

Sheffield Hallam University

Identification and mechanistic study of novel drug metabolites by LC-MS.

MARTIN, Scott.

Available from the Sheffield Hallam University Research Archive (SHURA) at:

<http://shura.shu.ac.uk/20713/>

A Sheffield Hallam University thesis

This thesis is protected by copyright which belongs to the author.

The content must not be changed in any way or sold commercially in any format or medium without the formal permission of the author.

When referring to this work, full bibliographic details including the author, title, awarding institution and date of the thesis must be given.

Please visit <http://shura.shu.ac.uk/20713/> and <http://shura.shu.ac.uk/information.html> for further details about copyright and re-use permissions.

SHEFFIELD HALLAM UNIVERSITY
LEARNING CENTRE
COLLEGIATE CRESCENT
SHEFFIELD S10 2BP

1402

102 121 732 8



ProQuest Number: 10702811

All rights reserved

INFORMATION TO ALL USERS

The quality of this reproduction is dependent upon the quality of the copy submitted.

In the unlikely event that the author did not send a complete manuscript and there are missing pages, these will be noted. Also, if material had to be removed, a note will indicate the deletion.



ProQuest 10702811

Published by ProQuest LLC (2017). Copyright of the Dissertation is held by the Author.

All rights reserved.

This work is protected against unauthorized copying under Title 17, United States Code
Microform Edition © ProQuest LLC.

ProQuest LLC.
789 East Eisenhower Parkway
P.O. Box 1346
Ann Arbor, MI 48106 – 1346

**IDENTIFICATION AND MECHANISTIC STUDY OF NOVEL DRUG
METABOLITES BY LC-MS**

Scott Martin

A thesis submitted in partial fulfilment of the requirements of

Sheffield Hallam University

for the degree of Doctor of Philosophy

July 2016

ABSTRACT

Understanding the metabolic fate of drug candidates *in vitro* and *in vivo* is a key component of drug development. Structural characterisation of drug candidate metabolites is important early in drug discovery to identify unwanted metabolic liabilities such as reactive, active, toxic or human specific metabolites. Reactive metabolite (RM) liability is a major concern for pharmaceutical companies during drug design, with most of the industry running primary RM trapping screens.

This thesis investigates Fenclozic acid, homopiperazine reactivity, homomorpholine reactive aldehyde and methanol adduct formation, where RMs were not detected through routine glutathione/cyanide trapping assays.

Fenclozic acid was withdrawn from clinical development due to hepatotoxicity; the mechanism of hepatotoxicity was never determined. *In vitro* covalent binding studies indicated phase I bioactivation in human liver microsomes, however no RMs were identified from *in vitro* experiments. As a part of this PhD thesis the metabolism of Fenclozic acid was investigated in bile duct cannulated rats using modern analytical techniques. Several new metabolites including glutathione related adducts formed through an epoxide RM were identified.

A series of homopiperazine compounds were found to react with endogenous formaldehyde during rat *in vivo* studies. This thesis describes a detailed investigation into the identification and mechanism of formation of the resulting product, a bridged homopiperazine formed through a reactive Schiff base intermediate.

A cysteineglycine conjugate observed for a series of homomorpholine compounds trapped by glutathione in human liver microsomes has been investigated in this thesis. NMR, detailed MS and methoxyamine trapping confirmed formation of a thiazolidine glycine product via a reactive aldehyde and subsequent glutathione rearrangement.

A compound series in an early drug discovery programme formed unusual methanol adducts post incubation in human liver microsomes. The work undertaken in this thesis revealed the generation of a reactive aldehyde metabolite that did not form an adduct with glutathione, but reacted with the methanol mobile phase to form a pair of hemiacetal diastereoisomers.

These examples would not have been detected using routine glutathione RM screening assays, this thesis highlights limitations of a screening approach, and where detailed metabolite identification studies employing modern LC-MS techniques are critical in understanding RM formation.

ACKNOWLEDGEMENTS

I would like to thank AstraZeneca for allowing me the time, resource and opportunity to complete this thesis.

The support and encouragement that I received from my supervisory team Dr Eva Lenz, Prof Malcolm Clench, Dr Simona Francese and Dr Dave Temesi was invaluable throughout this work and kept me motivated to the end.

I would like to acknowledge the technical support and expert knowledge from Dr Eva Lenz for conducting all the NMR analysis that was invaluable for the exact structural elucidation of several products. Also Dr Dave Temesi and Professor Malcolm Clench for the expert LC/MS support and advice throughout this project.

There have been a number of people who have generously provided their time and advice, but I would particularly like to thank Teresa Collins for her help with the Thesis formatting and Robin Smith for his help with generating *in vitro* samples for analysis.

Finally I would like to thank my parents Robert Martin and Linda Martin and partner Teresa Collins for their patience and support throughout the many years of this PhD.

TABLE OF CONTENTS

Identification and mechanistic study of novel drug metabolites by LC-MS.....	1
Abstract.....	2
Acknowledgements.....	3
Table of Contents.....	4
List of Figures	7
List of Tables.....	10
Abbreviations	11
1. Introduction.....	14
1.1 Drug metabolism and pharmacokinetics in drug discovery and development.....	14
1.1.1 Drug/Xenobiotic metabolism	14
1.1.2 Metabolite identification.....	16
1.1.3 Drug discovery/development process	26
1.2 LC-MS.....	26
1.2.1 Liquid chromatography.....	27
1.2.2 HPLC.....	28
1.2.3 UHPLC	30
1.2.4 MS Ionisation Source	30
1.2.5 Mass analyzers	32
1.3 MS scan approaches for metabolite identification studies	36
1.3.1 Nominal mass approaches to metabolite identification.....	36
1.3.2 High resolution accurate mass scan approaches	42

1.4	Non-MS based analytical techniques for metabolite identification	56
1.4.1	¹ H NMR.....	57
1.4.2	Ultraviolet Spectroscopy.....	57
1.4.3	Radio chemical detection	62
1.5	Detecting RMs	66
1.5.1	RM trapping assays.....	66
1.5.2	Bespoke trapping experiments.....	72
1.5.3	CVB.....	75
1.6	Aims and Objectives of this Project.....	76
2.	The metabolic fate of ¹⁴ C-Fenclozic acid in the hepatic reductase null (HRN) mouse	78
3.	Identification of the Reactive Metabolites of Fenclozic Acid in Bile Duct Cannulated Rats	89
4.	Reaction of Homopiperazine with Endogenous Formaldehyde: A Carbon Hydrogen Addition Metabolite/Product Identified in Rat Urine and Blood	99
5.	Reactive Metabolite Trapping Screens and Potential Pitfalls: Bioactivation of a Homomorpholine and Formation of an Unstable Thiazolidine Adduct	109
6.	Methanol adducts leading to the identification of a reactive aldehyde metabolite of CPAQOP in human liver microsomes by ultra-high performance liquid chromatography/mass spectrometry	123
7.	Summary and Conclusions	131
7.1	Fenclozic acid	131
7.1.1	<i>In vitro</i> studies	131
7.1.2	Fenclozic acid metabolism study in HRN mice (Chapter 2).....	133

7.1.3 Fenclozic acid metabolism study in bile duct cannulated rats (Chapter 3).....	133
7.2 Reaction of Homopiperazine with endogenous formaldehyde (Chapter 4) 137	
7.3 Bioactivation of a homomorpholine (Chapter 5).....	139
7.4 Methanol adducts leading to the identification of a reactive aldehyde metabolite (Chapter 6).....	140
7.5 Limitations of GSH LC-MS trapping screening assay	142
7.5.1 Detectability of RMs from compounds with little or no <i>in vitro</i> metabolic turnover	143
7.5.2 Bioactivation to a RM <i>in vivo</i> is not represented <i>in vitro</i>	144
7.5.3 GSH or cyanide trapping agents are unsuitable for the RM	144
7.5.4 Unexpected or unusual GSH rearrangement products not detectable by current LC-MS GSH trapping screening assays.	145
7.6 LC-UV-MS methodology	145
7.7 Overall conclusion	147
References	148
Word Count.....	157
Appendix A: Author contribution to multi-authored articles	158
Appendix B: Proposed structures for product ions identified from fenclozic acid and it's metabolites	160
Appendix C: Copyright Permission	167

LIST OF FIGURES

Figure 1 Compound optimisation by soft spot analysis and structural modification to block metabolism	17
Figure 2 Bioactivation of paracetamol and detoxification of the resulting RM by GSH	19
Figure 3 Drug discovery process (top) leading into drug development process (bottom).	26
Figure 4 Block diagram of a typical UHPLC or HPLC system connected to a mass spectrometer	27
Figure 5 Van Deemter plot showing the effect of flow rate on column efficiency (<i>HETP</i>) for different particle sizes and the optimal flow rate (red arrow) increases as the particle size decreases	29
Figure 6 Schematic diagram of a Q-ToF mass spectrometer.....	33
Figure 7 Schematic of quadrupole MS filter	34
Figure 8 Basic schematic diagram of a LTQ-Orbitrap XL mass spectrometer ..	35
Figure 9 Schematic of Orbitrap mass analyser	36
Figure 10 Diagram of the 4 scan modes on a triple quadrupole mass spectrometer: A Product ion scanning, B Selected reaction monitoring, C precursor ion scanning and D constant Neutral loss.....	37
Figure 11 CID Product ion scan (MS^2) for ibuprofen.....	38
Figure 12 Full scan TIC of a pre dose rat bile sample (top) and 0-7 hour post dose rat bile sample (bottom).....	39
Figure 13 Accurate mass spectrum and elemental composition results for Propranolol at 5 ppm and 20 ppm.....	44
Figure 14 Accurate mass simulated spectra for $C_{19}H_{32}ON_5$ (m/z 347.0934) and $C_{16}H_{16}N_3O_4S$ (m/z 347.2680) at 7500 peak resolution (a) and unit resolution (b).....	48

Figure 15 Fenclozic acid profile mass spectra at unit and 240,000 resolution. .49	
Figure 16 Elemental composition of a metabolite (m/z 864.4105) that is a glucuronide (bottom left) or cysteineglycine conjugate (bottom right).50	
Figure 17 Selected ion mass chromatograms of Fenclozic acid glutamyl metabolite in rat bile. (a) 1 Da mass window of the theoretical nominal $[M+H]^+$ 382 Da, (b) 10 ppm mass window of the theoretical exact $[M+H]^+$ 382.06228 Da.51	
Figure 18 Mass chromatograms of 3 co-eluting components highlighting which would be selected by DDA for MS^2 (a) Without dynamic exclusion (b) with dynamic exclusion.....55	
Figure 19 MS^2 scan of m/z 496.2097 (a) HCD CID and (b) IT CID55	
Figure 20 Electron transitions of σ , π and n electrons58	
Figure 21 Extracted UV chromatogram (330-350nm) of a test compound and its metabolites in human plasma (top) and extracted UV absorbances for metabolites and drug (bottom).60	
Figure 22 UV absorbance of a test compound (top) and extracted UV chromatograms of test compound and its metabolites in a rat hepatocyte extract (bottom).61	
Figure 23 Predose rat bile UV extracted chromatogram (280-290nm) (top) Test compound dosed 0-8 hour rat bile UV extracted chromatogram (bottom).62	
Figure 24 Partial positive ion mass spectrum of Chlozapine showing the $[M+H]^+$ ion and the signals arising from the presence of the 35 and 37 isotopes of Cl .64	
Figure 25 Theoretical mass spectrum for 1:1 mixture of Nortriptyline and stable labeled Nortriptyline ($3 \times {}^2H$) showing the two $[M+H]^+$ ions.65	
Figure 26 GSH structure showing the positive ion neutral loss fragments (A) negative ion precursor ion (B).67	

Figure 27 List of GSH analogues for RM trapping experiments: A Dansyl GSH, B GSH-ethylester C Quaternary ammonium GSH, D Stable labelled GSH and ³⁵ S labelled GSH.....	70
Figure 28 Cyanide addition to an iminium ion	72
Figure 29 Reactive aldehyde trapping by (A) methoxyamine and (B) semicarbazide.....	73
Figure 30 Metabolism/degradation of GSH adducts <i>in vivo</i>	74
Figure 31 ¹⁴ C Radiolabelled Fenclozic acid	131
Figure 32 Radio chromatogram from a Fenclozic acid GSH trapping experiment.	132
Figure 33 Fenclozic acid carnitine conjugate	135
Figure 34 Selected ion mass chromatograms for Fenclozic acid and the carnitine metabolite at pH 6.5 (ammonium acetate) (top) and pH 4.0 (formic acid) (bottom).....	135
Figure 35 Fenclozic acid Glutathione conjugate isomers.....	136
Figure 36 In vivo enzymatic degradation of GSH conjugates	136
Figure 37 AZX homopiperazine -CH ₂ bridged structure	138
Figure 38 Proposed structure for the AZXa cysteineglycine adduct.....	140
Figure 39 AZXb methanol adduct diastereoisomers	141
Figure 40 Selected ion mass chromatograms (+/-5 ppm narrow mass window) of Fenclozic acid (survey scan) and Fenclozic acid product ions (AIF) in rat urine.....	147

LIST OF TABLES

Table 1 Exact mass of the most abundant isotopes for common elements found in small organic drug-like molecules.	43
Table 2 Biotransformations reactions, where the metabolite formed has the same nominal mass but a different structure and accurate mass.	46

ABBREVIATIONS

^3H	Tritium
3 R's	Refine, reduce, replace
^{13}C	Carbon 13 isotope
^{14}C	Carbon 14 isotope
^{15}N	Nitrogen 15 isotope
ADME	Absorption, distribution, metabolism, excretion
AIF	All ion fragmentation
ADR	Adverse drug reaction
AUC	Area under the curve
CAD	Collision activated dissociation
CDER	Centre for drug evaluation and research
CID	Collision induced dissociation
Cl	Chlorine
CL	Clearance
Cl_{int}	Intrinsic clearance
C_{max}	Maximum concentration
CVB	Covalent binding
CYP	Cytochrome P450
Cys	Cysteine
Da	Daltons
DC	Direct current
DDA	Data dependent acquisition

DILI	Drug Induced Liver Injury
DMT	Design make test
DMPK	Drug metabolism and pharmacokinetics
ESI	Electrospray ionisation
FDA	Food and drug administration
GSH	Glutathione
GSH-EE	Glutathione ethyl ester
HCD	Higher-energy collisional dissociation
HETP	Height equivalent to a theoretical plate
HPLC	High performance liquid chromatography
ICH	International conference on harmonisation
IDA	Information dependent acquisition
IS	Internal Standard
IT	Ion trap
<i>i.v.</i>	Intravenous
IVIVE	<i>In vitro/in vivo</i> extrapolation
KCN	Potassium cyanide
LC	Liquid chromatography
LC-MS	Liquid chromatography mass spectrometry
<i>m/z</i>	Mass to charge ratio
MDF	Mass defect filtering
MIST	Metabolites in safety testing
MRM	Multiple reaction monitoring

MS ²	Product ion scanning
MS ⁿ	Infinite product ion scans
MS	Mass Spectrometry
MW	Molecular weight
NAC	N-Acetylcysteine
NLS	Neutral loss scanning
NMR	Nuclear magnetic resonance
PDA	Photodiode array detector
PIS	Precursor ion scanning
PK	Pharmacokinetic
QqQ	Triple quadrupole mass spectrometer
Q-ToF	Quadrupole time of flight
rf	Radio frequency
RM	Reactive metabolite
SAR	Structure activity relationship
SRM	Selected reaction monitoring
SWATH	Sequential window acquisition of all theoretical fragment ion spectra
tDRM	Total drug related material
Th	Thomson
UHPLC	Ultra high performance liquid chromatography
UV	Ultraviolet
vDIA	Variable data independent acquisition

1. INTRODUCTION

1.1 Drug metabolism and pharmacokinetics in drug discovery and development

Drug metabolism and pharmacokinetics (DMPK) is concerned with the fate of administered drug in the body. In the 1990s 40% of drug attrition was due to poor DMPK properties, and investment in DMPK had improved this statistic so that by the 2000s this had reduced to less than 10% attrition. However overall drug approval rates remained low¹. Pharmacokinetics (PK) examines drug concentrations over time, and is influenced by the drug's absorption, distribution, metabolism and excretion (ADME) properties. Both the rate and extent of absorption can be of concern, especially for orally administered drugs. When a drug is absorbed it passes through the liver first where metabolism of xenobiotics occurs and this is often described as first pass metabolism. Once in the systemic circulation the drug may become bound to plasma proteins or as free drug it is able to distribute into tissues/cells. Ultimately the drug will be excreted via urine or faeces unchanged or as a metabolite.

The rate of removal of active drug from the body can be referred to as Clearance (CL), which describes the volume of drug cleared per unit of time. It is important to understand the CL of a drug together with its volume of distribution to determine its plasma half-life. The optimisation of plasma half-life is critical (together with dose) to achieve sufficient duration of exposure of a drug to illicit efficacy for the desired therapeutic indication. Systemic CL can be due to metabolism, excretion of drug or a combination of both. It is therefore important to understand the routes of metabolism and elimination, which are studied in both *in vitro* and *in vivo* systems.

1.1.1 Drug/Xenobiotic metabolism

Xenobiotic metabolism is the biochemical modification of a drug or foreign compound by living organisms, typically to more polar water soluble metabolites which are more readily excreted from the body. Drug metabolism can generally be divided into two phases; Phase I and Phase II. Phase I metabolism involves oxidation, hydrolysis or reduction that typically increases the polarity of the drug.

These metabolites often maintain some parent drug activity, in the case of pro-drugs become more active, or they can be chemically reactive through bioactivation.

There are a number of enzymes that are known to catalyze Phase I biotransformation reactions such as the cytochrome P450 family (CYP), flavin-containing monooxygenases, aldehyde oxidase, alcohol dehydrogenase and monoamine oxidases. The most important of these for xenobiotic metabolism in humans is the CYP family²⁻⁵ which are responsible about 75% of all Phase I dependent drug metabolism⁴.

The human CYP family consists of numerous enzymes, however for drug metabolism; enzyme families 1-3 are the most important and are responsible for 10-80% of all phase I dependent metabolism of clinically used drugs⁴. These families can be divided up into sub families e.g. CYP3A and CYP3B and each individual member of a subfamily is labeled with Arabic numerals (e.g. CYP1A2)³. CYP3A4 is the most abundant CYP in the human liver and is the most important CYP for drug metabolism, responsible for about 50% of the metabolism of clinically used drugs^{4,6}. Drug metabolism by cytochrome P450s is a major cause of drug-drug interactions where co-administration of more than one drug leads to change in the exposure of one or more of the drugs and their metabolites. For example co-administration of a strong inhibitor of CYP3A4 such as ketoconazole with a drug that is primarily metabolized by CYP3A4 could lead to accumulation and increased exposure of that drug. This can have potentially dire consequences, such as life-threatening arrhythmias which occurred when 3A4 inhibitors were co-administered with terfenadine (an anti-histamine), which was later withdrawn⁷.

Phase II drug metabolism involves conjugation of small polar endogenous molecules (such as glutathione, sulphate, acetyl, glucuronic acid and amino acids) with specific functional groups on a drug, either directly to the drug or more often to a phase I metabolite. In contrast to phase I metabolism, phase II metabolism generally results in metabolites that are deactivated and or less reactive than the substrate, the exception being acyl-glucuronides where metabolites can be more chemically reactive.

1.1.2 Metabolite identification

Metabolite identification studies are fundamental to the discovery, refinement, optimization and development of small molecule therapeutics (xenobiotics) for humans. Metabolite identification studies are conducted from early design all the way through to life cycle management of a drug. Early discovery metabolite identification work focuses on drug design such as 'soft spot analysis' or identification of reactive/toxic metabolite liabilities to direct iterative synthetic chemistry make test cycles towards structures with favourable DMPK and safety profiles. Later drug development activities are more focused on quantifying and identifying metabolites in man, with a focus on major circulating metabolites. It is vital to avoid any unexpected occurrences such as the formation of reactive, active or circulating human specific/disproportionate metabolites in clinical trials, so it is important to identify, avoid or evaluate these issues during drug design.

1.1.2.1 Metabolite identification soft spot analysis

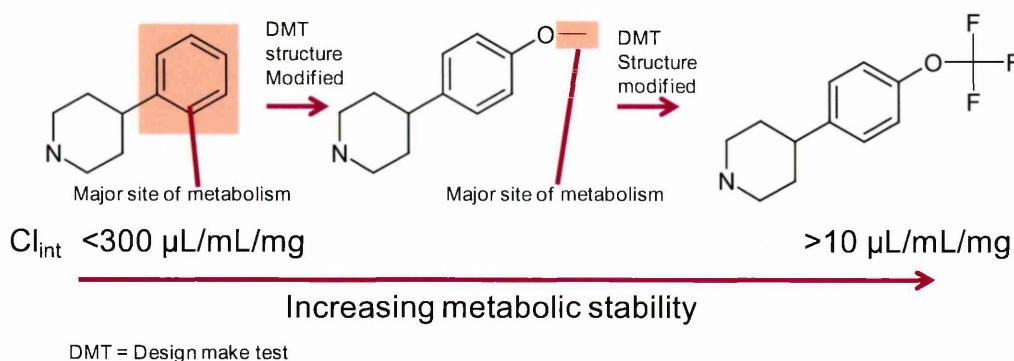
Metabolism studies begin early in drug discovery at lead identification or earlier, where large numbers of compounds are investigated to identify a promising series of compounds. At this stage it is important that there is sufficient exposure of a test compound in the efficacy species to be able to measure its *in vivo* efficacy. There are two important considerations to achieve good exposure of an orally administered drug; absorption and CL. It would be expensive and inefficient to dose large numbers of compounds to animals to optimise absorption and CL *in vivo* and would be against the 3 R's principles (Refine, reduce, replace animal usage), which all pharmaceutical companies are committed to. One way to reduce the number of compounds dosed to animals, is to optimise the CL *in vitro* first.

Metabolism is a major CL mechanism that primarily occurs in the liver, so measuring a test compound's metabolic stability or intrinsic CL (CL_{int}) will help understand the *in vivo* CL. These measurements can be determined *in vitro* using liver microsomes and/or hepatocytes, which contain enzymes for the most prevalent metabolic processes in the liver. Compounds are incubated in liver microsomes or hepatocytes where samples are taken at set times and

compound disappearance is measured allowing a Cl_{int} to be determined⁶. These *in vitro* experiments are high throughput and high numbers of compounds can be tested quickly and cheaply compared to *in vivo* testing.

One way to help reduce the Cl_{int} for a chemical series is to identify the major sites of metabolic liability on structure by *in vitro* soft spot metabolite identification. This metabolite identification is relatively simple, often only the top 2 or 3 metabolites are identified from the microsomal or hepatocytes incubation. Absolute confirmation of the metabolite structure is not always required and often just an idea of the site of metabolism is sufficient. Therefore the data can be generated quickly to direct iterative synthetic chemistry make-test cycles towards better compounds (Figure 1). Probe compounds with favourable Cl_{int} and potency are dosed to animals (rodents) to generate *in vivo* pharmacokinetic (PK) data to determine exposure.

Figure 1 Compound optimisation by soft spot analysis and structural modification to block metabolism



1.1.2.2 *In vitro-in vivo extrapolation disconnect*

Optimising Cl_{int} *in vitro* for a chemical series does not always correlate to the *in vivo* situation and there can be a significant disconnect in the *in vitro/in vivo* extrapolation (IVIVE) of CL. When this occurs, it is likely there is a CL mechanism *in vivo* that is not represented *in vitro* in microsomes or hepatocytes. This can be metabolic or non-metabolic, often the best way to identify the problem is to intravenously (*i.v.*) dose a bile cannulated animal (the species with the disconnect) and collect bile and urine. The parent drug is then quantified in the collected bile and urine (normally over a time course) and the % of dose excreted as parent compound can be calculated. If the majority of

the dose is excreted as parent compound then major CL mechanism is likely to be non-metabolic. If very little parent drug is quantified then the major CL mechanism is metabolic, which is not likely not to be represented in hepatocytes or microsomes and therefore potentially non-hepatic metabolism.

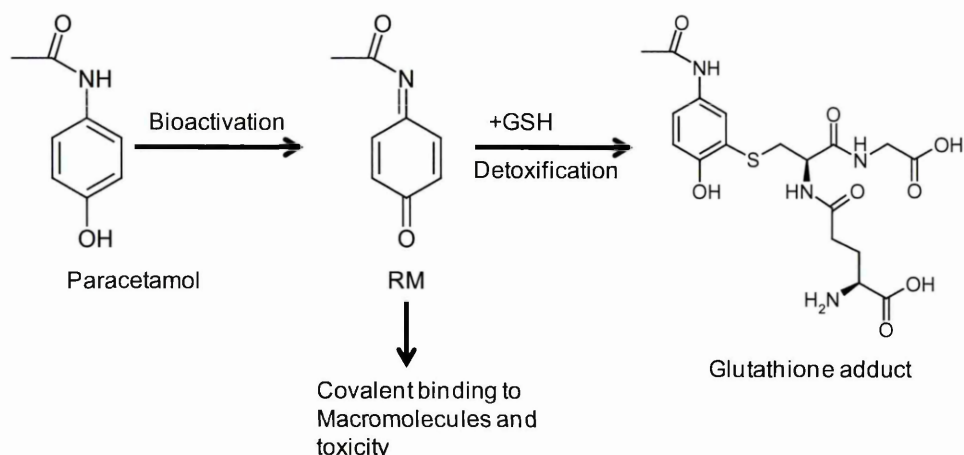
Non-hepatic metabolism was observed for compound AZX discussed in Chapter 4, where an unusual carbon hydrogen addition metabolite was observed *in vivo* in the rat, but not formed in rat microsomal or hepatocytes incubations. It is important to identify the exact metabolite to identify the structural liability so it can be avoided for future drug discovery programmes.

1.1.2.3 Reactive metabolites and toxicity

Metabolic processes normally transform xenobiotics into harmless, inactive water-soluble products to improve excretion from the body. However some metabolic transformations can result in products that are considerably more chemically reactive than the parent test compound or drug, this process is known as bioactivation. The product is referred to as a reactive metabolite (RM), but is in fact a reactive intermediate that undergoes further reaction. The most common of these reactive intermediates are electrophiles which can vary in nature from soft to hard. RMs may cause toxicity by binding to nucleophilic groups on macromolecules in the body such as protein, lipids and nucleic acids.

Glutathione (GSH), a tripeptide consisting of cysteine (Cys), glycine and glutamyl, present in animal cells, offers some protection from reactive/toxic compounds/metabolites⁸. It contains a thiol group which acts as a competing nucleophilic site for RMs to bind to rather than nucleophiles present on endogenous macromolecules. A good example of the protective properties of GSH is the bioactivation of paracetamol, a small molecule analgesic drug. Paracetamol is metabolized in man to a quinoneimine electrophilic RM that covalently binds to macromolecules which can cause hepatotoxicity. GSH protects against this covalent binding (CVB) by reacting with the quinoneimine metabolite/intermediate forming a non-reactive GSH adduct (Figure 2)⁹.

Figure 2 Bioactivation of paracetamol and detoxification of the resulting RM by GSH



This defensive mechanism is not always completely successful, and in some cases reactive electrophilic intermediates are not efficiently detoxified by GSH or in other cases may deplete GSH both resulting in CVB to cellular macromolecules. This type of *in vivo* CVB can lead to toxicity and adverse drug reactions (ADR) in the clinic^{10,11}.

1.1.2.3.1 Adverse drug reactions

The World Health Organization defines an adverse reaction as 'a response to a drug which is noxious and unintended, and which occurs at doses normally used in man for the prophylaxis, diagnosis, therapy of disease, or the modifications of physiological function'¹². ADRs are a serious concern for pharmaceutical companies, they are one of the most common causes for withdrawing a drug for the market and are estimated to be the 4th most common cause of death in the United States (US)¹³. It is estimated that about 2 million patients in the US experience serious ADRs each year from drugs on the market, which results in 100,000 deaths. In the United Kingdom, there were 557,978 ADR associated hospital admissions from 1999 to 2008, with approximately 5% mortality¹⁴.

ADRs are often classified into two important categories Type A and Type B, however there is an extended categorization that includes Type C, Type D and Type E¹⁵. Type A reactions are the result of a drugs primary or secondary pharmacological actions when given at the therapeutic dose and account

approximately 80% of all ADR's. These reactions are rarely life threatening and are normally dose dependent, so they are reversible on reducing dose or by withdrawing the drug¹⁶. Type A ADRs are generally predictable and can be identified from the pre-clinical toxicological studies in animals. Type B reactions are not related to the known pharmacology of the drug and are primarily related to the patient or individual dosed so are not predictable. They are referred to as an idiosyncratic adverse drug reaction (IADR) or idiosyncratic drug reaction (IDR). It is not currently possible to predict who will develop an IDR to a drug and there are no general animal models to predict the occurrence of IDR's. They can be dose dependent for the susceptible individuals; however most dosed patients will not have an IDR from a specific drug at any dose, so increasing the dose does not necessarily increase the risk or frequency of IDRs¹⁷. IDRs are rarer than type A with frequencies ranging from as high as 5% of users to as low as 1 in 10000 or 1 in 100,000¹⁸, however they are more serious and can be life-threatening. Due to the frequency and unpredictability these events are often only seen late in the development program or when the drug is licensed, both are likely to be after significant investment in its development.

1.1.2.3.2 RMs link to IDRs

IDRs can affect a number of different organs in the body, however drug induced liver injury (DILI) is the type that most commonly leads to drug withdrawals or failure to obtain market approval^{17,19}. DILI can be predictable (non-idiosyncratic, Type A), these are generally dose related and a result of direct toxicity of the parent drug or its metabolites, for example in the case of paracetamol⁹. This non-idiosyncratic DILI is more likely to be detected during the pre-clinical toxicological studies and therefore drugs generating these rarely get to market. In contrast, idiosyncratic (unpredictable, type B) DILI related events often materialize late in a drugs development or when the drug has been licensed, hence is responsible for most of the DILI related drug withdrawals^{17,19-21}. Withdrawing a drug late in its development or from the market is very expensive and can significantly damage a company's reputation, as well as putting patient health at risk, so idiosyncratic DILI is a serious concern for pharmaceutical companies.

The liver metabolizes xenobiotics in order to make them more polar to aid excretion, so will be exposed to high concentrations of drug and its corresponding metabolites after dosing. Bioactivation of the drug to a RM is believed to be the first step towards DILI and hepatotoxicity for most drugs^{17,19,21,22}; they can covalently bind to protein, lipids or nucleic acids. All of these have a direct effect on cell function, which can cause hepatic cell death leading to liver injury. A good way to reduce the risk of idiosyncratic DILI in the clinic is to try to avoid compounds that can generate RMs in man.

Over the last 15-20 years pharmaceutical companies have tried to identify compounds that generate RMs in early drug discovery and where possible modify chemistry to remove the liability. There are a number of ways to identify and avoid RMs, including *in silico* prediction, metabolite identification and *in vitro* trapping/*in vitro* trapping screens. The *in silico* metabolite predictive tools are beyond the scope of this thesis and are not discussed. Metabolite identification studies are generally low throughput and time consuming, so cannot be used to assess large numbers of compounds early in drug discovery, but can be applied sensibly by analyzing a selected compound representing a chemical series. *In vitro* trapping experiments are a tool that can be used by a metabolite identification scientist to help detect RMs and investigate their mechanism of formation. They can also be applied in a higher throughput manner using appropriate automation and analytical techniques (Section 1.5.1).

It is important to note that not all compounds that form a RM will lead to toxicity in man and that there are other factors that are important such as disease area, patient population and importantly the predicted human daily dose. In addition, it is not always possible to remove the RM liability by chemically altering compounds as the liability could be embedded in the pharmacophore, where structural changes would significantly impact its potency.

1.1.2.4 Active metabolites

Generally metabolism of an active drug leads to the formation of considerably less active or inactive metabolites. However, occasionally biotransformation of an active drug can lead to the generation of metabolites with equal or greater pharmacological activity (active metabolite). Active metabolites can be of

concern to drug discovery programmes due to the added complexity of understanding the metabolite contribution to the safety and efficacy profile of the drug, so are often avoided.

However, a metabolite identified in drug discovery may have superior pharmacological, pharmacokinetic, and safety profiles compared to its parent compound. In this case the metabolite may be developed in to a drug and there are several examples of this reported including oxyphenbutazone, oxazepam, cetirizine, fexofenadine and desloratadine²³. Confirming a metabolite has activity requires identifying its exact structure to enable metabolite synthesis for subsequent activity testing. Therefore it is important to try and determine the exact structure of metabolites when they are formed in high quantities from human *in vitro* experiments for promising compounds approaching development.

The pro-drug approach to drug design is where an inactive compound with favourable bioavailability is designed to be metabolised to an active drug via first pass metabolism. This is different to active metabolites, which have been defined as a pharmacologically active metabolic product with activity against the same pharmacological target as the parent molecule^{23,24}.

1.1.2.5 Metabolites in Safety testing

Non-clinical toxicological studies generally include the assessment of circulating concentrations of drug, which are used to compare the systemic exposure of the drug in the toxicological animal species with systemic exposure in humans to help guide clinical trials. This is likely to be sufficient if the metabolic profile in humans is similar to at least one of the animals used in the study, however metabolites can vary across species both quantitatively and qualitatively. Safety testing of drug metabolites is a serious consideration for drug development programmes and is concerned specifically with drug metabolites circulating in human plasma.

Circulating human metabolites can contribute to the primary target pharmacology, off target pharmacology/secondary pharmacology and/or toxicity of a drug through active, reactive and toxic metabolites. These metabolites

could represent a significant proportion of the dose or even be present at higher concentrations than the parent drug in plasma or tissues. In this circumstance it is important to understand if these metabolites are represented in one of the toxicological species and whether the metabolite exposure is equivalent to or high compared to humans.

In 2008 the Food and Drug Administration (FDA) centre for drug evaluation and research (CDER) issued 'the safety testing of metabolites' guidance also known as metabolites in safety testing (MIST)²⁵. Further guidance was published in 2009 following the International Conference on Harmonisation (ICH) of technical requirements for regulations of pharmaceuticals for human use²⁶. Both documents define levels of metabolite exposure in humans and pre-clinical species that would assure regulators.

The FDA guidance states that '*generally, metabolites identified only in human plasma or metabolites at disproportionately higher levels in humans than in any of the animal test species should be considered for safety assessment*'. Human metabolites that can raise a safety concern are those formed at greater than 10% of parent drug systemic exposure at steady state²⁷. Both the FDA and ICH guidance documents^{26,27} recommend the same 10% threshold value; however the ICH guidance refers to percentage of total drug related material (tDRM) rather than a percentage of parent drug. Percentage of tDRM is more commonly adopted within the pharmaceutical industry. Therefore metabolites that are unique or disproportionate in humans are not of concern if they are <10% relative to tDRM at steady state, and metabolites >10% are not of concern if there is equal or greater exposure of the metabolite in the toxicological species. Hence, it is necessary to either demonstrate there are no metabolites greater than 10% (quantification of circulating human metabolites) or to confirm equal exposure in the toxicological species (*in vivo* cross species comparison). Metabolite profile comparisons *in vitro* (hepatocytes or microsomes) are not sufficient to determine if a test compound has a unique/disproportionate metabolite^{26,27}, so both approaches require the analysis of human plasma and/or plasma from the toxicological species.

Radiolabelled ADME studies provide the most definitive metabolite identification and quantification *in vivo* in humans and pre-clinical toxicological species²⁸. Therefore a human radiolabelled ADME metabolite profiling study would determine if any metabolites were circulating greater than 10%. Comparison of the metabolite profiles from the radiolabelled ADME studies in human and the toxicological species, confirms if any of the human metabolites are unique or disproportionate. Human ADME studies are very expensive and often pharmaceutical companies prefer to backload these studies until there has been proof of concept around Phase IIb clinical trials. To perform this analysis earlier numerous non-radiolabelled methodologies have been reported in the literature for quantification, metabolite detection and profiling comparison.

1.1.2.5.1 Area under the curve pooling of samples for total metabolite exposure quantification or comparison

To quantify or compare the total exposure of all metabolites and drug plasma, concentrations can be determined from samples taken at several time-points during a dosing interval (typically 24 hours). The area under the curve (AUC) integrates concentrations over time and is used as a measure of total drug or metabolite exposure, unlike maximal concentration (C_{max}) that only compares amounts at a snapshot in time. The AUC of a metabolite can be used to judge whether there is a disproportionate amount in human to other species or if it represents more than 10% of tDRM. It would be time consuming and labour intensive to identify and quantify metabolites at each time-point, so the time-points available are pooled in order to construct a single sample for analysis. The volumes of each time point are pooled to reflect the relative proportions based on the PK profile needed to assess the AUC, and this is known as an AUC pooling as reported by Hamilton *et al.*²⁹.

1.1.2.5.2 Quantification of metabolites in human plasma for MIST assessments

This approach is to first identify and quantify all plasma circulating metabolites in an AUC pooled human plasma sample to determine if the exposure of any of the metabolites detected is greater than 10% of the tDRM. Quantification is not possible by mass spectrometry (MS) without a standard (Section 1.2.4), so

alternative techniques such as UV and nuclear magnetic resonance (NMR) have been used³⁰. Yu *et al.*³¹ reported the quantification of metabolites using a radiolabelled compound to generate *in vitro* metabolites, then determined a MS/radioactivity response factor to quantify human *in vivo* metabolites. If there are any metabolites at or above the 10% threshold then these are assessed to ensure their exposure in the toxicological species is at least equal to their exposure in humans. Due to this arbitrary 10% cut off and the accuracy of bioanalytical methodology metabolites slightly below this percentage will also likely be investigated.

1.1.2.5.3 *In vivo cross species metabolite comparison of circulating metabolites in human versus the toxicological species*

This approach focuses on determining if the toxicological species have been exposed in equal or greater levels to metabolites observed in humans. This is done by comparing the metabolite plasma profiles in a human AUC pooled sample with the metabolite profiles from the toxicological species. Comparison of all human metabolites with the equivalent metabolites (if formed) in the toxicological species is used to determine if any are disproportionate or unique to humans. This can be done using the techniques discussed in Section 1.1.2.5.2 or simply by liquid chromatography mass spectrometry (LC-MS) comparing the MS peak areas of each metabolite in human with the peak area of the equivalent metabolite in the toxicological species. Matrix matching of the human and animal samples is done to equalise any matrix or ion suppression effects (Section 1.2.4). Only the MS responses (peak area) of identical metabolites are compared with each other, so there should not be any variation in ionisation efficiency due to structural differences. If any metabolites are disproportionate or unique to humans then accurate quantification of these metabolites in humans is required to determine if they are greater than 10% of the total circulating drug related material. If no metabolites are human unique or disproportionate then no further work is required.

1.1.2.5.4 *MIST strategy summary*

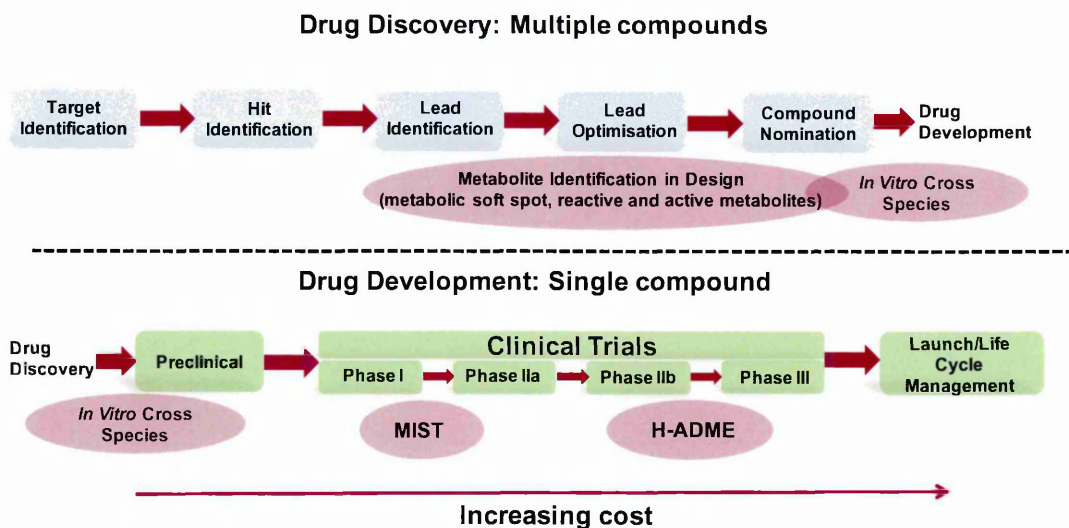
It is important to understand the metabolism of a drug in humans before it is tested on large numbers of patients. The best way to ensure there are no

problems later on in the clinic is to have synthetic standards for the major human circulating metabolites available before humans are dosed. Metabolites with analytical standards can be accurately quantified, tested for activity and dosed to toxicological species if specific or disproportionate in humans. Therefore identifying the exact structures of human metabolites *in vitro* and/or identifying them in other test species prior to the clinic is very important.

1.1.3 Drug discovery/development process

An overall view of the small molecule pharmaceutical drug discovery and development process is illustrated in Figure 3. Drug discovery is focused on the identification of a safe, potent, small molecule (from multiple potential compounds) to progress into clinical trials. Development studies are primarily to determine and understand the drug's effects on the human body including clinical toxicity and efficacy. The further a compound progresses in development the larger the number of patients/volunteers used, hence the increasing cost.

Figure 3 Drug discovery process (top) leading into drug development process (bottom).

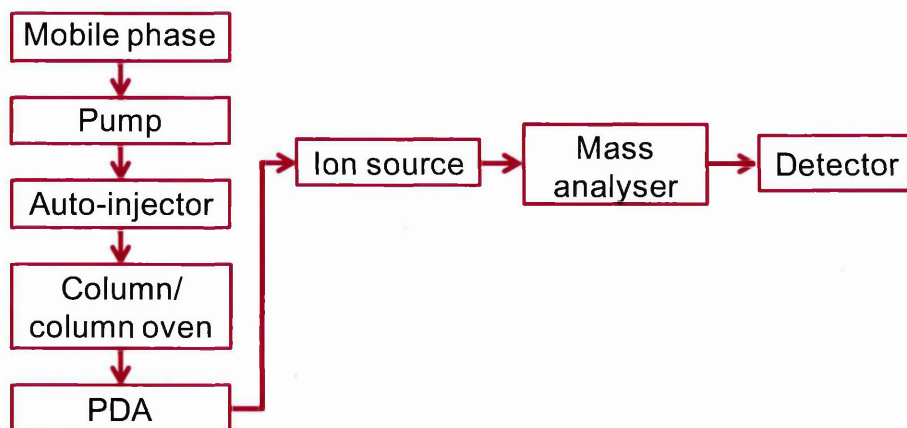


1.2 LC-MS

LC-MS is the most widely used analytical technique in drug research and is generally applied to the separation, quantification and/or structural characterisation of molecules from mixtures. It has become the predominant

analytical tool for the detection, quantification and characterisation of drugs and metabolites in biological matrices^{32,33}. MS instruments for metabolite identification studies are normally coupled to a high performance liquid chromatography (HPLC) system or ultra high performance liquid chromatography (UHPLC) system, see Figure 4 for a block diagram of a typical set up for these systems.

Figure 4 Block diagram of a typical UHPLC or HPLC system connected to a mass spectrometer



It is not uncommon for drugs to form multiple metabolites with the same accurate mass; such as multiple +O (hydroxylated) metabolites, therefore it is important to separate these by chromatography prior to MS analysis.

1.2.1 Liquid chromatography

Liquid chromatography (LC) is a technique used to separate components within a mixture through interactions with 2 phases; a mobile phase and a stationary phase. Components in a mixture are separated if they interact through hydrogen bonding, van der Waals forces or/and electrostatic forces to different extents with the mobile and/or stationary phases. There are different modes of liquid chromatography that include: normal-phase liquid chromatography, reverse phase liquid chromatography, ion-exchange liquid chromatography and size-exclusion chromatography. Reverse phase chromatography is the most compatible and the mostly commonly used separation mode with mass spectrometry. Reverse phase chromatography separates components using a polar mobile phase (typically water) and a non-polar stationary phase. Water in the mobile phase repels the non-polar regions of a molecule, which facilitates a

molecule stationary phase interaction through van der Waals forces. Molecules that are more polar will interact more with the mobile phase and elute earlier, conversely less polar molecules will interact more with the stationary phase and elute later. For this reason the vast majority of drug metabolites elute before drug by reverse phase chromatography.

1.2.2 HPLC

The mobile phase eluents consist of water and an organic solvent which is typically either acetonitrile or methanol for LC-MS applications. Mobile phase can be delivered in two ways, firstly isocratically, where the same composition of organic and aqueous is maintained across a run and is often used to separate a few compounds of similar polarity. Secondly by a gradient, where the mobile phase is changed across a run moving from mostly aqueous to more organic and is used to separate multiple components with varying polarities. Considering the potential for vastly differing polarities of metabolites and parent drug, gradient delivery is required for metabolite identification work.

Reverse phase HPLC stationary phases generally consist of a non-polar alkyl chain such as C18 bound to silica gel particles which are packed into a metal column. Column efficiency is measured in theoretical plates (N) and height equivalent to a theoretical plate ($HETP$):

$$HETP = \frac{L}{N}$$

Equation 1

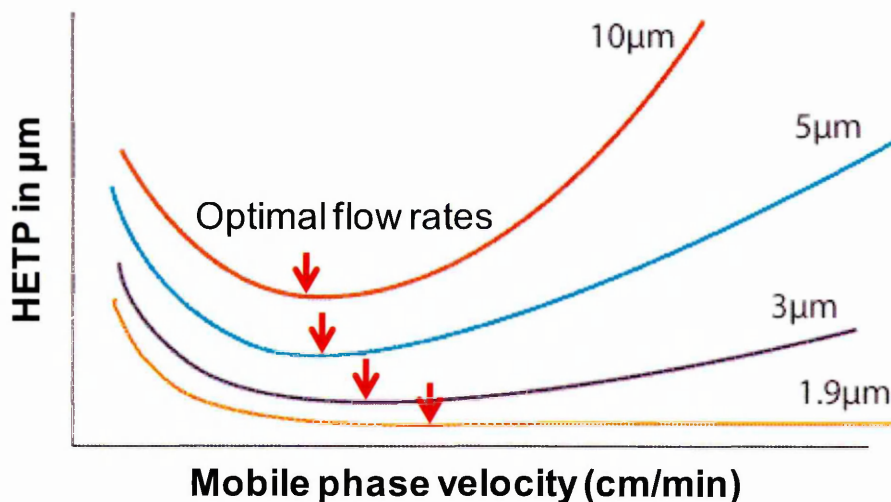
Where L is column length. The efficiency of chromatographic columns increases with the number of theoretical plates and when the $HETP$ is smaller. Equilibration rate between mobile and stationary phases is finite; therefore analyte band shape and column efficiency depend on the rate of elution, or mobile phase flow rate. The Van Deemter equation describes the mechanisms of band broadening:

$$HETP = A + \frac{B}{v} + Cv$$

Equation 2

A represents Eddy diffusion, which is a measure of the multiple paths of different lengths travelled by analytes between particles that is caused by small variations in particle size, so is broadly independent of flow rate. *B* represents longitudinal diffusion, since the longer the analyte spends on the column the greater its diffusive spreading; therefore it is dependent on flow rate. C_v represents the equilibration time between phases and this increases as flow rate increases. The band broadening effects due to *A* and C_v are reduced for smaller particle size columns, so in general smaller particle size columns are more efficient. Flow rate for a column is optimal when *HETP* is at its minimal value and is dependent on the particle size (Figure 5).

Figure 5 Van Deemter plot showing the effect of flow rate on column efficiency (*HETP*) for different particle sizes and the optimal flow rate (red arrow) increases as the particle size decreases



The smaller the particle size, the higher the optimum flow rate, the better the column efficiency; however flow rate is limited due to back pressure (pressures above 400 bar are not possible on HPLC systems). Smaller particle size columns suffer less diffusion so can accommodate higher flow rates without losing column efficiency (Figure 5), where 1.9 μm has the flattest curve.

Introducing a column heater reduces the viscosity of the mobile phase solvents to enable higher flow rates and improved column efficiency. Whilst this offers some improvement, generally HPLC pressure limitations restrict flow rates which are sub optimal for smaller particle size columns, and generally HPLC

particle sizes are typically around 3 to 5 μm . There are significant efficiency gains moving to smaller particle size columns if the back pressure limitations could be overcome.

1.2.3 UHPLC

UHPLC systems are essentially HPLC systems with pumps, columns and fittings that can cope with significantly higher pressures, typically 2x greater. The ability to run at higher pressures enables the use of smaller particle size columns typically 1.5-3 μm at more optimal flow rates. Using UHPLC systems with smaller particle size columns has three main effects; reduced HETP, optimal flow rate is higher and the loss in efficiency when flow rates are greatly above optimal are significantly reduced. The effects can be used to either dramatically speed up analysis times by running at higher flow rates or to improve separation on longer runs³⁴⁻³⁶. Castro-Perez *et al.*³⁷ demonstrated significant gains in chromatographic resolution, speed of analysis and sensitivity employing UHPLC for *in vitro* metabolite identification experiments.

Most modern LC-MS systems for metabolite identification applications have replaced HPLC with UHPLC systems; however peak widths are significantly smaller than standard HPLC and are often around 3 seconds wide. This would limit the number of MS experiments that can be acquired in a single scan.

1.2.4 MS Ionisation Source

Coupling a LC system directly to a mass spectrometer requires an interface to convert the liquid flow into gaseous ions prior to introduction into the mass spectrometer, which is under a high vacuum. Historically it was not easy to couple LC to MS using the conventional ionization methods at the time such as; electron ionisation (EI), fast atom bombardment or chemical ionisation. It was not until the advent of atmospheric pressure ionisation (API) techniques such as electrospray (ESI), atmospheric pressure chemical ionisation (APCI) and atmospheric pressure photo ionisation (APPI) that LC-MS became popular and it is currently amongst the most widely used analytical techniques.

API methods are well suited to LC-MS and essentially involve spraying a solution containing analyte at atmospheric pressure into the ion source and

through a combination of thermal and pneumatic processes, desolvation occurs. They are also referred to as 'soft ionisation techniques' where very little in-source dissociation of the analyte is observed and usually a protonated molecule ($[M+H]^+$ ion) is formed in positive ion mode and a deprotonated molecule ($[M-H]^-$ ion) in negative ion mode. Determining the molecular weight of an analyte from the $[M+H]^+$ or the $[M-H]^-$ ion simply involves adding or subtracting the mass of a proton.

For APCI and APPI, ions are formed chemically in the gas phase via gas phase reactions precipitated by a corona discharge needle and a krypton discharge lamp respectively. For ESI, an electric field is used to generate charged droplets and subsequently ions through evaporation. The best ionisation efficiency is achieved when analyte ions are already charged in solution and therefore ESI is best suited for the analysis of polar and ionic compounds. APCI and APPI are complimentary techniques to ESI and are generally applied to non-polar analytes which are not detectable or give poor responses by ESI-MS. If the parent compound is ionised effectively by ESI then it is highly likely all of the metabolites will also be ionised, since most metabolites are more polar than the parent compound, therefore ESI is often the first choice ionisation technique.

The main disadvantage of API ionisation techniques is ion suppression, where background ions may alter the MS response of the analyte of interest³⁸⁻⁴¹. King *et al.*⁴⁰ reported that ESI is more susceptible to ion suppression than APCI by comparing ion suppression effects from extracted dog plasma. They propose that gas phase effects are minimal and the major contributing factor to ion suppression is non-volatile material in the spray. Ion suppression is only serious concern for metabolite identification studies when attempting to quantify metabolite levels by mass spectrometry. Even if ion suppression effects could be overcome by sample clean up, differing ionisation efficiencies of the target metabolites from the parent compound and other metabolites^{28,42} make quantification impossible without authentic standards. Often other analytical techniques are utilised for quantification of metabolites such as NMR, UV or radiochemical detection.

1.2.5 Mass analyzers

Mass analyzers in mass spectrometry are used to separate ions of analytes by their mass/charge ratio (m/z) in the gas phase under high vacuum using electric and magnetic potentials. The monoisotopic mass can easily be determined by multiplying the m/z by the number of charges. Small organic molecule mass spectrometry often produces a single charged ion, however double or triply charged ions can occasionally be formed. It is easy to identify double or triple charged ions, simply by comparing the m/z difference between the ^{12}C and ^{13}C isotope peaks in the mass spectrum. For single charge ions it will be 1 Th, for doubly charge it will be 0.5 Th and for triply charged ~ 0.33 Th. The ability to separate components by mass (m/z) makes mass spectrometry extremely useful technique for quantitative and qualitative analysis of molecules in biological samples.

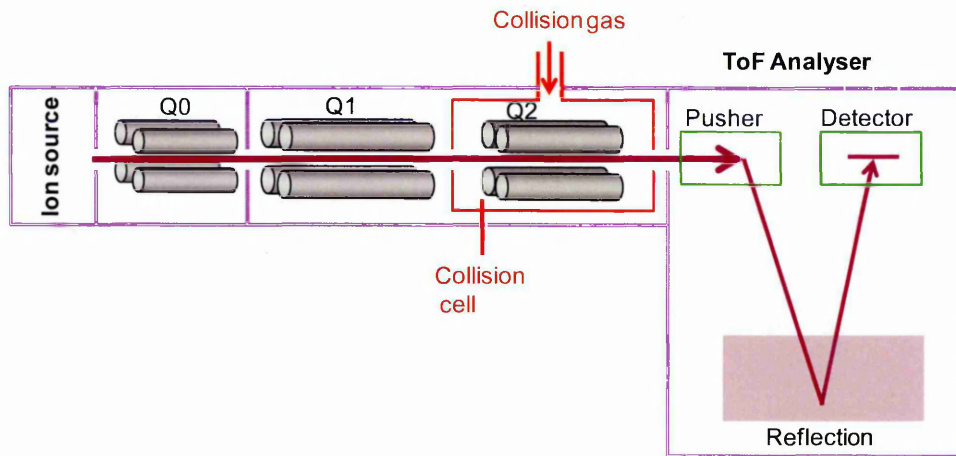
Historically metabolite identification studies were conducted on low resolution mass analysers such triple quadrupole (QqQ) and ion trap (IT) LC-MS systems. These mass spectrometers offered several useful scan functions to find metabolites and help elucidate their structure (Section 1.3.1.1 and 1.3.1.2).

More recently, the introduction of hybrid high resolution accurate mass LC-MS systems have replaced the low resolution instruments for metabolite identification work. The benefits of accurate mass data over nominal mass data are very significant for the identification and structural elucidation of metabolites and are discussed in Section 1.3.2.1. There are two main types of hybrid mass spectrometers; ToF hybrids or orbitrap hybrids, both can be coupled with either an IT or a quadrupole mass analyser. The two instruments available for this PhD thesis are the quadrupole Time of Flight (Q-ToF) and the IT orbitrap (LTQ-Orbitrap XL).

1.2.5.1 Q-ToF

Q-ToF mass spectrometers generally consist of an ion source, a quadrupole mass filter, a collision cell and an orthogonal acceleration time of flight (oaToF) mass analyser (Figure 6).

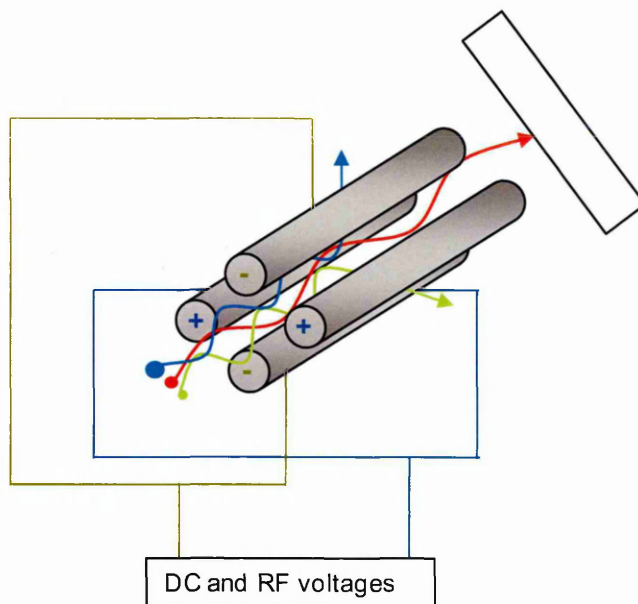
Figure 6 Schematic diagram of a Q-ToF mass spectrometer



1.2.5.1.1 Quadrupole mass filter

The quadrupole mass filter consists of two pairs of parallel metallic rods arranged so the ion beam will be focused axially between them. Each pair of rods is connected electrically and a DC voltage is applied to each pair, one at a positive potential and the other negative. Variable radio frequency ac potentials are also applied to each pair of rods which are 180° out of phase from each other. Ions enter the quadrupole and orbit around the central axis of the quadrupole, varying the DC/rf electric field can create a suitable path through the field for a single m/z . Heavier or lighter ions will not have stable trajectories causing them to spin out of the central axis ion path before reaching the detector (Figure 7). Thus ions of a selected m/z can be filtered through the quadrupole by varying the electric field. In the Q-ToF MS Q1 (quadrupole mass filter) is used to either filter selected ions into the collision cell for discrete MS^2 experiments or to operate in rf only mode allowing all ions into the collision cell for full scan ToF experiments. The collision cell can be used to generate collision induced dissociation (CID) with collision gas or allow the ions to pass without CID. The Q-ToF scan modes used for metabolite identification work are discussed in Section 1.3.2.8.

Figure 7 Schematic of quadrupole MS filter



1.2.5.1.2 OaToF Mass analyser

oaToF mass spectrometry determines the m/z of ions by measuring the time it takes for them to travel down a flight tube. In oaToF the ion beam from the collision cell is focused into the pusher parallel to the flight tube, it then applies high voltage push out pulse on a section of the beam, orthogonally accelerating a package of ions into the flight tube. Because the m/z of each ion is determined by its flight time, the flight tube needs to be under ultra high vacuum to avoid any ion collisions with residual background molecules. Any collision will alter an ions flight time and therefore the accuracy of its calculated m/z . At the opposite end of the flight tube there is a reflectron which is a stack of ring electrodes held at increasing voltages at the same polarity as the analyte ion.

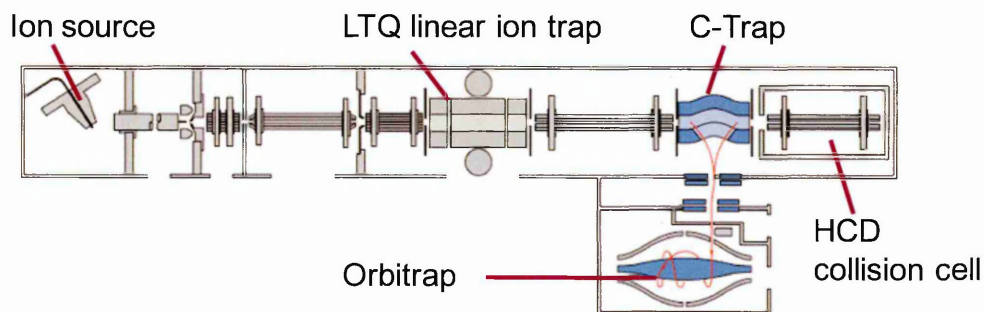
As the ions enter the reflectron they are decelerated, stopped and their kinetic energy is stored as potential energy, which is released when their direction is reversed and they are re-accelerated towards the detector. There are two distinct benefits with a reflectron in the flight tube; the length of the flight is increased (x2) and a reduction in the arrival time distribution, both improve the spectral resolution. Generally there are two detector types for ToF mass

spectrometry; analogue to digital conversion detectors that measure ion current and time to digital conversion detectors that measure individual ion counts.

1.2.5.2 Linear trap quadropole (LTQ) Orbitrap XL

The LTQ orbitrap XL is a linear IT connected to an orbitrap equipped with a higher-energy collisional dissociation (HCD) collision cell (Figure 8).

Figure 8 Basic schematic diagram of a LTQ-Orbitrap XL mass spectrometer



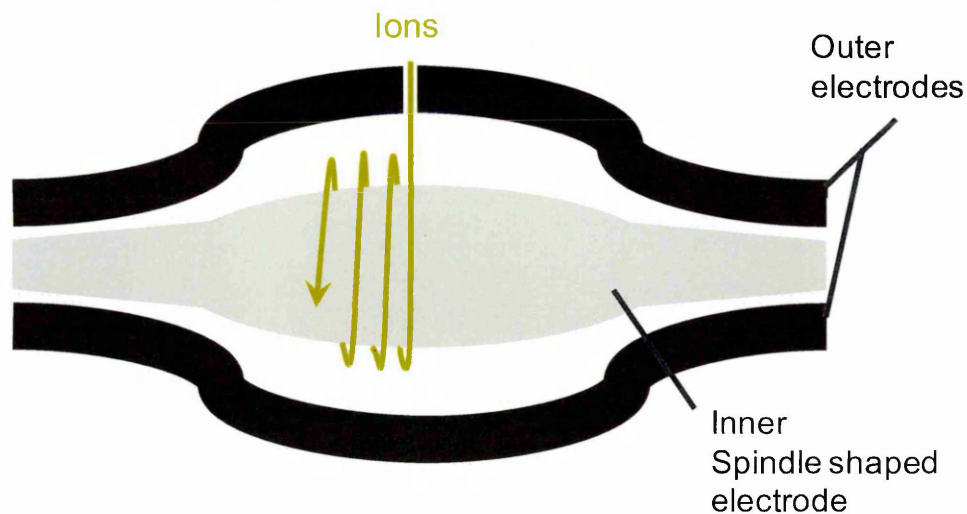
1.2.5.2.1 *Linear IT*

The linear IT consists of 4 parallel hyperbolic shaped rods (similar to a quadrupole) which are split into 3 sections and rf or DC voltages can be applied to each section. The ions are trapped radially by a two dimensional rf electric field and axially by a static DC electric field. Mass analysis is done by ejecting the ions in the radial direction through a slot in a pair of the central rods. Helium is used in the mass analyser to slow down ions, so that the rf field can more efficiently trap them. Helium also acts as a collision gas and when an AC excitation voltage is applied to the exit rods the ions are driven into the helium atoms generating CID. The IT can acquire spectra independently, send ions to the orbitrap for mass analysis, or the HCD collision cell for CID.

1.2.5.2.2 *Orbitrap mass analyser*

The Orbitrap mass analyser consists of two outer electrodes around an interior spindle shaped electrode, the electrodes are connected to independent voltage supplies. The space between the inner and outer electrodes, where the ions are analysed, is at ultra high vacuum ($<10^{-8}$ torr), Figure 9.

Figure 9 Schematic of Orbitrap mass analyser



Applying a voltage between the inner and outer electrodes creates an electric field which will bend the path of the ions towards the central spindle electrode, while the circular motion of the ions creates an opposing centrifugal force. An axial electric field pushes the ions towards the widest part of the central spindle electrode creating axial oscillations at the same time as the circular motion around the spindle. The outer electrodes measure the ion current in the time domain, which is transformed into frequency domain by Fourier transform and then converted into a mass spectrum. The orbitrap is capable of generating high resolution and excellent mass accuracy (often <1ppm), which is invaluable for metabolite identification work.

1.3 MS scan approaches for metabolite identification studies

It is important to select the most appropriate scan technique for the type of analytical work to be undertaken and the MS system employed. All metabolite identification scan types are based around similar principles, so it is important to understand the advantages and disadvantages for each of them across different instrumentation.

1.3.1 Nominal mass approaches to metabolite identification

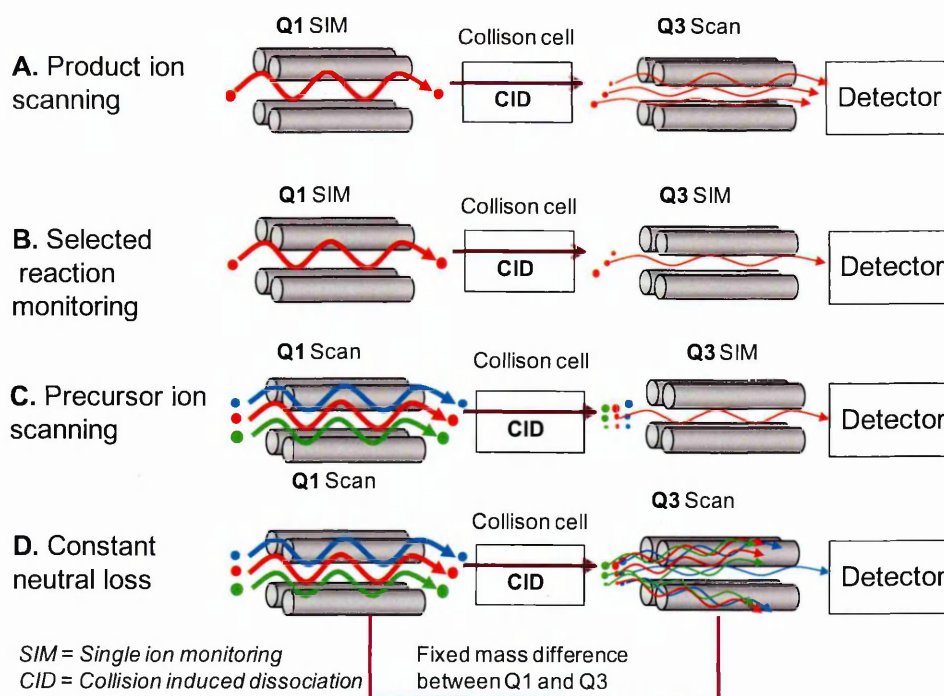
For metabolite identification studies there are many low resolution nominal mass MS scan approaches available on a range of mass spectrometry instrumentation, including: QqQ, IT and Quadrupole Iontraps. Described below

are some of the most commonly nominal mass scan modes employed during the last 20 years.

1.3.1.1 Triple Quadrupole scan modes in biotransformation studies

Historically low resolution nominal mass scans such as selected reaction monitoring (SRM), precursor ion scanning (PIS), neutral loss scanning (NLS) and product ion scanning (MS^2) were routinely acquired on triple quadrupole mass spectrometers (QqQ) for metabolite identification studies⁴³. These methods are still used today in biotransformation studies for specific applications such as GSH RM trapping assays, which can be done using PIS in negative ion for m/z 272 or NLS in positive ion of -129 Da to find any GSH conjugates (Section 1.5.1.1). These scan functions form the basic principles for all modern metabolite identification mass spectrometry methods and are therefore important for any metabolite identification scientist to understand.

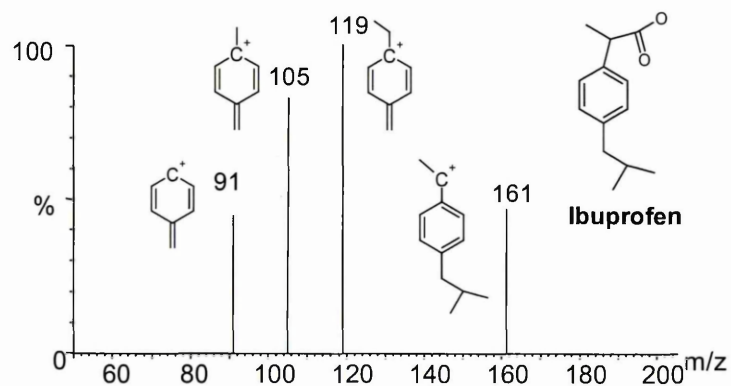
Figure 10 Diagram of the 4 scan modes on a triple quadrupole mass spectrometer: A Product ion scanning, B Selected reaction monitoring, C precursor ion scanning and D constant Neutral loss.



MS^2 is one of the most commonly employed scan types on mass spectrometers, it is used to generate structural information on an analyte for confirmation or elucidation of its structure. The MS^2 scan mode for a triple

quadrupole MS is shown in Figure 10. The m/z of the $[M+H]^+$ ion of the analyte is selected in Q1 to allow only ions with this m/z to pass, thus filtering out any other ions with different m/z values from reaching to the collision cell. Once it is in the collision cell it is broken down by collision induced dissociation (CID), also known as collision activated dissociation (CAD), and the ensuing product ions are scanned in Q3 prior to hitting the detector. The result is a product ion spectrum which will contain structural information about the analyte, see example spectrum ibuprofen (Figure 11).

Figure 11 CID Product ion scan (MS^2) for ibuprofen



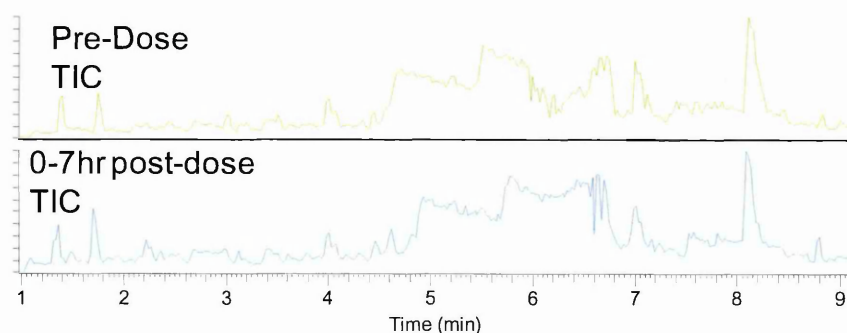
SRM, precursor ion scanning (PIS) and neutral loss scanning (NLS) are all used to identify or/and quantify metabolites/products from complex matrices, so require liquid chromatography (LC) to separate components prior to introduction to LC-MS analysis. Unlike MS^2 no full scan data or structural information is acquired and these techniques are purely used to generate a signal when the scan criteria are met.

Before conducting an SRM, PIS or NLS experiment, a MS^2 is acquired on the test compound to identify a product ion m/z for PIS/MRM and a neutral loss value for the NLS. Of these three scan modes SRM (Figure 10) is the most commonly used with QqQ. Q1 is set to filter a single ion into the collision cell which breaks up the ion by CID generating several product ions. Q3 is also set filter a single ion and will only allow a selected product ion from the selected precursor ion to hit the detector, the m/z from the selected ions can be written as: precursor>product ion (e.g.500>250) and is referred to as a mass transition.

It is possible to monitor multiple mass transitions at the same time; this technique is often called multiple reaction monitoring (MRM). SRM and MRM modes are very selective/sensitive for analytes of interest on QqQ instruments, so are predominately used in quantitative analysis⁴⁴⁻⁴⁶. Though these scan modes can be applied to metabolite identification studies to determine the presence of or to quantify expected metabolites on QqQ instruments⁴⁷, they have limited applicability in drug discovery. Metabolites are mostly unknown prior to analysis, so there would be significant risk of missing unexpected metabolites from new novel compounds.

Unlike SRM, PIS and NLS in metabolite identification studies are employed to find unknown products or metabolites related to a test compound or drug from a complex biological sample extract. These searching scans are required because it is very difficult to identify metabolites using full scan total ion chromatograms alone, due to the amount of background interference. For example Figure 12 shows the total ion chromatograms for a pre-dose and 0-7 hour post dose rat bile sample, comparing the traces it is not possible to identify a peak for the test compound or its metabolites.

Figure 12 Full scan TIC of a pre dose rat bile sample (top) and 0-7 hour post dose rat bile sample (bottom).



For metabolite identification studies the ions arising from molecular species of analyte related metabolites/products are unknown, so Q1 is set to scan a mass range and all the ions from Q1 are dissociated in the collision cell sequentially in both PIS and NLS. In PIS Q3 is set to a specific m/z (a product ion identified from test compound) so only ions with this m/z will reach the detector and generate a signal. If an ion reaches the detector its precursor ion can be identified from the Q1 scan. The NLS is identical to a precursor scan until Q3,

which is set to scan a mass range rather than a selected ion. Q3 is offset from Q1 by a specified m/z (neutral loss identified from test compound), so only product ions that have lost the specified m/z offset from the precursor ion scanned in Q1 will hit the detector and generate a signal. The result from both of these scan experiments is a series of peaks in mass chromatograms, each peak corresponding to a precursor ion that met the scan criteria. The peaks contain m/z values for the precursor ion responsible for the signal, but no structural information.

A second experiment is required to elucidate the structures using the m/z values identified from the PIS/NLS run to generate a MS^2 of the potential metabolites^{48,49}. It is possible with modern software and faster scanning instrumentation to automatically trigger further scan modes such as a MS^2 scan for structural information; this technique is data dependant acquisition (DDA) and will be discussed in Section 1.3.1.2.1. While DDA on a QqQ could reduce the need to re-run samples for product ion spectra; it can be difficult to achieve enough data points across a peak especially if using UHPLC. PIS and NLS methodology have been used successfully to detect expected and unexpected metabolites for several applications in metabolism⁵⁰⁻⁵². It is also possible to acquire PIS and NLS in a single experiment to improve detection, Kasshun *et al.*⁵³ reported a method for the detection of GSH and N-acetylcysteine (NAC) conjugates using 129 NLS and 164 PIS respectively.

1.3.1.2 IT scan modes.

Historically ITs were a good alternative to QqQ analysis for metabolite identification; however conventional ITs do not have the ability to acquire PIS or NLS. ITs acquire full scan data faster and with more sensitivity than QqQ instruments and have the ability to carry out MS^n experiments. The MS^n capability of an IT enables the acquisition of CID data on an ion, its resulting product ions and their product ions and so on, thus ITs can hypothetically generate infinite sequential product ion data.

This data can be very effective in generating detailed dissociation pathways aiding the structural elucidation of unknowns. Kolliker *et al.*⁵⁴ reported the use of MS^n (MS^3 and MS^4) to facilitate the elucidation of 2,4-dinitrophenylhydrazine

derivatives of carbonyl compounds. Sequential product ion spectra can be a powerful tool to help elucidate structures of unknown metabolites and determine the sites of biotransformation (Chapter 4). However, there is a major drawback with conventional ITs which is the $\frac{1}{3}$ low mass cut off where any m/z below $\frac{1}{3}$ of the precursor ion selected for MS^n will not be detected. This can be significant disadvantage for metabolite identification studies, where the compound of interest generates low m/z product ions which are key to identifying the site of metabolism. Product ion data can be acquired by selecting a single or multiple m/z for MS^2 experiments across an analytical run or by DDA.

1.3.1.2.1 DDA

The DDA mode enables experiments to be automatically created in real-time based on results from the previous scan. For metabolite identification studies the DDA experiment is used to generate MS^2 data on expected or unexpected metabolites based on the ions detected in a survey scan. For expected metabolites this is performed in a targeted manner using a predefined list of m/z values, which are selected for MS^2 if detected in the survey scan. For unexpected metabolites, non-targeted m/z selection criteria are employed such as most intense ion, least intense ion, highest charge state, highest m/z etc. It is also possible to use a targeted list in combination with non-targeted selection criteria for both expected and unexpected metabolites. For example if no ions are detected from the targeted m/z list, then the most intense ion from the previous survey scan will be selected for MS^2 . DDA is an efficient method for acquiring MS^2 data on expected metabolites and more importantly unexpected metabolites, however scan speed can limit the number of MS^2 experiments acquired in a run, so potentially metabolites could be missed when analysing complex biological samples.

1.3.1.3 Quadrupole linear ITs

More modern IT mass spectrometers such as hybrid quadrupole linear ITs do not suffer from the $\frac{1}{3}$ cut off and can acquire all of the QqQ scan functions with any of the IT scan functions. Hopfgartner *et al.*⁵⁵ demonstrated rapid screening and characterisation of drug metabolites using a quadrupole linear IT, which was set to acquire PIS, NLS, targeted product ion and information dependant

acquisition (another term for DDA) in a single run. Another advantage of this hybrid instrumentation is the ability to generate quantitative MRM data and qualitative MSⁿ data. Xia *et al.*⁵⁶ described the use of a quadrupole linear IT for the identification of metabolites of Gemfibrozil in HLM and the quantification of propranolol in rat plasma bioanalysis.

1.3.2 High resolution accurate mass scan approaches

There are two types of high resolution accurate mass analysers used for metabolite identification studies; ToF and Orbitrap. However, there are various hybrid combinations of these such as Q-ToF, IT time of flight, LTQ-orbitrap Q-exactive (quadrupole orbitrap) and Fusion (quadrupole IT orbitrap). The most significant advantage of these instruments is the ability to acquire full scan accurate mass data, which enables the use of several post acquisition data processing techniques.

1.3.2.1 Accurate Mass

Accurate mass data significantly improves quality and confidence of correct structural assignments in metabolite identification studies through the use of several data processing/stripping techniques that include elemental composition, mass defect filtering (MDF), accurate mass chromatograms with narrow mass window and accurate mass product ion spectra. Accurate mass is often required to determine the elemental change from a metabolite compared to the parent compound: this is impossible with nominal mass data. Mass accuracy is often measured in parts per million (ppm) which is the relative error between the theoretical and measured accurate mass:

$$\text{Mass_accuracy} = \frac{m/z_{\text{measured}} - m/z_{\text{theoretical}}}{m/z_{\text{theoretical}}} \times 10^6$$

Equation 3

Mass accuracy is measured in ppm to normalise the error across a mass range, i.e. 5 mDa mass error at *m/z* 100 is 50 ppm, 10x greater than 5 mDa error at *m/z* 1000 (5 ppm).

1.3.2.2 Elemental composition

Each element has a specific accurate mass which is the sum of its protons (1.00728 Da), neutrons (1.00867 Da) and electrons (0.00055 Da) minus its mass defect. The mass defect for an element is the loss in mass required to create the energy to bind protons and neutrons together in the nucleus ($E=MC^2$), thus mass defect is the difference between the measured accurate mass of an atom and the sum of its individual particles. For example the mass of a nitrogen atom should be $(7 \times 1.00728) + (7 \times 1.00867) + (7 \times 0.00055) = 14.11158$, but it is in fact 14.00307 Da due to the mass defect. Every isotope has a unique mass defect, so it is possible to determine the elements present in a molecule from its measured mono isotopic accurate mass using the theoretical exact mass of the most abundant isotopes for each element (Table 1). In Mass spectrometry the mass defect is often only referred to as the difference between the integer mass and the exact mass of a molecule.

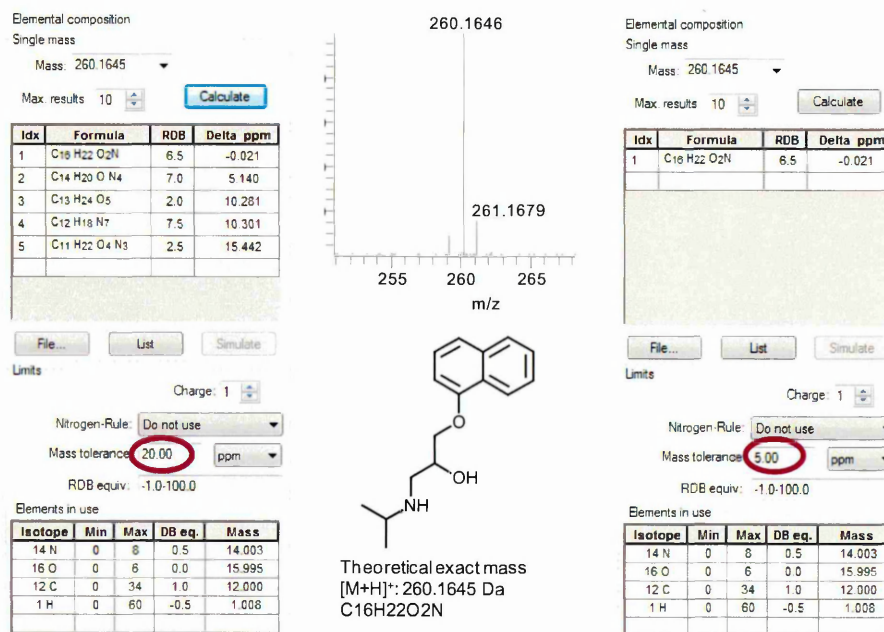
Table 1 Exact mass of the most abundant isotopes for common elements found in small organic drug-like molecules.

Isotope	Exact mass (Da)
^1H	1.0078
^{12}C	12.0000
^{14}N	14.0031
^{16}O	15.9949
^{19}F	18.9979
^{32}S	31.9721
^{35}Cl	34.9683
^{79}Br	78.9178

Most MS software contains an elemental composition programme, which can calculate possible molecular formulae from the measured accurate mass of

unknowns^{55,57,58}. Modern accurate mass instrumentation can reliably measure m/z to <5 ppm of the theoretical value, which significantly reduces the number of possible molecular formulae. For example, accurate mass data for Propranolol was generated on an LTQ orbitrap and the elemental composition calculated at 5 ppm and 20 ppm, there was only 1 molecular formula at 5 ppm where as at 20 ppm there were five possible formulae (Figure 13). Biotransformation reactions generally only add hydrogen, carbon, nitrogen oxygen or sulphur atoms, so it's possible to restrict the number of potential elements, which also reduces the number of potential molecular formulae.

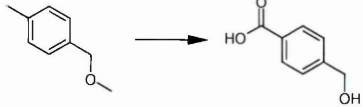
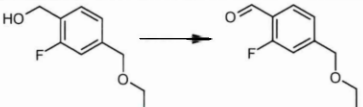
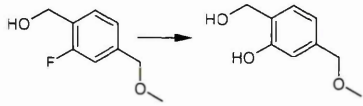
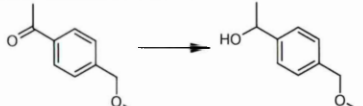
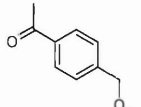
Figure 13 Accurate mass spectrum and elemental composition results for Propranolol at 5 ppm and 20 ppm.



Without accurate mass data there is significant risk of generating incorrect or ambiguous structures for metabolites, as it is possible that a nominal mass change can represent more than one structure. For example, it may appear obvious that addition of 16 Da is simply addition of oxygen, but it could also be oxidation of a methyl to the corresponding acid (+2xO -H₂) +30 Da and demethylation (-CH₂) -14 Da equalling an overall addition of 16 Da. The nominal mass addition for both is +16 Da, but the accurate mass addition for +O is 15.9949, where as the oxidation to an acid and demethylation metabolite would be 15.9585. There are several examples of common biotransformations

where the nominal mass changes can be ambiguous/misinterpreted without accurate mass data, see Table 2 describing several examples.

Table 2 Biotransformations reactions, where the metabolite formed has the same nominal mass but a different structure and accurate mass.

Nominal mass change (Da)	Elemental change	Mass change (Da)	Biotransformation (fictional molecules) includes theoretical mono isotopic accurate mass and elemental composition
+16 Da	+O	+16	 154.07 $C_9H_{11}FO$ → 170.0738 $C_9H_{11}FO_2$
	+O ₂ -H ₂ -CH ₂	+32 -2 -14	 154.0788 $C_9H_{11}FO$ → 170.0374 $C_8H_7FO_3$
-2 Da	-H ₂	-2	 184.0894 $C_{10}H_{13}FO_2$ → 182.0738 $C_{10}H_{11}FO_2$
	-HF +H ₂ O	-20 +18	 184.0894 $C_{10}H_{13}FO_2$ → 182.0937 $C_{10}H_{14}O_3$
+2 Da	+H ₂	+2	 164.0832 $C_{10}H_{12}O_2$ → 166.0988 $C_{10}H_{14}O_2$
	+O -CH ₂	+16 -14	 164.0832 $C_{10}H_{12}O_2$ → 166.0624 $C_9H_{10}O_3$
No nominal mass change	Parent compound	+/- 0 Da	 136.0883 $C_9H_{12}O$
	+O -H ₂ -CH ₂	+16 -2 -14	 136.0883 $C_9H_{12}O$ → 136.0519 $C_8H_8O_2$

It is also possible to incorrectly assign product ion spectra when attempting to elucidate metabolite structures by nominal mass, for example loss of $-\text{CO}$ and C_2H_4 are both -28 Da, however by accurate mass they are -27.9944 Da and -28.0308 respectively, so can easily be distinguished.

1.3.2.3 Mass Defect Filtering

Biological samples contain a large variety of endogenous components that complicate mass spectrometry data, so searching for unexpected drug related metabolites in a complex biological matrix such as: urine, plasma, bile or faeces by LC-MS is very difficult. Drug related metabolites often have similar mass defects to the parent drug as most biotransformation reactions do not drastically change the molecular formula. Therefore, the mass defect of an analyte could be used to remove endogenous component mass spectrum peaks that have significantly different molecular formula to the analyte/metabolites of interest. This is the principle behind MDF, which is essentially a post acquisition technique to help clean spectra/find parent compound and drug related metabolites.

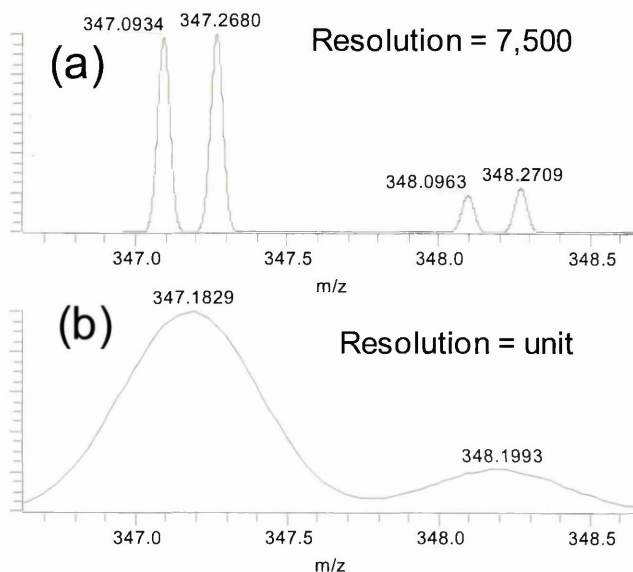
Zhang *et al.*⁵⁹ developed MDF software to process accurate mass data from complex biological matrices for metabolism studies. They demonstrated significant simplification of mass spectra data for four compounds in animal bile, plasma and human faeces using the MDF software. The method assumes that the majority of biotransformation reactions fall within a 50 mDa window of the analyte's mass defect with the exception of GSH (+68 mDa), hydrolysis metabolites or amino acid conjugates.

Since this work there have been many publications on MDF metabolism applications and improving the methodology⁶⁰⁻⁶⁶. MDF is now included in most vendors MS software as a routine application. Whilst this technique has proven to significantly improve mass spectral data, unexpected/unusual biotransformations may fall outside of the selected mass defect window and will therefore be removed from the data.

1.3.2.4 Resolution

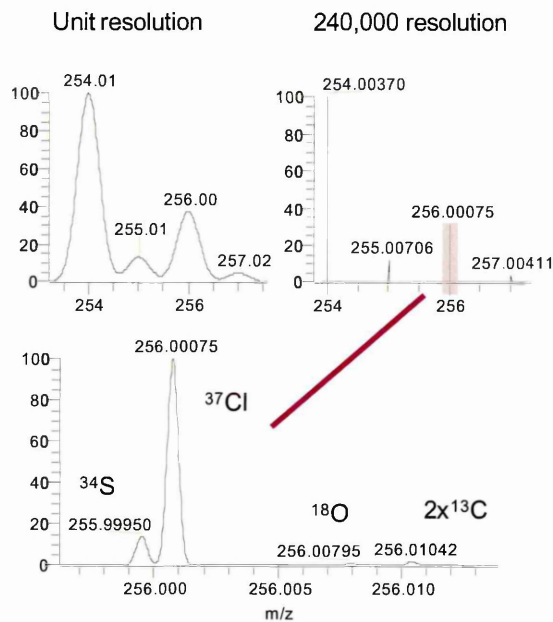
High resolution MS scanning is important for accurate mass measurements when acquiring data on biological extracts where co-elution of components with the same nominal mass or overlapping isotope peaks with the analyte could contaminate accurate mass measurements. Acquiring high resolution data reduces the potential for peak contamination from components with the same nominal mass (Figure 14).

Figure 14 Accurate mass simulated spectra for $C_{19}H_{32}ON_5$ (m/z 347.0934) and $C_{16}H_{16}N_3O_4S$ (m/z 347.2680) at 7500 peak resolution (a) and unit resolution (b)



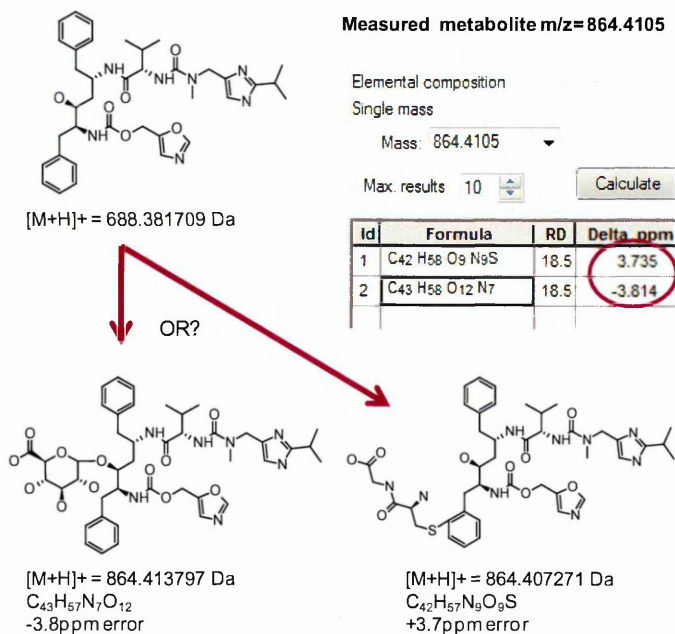
It is possible to separate the lower abundant isotopes using high resolution scanning, for example to determine whether sulphur is present in a molecule. sulphur has a lower abundant isotope ^{34}S at ~4.5%, which makes it very difficult to identify its isotope pattern in a spectrum due to the contamination with the $2 \times ^{13}C$ isotope peak or potentially other isotopes such as chlorine (Cl). Fenclozic acid contains a sulphur and a Cl so is a good example to demonstrate the power of separating lower abundant isotopes. The mass spectra of Fenclozic acid has been acquired at unit (low resolution instruments) and 240,000 resolution (routinely achievable on modern orbitraps) (Figure 15). At unit resolution it is impossible to determine if a sulphur is present, but at 240,000 resolution the ^{34}S , ^{18}O , ^{37}Cl and $2 \times ^{13}C$ are resolved and easily identified.

Figure 15 Fenclozic acid profile mass spectra at unit and 240,000 resolution.



It is possible that the measured accurate mass of the $[\text{M}+\text{H}]^+ / [\text{M}-\text{H}]^-$ for a glucuronide metabolite could be within 5 ppm of the $[\text{M}+\text{H}]^+ / [\text{M}-\text{H}]^-$ for a cysteineglycine conjugate (Figure 16) making it difficult to identify which was formed. A high resolution MS scan can be used to determine the presence of a sulphur and therefore differentiate between a potential Cysteineglycine conjugate or a glucuronide metabolite, even though both have the same nominal mass and very similar mass defects.

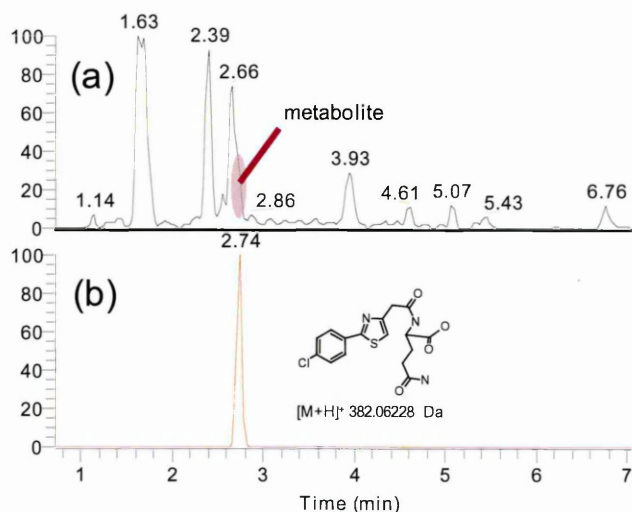
Figure 16 Elemental composition of a metabolite (m/z 864.4105) that is a glucuronide (bottom left) or cysteineglycine conjugate (bottom right).



1.3.2.5 Mass chromatograms with a narrow mass window

Biological samples contain endogenous components that can obscure metabolites in nominal mass selected ion chromatograms as interfering peaks (Figure 17a). With accurate mass data it is possible to display metabolite peaks using a theoretical exact mass and a narrow mass window of 10 ppm (± 5 ppm of the theoretical exact mass), which greatly reduces background and simplifies the data (Figure 17b).

Figure 17 Selected ion mass chromatograms of Fenclozic acid glutamyl metabolite in rat bile. (a) 1 Da mass window of the theoretical nominal $[M+H]^+$ 382 Da, (b) 10 ppm mass window of the theoretical exact $[M+H]^+$ 382.06228 Da.



1.3.2.6 Accurate mass MS^2 spectra.

With accurate mass product ion spectra it is possible to generate an elemental composition for each product quickly which greatly simplifies the structural interpretation. Product ion spectra are generated by selecting a precursor ion then subjecting it to CID which generate a series of breakdown product ions that are measured. If the molecular formula of the precursor ion is known (determined by accurate mass), then it is possible to restrict the number and type of elements available in the elemental composition software for each product ion to the precursor molecular formula. The result of this is a significant reduction in possible formula hits for the ions detected in the product ion spectra.

1.3.2.7 ToF MS scan modes

The scan modes on a ToF MS are limited and these instruments only acquire full scan data, though it is possible to generate some product ion data using in-source dissociation. Acquiring full scan with in-source dissociation can generate some useful product ion information^{67,68}, but the product ion spectra are often complicated by background ions. ToF MS has been used to support early *in vitro* turnover assays for quantification and some limited metabolite identification^{69,70}. However, ToF MS has limited capability for metabolite

identification studies as it cannot generate discrete product ion spectra. Hybrid ToF instruments such as the QToF mass spectrometers can acquire discrete product ion spectra, so are more suited to metabolite identification studies.

1.3.2.8 Q-ToF MS scan modes

Q-ToF instruments offer several scan options for metabolite identification studies such as accurate mass full scan, MS^2 , Mass spectrometry collision energy MS^E , sequential window acquisition of all theoretical fragment ion spectra (SWATH) and DDA MS^2 (also known as IDA). The benefit of accurate mass full scan and accurate mass MS^2 have been discussed previously, whilst MS^E and SWATH are scans that can only be acquired on hybrid accurate mass instruments. DDA experiments on the Q-ToF, consist of MS^2 scans triggered on predefined precursor list or via information acquired in a ToF survey scan. This technique has not been used extensively for metabolite identification studies by Q-ToF MS due to the potential to miss precursor ions⁷¹.

1.3.2.8.1 MS^E

To acquire full scan accurate mass data on a Q-ToF the quadrupole mass analyser is set to wide band mode (RF-only), allowing all ions to be transmitted into the collision cell, and subsequently the ToF for analysis. In MS^E mode two full scan data are acquired, the first with no collision energy (low energy scan) applied to the collision cell and the second with collision energy applied to the collision cell (high energy scan), the result is an all ion precursor survey scan and an all ion product ion scan. Bateman *et al.*⁷² first reported this technique to study protein phosphorylation, however since then it has been utilised across numerous applications.

This technique is very powerful when used in metabolite identification studies especially when searching for unexpected metabolites, as no compound or metabolite information is required prior to analysis⁶⁶. Since all precursors and their product ions are acquired in MS^E , it is possible to perform post acquisition data mining such as pseudo neutral loss and common product ion searching as well as MDF. These post acquisition techniques are similar to PIS/NLS on a QqQ and the fundamental principle is the same. Common product ion

searching is similar to PIS, product ions from the test compound are identified and used to find related products/metabolites. Unlike PIS product ions are found by searching the high energy scan data using a selected ion chromatogram at the theoretical exact m/z for each product ion and applying a narrow mass window. Each peak in the chromatogram is potentially a product ion from a test compound related metabolite; however the precursor ion is not automatically determined. The precursor ion can be identified in the low energy scan at the retention time of the product ion peak detected in the high energy scan.

It is also possible to generate pseudo neutral loss data using the all ion product scan, by looking for test compound accurate mass losses in the high energy scan. This is similar to common product ion searching where an accurate mass neutral loss chromatogram can be generated, highlighting where potential test compound related metabolites elute.

Another advantage of the MS^E approach, is product ion information on all components injected, so it may be possible to interpret numerous metabolites without the need for further discrete MS^2 experiments. However, endogenous co-eluting components can complicate the product ion spectra and if two metabolites co-elute then discrete MS^2 experiments would be required.

1.3.2.8.2 SWATH

Recently a new scan mode on the Q-ToF has been introduced; SWATH, also known as global precursor ion scan mode. In this scan mode the quadrupole is set to transmit a small mass range (typically 20 Da) sequentially to the collision cell generating product ions which are analysed in the ToF. This scan mode is more selective than MS^E , as fewer precursor ions pass to the collision cell for each mass range, yet it maintains similar precursor coverage owing to the acquisition of sequential mass windows across the whole m/z range⁷¹. Hopfgartner *et al.*⁷³ and Zhu *et al.*⁷¹ reported the application of SWATH for metabolite identification studies, demonstrating cleaner product ion spectra compared to those acquired by MS^E . Even though a 20 mDa mass range is used for SWATH, it is still possible to get contamination from endogenous material or co-eluting phase I metabolites, which generally have small additions/losses of >20 Da.

1.3.2.9 Orbitrap scan modes

Orbitrap mass analysers are all hybrid instruments and are either connected to an IT (LTQ-Orbitrap), a Quadrupole (Q-Exactive) or both (Fusion orbitrap).

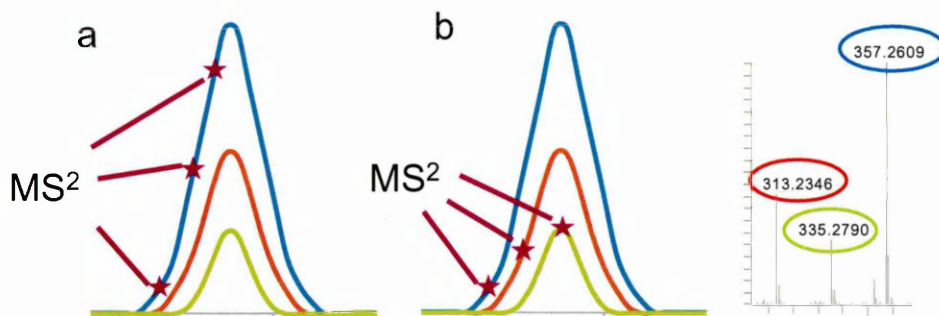
1.3.2.9.1 *LTQ-Orbitrap XL*

The LTQ-orbitrap XL mass spectrometer consists of an IT, a higher collisional dissociation (HCD) cell and the high resolution accurate mass capability of the orbitrap mass analyser. The IT is capable of acquiring data independently, creating additional scan functionality and some potential for parallel analysis. The LTQ-orbitrap offers several scan modes for metabolite such as accurate mass full scan, MS^n , accurate mass MS^n , accurate mass HCD MS^2 , DDA, DDA with accurate mass, all ion fragmentation (AIF) or combinations of these. MS^n , DDA and full scan accurate mass data have been discussed previously, however the LTQ-orbitrap offers some additional functionality for the DDA scans.

1.3.2.9.1.1 *DDA dynamic exclusion*

A problem with DDA is the potential to miss ions in a complex mixture, as there is a limit to the number of MS^2 scans that can be acquired in a run. To increase the number of precursor ions sent for MS^2 dynamic exclusion can be activated. Dynamic exclusion works by ignoring the precursor ion that has just been sent for MS^2 for a period of time, (normally the width of an LC-MS peak) then the next most intense peak can be selected for MS^2 . For example if three components co-elute only the most intense ion across the peak is selected by DDA, however with dynamic exclusion all three would be selected (Figure 18).

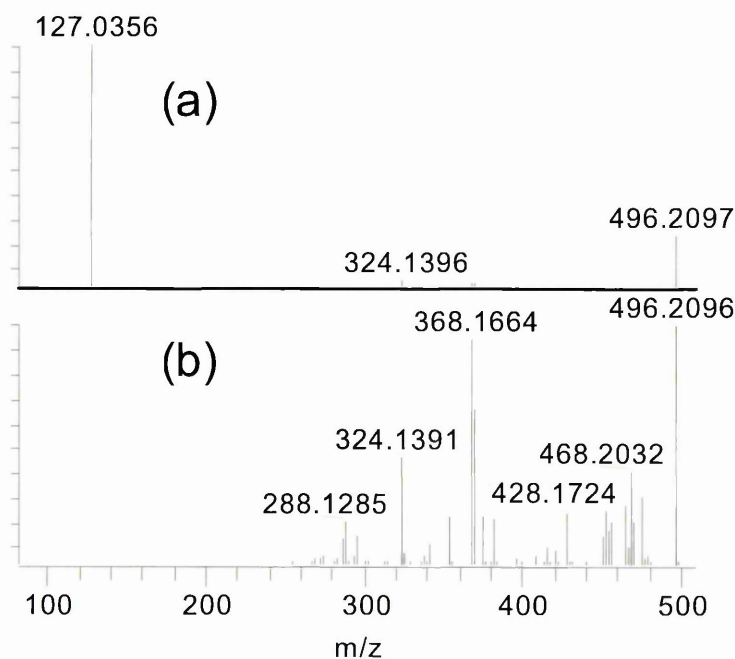
Figure 18 Mass chromatograms of 3 co-eluting components highlighting which would be selected by DDA for MS² (a) Without dynamic exclusion (b) with dynamic exclusion.



1.3.2.9.1.2 LTQ-Orbitrap, IT and HCD Product ion spectra

It is possible to generate product ion spectra through HCD (similar to a collision cell) or through IT CID (limited by the $\frac{1}{3}$ cut off). IT CID is softer than HCD CID and more likely to generate high m/z product ions, whereas HCD is harsher and more likely to generate lower m/z product ions. HCD product ion data is not restricted by the $\frac{1}{3}$ cut off (Figure 19).

Figure 19 MS² scan of m/z 496.2097 (a) HCD CID and (b) IT CID



Bushee *et al.*⁷⁴ reported a DDA method to generate HCD and IT MS² data for metabolite identification studies on an LTQ orbitrap. This method significantly improved spectral information for structural elucidation over DDA with IT MSⁿ alone. It is also possible to apply a product ion filter and a neutral loss filter to all of the MS² data from a DDA experiment⁷⁵. Product ion and neutral loss filters work on the same principles as PIS/NLS, MS² information on the test compound is used to find related metabolites. However complex biological matrices, which are likely to have a large number of intense background ions by MS, can interfere with DDA experiments. DDA works by sending the most intense ion for an MS² experiment, so if there are many intense background ions, it is likely that some metabolites will not be selected for an MS² experiment.

Cho *et al.*⁷⁶ reported a new method for metabolite identification on a LTQ-Orbitrap velos that acquired AIF with DDA, HCD MS² and IT MSⁿ. AIF on the orbitrap generates data similar to the MS^E method on a Q-ToF, however it is not possible to generate the data in exactly the same way as MS^E. In the LTQ-Orbitrap, it is done in an MS² by selecting an *m/z* in the middle of the *m/z* range of interest and applying an isolation width the size of the required mass range. For example if the mass range to be analysed is *m/z* 200 to *m/z* 800 then the mass selected would be *m/z* 500 with an isolation width of 600 Da. This is the most comprehensive method for metabolite identification discussed so far for high resolution accurate mass instruments.

1.3.2.9.2 Q-Exactive

The Q-Exactive mass spectrometer can acquire all the same scan modes as a Q-ToF including MS^E and SWATH which are referred to as AIF and vDIA (variable data independent acquisitions). The Q-Exactive has one major advantage over the Q-ToF, its ability to polarity switch and acquire both positive and negative ion data in a single analysis. This is very useful for metabolite identification studies where the parent may be basic and fly well in positive ion mode, but some metabolites could be acidic and only give a good response in negative ion mode.

1.3.2.9.3 *Fusion Mass spectrometer*

This is a relatively new advance in mass spectrometry and is the world's first tribrid mass spectrometer, containing three mass analysers (quadrupole/IT/Orbitrap). This instrument is able to acquire the all scan modes discussed previously and additional ones to unique to tribrid instruments.

1.4 Non-MS based analytical techniques for metabolite identification

There are various MS scanning techniques that have proven to be very efficient when applied to metabolite searching as outlined in Section 1.3, however these rely on metabolites retaining similar mass spectrometry characteristics as the parent compound such as ionisation polarity, product ion formation, isotope pattern, or ionisation efficiency. Even simple biotransformation reactions of test compounds can dramatically change the MS ionisation, isotope pattern or dissociation properties potentially leading to important metabolites being missed. Therefore there are several complimentary analytical techniques for the detection, quantification and identification of metabolites including NMR, UV spectroscopy and radiochemical detection.

1.4.1 ¹H NMR

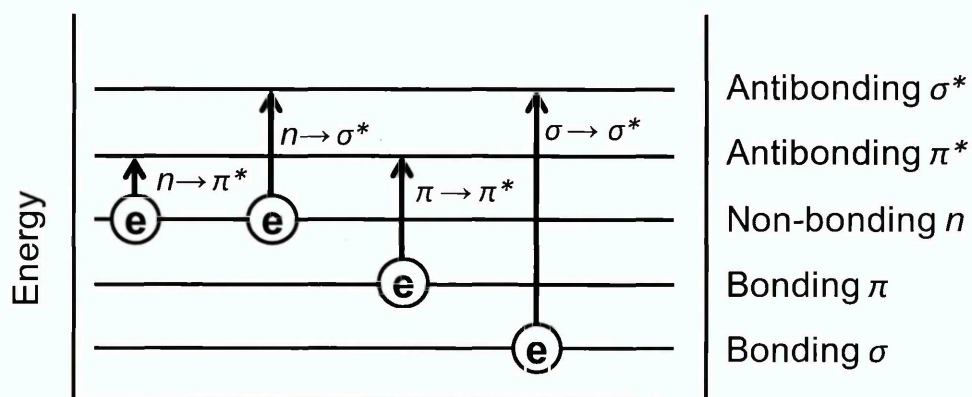
Atomic nuclei with an even number of neutrons and protons have no spin and nuclei with odd numbers of both neutrons and protons have integer spins. When the number of protons and neutrons in a nucleus add up to an odd number they have half-integer spin such as ¹H or ¹³C and ¹⁹F. Applying a magnetic field to these nuclei will cause the nuclear spin states to be parallel or anti-parallel to the magnetic field. The parallel spin state has less energy than the anti-parallel state and the lower energy spin state has slightly more nuclei. Introducing a rf energy pulse to the nuclei at its Larmor frequency will cause some of the low energy spin nuclei to absorb energy and flip spin states. When these nuclei revert back to the lower spin state they will release energy at the same frequency, which can be measured to generate a proton NMR spectrum. Protons in an organic molecule in different environments (non-equivalent

protons) will experience different magnetic fields and therefore give separate signals. Information such as the chemical shift, signal splitting and relative intensity of the signal can be used to elucidate structures of organic molecules. For metabolite identification work NMR has proven to be very useful to elucidate metabolite structures⁷⁷⁻⁷⁹ and in some applications quantify metabolites^{30,80,81}. The main difficulties with NMR are its low sensitivity, requiring μg quantities of a metabolite to generate useful spectra and its lack of selectivity, as metabolites generally require isolation from the matrix prior to analysis. Isolation of a metabolite from a matrix is fairly simple by LC and can be collected by time slicing or by mass direction (LC-MS).

1.4.2 Ultraviolet Spectroscopy.

Ultraviolet light (UV) absorption spectroscopy is an analytical technique which is applied to the quantitative and qualitative determination of molecular species. The absorption of UV light in organic molecules usually results from the excitation of bonding electrons or unbound outer electrons in atoms such as oxygen, halogens, sulphur or nitrogen. All organic molecules are capable of absorbing UV light, because they contain valence electrons that can be excited and transitioned to higher levels. There are 4 types of electron transitions (Figure 20) that involve σ bond electrons, π bond electrons and nonbonding electrons (n) to the excited antibonding σ^* and π^* orbitals.

Figure 20 Electron transitions of σ , π and n electrons



Relative to the other transitions the energy required to induce σ to σ^* transitions is large, so single bond electrons will absorb in the 'vacuum ultraviolet region'

(<185 nm), where components from the atmosphere strongly absorb. Therefore these absorbances are not observed in UV absorbance spectra, which typically range from 200-400 nm. The n to σ^* transition require less energy and gives absorbances in the range 150-200 nm, but most are below 200 nm so are outside the UV spectral region 200-400 nm. Energies for the n to π and π to π^* electron transitions are lower and within the spectral region, so most organic molecule applications of UV absorbance spectroscopy are based on these transitions. Both of these transitions require the presence of π orbitals, so the analyte molecule must contain an unsaturated functional group. For organic molecules the term chromophore applies to these absorbing unsaturated functional groups. Multiple chromophores in a single molecule are additive provided they are separated from each other by more than one single bond. π electrons are further delocalised through conjugation lowering the energy level of the π orbitals giving it less antibonding character, so the absorption maxima (λ_{max}) are shifted to higher wavelengths. Drug like structures often contain conjugated ring systems and multiple chromophores, so are likely to absorb UV at higher wave lengths.

1.4.2.1 UV in metabolite identification

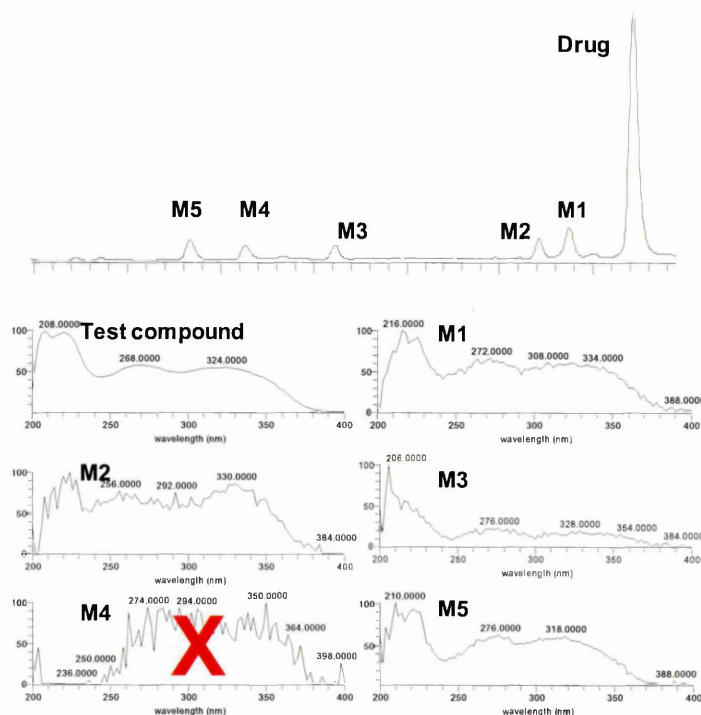
UV absorption spectroscopy is often coupled to LC-MS systems for metabolite identification via a photodiode array detector (PDA) that sits between the end of the HPLC column and the mass spectrometer (LC-UV-MS). UV detection is a non-destructive technique and can be acquired without impacting mass spectral data or analysis time so there are no disadvantages acquiring UV scan data prior to sample introduction into the mass spectrometer. For metabolite identification studies UV scan data offers two distinct advantages; semi-quantification and finding test compound related metabolites.

1.4.2.2 UV metabolite semi-quantification

UV is a quantitative technique⁸²⁻⁸⁴ and like LC-MS/MS relies on analytical standards to determine concentrations accurately, however it does not suffer from ion suppression or variable ionisation. Biotransformation reactions rarely destroy the conjugation of drug molecules, so the UV absorbance of most metabolites will be similar to the parent compound. It is therefore possible to

semi-quantify metabolites and parent compound without analytical standards more accurately than by MS. However, it is important to check the UV absorbance spectra for each metabolite to ensure there that there is no significant difference from the parent molecule (Figure 21).

Figure 21 Extracted UV chromatogram (330-350nm) of a test compound and its metabolites in human plasma (top) and extracted UV absorbances for metabolites and drug (bottom).



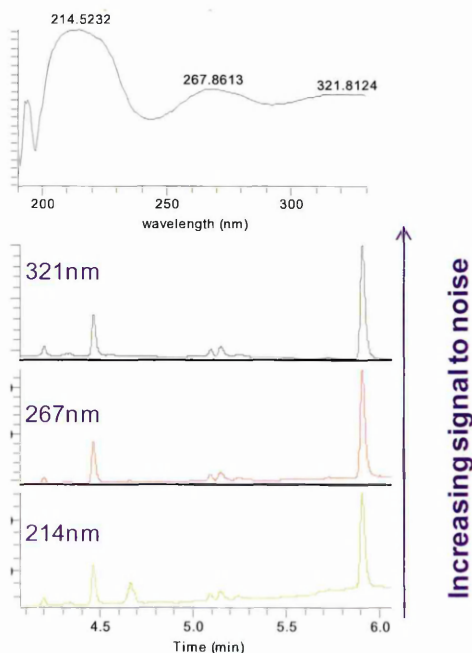
X = Cannot quantify (peak contamination or change in UV absorbance)

If the absorbance spectra are significantly different from the parent drug then it is not possible to quantify the metabolite. Another problem with UV quantification is the contamination of metabolite UV peaks with endogenous components in complex biological matrices that have an overlapping UV absorbance. A control sample or predose sample can identify the potential for UV peak contamination. However the application of UV quantification is generally only applied to relatively clean UV matrices such as plasma or *in vitro* samples.

Improved signal to noise, sensitivity and cleaner chromatograms are achieved for compounds that have greater conjugation due to the shift in λ_{max} to higher wavelengths. Quantification at higher wavelengths (>300 nm) is more selective

due to fewer endogenous biological components generating overlapping absorbances. Therefore when compounds contain multiple chromophores it is better to use the highest wavelength absorbance rather than the most intense absorbance (Figure 22).

Figure 22 UV absorbance of a test compound (top) and extracted UV chromatograms of test compound and its metabolites in a rat hepatocyte extract (bottom).



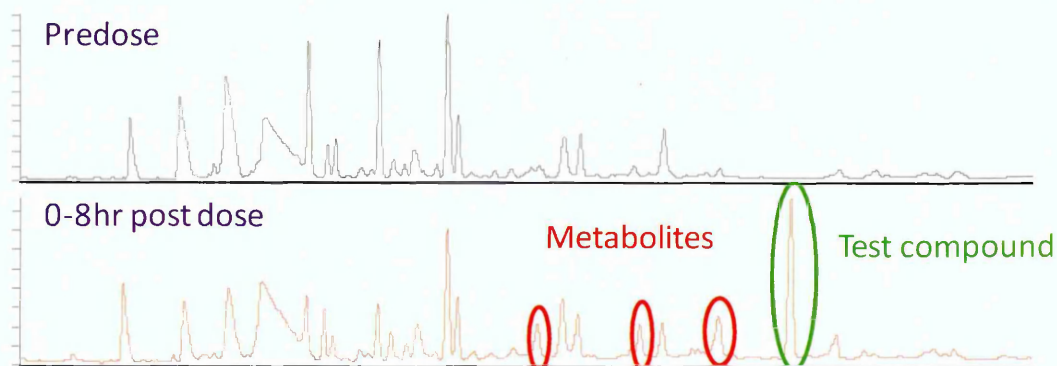
UV semi-quantification of metabolites is more suited to discovery metabolite identification studies where turnaround of data needs to be quick and design teams are generally only interested in major metabolic liabilities. Whilst UV is a good generic technique for the semi-quantification of metabolites, not all compounds give a strong UV absorbance, so sensitivity can be an issue for certain compound types.

1.4.2.3 Finding metabolites by UV

Metabolites often retain similar UV absorbance spectra to the parent compound, however when the UV chromophore is altered by metabolic modification the metabolite could be missed. Drug like compounds often contain multiple chromophores and therefore can generate more than one wavelength absorbance. If one chromophore was altered through metabolism it may still be possible to find metabolites using a different absorbance wavelength (Figure

22). UV is not as selective as mass spectrometry, so there is potential for endogenous components in biological extracts to have overlapping UV absorbances giving rise to background peaks that complicate chromatograms. If a compound has a good chromophore and absorbs at a high wavelength, it is possible to generate a relatively clean selected UV wavelength absorbance chromatogram. This is especially true for plasma or *in vitro* extract samples which are fairly clean matrices, so generally do not suffer from significant contaminating peaks (Figure 22). In more complicated matrices such as bile, urine or faeces there are considerably more endogenous components that can interfere with selected wavelength chromatograms, even at high UV absorbances. In this situation it is possible to improve the detection of major metabolites using a predose as a control for a chromatogram comparison (Figure 23).

Figure 23 Predose rat bile UV extracted chromatogram (280-290nm) (top) Test compound dosed 0-8 hour rat bile UV extracted chromatogram (bottom).



1.4.3 Radio chemical detection

Radiolabelled metabolite identification studies are the gold standard for the detection and quantification of drug metabolites⁸⁵. Accurate quantification of metabolites by MS and UV require analytical standards as the response can change with metabolic modifications of the chemical structure (Section 1.4.2 and 1.2.4). Whereas measurement of radioactivity is independent of chemical structure (provided the analyte contains a radioactive isotope), so no analytical standards are required. The most common radioisotopes used in drug metabolism studies are ¹⁴C or ³H⁸⁶, which can be incorporated into a drug's

chemical structure, producing a radioisotope analogue that is chemically identical to the original material. ^3H is often used in early drug development as it is quicker, cheaper and easier to incorporate into a structure than ^{14}C , and can be done by direct iridium catalysed hydrogen exchange of drug or modification of a precursor to include ^3H ²⁸. The problem with a ^3H label is the potential for it to chemically or metabolically exchange resulting in unlabelled products⁸⁷ or the ^3H isotope label altering the metabolic profile or metabolite formation rate^{28,86}. Therefore ^{14}C is superior to ^3H for drug metabolism studies, but it is more costly, so is generally only employed in later drug development where more accurate data is required. All of the radioisotope work undertaken in this PhD will be with ^{14}C labelled Fenclozic acid.

The total radioactivity in a sample can be measured by liquid scintillation counting (LSC), solid scintillation counting (SSC) or accelerator mass spectrometry. Accelerator mass spectrometry is a very expensive technique which involves intensive sample preparation and is beyond the scope of this PhD thesis. The principles of scintillation counting are the same regardless of the nuclei used or whether the technique is SSC or LSC, which both involve mixing the radioactive material with a scintillant. Energy is released as a part of the radioactive decay of the isotope and some of this energy is transformed into detectable light photons that are measured by photo multiplier tubes in the detector.

Scintillation counting is susceptible to quenching, where sample components can interfere with the measurement of photons and reduce the number of photons detected. For this reason instruments measure counts per minute (CPM), rather than decays per minute (DPM), the ratio between these is the counting efficiency. There are quenching correction methods available and the most common for modern instruments is to use an external source of known radioactivity at close proximity to the sample.

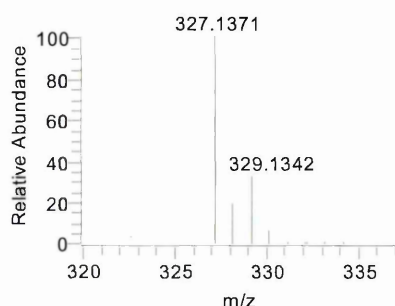
Generating a metabolite profile by radio chemical detection requires either a flow radiochemical detector for LSC or fractionating the sample, then analysing the fractions by SSC. For both methods a flow splitter is often employed to divert some of the sample to a MS for metabolite identification and the rest to a

flow radiochemical detector or a fraction collector and SSC for metabolite detection and quantification.

1.4.3.1 Stable label

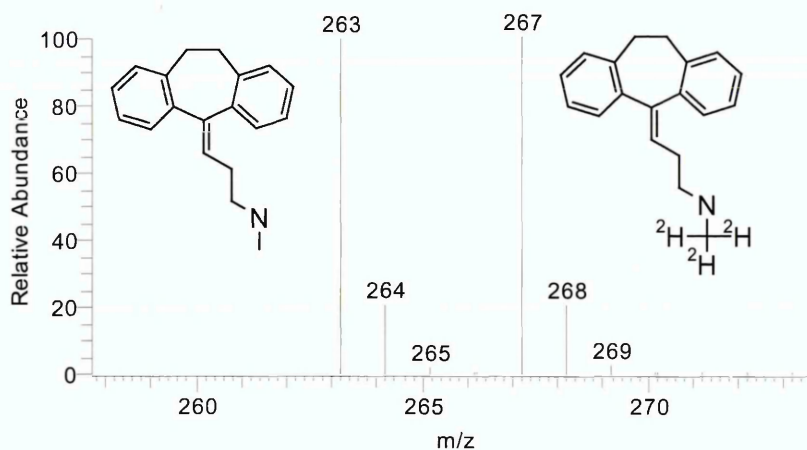
Compounds containing elements such as Cl or bromine give a distinct isotope pattern by mass spectrometry due to their natural isotopic abundance. Cl has two abundant isotopes, ^{35}Cl and ^{37}Cl at a ratio of 3:1 so generates two distinct ions 2 Da apart at a ratio of 3:1 see Figure 24. This isotopic ratio is extremely useful to help identify parent related metabolites from complex biological matrices. It is obviously not possible for every potential drug to incorporate an element with multiple abundant isotopes, but it is possible to create a pseudo isotope pattern using stable labels.

Figure 24 Partial positive ion mass spectrum of Chlozapine showing the $[\text{M}+\text{H}]^+$ ion and the signals arising from the presence of the 35 and 37 isotopes of Cl



The stable labels of drug candidates have been exploited by scientists in drug metabolite identification and profiling studies⁸⁸⁻⁹⁰. For example in 1971 Knapp *et al.*⁸⁹ reported the use of a stable labelled Nortriptyline replacing three hydrogens for three deuterium atoms (^2H) equating to an overall mass increase of +3 Da over unlabelled Nortriptyline. A mixture of 50% labelled and 50% unlabelled Nortriptyline would create a very distinct pseudo isotope pattern (Figure 25), which could be used to help identify drug/analyte related metabolites by mass spectrometry.

Figure 25 Theoretical mass spectrum for 1:1 mixture of Nortriptyline and stable labeled Nortriptyline (3x ^2H) showing the two $[\text{M}+\text{H}]^+$ ions.



Using this 1:1 mixture in metabolism studies generates parent related metabolites or products with two isotope peaks (M and M+3) at ratio of 1:1, greatly simplifying the identification of drug related metabolite peaks by mass spectrometry in complex biological matrices.

Today there are a host of automated software data stripping techniques which can aid metabolite searching and includes programmes such as cluster pattern or isotopic pattern recognition that will automate the detection of MS peaks with pseudo isotope pattern such as M:M+3 at 1:1. This technique is rarely used for optimisation of compound series in drug discovery due to the cost associated with the synthesis of multiple stable labelled test compounds.

For development studies where the compound is in the clinic there is often a radioisotope labelled analogue available, which is far superior for metabolism studies. Therefore these stable labelled metabolite identification studies are not conducted routinely, but are often applied ad hoc for specific investigations. A review on stable labelled compounds in metabolism by Mutlib⁹¹ describes using ^{13}C labelled DpC961⁹² in an *in vivo* study to confirm a GSH adduct was formed via oxidation on an alkyne moiety.

Another application for this technique is in the area of detecting GSH adducts from RM GSH trapping experiments of test compounds incubated in microsomes. Yan *et al.*⁹³ described the use of stable labelled GSH (2x ^{13}C and 1x ^{15}N on the glycine moiety) to improve detection of adducts and reduce false

positives observed from constant neutral loss scanning of -129 Da (loss of the glutamyl). A mixture of 50% labelled and 50% unlabelled GSH was added to microsomal incubations of test compounds which resulted in RMs that formed two GSH adducts 3 mass units apart. Both the labelled and unlabelled GSH adducts could generate the -129 Da neutral loss, therefore each RM trapped with GSH would give 2 neutral losses 3 mass units apart, generating a unique pattern for an unambiguous result.

1.5 Detecting RMs

RMs are very difficult to detect analytically due to their inherent chemical reactivity. There are several *in vitro* techniques available to help identify compounds that form RMs and/or determine potential sites of bioactivation.

1.5.1 RM trapping assays

The pharmaceutical industry standard for identifying RMs in early discovery is RM trapping assays or screens^{94,95}, where the reactive intermediate is produced under conditions that favour a particular, known endpoint. Test compounds are incubated in liver microsomes (usually human), metabolising them by the most prevalent phase I metabolic processes occurring in the liver. The microsomal incubation of test compound is fortified with an excess of nucleophilic trapping agent, to convert any reactive electrophilic species into a stable detectable conjugate.

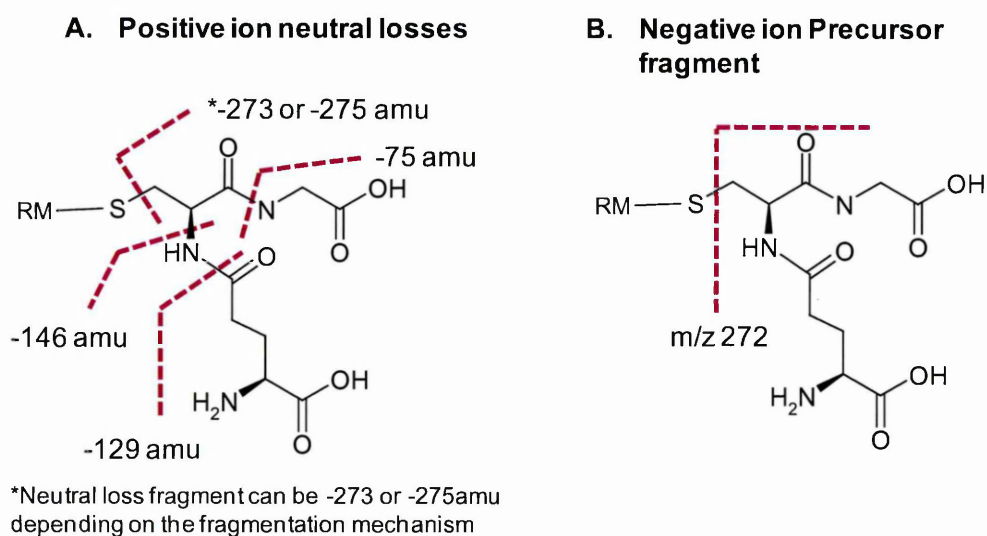
GSH is the most commonly used nucleophilic trapping agent for RM trapping screens⁹⁶⁻¹⁰², and as it is a naturally occurring tripeptide in the body, it is favoured over chemically synthetic nucleophiles. GSH is the body's natural defence against toxic/reactive products, forming adducts with them to generate inactive stable products, that are easily excreted from the body. GSH will efficiently adduct with soft electrophiles such as epoxides, quinonemines Michael acceptors etc, but does not react with hard electrophiles such as iminium ions. Hard electrophiles (iminium ions) are detected using potassium cyanide (KCN) as a nucleophilic trapping agent forming stable detectable -CN adducts. *In vitro* RM screening has become more routine within the

pharmaceutical industry with many companies now running primary GSH and KCN screens in parallel for maximum coverage¹⁰³.

1.5.1.1 GSH RM screening assay

GSH adducts with soft electrophiles forming a stable LC-MS detectable product. Analysis of the microsomal GSH trapping assays are primarily by LC-MSMS, which offers the sensitivity, selectivity and throughput required. A wide range of LC-MS methodology can be used to detect GSH adducts, currently the most popular are; PIS, NLS, DDA or accurate mass scanning with MDF. Positive ion NLS on a QqQ monitoring for -129 Da⁵² is by far the most well known. The -129 Da neutral loss corresponds to loss of the glutamyl moiety from GSH, however there are additional neutral loss values such as -75, -146, -273 or -275 Da (Figure 26A) which can be used independently or in combination with -129 Da. Negative PIS monitoring for m/z 272 product ion (Figure 26B) is an alternative scan mode on a QqQ, Dieckhaus *et al.*¹⁰¹ reported this to be more sensitive and less likely to give false negatives over positive ion -129 NLS.

Figure 26 GSH structure showing the positive ion neutral loss fragments (A) negative ion precursor ion (B).



Both PIS and NLS do not require any information about the test compound and are simple to set up for relatively high throughput analyses with minimal data interpretation. The analytical output is limited and only provides a yes/no answer without any information on the site of bioactivation. The methodology is

amenable to screening high numbers of compounds, which can be used to generate some structure activity relationship (SAR)^{104,105} early in drug discovery programs.

Quadrupole linear IT instruments have the capability to acquire data dependent scans (DDA) using NLS and/or PIS in combination with full scan data including MS² scans. The DDA experiment for GSH trapping uses information from a survey PIS or NLS to trigger MS² scans to generate structural information. This technique removes the need to run a second experiment to acquire MS² scans on all the potential GSH adduct ions detected from PIS/NLS. Wen *et al.*⁹⁷ compared the effectiveness of negative ion PIS and positive ion NLS methods to trigger MS² spectra for GSH adducts, demonstrating negative ion PIS was more effective.

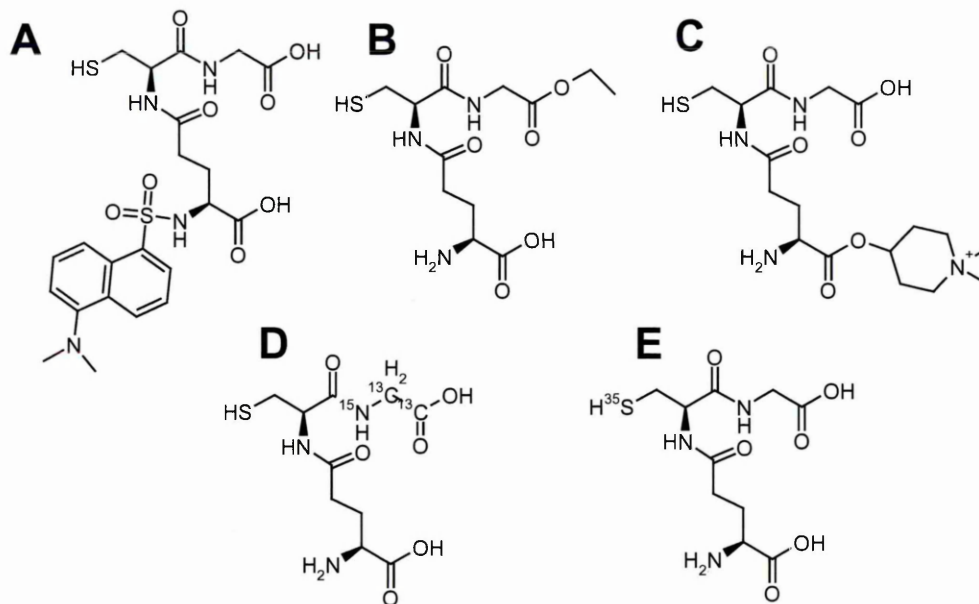
More recently Jian *et al.*¹⁰³ reported using both negative ion PIS and positive ion NLS to trigger product ion scans in a single experiment for a GSH RM trapping screen. This data dependent methodology creates fewer false negatives/positives offering greater confidence over triplequadrupole NLS and PIS analysis, whilst acquiring additional structural information. High resolution accurate mass instrumentation is an alternative to these low resolution nominal mass techniques, however they often require more in depth expertise in mass spectrometry interpretation. It is not possible to acquire NLS or PIS on a Q-ToF mass spectrometer, however Castro-Perez⁹⁶ presented a method acquiring MS^E (Section 1.3.2.8.1) looking for a pseudo accurate neutral loss difference of 129.0426 (+/- 20 mDa mass window) between the high energy and low energy scans. This is not technically neutral loss scanning as no neutral loss is measured, just an assumed neutral loss when comparing the *m/z* difference between the high and low energy scans. They report an increase in selectivity for this methodology over nominal mass NLS, though no comparison is made with superior nominal mass GSH detection techniques such as negative ion PIS. All of the techniques discussed so far, rely on GSH adducts generating expected common neutral losses or product ions for detection; however this is not always the case for GSH adducts¹⁰¹. This is a major disadvantage of these techniques and is likely to lead to significant number of false negatives.

Alternative MS methodology utilising accurate mass full scan data and post acquisition mass defect filtering rather than GSH fragmentation characteristics has been reported in the literature with some success. Zhu *et al.*¹⁰⁶ have compared traditional NLS data with LTQ-Orbitrap high resolution accurate mass data processed with MDF. They set the MDF window to +/- 0.04 Da around a calculated mass defect for a GSH adduct template ($[M+H]^+$ of drug + GSH $-H_2$). The MDF window was applied over a mass range of +/-50 Da around the calculated mass for the GSH adduct. Unlike all of the GSH adduct LC-MS screening methods discussed previously, the sensitivity of the MDF approach is not dependent on MS² dissociation efficiency of GSH adducts. The MDF approach was reported to be more sensitive and selective over -129 NLS¹⁰⁶, especially for GSH adducts that do not produce the -129 neutral loss effectively. MDF appears to offer significant improvements over traditional approaches, however the small mass window (+/- 50 Da) employed by Zhu *et al.*¹⁰⁶ would likely to miss GSH where the bioactivation step involves an increase or decreases in its mass by more than 50 Da (e.g. hydrolysis).

1.5.1.1.1 Derivatised GSH trapping studies

Several GSH analogues (Figure 27) have been used to enhance the detection and quantification of RMs in microsomal trapping assays, significant improvements over GSH trapped adducts have been reported.

Figure 27 List of GSH analogues for RM trapping experiments: A Dansyl GSH, B GSH-ethylester C Quaternary ammonium GSH, D Stable labelled GSH and ³⁵S labelled GSH.



1.5.1.1.2 **Dansylated GSH**

Gan *et al.*¹⁰⁷ demonstrated it was possible to attach a fluorescence tag to GSH by derivatisation with dansyl chloride. The resulting dansyl-glutathione product (Figure 27A) can be analysed by fluorescent detection rather than mass spectrometry, offering analytical advantages in sensitivity, selectivity and quantification over standard GSH RM trapping experiments.

1.5.1.1.3 **GSH ethyl ester**

Soglia *et al.*¹⁰⁸ compared the LC-MS analysis (SRM) of GSH ethylester (GSH-EE) (Figure 27B) and GSH microsomal trapping experiments on twelve compounds known to form RMs. Of the twelve compounds tested only 4 GSH adducts were detectable by mass spectrometry, whereas ten GSH-EE adducts were detected. The GSH-EE adducts were shown to give increased MS response (up to 80x) over the equivalent GSH adducts.

1.5.1.1.4 **Quaternary ammonium ion GSH**

An attempt to improve quantification of GSH adducts by incorporation of a fixed positive charge into GSH through addition of a quaternary ammonium ion (QA-

GSH) (Figure 27C) was reported by Soglia *et al.*¹⁰⁹. The addition of a fixed positive charge reduced the variability in ionisation between different QA-GSH-adducts. Comparison of MS responses for 3 QA-GSH adducts standards and a QA-GSH free thiol, were within about 3 fold of each other, whereas parent compound MS responses differed by more than 19 fold. Semi-quantification was achieved by the addition of a QA-GSH free thiol internal standard (IS) post incubation at a known concentration. Direct comparison of the QA-GSH peak area versus the detected GSH adduct enabled semi-quantification.

1.5.1.1.5 Stable labelled GSH

Stable label GSH (¹⁵N and 2 x ¹³C on the glycine, Figure 27D) has been used effectively to improve GSH adduct detection and sensitivity in high throughput RM screens^{93,110} (Section 1.4.3.1)

1.5.1.1.6 Radiolabelled GSH

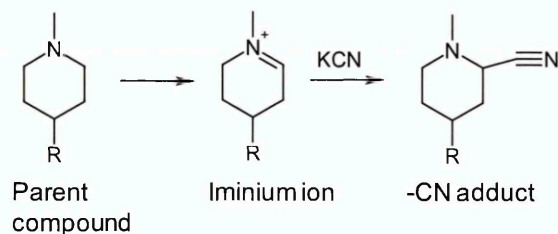
Hartman *et al.*¹¹¹ reported incorporating ³⁵S isotope into intracellular GSH by exposing hepatocytes to ³⁵S-labelled methionine, replacing cellular GSH with intracellular generated ³⁵S labelled GSH (³⁵S-GSH) (Figure 27E). Incubation of acetaminophen (known to form GSH adducts) demonstrated it was possible to detect and quantify ³⁵S-GSH adducts by radiochemical detection. This approach has significant advantages over all other trapping methods and will detect all GSH adduct types while quantifying them accurately. However using ³⁵S radioisotope in a high throughput setting is extremely difficult, potentially time consuming and expensive, so it is not a viable option for early drug discovery.

1.5.1.2 Cyanide trapping assays

GSH does not adduct with hard electrophiles such as iminium ions, so trapping this type of RM requires an alternative trapping agent. The cyanide anion is a hard nucleophile and will adduct with iminium ions efficiently, generating a stable detectable product of 25 Da (+C+N –H) higher than the parent compound mass (Figure 28). Cyanide adducts often generate a single diagnostic neutral loss (-27 Da) by CID, which greatly simplifies their detection by MS. The analysis of the microsomal KCN trapping assays is therefore primarily carried

out by LC-MS and often run in conjunction with the GSH trapping screen^{103,112}. Argoti *et al.*¹¹² reported using a mixture of stable labelled $K^{13}C^{15}N$ and non labelled KCN generating a pseudo isotope pattern by MS to reduce false positives. Gorrod *et al.*¹¹³ used radiolabelled $Na^{14}CN$ to determine the formation of an iminium ion intermediate through nicotine metabolism.

Figure 28 Cyanide addition to an iminium ion



KCN trapping offers additional information over GSH trapping experiments, however it has the potential for false positive through the formation of cyanide adduct artefacts¹¹⁴.

1.5.1.3 Peptide screening assays

Mitchell *et al.*¹¹⁵ and Laine *et al.*¹¹⁶ have both described the use of synthetic peptides for RM screening. Mitchell reported using an 11 amino acid peptide that included Cys and other nucleophilic amino-acid groups to trap electrophilic RMs. Analysis was by surface enhanced laser detection/ionisation-ToF MS, which is a surface ionisation technique and does not require LC separation to introduce the sample into the instrument. Whereas Laine *et al.*¹¹⁶ described an LC-MS based peptide trapping assay which would be more amenable to instrumentation available within drug metabolism groups.

1.5.2 Bespoke trapping experiments

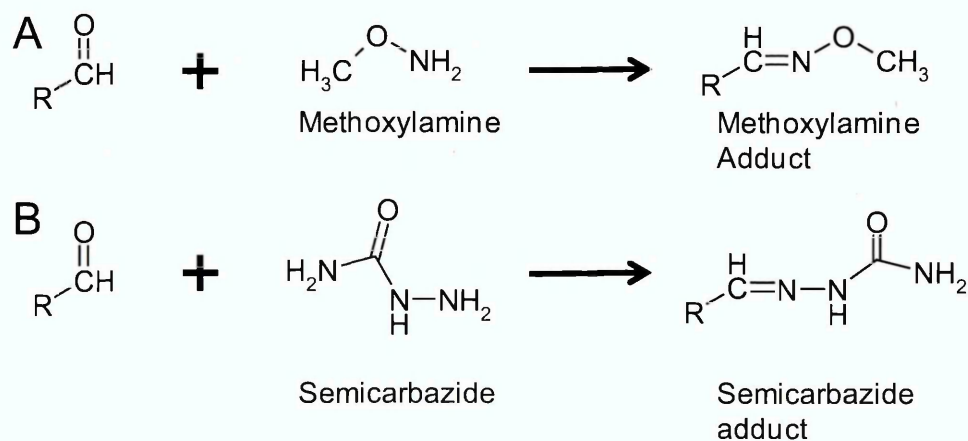
There are a number of trapping experiments employed by biotransformation scientists to detect, identify and understand bioactivation of test compounds or drugs to RMs. In contrast to RM screening, that often only offers a yes/no answer; these studies are targeted at identifying and understanding the reactive intermediate. The work is low throughput, and often used to investigate a single compound where CVB, toxicity, mechanism based inhibition or a positive RM trapping result are observed. GSH and KCN trapping have been discussed

already, but there are a number of other additional trapping agents that have been utilized including; semicarbazide, methoxyamine, Cys or NAC.

1.5.2.1 Semicarbazide and Methoxyamine Aldehyde Trapping

KCN and GSH trapping agents form adducts with most electrophilic RMs, although reactive aldehyde metabolites are not always trapped. There are two commonly used agents to trap reactive aldehyde metabolites; methoxyamine (Figure 29A) and semicarbazide (Figure 29B).

Figure 29 Reactive aldehyde trapping by (A) methoxyamine and (B) semicarbazide

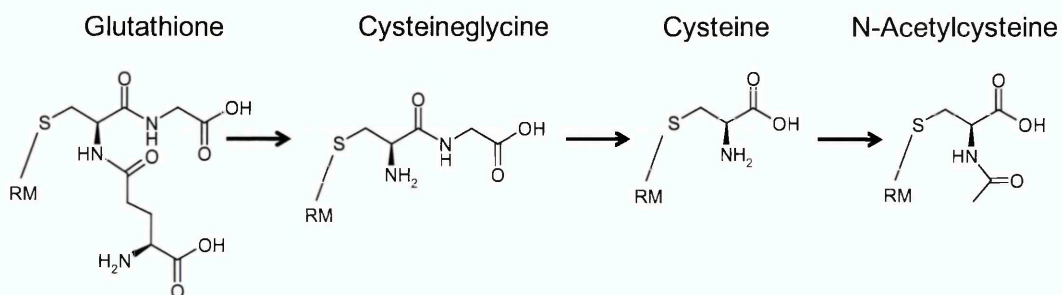


There are several excellent examples of methoxyamine and semicarbazide confirming the formation of reactive aldehyde metabolites¹¹⁷⁻¹²⁰. Unlike GSH and cyanide adducts, there are no straight forward product ions or neutral losses consistently generated from semicarbazide adducts. Thus it is not possible to use automated scan functions such as PIS/NLS or data processing to detect and find these adducts making them less amenable to LC-MS screening assays. An additional drawback using methoxyamine as a trapping agent in microsomal incubations is the potential for it to interfere with the metabolising enzymes, altering the metabolic profile or even inhibiting aldehyde formation. Zhang *et al.*¹²¹ described the inhibitory properties of GSH, KCN and methoxyamine in liver microsomes. GSH and KCN did not inhibit any P450 enzyme isoforms at concentrations up to 10mM; however methoxyamine inhibited CYP1A2, CYP2C9, CYP2C19, CYP2D6 and CYP3A4/5.

1.5.2.2 Cys and NAC Trapping Agents

Detoxification of RMs by GSH *in vivo*, can lead to a series of conjugates generated from the metabolism/degradation of GSH conjugates (Figure 30).

Figure 30 Metabolism/degradation of GSH adducts *in vivo*.



Cys and NAC are two of the breakdown products from GSH and have both been used *in vitro* to trap RMs with some degree of success. Ravindranath *et al.*¹²² reported that Cys was a better trapping agent than GSH for the RM of 2-methyl furan. Whereas Jian *et al.*¹²³ presented a high throughput method for the detection of NAC-adducts using -129 NLS and MRM approaches to triggering MS² experiments for detection and identification in a single LC-MS run. They reported the potential for NAC-adducts to generate more product ions from cleavages of the test compound/drug providing more information about the site of bioactivation.

1.5.2.3 Acyl-glucuronide screening

Acyl-glucuronides are formed by the phase II metabolism of carboxylic acids, so it is easy for a chemist to visually inspect the structure of a test compound and identify whether it is possible to form an acyl-glucuronide. The detection of an acyl-glucuronide metabolite is not confirmation of a RM, as not all acyl-glucuronides are reactive. Therefore acyl-glucuronide *in vitro* screening is to determine whether acyl-glucuronide metabolites are likely to be chemically reactive rather than focusing on their detection.

Acyl-glucuronides are able to undergo acyl migration and through this process generate a chemically reactive intermediate that can covalently bind to proteins. This chemical reactivity can be linked to the stability of an acyl-glucuronide¹²⁴ and Bolze *et al.*¹²⁵, Chen *et al.*¹²⁶, Jinno *et al.*¹²⁷ and Zhong *et al.*¹²⁸ all describe

methods to measure the stability of acyl-glucuronide metabolites. The basic principle across all the methods reported, is to first biosynthesize the acyl-glucuronide metabolite *in vitro*, incubating test compound/drug in human microsomes activated for glucuronidation. The rate of degradation of the resulting acyl glucuronide is then measured by LC-MS in buffer, plasma or albumin. The faster this rate the more reactive the acyl-glucuronide and therefore the higher the potential for CVB to protein and toxicity.

1.5.3 CVB

The most common way to assess RM risk is to measure the CVB of a compound and its metabolites in human microsomes or hepatocytes using radiolabelled compound. CVB of xenobiotic metabolites to endogenous macro molecules *in vivo* has been associated with toxicity (Hapten hypothesis)^{10,11,22,124}. In theory measuring the CVB of a drug and its metabolites could indicate their reactivity and help determine how likely they are to generate RM mediated toxicity. Measuring CVB of a drug and its metabolites is not a new idea; Gillette *et al.*¹²⁹ reported the merits of investigating CVB for drug toxicity in 1974.

CVB is simply a measure of the amount of drug/compound related material covalently bound to endogenous macromolecules, after dosing (*in vivo* CVB) or after incubation in a metabolizing system (*in vitro* CVB). These studies require radioisotope labelled test compound or drug and radio chemical detection is used to determine the quantity of bound drug. *In vitro* CVB experiments are often used to assess the RM risk of compounds that are close to progression into drug development and there are various methods reported in the literature¹³⁰. The data is usually reported in pMol/mg of protein and is used to help evaluate whether a compound is safe enough to progress into development and studies in humans.

Evans *et al.*¹³⁰ reported that Merck Sharp and Dohme used a threshold of 50pMol/mg. This was based on the levels of covalent adducts found in the liver associated with hepatic necrosis of known hepatotoxins, approximately 1 nmol of drug/mg of protein, which was reduced 20 fold for a 'conservative target'. They state that 50 pMol/mg is a target upper limit and not an absolute threshold

above which compounds cannot progress, since other factors need to be considered.

The predicted daily human dose is a very important consideration; drugs given at a daily dose of 10mg or less are rarely if ever associated with idiosyncratic drug reactions¹⁰. Nakayama *et al.*¹³¹ measured the CVB of 42 marketed drugs *in vitro* and *in vivo* to determine if CVB predicted the clinical situation. These were classified as either safe, or had a warning, black box warning or were withdrawn based on their clinical safety profiles. The CVB results on their own did not clearly discriminate between the categories, however when the daily dose was considered as well, a much better prediction was achieved.

More recent CVB assessments methods, factor in the relative *in vitro* metabolic turnover (Cl_{int}) with the predicted daily dose to calculate a predicated daily CVB burden^{132,133}. These methods do not accurately predict toxicity for all drugs, so the question remains: is toxicity predictable based on a quantity of CVB?

1.6 Aims and Objectives of this Project.

The aims of this project are to apply the methodology discussed in the introduction to;

- Investigate the metabolism of Fenclozic acid in HRN mice and bile duct cannulated rats to identify any new reactive/toxic metabolites that could explain the reported hepatotoxicity observed in the clinic or covalent binding observed in microsomes (Chapter 2 & 3).
- Identify and determine the mechanism of formation of a novel carbon hydrogen addition metabolite formed *in vivo* in the rat (Chapter 4).
- Investigate the formation of a Homomorpholine GSH rearrangement metabolite in human liver microsomes fortified with GSH (Chapter 5).
- Study the formation of isomeric methanol adducts identified from a human liver microsomal incubation (Chapter 6).

From the investigation of these RM examples, it is intended to;

- Determine the limitations of current RM trapping screening methodology employed within the pharmaceutical industry.

- Identify of any unfavourable chemical moieties that should be avoided for drug research programmes.
- Discover areas of improvement in the current LC-MS methodology for metabolite identification.

2. THE METABOLIC FATE OF ¹⁴C-FENCLOZIC ACID IN THE HEPATIC REDUCTASE NULL (HRN) MOUSE

Reprinted with permission of Informa UK Ltd. All rights reserved.

RESEARCH ARTICLE

The metabolic fate of [¹⁴C]-fenclozic acid in the hepatic reductase null (HRN) mouse

Kathryn Pickup¹, Jonathan Wills¹, Alison Rodrigues², Huw B. Jones³, Chris Page⁴, Scott Martin¹, Sunil Sarda¹, and Ian Wilson^{1*}

¹Drug Metabolism and Pharmacokinetics IM Alderley Park, AstraZeneca UK Ltd, Macclesfield, Cheshire, UK, ²MRC Centre for Drug Safety Science, University of Liverpool, Liverpool, UK, ³Global Safety Assessment, Alderley Park, AstraZeneca UK Ltd, Macclesfield, Cheshire, UK, and ⁴eADMET Argenta, Harlow, Essex, UK

Abstract

1. The distribution, metabolism, excretion and hepatic effects of fenclozic acid were investigated following a single oral dose of 10 mg/kg to hepatic reductase null (HRN) mice.
2. The majority of the [¹⁴C]-fenclozic acid was eliminated via the urine/aqueous cage wash, (55%) with a smaller portion excreted in the faeces, (5%). The total recovery of radioactivity in the excreta over the 72 h period studied was ca. 60%.
3. Metabolism of fenclozic acid in the HRN mice was entirely to the carboxylic acid function and was dominated by amino acid conjugation to glycine and taurine, with lesser amounts of an acyl glucuronide.
4. Whole body autoradiography of mice showed general distribution into all tissues except the brain. Radioactivity was still detectable in the kidney and liver of the HRN mice at 72 h post-dose. Covalent binding studies showed evidence of binding to kidney, liver and plasma proteins however, the degree of binding was less than 50 pmol equiv/mg protein for all tissues.
5. The HRN mouse appears to be a useful *in vivo* model for the study of the Phase II conjugation metabolism of fenclozic acid in the absence of hepatic cytochrome P450-related oxidative metabolism.

Keywords

Drug metabolism, fenclozic acid, HRN mouse

History

Received 25 September 2013

Revised 11 November 2013

Accepted 12 November 2013

Published online 10 December 2013

Introduction

Fenclozic acid (2-(4-chlorophenyl)-thiazol-4-ylacetic acid) (Myalex) was identified as a potential anti-rheumatic by ICI Pharmaceuticals in the 1960's (Newbould, 1969) and, in early clinical trials, (Chalmers et al., 1969a,b) ascending doses (100–400 mg) were found to be well tolerated. The results of these, and subsequent, trials suggested that the drug would make a suitable alternative to aspirin as a treatment for rheumatoid arthritis as it had equal efficacy but higher potency with less side effects. However, when large scale studies were undertaken, patients at the higher dose of 400 mg daily showed adverse effects after 4 weeks of treatment, with two cases of jaundice out of 12 patients in one centre (Hart et al., 1970). Numerous cases of jaundice and abnormal hepatic function emerged at other centres in patients

administered with the 400 mg dose of fenclozic acid for over 14 days and consequently trials were stopped (Alcock, 1971) and the compound was withdrawn from further development. Biochemical analysis indicated that the jaundice was cholestatic (suppression of bile flow) and it was accompanied by raised alkaline phosphatase, serum glutamic oxaloacetic transaminase and serum glutamic pyruvic transaminase levels (Hart et al., 1970). The withdrawal of fenclozic acid led to a reappraisal of the pre-clinical data, and additional work in a wider range of pre-clinical species (Alcock, 1971) however, no hepatotoxicity was identified in animals. Fenclozic acid thus represents an example of a compound causing serious and unpredicted non-idiosyncratic adverse drug reactions (ADRs) in man despite rigorous preclinical testing.

As part of a series of studies to examine whether modern methods of safety testing would have detected the hepatotoxic potential of fenclozic acid, we recently undertook a range of *in vitro* investigations (Rodrigues et al., 2013), based on a panel of assays, designed to look for effects on the liver (Thompson et al., 2012). These studies showed that, in microsomal and hepatocyte incubations, fenclozic acid underwent NADPH-dependant metabolism to reactive species that covalently bound to protein. However, incubation of the drug together with reactive metabolite-trapping reagents

*Present address: Department of Surgery and Cancer, Imperial College, Exhibition Rd, South Kensington, London, UK

Address for correspondence: Kathryn Pickup, Drug Metabolism and Pharmacokinetics IM, Alderley Park, AstraZeneca UK Ltd., Macclesfield, Cheshire SK10 4TG, UK. Tel: +44-1625-518418. Fax: +44-1625-230614. E-mail: Kathryn.pickup@astrazeneca.com

failed to identify any reactive metabolites even when compounds such as glutathione, clearly modified the extent of covalent binding. This is interesting because, in the *in vivo* studies undertaken during the development of fenclozic acid, studies in rat, dog and monkey showed extensive metabolism of the drug. In rat and dog, the major metabolites identified included 2-(4-chlorophenyl)-4-methyl-thiazole, 2-(4-hydroxyphenyl)-thiazol-4-ylacetic acid and 2-(4-hydroxy-3-chlorophenyl)-thiazol-4-ylacetic acid (Foulkes, 1970). These three metabolites, together with fenclozic acid itself were also converted to acyl glucuronide conjugates. In monkey, the fenclozic acid acyl glucuronide was the only significant metabolite produced. Later studies in the rat, identified glucuronide and taurine conjugates in the bile and urine, the proportions of which were dose-dependent, with the proportions of the taurine conjugate increasing from 16% to 32% of the total in urine when the dose was raised from 2 to 100 mg/kg fenclozic acid, respectively (Bradbury et al., 1981). The ability of fenclozic acid to undergo both Phase I oxidative and Phase II metabolic conjugation reactions clearly offers the potential for several different types of reactive metabolite to be formed *in vivo*. As such it can be difficult to determine whether one, or both types of biotransformation, are responsible for the generation of a chemically reactive species *in vivo*. Recently, we have shown (Pickup et al., 2012) that using the hepatic reductase null (HRN) mouse model (Le & Sauer, 2001), which has no functional hepatic cytochrome P450 enzymes, resulted in the production of only conjugated diclofenac metabolites. We have therefore undertaken a study of [¹⁴C]-fenclozic acid in the HRN mouse model to examine the disposition, metabolism and covalent binding of fenclozic acid drug in order to see if this might cast further light on the involvement, if any, of Phase II metabolism in the toxicity of the drug.

Experimental procedures

Chemicals

Unlabelled fenclozic acid [2-(2-(4-chlorophenyl)thiazol-4-yl)acetic acid] was obtained from Compound Management (AstraZeneca, Alderley Park, UK, Batch number: AZ10002189-024) [¹⁴C]-fenclozic acid [2-(2-(4-chlorophenyl)[2-¹⁴C]thiazol-4-yl)acetic acid; refer Table 4 for position of radiolabel] was synthesised and supplied by Isotope Chemistry (AstraZeneca, Alderley Park, UK) at 237 µCi/mg and a radiochemical purity >99%. Ultima Gold and Ultima Flo M scintillation cocktails were purchased from Packard Instruments (Pangbourne, UK). CarboSorb oxidiser absorbent and Permafluor E + scintillant were obtained from PerkinElmer (Beaconsfield, UK) whilst FLUOTHANE™ was obtained from the AstraZeneca Group of Companies. Pierce BCA protein assay kit was obtained from Perbio Science (Cramlington, UK). Acetonitrile, ethanol, formic acid, hexane, tetrahydrofuran (THF), trifluoroacetic acid (TFA) and xylene were all of analytical grade and supplied by Fisher Scientific (Loughborough, UK). Phosphate buffer (pH 7.4) was supplied by AZ media (AstraZeneca, Alderley Park, UK). All other chemicals or solvents were purchased from commercial suppliers and were of analytical grade or the best equivalent.

Animals

In total, 12 male Hepatic Reductase Null [HRN; B6.Cg-*Por^{mut}Wolf^{Tg}*(Alb-cre)21Mgn N7] mice aged approximately 8 weeks and weighing between 18.5 and 26.0 g were purchased from Taconic (Taconic Farms Inc., Germantown, NY). All animal procedures and treatments were carried out in accordance with approved animal licenses and guidelines issued by the British Home Office [Animals (Scientific Procedures) Act (1986)].

Methods

Two studies were performed as follows.

Study 1: To determine the route and rate of excretion, and metabolic fate of [¹⁴C]-fenclozic acid (target 1100 µCi/kg) in the HRN mouse.

Study 2: To determine the distribution of [¹⁴C]-fenclozic acid (target 200 µCi/kg) by semi-quantitative whole body autoradiography (WBA) in HRN mice.

Individual mice were identified by tail markings, and acclimatised in groups to the environmental conditions for 3 days prior to dosing. Mice were kept at room temperature and exposed to a 12 h dark/12 h artificial light cycle and an R&M No. 1 Modified Irradiated diet; potable water was available *ad libitum*. Mice were fasted for 12 h prior to oral administration (by gavage) of either [¹⁴C]-fenclozic acid (10 mg/kg) or phosphate buffer (dosing volume of 5 mL/kg). After dosing, the mice designated to the WBA study and the mice dosed with vehicle control were housed individually in polycarbonate cages with stainless steel mesh inserts. Mice for the [¹⁴C] excretion-balance study were housed individually in glass metabolism cages.

Two dose solutions were prepared, one for each study. [¹⁴C]-fenclozic acid, supplied with a specific activity of 237 µCi/mg, was diluted with unlabelled fenclozic acid to give material with the target specific activity for each study. Unlabelled fenclozic was dissolved in phosphate buffer (pH 7.4) and an appropriate volume of this solution was added to the [¹⁴C]-fenclozic acid to give a solution at the target specific activity (110 µCi/mg for the balance study and 20 µCi/mg for the WBA study), and a target concentration of 2 mg/mL. Phosphate buffer (pH 7.4) was used as the vehicle control dose.

Sample collection

Study 1: Urine, faeces and aqueous cage wash were collected over a 72 h period (urine and cage wash; 0–6 h and 6–12 h then daily to 72 h post-dose, faeces; daily post-dose), after which animals were sacrificed by FLUOTHANE™ inhalation. Urine and faeces were collected over dry ice to ensure sample stability. Following death, the mice were exsanguinated and the blood collected into heparinised blood tubes before being spun for 2 min, at approximately 7800 g and ambient temperature to produce plasma. The liver (with gall bladder removed) and kidneys from each animal were collected and a small sample of each liver was taken and fixed for histopathology. The remainder of the liver and kidneys were snap-frozen in liquid nitrogen and stored at –80 °C until required.

Study 2: Two HRN mice were sacrificed at 6, 24 and 72 h post-dose by FLUOTHANE™ inhalation. Carcasses were immediately frozen in a mixture of hexane and dry ice then stored at *ca.* -80°C until WBA was performed as described below.

Histopathology

Liver samples were fixed in 10% neutral buffered formaldehyde for 5 days before dehydrating in increasing concentrations of industrial methylated spirits (IMS), IMS and xylene (70, 80 and 95%) then xylene alone, over a total of 7 h. Dehydrated samples were embedded in paraffin wax, after which sections (3 μm thick) were prepared and stained with Haematoxylin and Eosin (H&E). Stained sections were observed using a light microscope.

Determination of routes and rates of excretion

The radioactive content of liquid samples (dose solutions, urine, aqueous cage wash and plasma) was determined by liquid scintillation counting (LSC). Weighed aliquots (in duplicate) of sample were made up to 1 mL with deionised water, after which 10 mL scintillation cocktail (Ultima Gold) was added and the samples analysed using a Packard TriCarb scintillation counter (Pangbourne, UK) for 10 min or until 10^6 counts had accumulated. Solid samples, such as faeces, liver and kidney, were first homogenised in water (1:3 w/v) and then combusted using a Packard Oxidiser (model 307). The products of combustion were trapped in 9 mL of CarboSorb and then 12 mL Permafluor E+ scintillation cocktail were added prior to LSC as described above. The amount of radioactivity in the excreta and tissue samples was compared with that dosed to the animals in order to calculate the percentage recovery from each animal.

Whole body autoradiography

Following the freezing of the animals the hind legs and tail were removed. Each carcass was then embedded left side uppermost in a block of carboxymethylcellulose (*ca.* 2% in water) then mounted on the stage of a Leica CM3600 cryomacrotome (Leica Microsystems, Germany) maintained at approximately -20°C . Sagittal sections (30 μm) were prepared from each animal based on the work of Ullberg (1954) to include as many tissues as possible. Sections were then allowed to freeze-dry prior to exposure to FUJI phosphor imaging plates (Raytek, Sheffield, UK). Sections for imaging were enclosed in a light-tight cassette and were exposed for 7 days. After exposure the imaging plates were removed from the cassettes under dark room conditions and the plates scanned using a FUJI FLA 5000 phosphor imager (Raytek) and radioactive content of selected tissues determined using AIDA image analysis software (Raytest UK, Sheffield, UK).

Covalent binding

Individual plasma samples were used untreated whilst liver and kidney homogenates from each animal in Study 1 were used to assess the extent of covalent binding. The radioactive

content for each sample was measured by scintillation counting. The protein content of the homogenates and plasma was determined using a Pierce BCA protein assay kit, samples were subsequently diluted to give 2 mg/mL protein using 0.1 M phosphate buffer (pH 7.4). Aliquots (200 μL in triplicate) were then placed in the wells of a 96-well plate and 300 μL of acidified (3% formic acid) acetone added, and the samples then agitated for 1 min. A further 500 μL acidified acetone was then added and the samples agitated again for 1 min to allow the protein to precipitate. The protein pellet was washed with 80% methanol in water using a Brandel cell harvester (Gaithersburg, MD). The protein concentration and radioactive content of the remaining pellet were determined by scintillation counting, and the extent of covalent binding calculated by difference using Microsoft Excel. The statistical significance of the difference was calculated using the Student's *t*-test function in Microsoft Excel.

Sample preparation for metabolite identification

Urine and faeces samples were pooled by excreta type to include any sample containing greater than 1% of the administered dose. For urine the pool was 6–72 h whilst for the faeces the pool was 24–48 h. The radioactive content of each pool was determined either by LSC directly (urine) or following combustion (faecal homogenates) as described previously. Pre-dose urine and faeces samples were also prepared in the same way as the post-dose samples.

Pooled urine samples were concentrated to approximately 400 000 dpm/mL under a stream of oxygen-free nitrogen and analysed directly, whereas faecal homogenates were extracted by adding acetonitrile to each homogenate in the ratio 3:1 (vol/weight) and the sample mixed on a rotary mixer for 10 min before centrifuging at 3345 g for 10 min at 20°C . The supernatant was removed and the radioactive recovery determined by LSC. Two extractions sufficed to give complete recovery, and these were combined prior to concentration using a Büchi R-114 rotavapor (BUCHI Labortechnik AG, Switzerland) at 30°C followed by further concentration to approximately 400 000 dpm/mL under a stream of oxygen-free nitrogen. The resulting concentrated samples were centrifuged at 25 000 g for 3 min to remove any particulate matter.

Profiling and structural characterisation of metabolites by UPLC-LTQ-Orbitrap and top count

Accurate mass structural characterisation work was acquired on an LTQ Orbitrap XL connected to a Waters Acquity Ultra high-Performance Liquid Chromatography (UPLC) system. The Waters Acquity system consisted of a binary UPLC pump, Column oven, autoinjector equipped and a photodiode array detector. Separations were carried out on a Waters BEH C18 (100 \times 2.0 mm, 1.8 μm), preceded by a guard filter in a column oven at 50°C . The mobile phase consisted of aqueous formic acid (0.1% in water, eluent A) and methanolic formic acid (0.1%, eluent B).

The following elution profile was employed: An initial step of 5–20% at 1.00 min, a linear gradient 20% A to 55% A,

1.01–15.00 min, a fast linear gradient 55% A to 98% A 15.00–min, isocratic hold, 2% A 16.00–17.00 min; re-equilibration 95% A, 17.00–19.00 min. The flow rate was 0.45 mL/min and was split post-column 5:1 (v/v) using a QuickSplit™ fixed-flow splitter (Analytical Scientific Instruments, Elsobrante, CA) to a HTC-PAL fraction-collector/autosampler (CTC Analytics, Presearch, Baskingstoke, UK) for fraction collecting and an LTQ Orbitrap (Thermo Fisher Scientific, Bremen, Germany) for mass spec analysis.

Using an injection volume of 20 μL , fractions were collected into 96 deep-well Luma™ plates (Perkin Elmer Inc., Cambridge, UK) across the whole run at a rate of 2.4 s per well. These plates were then dried and analysed for radioactivity on a Packard HTS-Topcount-NXT (Pangbourne, UK). The data were imported into LAURA software version 4.1.12.89 (Lablogic systems Ltd., Sheffield, UK) to reconstruct the radio chromatograms. The LTQ-Orbitrap XL was equipped with an electrospray ionisation (ESI) source (Thermo Fisher Scientific, Bremen, Germany) which was operated in positive mode. Source settings were: Capillary temperature 300 °C, sheath gas flow 25, auxiliary gas flow 17, sweep gas flow 5, source voltage 3.5 kV, source current 100 μA , capillary voltage 18 V, tube lens 75.0 V. Full scan MS data were obtained over the mass range of 100–1000 Da at a peak resolution of 7500 FWHM. Targeted MSMS experiments were acquired using Higher energy Collisional Dissociation (HCD) fragmentation, isolation width 2 Da, normalised collision energy 45, and activation time 30 ms. HCD fragment ions were monitored by the Orbitrap using 7500 resolution. LTQ and Orbitrap mass detectors were calibrated within one day of commencing the work using Proteomass LTQ/FT-Hybrid ESI positive mode calibration mix (Supelco, Bellefonte, PA).

Data analysis

The assessment of the metabolism of fenclozic acid was made by both quantitative and qualitative analyses of the chromatographic profiles obtained *via* [^{14}C]-detection and LC-MS respectively. Radio-labelled components were assumed to have the same specific activity as parent molecule.

Mass spectrometric data were collected using Xcalibur version 2.0.7 (Thermo Fisher Scientific, Waltham, MA). Components were identified as being derived from [^{14}C]-fenclozic acid if they displayed the retention times corresponding with radio-labelled peaks and demonstrated the characteristic, isotopic and fragmentation patterns observed with the parent molecule. All accurate mass measurements including the MSMS fragmentation and MSMS isolation were taken from the fenclozic acid [^{12}C] isotope peak. This was done due to the interference of the unlabeled fenclozic [^{37}Cl] isotope peak contaminating the [^{14}C]-labelled fenclozic acid accurate mass. Comparisons with pre-dose control samples were conducted to minimise the potential for false positives from endogenous compounds.

Results and discussion

Histopathology

Liver sections treated with H&E stains observed under light microscopy for HRN mice dosed with [^{14}C]-fenclozic acid

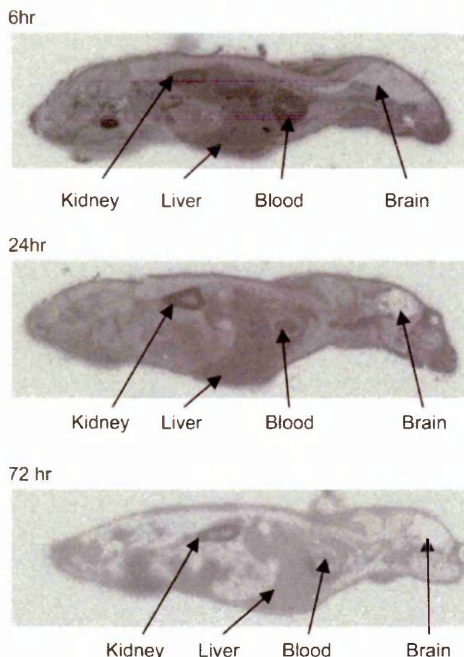


Figure 1. Autoradiography images of hepatic cytochrome P450 reductase null (HRN) mice following a single 10 mg/kg oral dose of [^{14}C]-fenclozic acid. Fenclozic acid related material is well distributed in all tissues with the exception of the central nervous system, and still remains in tissues at 72 h post-dose.

showed no alterations in liver morphology in comparison with the corresponding vehicle controls.

Whole body autoradiography

Whole body autoradiography (WBA) of HRN mice showed that the radioactivity was widely distributed in to all the tissues (with the exception of the CNS where only very low levels were detected) (Figure 1). The radioactive content determined by imaging analysis software AIDA version 4.22 (Raytest UK, Sheffield, UK) for selected tissues including tissue:blood ratios, illustrating retention of the radioactivity compared with circulating drug-related material is presented in Table 1. The highest concentrations of radioactivity were detected in the blood, liver and kidney. The results of the WBA study showed retention of the radioactivity in the tissues of animals 72 h post-dosing (Figure 1). The amount of radioactivity remaining in the liver and kidneys at 72 h was quantified as part of the mass balance study and is described as follows.

Routes and rates of excretion of radioactivity

Following oral administration of [^{14}C]-fenclozic acid at 10 mg/kg to HRN mice, the majority of the recovered radioactivity was eliminated *via* the urine (Table 2). A significant portion of the dose was also recovered in the cage wash, which was attributable to the low volumes of urine produced by the mice, resulting in a portion being recovered from the wall of the meta-bowls when cage washing was undertaken at sample collection. For this reason, the urine and

Table 1. The mean ($n=2$) radioactive content (dpm/g) of selected tissues in hepatic cytochrome P450 reductase null (HRN) mice, 6, 24 and 72 h after a single 10 mg/kg oral dose of [14 C]-fenclizic acid.

Tissue	6 h		24 h		72 h	
	dpm/g	Tissue:blood	dpm/g	Tissue:blood	dpm/g	Tissue:blood
Blood	1 495 895	1.00	324 417	1.00	40 204	1.00
Brain	30 382	0.02	7 803	0.02	439	0.01
Kidney cortex	1 306 595	0.87	684 612	2.11	163 856	4.08
Kidney medulla	692 149	0.46	141 989	0.44	20 772	0.52
Liver	918 417	0.61	306 996	0.95	49 330	1.23

Table 2. The mean ($n=3$) percentage of fenclizic acid related material recovered in the excreta of hepatic cytochrome P450 reductase null (HRN) mice over time.

	Percentage of the dose recovered in excreta (%) (Mean \pm SD)				
	0-6 h	6-12 h	12-24 h	24-48 h	48-72 h
Urine	1.45 \pm 2.02	2.05 \pm 2.08	10.93 \pm 11.62	14.87 \pm 2.16	5.62 \pm 0.92
Cagewash	4.03 \pm 0.76	4.17 \pm 3.77	5.98 \pm 5.99	4.26 \pm 2.55	1.17 \pm 0.39
Subtotal	5.49 \pm 2.48	6.24 \pm 5.04	16.91 \pm 11.75	19.11 \pm 4.54	6.80 \pm 0.89
		0-24 h		24-48 h	48-72 h
Faeces		2.86 \pm 2.25		2.08 \pm 0.67	0.37 \pm 0.06
Subtotal		31.50 \pm 10.80		21.18 \pm 4.97	7.17 \pm 0.84
Total				59.84 \pm 6.30	

Table 3. Covalent binding of fenclizic acid related material in hepatic cytochrome P450 reductase null (HRN) mice, 72 h after a single 10 mg/kg oral dose of [14 C]-fenclizic acid.

Animal	pmol equiv/mg protein		
	Liver	Kidney	Plasma
4	9.96 \pm 0.54	21.93 \pm 0.34	2.37 \pm 0.75
5	16.64 \pm 0.32	29.82 \pm 3.43	2.14 \pm 0.24
6	13.69 \pm 0.31	27.21 \pm 1.18	3.97 \pm 1.56
Mean	13.43 \pm 3.35	26.32 \pm 4.02	2.83 \pm 1.00

cage wash values were combined, with cage wash-derived radioactivity assumed to result from urinary excretion. Recovery of radioactivity via the urine/cage wash amounted to *ca.* 55 \pm 5% (mean \pm SD) by 72 h post-dose.

A smaller portion of the administered dose was excreted in the faeces (Table 2), with *ca.* 5 \pm 2% eliminated via this route over 72 h collection period. Therefore, the overall recovery of compound-related material in the excreta was approximately 60 \pm 6% (mean \pm SD) over the 72 h period studied. The reason(s) for the relatively low recovery in the excretion balance part of the study are not clear. The site of incorporation of the radiolabel should ensure metabolic stability so the low recovery more likely reflects either the administration of less [14 C]-fenclizic acid than expected, or difficulties in ensuring the complete recovery of excreted radiolabel from the meta-bowls. As a result of the observation of retention of the radiolabel in certain tissues by WBA at 72 h post dose, covalent binding studies were performed on plasma, liver and kidney samples to determine whether this relatively long-retained radioactivity was due to covalent binding to cellular macromolecules. Covalent binding results revealed low levels (<50 pmol equiv/mg protein) of bound radioactivity in the plasma, liver and kidneys (Table 3). The highest levels of binding were seen in the kidneys (26.32 \pm 4.02 pmolequiv/mg protein) with much lower levels

of binding in the liver and plasma (13.43 \pm 3.35 and 2.83 \pm 1.00 pmol equiv/mg protein respectively). Quantification of the total amount of the dose (i.e. free and covalently bound) present in the homogenates of the excised livers and kidneys by sample oxidation showed that this amounted to 1.01 \pm 0.06% in the liver and 0.39 \pm 0.06% (mean \pm SD) in the kidneys.

Metabolite profile of [14 C]-fenclizic acid in urine and faecal extracts

Radiochromatograms generated the Topcount data of the excreta from HRN mice are shown in Figure 2(A) and (B). HRN mice excreted four major radio-labelled components via the urine eluting between 10 and 14 min (Figure 2A). These were identified by mass spectrometry as unchanged fenclizic acid an acyl glucuronide (as a mixture of transacylated isomers) and two amino acid conjugates. The latter were identified as a glycine conjugate, which formed the major metabolite in urine and a taurine conjugate (refer Table 4 for structures and proportions of the dose).

The faecal extract from HRN mice (Figure 2B) showed two major radio-peaks, identified as parent compound and the taurine conjugate. In addition, a small peak corresponding to the glycine conjugate was also seen. Full scan and fragmentation mass spectra for the glycine, taurine and acyl-glucuronide conjugates are shown in Figure 4.

No loss of radioactivity on the HPLC column was observed for any of the samples studied and we therefore assume that the profiles obtained represent the contents of the samples.

Structural characterization of drug and metabolites by UPLC-MS

To ensure good quality accurate mass measurements all structural characterisation was conducted on the unlabeled

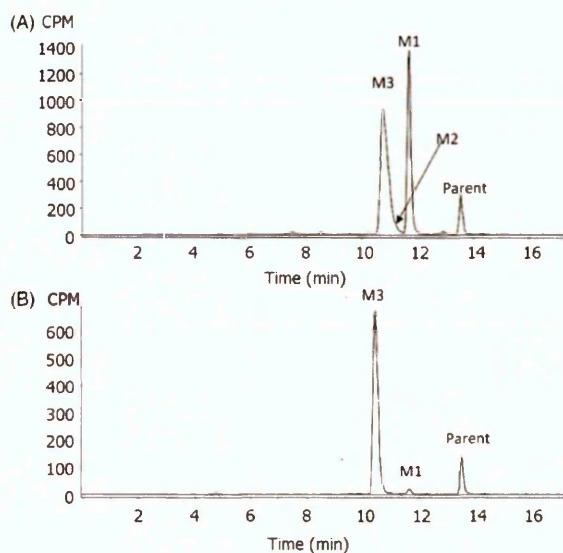


Figure 2. The radiochromatograms generated from the Topcount data of the excreta from hepatic cytochrome P450 reductase null (HRN) mice after a single 10 mg/kg oral dose of [¹⁴C]-fenclzic acid. (A) urine, (B) faeces. Labels indicate peaks whose chemical structures were determined using mass spectrometric data.

fenclzic acid and metabolite MS peaks. This was due to the contamination of the [¹⁴C]-labelled fenclzic acid isotope MS peak with the unlabeled [³⁷Cl]-fenclzic acid isotope. Drugs often contain structural motifs similar to those of their metabolites; it is therefore common practice to first fully characterize the structure of the parent compound with accurate mass MS/MS fragmentation. Characteristic fragment ions identified from the drug can then be used to elucidate metabolite structures.

Structural characterization fenclzic acid

Analysis of fenclzic by LC-MS/MS/MS yielded a protonated molecular ion for unlabeled [¹²C] with an accurate mass of $[M + H]^+$ 254.0035 (−1.00 ppm). The proposed fragmentation pattern and LTQ Orbitrap HCD MS/MS spectrum fenclzic acid (Figure 3) revealed three fragment ions m/z 207.9982 (corresponding to decarboxylation) m/z 138.105 and m/z 70.9951 (corresponding to thiazole ring opening products).

Structural characterization of the major metabolites observed in the radiochromatogram

The UPLC peak corresponding to **M1** yielded a protonated molecular ion with an accurate mass of $[M + H]^+$ 311.0239, which was consistent with glycine conjugation (+1.81 ppm mass error). The accurate mass fragmentation of m/z 311 (Figure 4) yielded two key fragment ions m/z 265.0197 resulting from the loss of CO₂ and m/z 235.9934 for the loss of the glycine moiety, which are both indicative of a glycine conjugate. It is believed that the ion at m/z 254.0039 is an artefact, which has been formed through the addition of water to the m/z 235.9931 fragment ion in the MS (+0.77 ppm mass error).

The metabolite **M2** yielded a protonated molecular ion with an accurate mass of $[M + H]^+$ 430.0381 (−1.61 ppm mass error) and this, and the proposed fragmentation pattern (Figure 4), were both indicative of direct glucuronidation on the acid moiety. A cluster of four MS peaks were detected for m/z 430.0381, which is consistent with transacylated products from an acyl-glucuronide.

The mass spectra data for **M3** yielded a protonated molecular ion with an accurate mass of $[M + H]^+$ 361.0083, which was consistent with taurine conjugation (+1.378 ppm mass error). The accurate mass fragmentation of m/z 361 (Figure 4) yielded two key fragment ions, m/z 279.0353 showing the loss of SO₃H and m/z 235.9934 for the loss of the taurine moiety, which are both characteristic of a taurine conjugate.

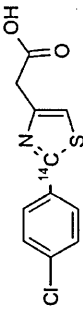
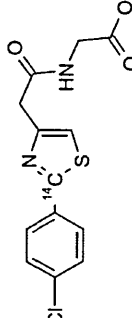
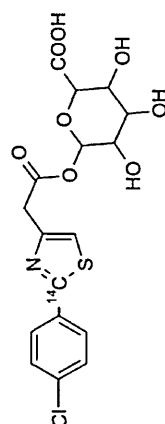
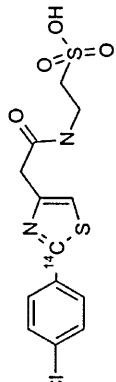
Discussion

As described in the ‘‘Introduction’’ section, the development of fenclzic acid was discontinued due to hepatotoxicity in man. This study was undertaken to examine the distribution, metabolism, excretion and hepatic effects, if any, of fenclzic acid using the HRN mouse, which is deficient in hepatic Phase I metabolism (via CYP P450’s) but capable of Phase II conjugation reactions. Histopathological examination did not reveal any evidence of adverse hepatic effects for fenclzic acid in these animals after a single dose of 10 mg/kg. From the autoradiographic data the radiolabel was well distributed into tissues (apart from the brain), particularly into tissues such as liver and kidney. The majority of radioactivity (55%) was recovered in the urine/aqueous cage wash, with a smaller amount (5%) in the faeces giving an overall recovery of radioactivity in the excreta, over the 72 h period studied, of *ca.* 60%. Whilst the bulk of the radiolabel recovered in the urine and faeces was excreted in the first 48 h, appreciable amounts were still being excreted at the end of the study, and radioactivity was still detectable in tissues such as liver and kidney at 72 h post-dose.

The profiles of urine and faecal extracts showed that metabolism proceeded largely via conjugation reactions, as might be expected from animals where hepatic P450-based metabolism had been abolished. The major metabolites in the HRN mouse were amino acid conjugates to glycine and taurine, with quantities of the transacylated acyl glucuronide.

The detection of transacylated acyl-glucuronide metabolites of fenclzic acid in urine suggests a source of chemically reactive metabolites with the potential to form adducts to proteins (Stachulski et al., 2006) and indeed such metabolites have been designated as toxic in some regulatory guidances (FDA Guidance on safety testing of drug metabolites, 2008). However, in the *in vitro* investigations undertaken prior to this study (Rodrigues et al., 2013), high covalent binding was only observed in rat, dog and human microsomal incubations in the presence of NADPH (125.8 ± 20.1, 70.2 ± 19.8 and 38.5 ± 6.8 pmol equiv/mg of protein for human, dog and rat liver microsomes, respectively). (For comparison when [¹⁴C]-diclofenac was used as a positive control covalent binding was 108.6 ± 3.6, 145.8 ± 20.5 and 126.9 ± 18.0 pmol equiv/mg of protein for human, rat and dog, respectively). When the ability of the acyl glucuronide to bind to proteins was

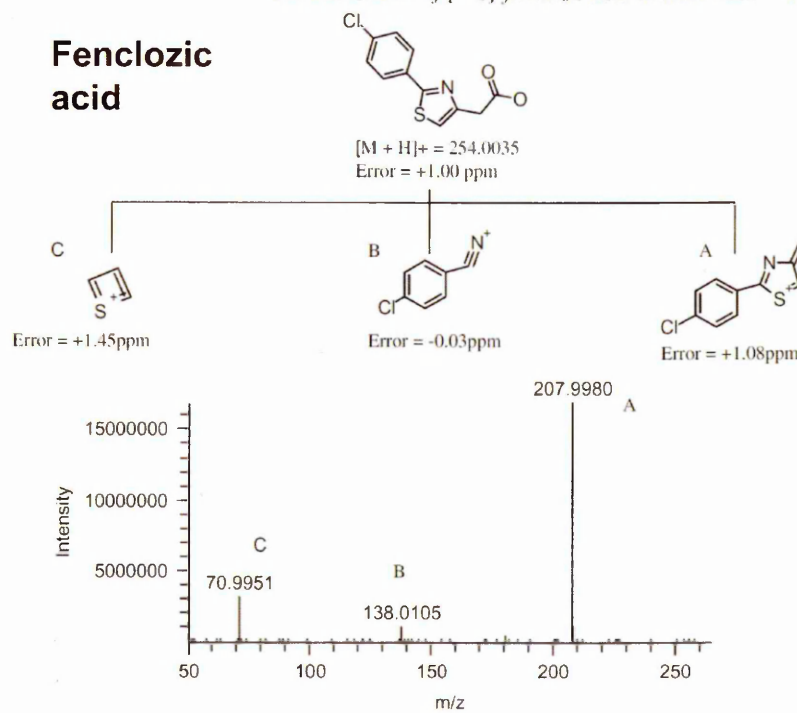
Table 4. Metabolites identified within the urine and faeces from hepatic cytochrome P450 reductase null (HRN) mice following a single 10 mg/kg oral dose of [¹⁴C]-fenclozic acid.

Peak label	Retention time (minutes)	[M + H] ⁺ in positive ion mode [¹² C]/[¹⁴ C]	Metabolite	Structure	Percentage dose (%)	
					Urine	Faeces
P	13.32	254.0037/256 ^a	Fenclozic acid (parent compound)		3.38	0.21
M1	11.42	311.0252/313 ^a	Glycine conjugate		16.82	0.05
M2	11.09	430.0358/432 ^a	Acyl glucuronide		1.3	-
M3	10.45	361.0078/363 ^a	Taurine conjugate		21.97	1.48

Metabolites were identified by high performance liquid chromatography coupled to mass spectrometry (LC-MS). Figures quoted represent the percentage administered dose.

^aAccurate masses were taken from the fenclozic acid [¹²C] isotope peak.

Figure 3. Proposed LTQ Orbitrap HCD fragmentation of fenclozic acid including mass error in ppm (top) and accurate mass spectrum (bottom).



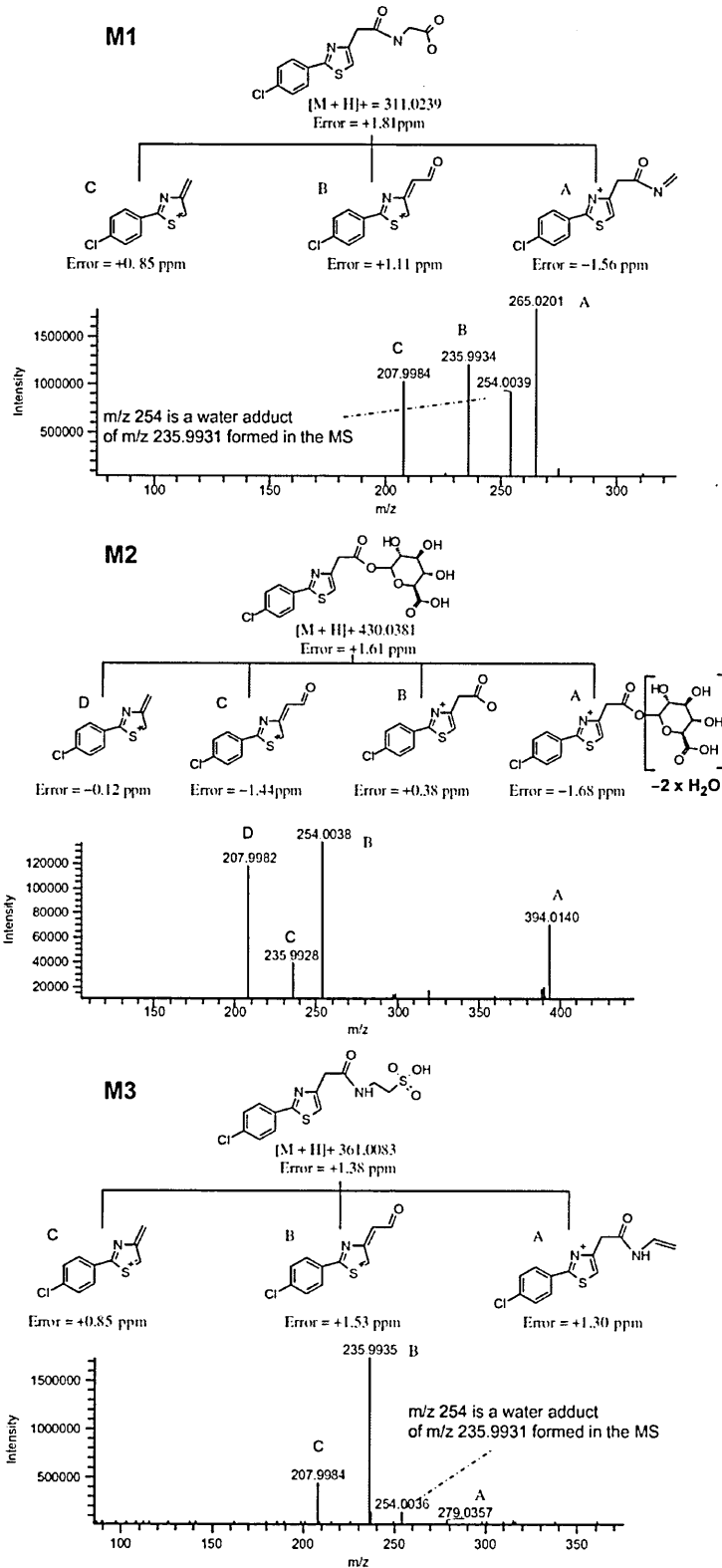
examined, in microsomal incubations supplemented with UDPGA (where the acyl glucuronide accounted for 4.5, 0.9 and 4.9% of the total for human, rat and dog respectively) no covalent binding was observed. In contrast, when [^{14}C]-diclofenac, as a positive control, was incubated in the presence of UDPGA the covalent binding to liver microsomes amounted to 155.1 ± 17.7 , 113 ± 21.4 and 131.4 ± 21.2 pmol equiv/mg of protein for human, rat and dog, respectively. This suggests that, unlike diclofenac, the propensity for covalent binding of the fenclozic acid acyl-glucuronide is low, supporting the results obtained *in vivo* in this study in the HRN mouse.

Metabolism to amino acid conjugates provides an alternative route to reactive metabolite formation as it proceeds via an acyl-coenzyme A thioester intermediate. As has been shown experimentally, such CoA-thioester metabolites have the potential to react with proteins (Boelsterli, 2002; Knights et al., 2007; Skonberg et al., 2008). In the *in vitro* hepatocyte study the taurine conjugate of [^{14}C]-fenclozic acid was observed in rat and dog (but not human) hepatocyte incubations, and was highest in rat accounting for 9.6% of the total radioactivity after 180 min (Rodrigues et al., 2013). When covalent binding was investigated the greatest amount of non-extractable binding in hepatocytes also followed this trend with the highest binding seen for rat, then dog and finally human hepatocytes, amounting to 539.0 ± 69.6 , 269.7 ± 143.5 and 74.9 ± 13.6 pmol equiv/mg of protein, respectively, and such a result might be taken as support for a CoA-thioester-binding mechanism. However, in these *in vitro* hepatocyte studies, interpretation of the covalent binding data was complicated since the cells had the ability to perform P450 related oxidative metabolism as well as Phase II metabolism.

Despite the clear opportunity to covalently bind to proteins via either acyl CoA thioesters or due to acyl-glucuronide reactivity, and clear exposure to these metabolites *in vivo*, the determination of the extent of tissue and plasma covalent binding detected in the HRN mouse has shown this to be modest. Thus, for the tissues examined, covalent binding amounted to much less than 50 pmol equiv/mg protein. In addition, the highest levels of binding were seen in the kidney, at ca. 26 pmolequiv/mg protein, twice that seen for liver (ca. 13 pmolequiv/mg protein) whilst that seen for plasma (ca. 3 pmol equiv/mg protein) was negligible. In attempting to interpret the higher covalent binding of the radiolabel in kidney compared to liver it has to be borne in mind that, whilst hepatic metabolism can be reasonably considered to lack any P450-related contribution the same cannot be considered for kidney, which can perform both Phase I oxidative and Phase II conjugation reactions. Whilst based on the data obtained in the previous *in vitro* study (Rodrigues et al., 2013), it may be assumed that the higher levels of covalent binding in kidney compared to liver were the result of the presence of active P450's in the former, further studies would be required to confirm this.

The results of this study show that it is possible to use the HRN to separate the contributions hepatic conjugative and P450-related oxidative metabolism from each other for fenclozic acid (as indeed it was for diclofenac – Pickup et al., 2012). The results obtained in the HRN mouse suggest that the Phase II conjugation of fenclozic acid does not result in the production of large amounts of covalent binding, supporting the findings of the *in vitro* studies carried out with microsomes (Rodrigues et al., 2013). Further work will examine the metabolic fate of the drug in normal mice to explore the effects of P450-dependant oxidative metabolism.

Figure 4. Proposed LTQ Orbitrap collision cell fragmentation of metabolites **M1** (glycine conjugate), **M2** (glucuronide) and **M3** (taurine conjugate) with accurate mass spectra and mass error in ppm.



Acknowledgements

We thank Paul Evenden and Sarah Simcoe (Global Safety Assessment, Alderley Park, AstraZeneca) for technical assistance during the live phase of these studies.

Declaration of interest

The authors report no declarations of interest.

References

- Alcock S. (1971). An anti-inflammatory compound: non-toxic to animals but with an adverse action in man. *Proc Eur Soc Study Drug Toxic* 12:184–90.
- Boelsterli UA. (2002). Xenobiotic acyl glucuronides and acyl CoA thioesters as protein-reactive metabolites with the potential to cause idiosyncratic drug reactions. *Curr Drug Metab* 3:439–50.
- Bradbury A, Powell GM, Curtis CG, Rhodes C. (1981). The enhanced biliary secretion of a taurine conjugate in the rat after intraduodenal administration of high doses of fenclozic acid. *Xenobiotica* 11: 665–74.
- Chalmers TM, Kellgren JH, Platt DS. (1969a). Evaluation in man of fenclozic acid (I.C.I. 54,450; Myalex), a new anti-inflammatory agent. II. Clinical trial in patients with rheumatoid arthritis. *Ann Rheum Dis* 28:595–601.
- Chalmers TM, Pohl JE, Platt DS. (1969b). Evaluation in man of fenclozic acid (I.C.I. 54,450; Myalex), a new anti-inflammatory agent. I. Serum concentration studies in healthy individuals and in patients with rheumatoid arthritis. *Ann Rheum Dis* 28:590–4.
- FDA. (2008). FDA Guidance for Industry: Safety Testing of Drug Metabolites. FDA Guidance on safety testing of drug metabolites. *The metabolism of [¹⁴C]-fenclozic acid in HRN mice* 173 (2008). Retrieved from <http://www.fda.gov/downloads/Drugs/GuidanceComplianceRegulatoryInformation/Guidances/ucm079266.pdf> [last accessed 2 Dec 2013].
- Foulkes DM. (1970). The metabolism of C14-ICI 54,450 (myalex) in various species – an in vivo NIH shift. *J Pharmacol Exp Ther* 172: 115–21.
- Hart FD, Bain LS, Huskisson EC, et al. (1970). Hepatic effects of fenclozic acid. *Ann Rheum Dis* 29:684.
- Knights KM, Sykes MJ, Miners JO. (2007). Amino acid conjugation: contribution to the metabolism and toxicity of xenobiotic carboxylic acids. *Expert Opin Drug Metab Toxicol* 3:159–68.
- Le Y, Sauer B. (2001). Conditional gene knockout using Cre recombinase. *Mol Biotechnol* 17:269–75.
- Newbould BB. (1969). The pharmacology of fenclozic acid (2-(4-chlorophenyl)-thiazol-4-ylacetic acid; I.C.I. 54,450; 'Myalex'); a new compound with anti-inflammatory, analgesic and antipyretic activity. *Br J Pharmacol* 35:487–97.
- Pickup K, Gavin A, Jones HB, et al. (2012). The hepatic reductase null mouse as a model for exploring hepatic conjugation of xenobiotics: application to the metabolism of diclofenac. *Xenobiotica* 42: 195–205.
- Rodrigues AVM, Rollison HE, Martin S, et al. (2013). In vitro exploration of potential mechanisms of toxicity of the human hepatotoxic drug fenclozic acid. *Arch Toxicol* 87:1569–79.
- Skonberg C, Olsen J, Madsen KG, et al. (2008). Metabolic activation of carboxylic acids. *Expert Opin Drug Metab Toxicol* 4:425–38.
- Stachulski AV, Harding JR, Lindon JC, et al. (2006). Acyl glucuronides: biological activity, chemical reactivity, and chemical synthesis. *J Med Chem* 49:6931–45.
- Thompson RA, Isin EM, Li Y, et al. (2012). In vitro approach to assess the potential for risk of idiosyncratic adverse reactions caused by candidate drugs. *Chem Res Tox* 25:1616–32.
- Ullberg S. (1954). Studies on the distribution and fate of [³⁵S]-labelled benzylpenicillin in the body. *Acta Radiol Suppl* 118:1–110.

**3. IDENTIFICATION OF THE REACTIVE METABOLITES OF FENCLOZIC
ACID IN BILE DUCT CANNULATED RATS**

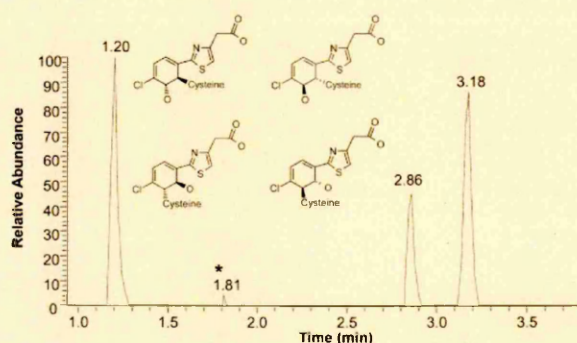
Reproduced with permission from Anal. Chem. (2014) 86:11281-11289.
Copyright 2014 American Chemical Society.

Identification of the Reactive Metabolites of Fenclozic Acid in Bile Duct Cannulated Rats

Scott Martin,^{*,†} Eva M. Lenz,[†] Warren Keene,[†] and Malcolm R. Clench[‡][†]DMPK Department, AstraZeneca UK Ltd., Alderley Park, Macclesfield, Cheshire SK10 4TG, United Kingdom[‡]Biomedical Research Centre, Sheffield Hallam University, Howard Street, Sheffield, South Yorkshire S1 1WB, United Kingdom

Supporting Information

ABSTRACT: Fenclozic acid (Myalex) was developed by ICI pharmaceuticals in the 1960s for the treatment of rheumatoid arthritis and was a promising compound with a good preclinical safety profile and efficacy. While it did not show adverse hepatic effects in preclinical animal tests or initial studies in man [Chalmers et al. *Ann. Rheum. Dis.* **1969**, *28*, 595 and Chalmers et al. *Ann. Rheum. Dis.* **1969**, *28*, 590], it was later withdrawn from clinical development. Hepatotoxicity was observed in humans at daily doses of 400 mg but was not replicated in any of the animal species tested. Rodrigues et al. [*Arch. Toxicol.* **2013**, *87*, 1569] published a mechanistic investigation using modern *in vitro* assays/techniques in order to investigate the hepatotoxicity; however, only the covalent binding in rat, dog, and human microsomes was identified as a potential indicator for hepatotoxicity. Metabolites associated with or responsible for covalent binding could not be detected, likely due to the low *in vitro* metabolic turnover of fenclozic acid in microsomes. Foulkes [*J. Pharmacol. Exp. Ther.* **1970**, *172*, 115] investigated the *in vivo* metabolism of fenclozic acid which included a rat bile duct cannulated (BDC) study characterizing the biliary and urinary metabolites; however, no reactive metabolites were identified. This study aimed to reinvestigate the *in vivo* metabolism of fenclozic acid in rat, with a focus on identifying any reactive metabolites that could explain the *in vitro* covalent binding in microsomes observed across the species. Using modern analytical techniques, we were successful in identifying an epoxide reactive metabolite, which upon conjugation with glutathione (GSH), formed up to 16 GSH-related products including positional and diastereoisomers. Not including the GSH related conjugates, 7 additional metabolites were identified compared to these previous metabolism studies.



Fenclozic acid ([2-(4-chlorophenyl)-1,3-thiazol-4-yl]acetic acid, Myalex) was developed by ICI pharmaceuticals in the 1960s as a nonsteroidal anti-inflammatory drug for the treatment of rheumatoid arthritis and was a promising compound with a good preclinical efficacy.⁵ While it did not show adverse hepatic effects in preclinical animal tests or initial studies in man,^{1,2} it was later withdrawn from clinical development. This was due to nonidiosyncratic hepatotoxicity at daily doses of 400 mg where several incidences of jaundice and abnormal hepatic function were reported.⁶ The cholestatic jaundice was also associated with elevated liver toxicity biomarkers such as alkaline phosphatase, serum glutamic oxaloacetic transaminase, and serum glutamic pyruvic transaminase. This hepatotoxicity was not observed in any of the preclinical animal species prior to dosing to man or later in additional animal studies where a variety of species were used.⁷ More recently, Rodrigues et al.³ published a mechanistic investigation using a cascade of modern *in vitro* toxicity assays⁸ in order to investigate the hepatotoxicity; however, only the NADPH dependent covalent binding to protein in rat, dog and human microsomes was identified as a potential indicator for the hepatotoxicity. Additionally, there was a reduction in the covalent

binding in microsomes when fenclozic acid was incubated in the presence of glutathione (GSH) or cysteine. However, they were unable to identify any metabolites or adducts from any of the incubations including those fortified with nucleophilic trapping agents such as GSH, despite the use of radiolabeled fenclozic acid.

In contrast, *in vivo* studies undertaken with fenclozic acid by Foulkes⁴ and by Bradbury et al.⁹ showed extensive metabolism of the drug. A more recent *in vivo* study conducted in hepatic CYP reductase null (HRN) mice¹⁰ aimed to further evaluate the involvement of any phase II metabolism in the toxicity of the drug. The HRN mice lack functional hepatic cytochrome P450 leading to the formation of direct conjugated metabolites exclusively. In both, the *in vivo* and the hepatocytes incubation study, an acylglucuronide was identified which can cause covalent binding to protein.¹¹ However, Rodrigues et al.³ showed a higher level of covalent binding in microsomes compared to hepatocytes or microsomes supplemented with UDPGA

Received: August 6, 2014

Accepted: October 16, 2014

Published: October 16, 2014

(uridine 5'-diphospho-glucuronosyltransferase), which suggests that phase I metabolites were responsible or significantly contributing to the covalent binding.

This paper describes the characterization of the biliary and urinary metabolites of fenclazic from a bile duct cannulated (BDC) study in rats utilizing UPLC (ultra high-performance liquid chromatography) and Fourier transform-mass spectrometry. The emphasis is on identifying metabolites that indicate the formation of reactive intermediates which may have been missed in the previous studies by Foulkes⁴ and by Bradbury et al.⁹

EXPERIMENTAL SECTION

Chemicals. Fenclazic acid, [2-(4-chlorophenyl)-1,3-thiazol-4-yl]acetic acid, was obtained from Compound Management (AstraZeneca, Alderley Park, UK, Batch number: AZ10002189-024). Methanol (MeOH), formic acid, and ammonium acetate were all of analytical grade and supplied by Fisher Scientific (Loughborough, UK). All other chemicals or solvents were purchased from commercial suppliers and were of analytical grade. No specific safety considerations apply to any of these agents, although the agents should be handled with care in a fumehood to avoid inhalation or ingestion.

Fenclazic Acid Stock Solution. Fenclazic acid was dissolved in MeOH at a concentration of 200 μ M.

Animal Dosing and Sample Collection (Bile and Urine) of the BDC Rats. Two male Han Wistar rats, aged between 7 and 12 weeks and weighing between 180 and 250 g at the time of dosing, were supplied by AstraZeneca's rodent breeding unit. The animals were surgically fitted with bile duct cannuli under full anesthetic.

Each animal received a single *i.v.* bolus dose of fenclazic acid at 2 mg/kg at a dose volume of 2 mL/kg in a dose vehicle consisting of dimethylamide (DMA)/phosphate buffered saline (PBS, pH 7.4) (30%/70%, v/v). Urine and bile were collected on ice predose and at 0–6 h, 6–12 h, and 12–24 h postdose and stored frozen at -20 °C until analysis. All animal procedures and treatments were carried out in accordance with approved animal licenses and guidelines issued by the British Home Office (Animals (Scientific Procedures) Act (1986)).

Sample Preparation. Urine. 100 μ L aliquots were taken from each time point for both animals and pooled to produce a 600 μ L, 0–24 h postdose sample for metabolite identification. A 600 μ L aliquot of predose urine was spiked with 1.5 μ L of the fenclazic acid stock solution (2 mM).

Bile. 100 μ L aliquots were taken from each time point for both animals and pooled to produce a 600 μ L, 0–24 h postdose sample for metabolite identification. A 600 μ L aliquot of predose bile was spiked with 1.5 μ L of the fenclazic acid stock solution (2 mM).

The spiked predose and pooled 0–24 h postdose urine and bile samples were centrifuged at ca. 12 000g for 5 min prior to analysis. The supernatants were transferred to an equal volume of ultrapurified distilled water in Waters HPLC 2 mL vials for LC-MS analyses.

Profiling and Structural Characterization of Metabolites by UPLC-LTQ-Orbitrap Mass Spectrometry. Accurate mass structural characterization work was acquired on a LTQ Orbitrap XL (Thermo Fisher Scientific, Bremen, Germany) connected to a Waters Acquity UPLC system. The Waters Acquity system (Waters, Milford, MA, USA) consisted of a binary UPLC Pump, column oven, a sample manager, and a photodiode array detector. Separation was carried out on a Waters BEH C18 (100 \times 2.1 mm, 1.7 μ M) (Waters, Milford,

MA, USA), preceded by a guard filter in a column oven at 50 °C. Two chromatographic methods were used.

Method 1. The mobile phase consisted of formic acid (0.1% in water, eluent A) and methanolic formic acid (0.1%, eluent B).

Method 2. The mobile phase consisted of ammonium acetate (5 mM, eluent A) and methanolic ammonium acetate (5 mM, eluent B). The elution profile for both methods was: An initial hold at 95% A and then a step from 95% to 80% A at 1.00 min, a linear gradient from 80% to 50% A at 1.01 to 15.00 min, a fast linear gradient from 50% to 2% A at 15.00 to 16 min, isocratic hold, 2% A from 16.00 to 17.00 min; re-equilibration at 95% A from 17.00 to 19.00 min. The flow rate was 0.45 mL/min, and the eluent was introduced into the mass spectrometer via the LTQ divert valve at 1 min. The injection volume was 20 μ L, and UV spectra were acquired over 190–330 nm. The LTQ-Orbitrap XL was equipped with an electrospray ionization (ESI) source which was operated in either positive or negative ion mode. Positive ion source settings were: Capillary temperature 300 °C, sheath gas flow 25, auxiliary gas flow 17, sweep gas flow 5, source voltage 3.5 kV, source current 100.0 μ A, capillary voltage 18 V, and tube lens 75.0 V. Full scan MS data were obtained over the mass range of 100 to 1200 Da. Negative ion source settings were capillary temperature 300 °C, sheath gas flow 25, auxiliary gas flow 17, sweep gas flow 5, source voltage 3.0 kV, source current 100.0 μ A, capillary voltage -1 V, and tube lens -128.3 V. Full scan MS data were obtained over the mass range of 100 to 1200 Da. Targeted MSMS experiments were acquired in the Orbitrap using higher energy collisional dissociation (HCD) fragmentation, isolation width 3 Da, normalized collision energy 60 eV, and activation time 30 ms. All Ion trap MSⁿ experiments were acquired using collision induced dissociation (CID), isolation width 3 Da, normalized collision energy 35 eV, and activation time 30 ms. All ions acquired in the Orbitrap were monitored at 7500 resolution fwhm (full width at half-maximum). LTQ and Orbitrap mass detectors were calibrated within 1 day of commencing the work using Proteomass LTQ/FT-Hybrid ESI positive mode calibration mix (Supelco, Bellefonte, USA).

Data Analysis. Mass spectrometric data were collected using Xcalibur version 2.1 (Thermo Fisher Scientific, Bremen, Germany). Components were identified as being derived from fenclazic acid by common fragments, isotopic pattern (chlorine), UV absorbance, and accurate mass. Comparisons with predose control samples spiked with fenclazic acid were conducted to minimize the potential for false positives from system impurities and endogenous components. All accurate mass measurements including the MSMS fragmentation were within ± 3 ppm of the theoretical accurate mass.

RESULTS

Structural Characterization of Fenclazic Acid. It is common practice to first fully characterize the structure of the drug/test compound with accurate mass MSMS fragmentation as they often contain structural motifs similar to those of their metabolites. Characteristic fragment ions identified from the drug can then be used to help elucidate metabolite structures. Where required, MSMS fragmentation experiments were undertaken in positive and negative ion mode to maximize structural elucidation of the metabolites.

In positive ion mode, fenclazic acid yielded a protonated molecular ion at $[M + H]^+$ 254.0037 Da (-1.00 ppm mass error) and showed a characteristic chlorine pattern. The proposed fragmentation pattern and LTQ Orbitrap HCD MSMS spectrum (Figure 1a) revealed 3 key fragment ions at m/z 207.9980

(corresponding to decarboxylation) and m/z 138.0105 and m/z 70.9951 (both representative of cleavage of the thiazole ring)

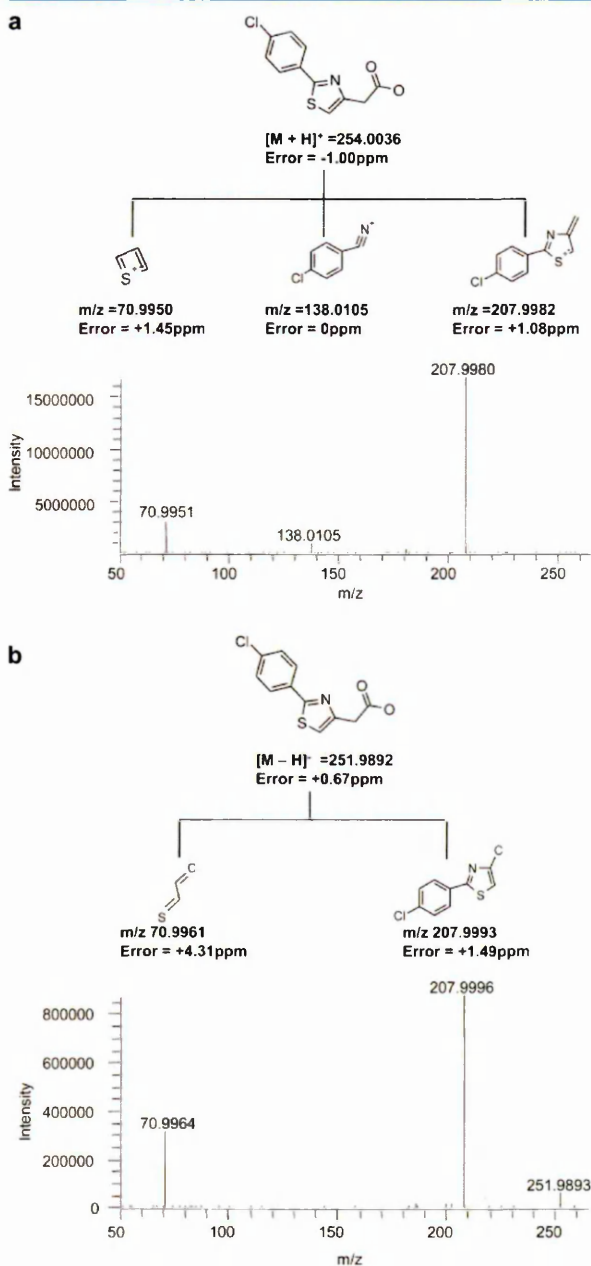


Figure 1. Accurate mass HCD MSMS positive ion (a) and negative ion (b) spectra of fenclozic acid and their associated fragmentation patterns with theoretical accurate mass shown below each structure.

In negative ion mode, fenclozic acid yielded a deprotonated molecular ion at $[M - H]^-$ 251.9893 Da (+0.67 ppm mass error) and showed a characteristic chlorine pattern. The proposed fragmentation pattern and LTQ Orbitrap HCD MSMS spectrum (Figure 1b) revealed 2 fragment ions m/z 207.9996 (corresponding to decarboxylation) and m/z 70.9964 (corresponding to a thiazole ring cleavage product).

Structural Characterization of the Urinary and Biliary Metabolites of Fenclozic Acid. Fenclozic acid was found to be

extensively metabolized in the rat. In total, 18 metabolites were detected and identified in bile and urine, of which 7 metabolites had not been identified previously, not including the multiple GSH related adducts (see Table 1).

Metabolite Formation via Direct Conjugation. Acylglucuronide Conjugate. The β -1-*O*-acylglucuronide conjugate of fenclozic acid (Table 1, M10) with $[M + H]^+$ 430.0352 (-1.38 ppm mass error) was detected in both the urine and bile samples with evidence of acyl migration products (Figure 2). The reactivity of acylglucuronide conjugates and the associated idiosyncratic toxicity is well documented in the literature,^{11,12} and as it has been observed previously by Pickup et al.,¹⁰ it will not be further characterized and discussed here.

Metabolite Formation via Coenzyme A. In this study, several conjugates were detected which are known to be formed through a coenzyme A intermediate,¹³ such as the carnitine, glutamyl, glycine, and taurine conjugates. The taurine and glycine metabolites have been detected and characterized previously by Foulkes,⁴ Newbould,⁵ and Pickup et al.¹⁰ The glutamyl conjugate has not been reported for fenclozic acid previously; however, it is a fairly common metabolite which is not associated with toxicity. In contrast, carnitine conjugation is not a common biotransformation for xenobiotics. More importantly, carnitine depletion has been associated with potential toxicity (i.e., valproic acid,^{14,15}), so it is characterized here.

Characterization of the Carnitine Conjugate. The carnitine metabolite (Table 1, M11) produced a protonated molecular ion with a characteristic chlorine pattern and an accurate mass of $[M + H]^+$ 397.0979 Da (Figure 3), consistent with carnitine conjugation (-1.09 ppm mass error). Accurate mass HCD fragmentation of $[M + H]^+$ 397.0979 Da (Figure 3) yielded four key fragment ions with m/z 338.0246 (resulting from loss of NC_3H_9), m/z 254.0033 (loss of carnitine), m/z 207.9981 (loss of CO_2 and carnitine), and m/z 144.1015 (characteristic of the carnitine ion).

The zwitterionic nature of the carnitine-metabolite was demonstrated in a brief experiment with two different mobile phase modifiers (formic acid, approximately pH 4.0 (LC method 1), and ammonium acetate, approximately pH 6.5 (LC method 2)). The difference in pH had no effect on the ionization state and therefore little effect on the retention time of the carnitine conjugate, based on its low pK_a (<3), compared to a change in the ionization state and retention characteristics of fenclozic acid, as shown in Figure 4.

Glutathione (GSH)-Related Conjugates Formed via Epoxidation. Several GSH-related conjugates were detected consistent with GSH, cysteine-glycine, cysteine, and N-acetylcysteine conjugation. For each of these conjugates, up to 4 isomers were detected (consisting of pairs of positional and diastomeric isomers). These adducts and isomers were formed via an epoxide intermediate which was confirmed by accurate mass MSMS fragmentation data to be on the chlorobenzene ring. The cysteine conjugate, the simplest representative of this class, is described here in detail.

Characterization of the Cysteine Conjugate. Multiple isomers were detected for the cysteine conjugate (M15, Figure 5) all of which generated identical fragmentation data. Positive as well as negative ion spectra were required to determine the site of metabolism, confirming the chlorobenzene ring to be both, the site of oxidation (+O) and cysteine conjugation.

In positive ion mode, a protonated molecular ion with a chlorine pattern and an accurate mass of $[M + H]^+$ 391.0192 Da was observed, which was consistent with cysteine conjugation

Table 1. Metabolites of Fenclozic Acid Identified in Rat Bile and Urine^a

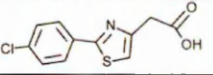
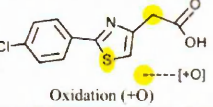
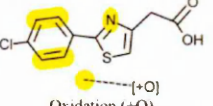
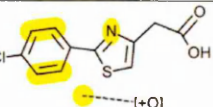
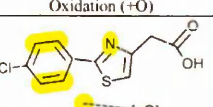
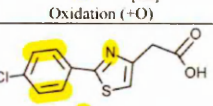
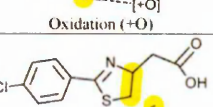
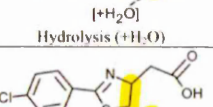
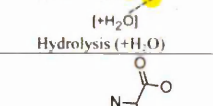
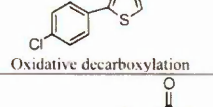
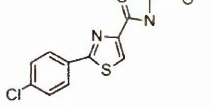
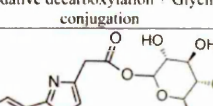
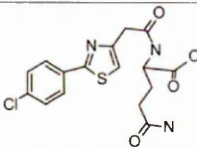
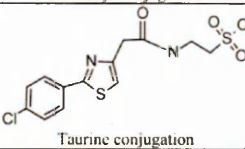
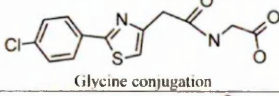
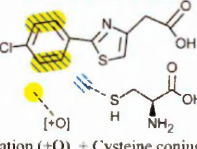
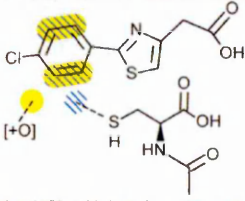
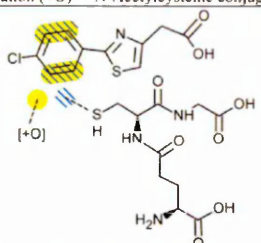
Metabolite	Matrix detected	Observed [M+H] ⁺ [M-H] ⁻	Structure/description	New	Key fragment ions observed (positive ion)
Fenclozic acid	Bile /Urine	254.0037 251.9892			70.9950 138.0105 207.9982
M1	Bile/Urine	269.9986 267.9841	 Oxidation (+O)	Yes	86.9905 114.9848 138.0105 154.9722 195.9982 223.9928
M2	Bile/Urine	269.9986 267.9841	 Oxidation (+O)		223.9931 154.0053 70.9950
M3	Bile/ Urine	269.9986 267.9841	 Oxidation (+O)		223.9930 154.0051 70.9949
M4	Urine	269.9986 267.9841	 Oxidation (+O)		223.9931 154.0056 70.9950
M5	Urine	269.9986 267.9841	 Oxidation (+O)		223.9932 154.0054 70.9950
M6	Bile/Urine	272.0128 ND	 Hydrolysis (+H ₂ O)	Yes	195.9982 154.9717 138.0105 89.0054
M7	Bile/Urine	272.0128 ND	 Hydrolysis (+H ₂ O)	Yes	195.9981 154.9717 138.0108 89.0055
M8	Bile/Urine	239.9877 ND	 Oxidative decarboxylation	Yes	221.9774 193.9824 150.0103
M9	Bile	297.0095	 Oxidative decarboxylation + Glycine conjugation	Yes	239.9883 221.9776 193.9828 150.0105
*M10	Bile/Urine	430.0352 ND	 Glucuronidation		207.9987 70.9947
M11	Bile/Urine	397.0979 ND	 Carnitine conjugation	Yes	338.0246 254.0033 297.9981 144.1015

Table 1. continued

Metabolite	Matrix detected	Observed $[M+H]^+$ $[M-H]^-$	Structure/description	New	Key fragment ions observed (positive ion)
M12	Bile	382.0621 ND	 Glutamyl conjugation	Yes	235.9931 207.9882 130.0499 84.0444 70.9950
M13	Bile/Urine	361.0077 ND	 Taurine conjugation		279.0353 235.9939 126.0219
M14	Bile	311.0252 ND	 Glycine conjugation		265.0195 235.9932 207.998
*M15	Bile/Urine	391.0192 389.0035	 Oxidation (+O) + Cysteine conjugation	Yes	70.9951 154.0056 194.0094 207.9985 222.0045 223.9937 283.9603
*M16	Bile	448.0398 446.0254	 Oxidation (+O) + Cysteinylglycine conjugation	Yes	283.9601 223.9935 194.0094 154.0044 70.9950
*M17	Bile	433.0294 431.0144	 Oxidation (+O) + N-Acetylcysteine conjugation	Yes	415.0190 223.9935 154.0054 70.9950
*M18	Bile	577.0830 575.0679	 Oxidation (+O) + Glutathione conjugation	Yes	448.0404 373.0083 354.9978 283.9603 177.0335 154.0042 130.0506

*Note: M6 and M7 are potentially diastereoisomers. * denotes the presence of positional and diastereoisomers. New = not previously identified in published data.

(2.13 ppm mass error). The accurate mass HCD fragmentation of $[M + H]^+$ 391.0192 Da (Figure 5a) yielded several diagnostic ions with one key fragment at m/z 154.0056 (equivalent to the m/z 138.0105 +O product of fenclazac acid) which confirmed oxidation on the chlorobenzene ring.

In negative ion mode, a molecular ion of $[M - H]^-$ 389.0037 Da (Figure 5b) was observed, which was consistent with cysteine conjugation (0 ppm mass error). The accurate mass HCD fragmentation of $[M - H]^-$ 389.0037 Da (Figure 5b) yielded 3 key fragment ions at m/z 283.9610, a characteristic fragment of GSH-related conjugates, corresponding to cleavage of the

cysteine leaving the thiol attached to chlorobenzene ring. The fragment ions at m/z 239.9710 and at m/z 167.9678 are representative of decarboxylation and thiazole ring cleavage, respectively, while preserving the thiol-chlorobenzene ring.

Characterization of the GSH-Related Metabolites, Epoxide, and Isomer Formation. The key fragments at m/z 167 (in negative ion) and m/z 154 (in positive ion) were present in all the GSH-related conjugates. This suggests that they were all formed through bioactivation via oxidation of the chlorobenzene ring forming an epoxide intermediate, followed by GSH addition

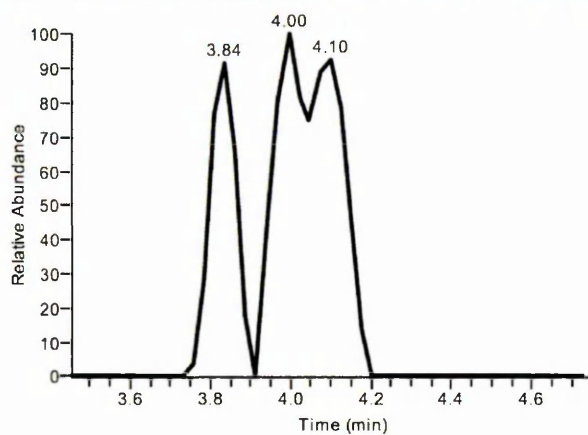


Figure 2. LCMS selected ion (m/z 430.0352) mass chromatogram showing partially resolved transacylated products of fenclozic acid acylglucuronide.

and subsequent metabolism/degradation to the cysteine–glycine, cysteine, and finally acetylation to the N-acetylcysteine.

Up to four LCMS peaks were detected for each of the GSH-related conjugates with literally identical accurate masses (within ± 2 ppm mass error). In each case, the chlorobenzene ring was identified as the site of conjugation based on the accurate mass MSMS data, confirming that the cysteine–glycine, cysteine–glycine, and N-acetylcysteine were derived from the same GSH adduct.

As an example, the cysteine conjugate, the simplest representative of the GSH family, showed three distinct chromatographic peaks and a very minor fourth peak for which MSMS fragmentation was not possible, although the accurate mass was within ± 5 ppm. Following epoxidation of the chlorobenzene ring and subsequent conjugation with GSH, a

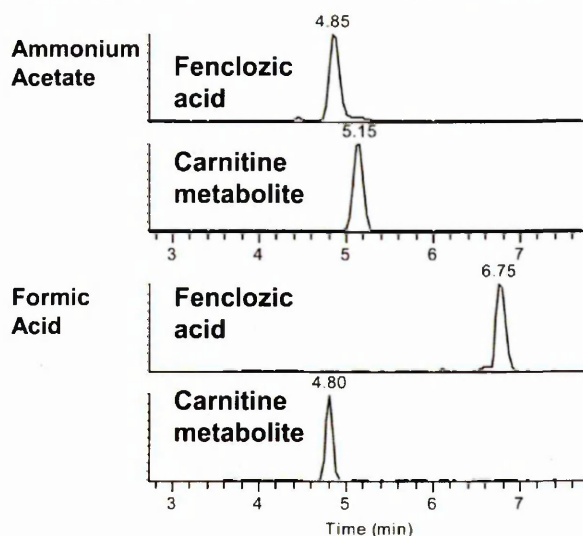


Figure 4. Selected ion mass chromatograms for fenclozic acid and the carnitine metabolite (M11) with LC method 2 at pH 6.5 (top) and LC method 1 at pH 4 (bottom).

pair of diastereoisomers and two positional isomers are formed which can be separated chromatographically (Figure 6). Overall, up to 16 GSH-related products were formed from the single epoxide reactive intermediate, with four GSH-related conjugates (GSH, cysteine–glycine, cysteine, and N-acetylcysteine) and up to four isomers for each (consisting of positional isomers and diastereoisomers).

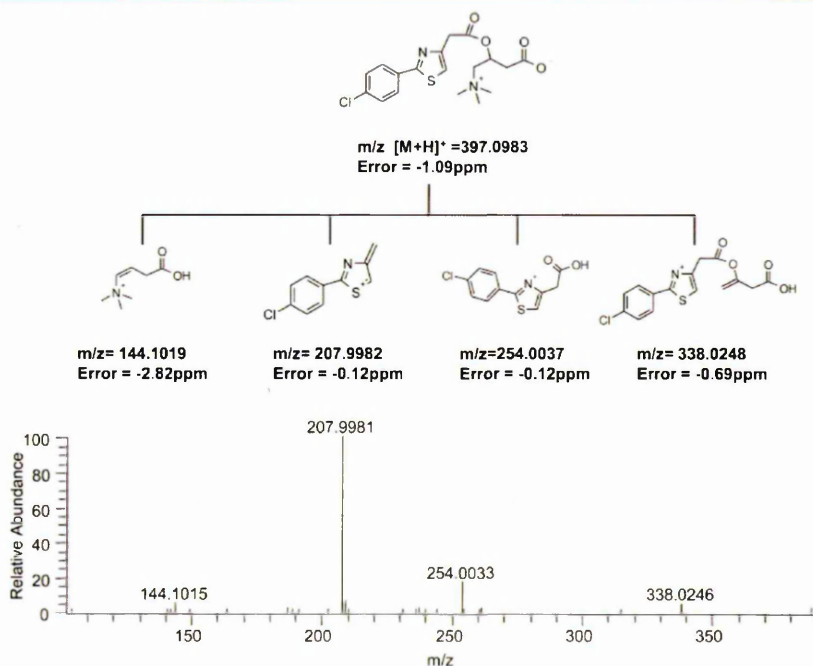


Figure 3. Accurate mass HCD MSMS spectrum of the carnitine metabolite (M11) in positive ion mode and its associated fragmentation pattern with theoretical accurate mass shown below each structure.

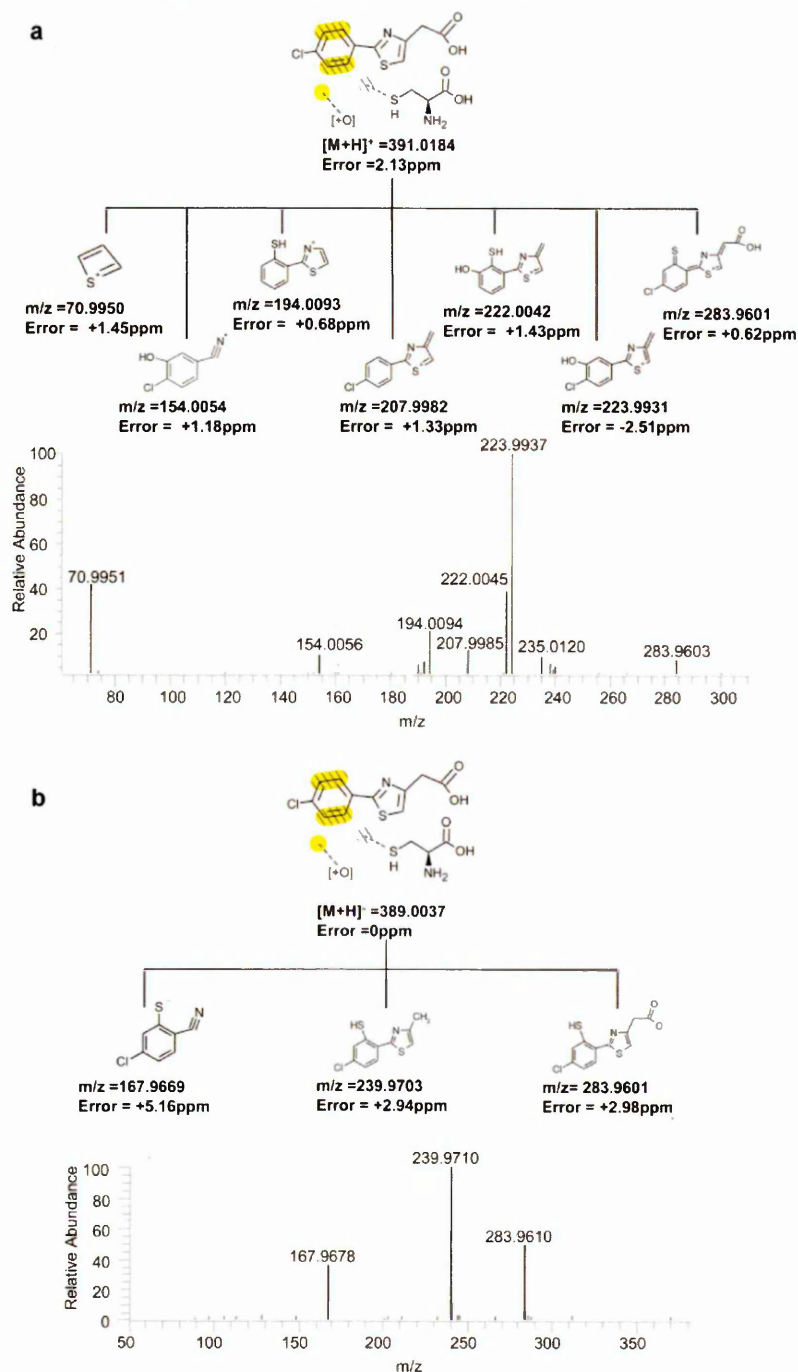


Figure 5. Accurate mass HCD MSMS spectra and fragmentation patterns with theoretical accurate mass shown below each structure for the cysteine metabolite (M15) of fenclazac acid, acquired in positive ion mode (a) and negative ion mode (b). Note: The exact positions of the OH- and cysteine-substituents on the benzyl-ring of the fragment ions are not confirmed.

DISCUSSION

This study has demonstrated that fenclazac acid is extensively metabolized in the BDC rat, with a total of 18 metabolites detected and identified, exclusive of the multiple GSH-related conjugate isomers. Several previously unreported metabolites were identified including a carnitine conjugate as well as a series of GSH-related adducts formed through bioactivation of the chlorobenzene ring via epoxidation.

The *in vivo* metabolite identification studies conducted in the rat by Foulkes⁴ and by Bradbury⁹ showed fairly extensive metabolism of fenclazac acid. Foulkes⁴ reported 7 metabolites, including 4 oxidation products on the chlorobenzene ring (including an oxidative dechlorination product), an acylglucuronide, a taurine, and a reductive decarboxylation product. Bradbury⁹ reported an increase in taurine conjugation when the dose was increased from 2 to 100 mg/kg. There is a significant

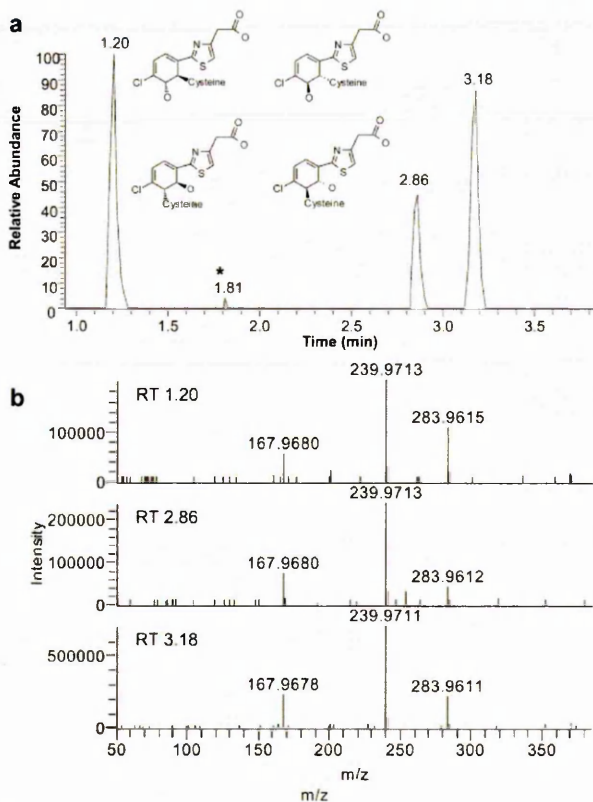


Figure 6. Cysteine conjugate with the structures of the four isomers (consisting of positional and diastereoisomers) formed upon conjugation. The MS selected chromatogram (a) shows 3 major peaks/isomers, with the 4th isomer present at trace level*. Accurate mass HCD MSMS spectra of the 3 main cysteine conjugate isomer MS peaks are shown (b). Note: the cysteine serves as a representative of the GSH family (GSH, cysteine–glycine, cysteine, and N-acetylcysteine).

difference in the number and type of metabolites identified between these studies and those reported in this paper. A simple explanation for the differences observed could be the harsh extraction and chromatographic conditions employed by both groups. Foulkes⁴ extracted metabolites from urine samples with chloroform or a mixture of methylene chloride/chloroform at pH 4.5 initially and then adjusted the aqueous phase (the residual urine) to pH 2 and re-extracted with the same solvents. The bile was either diluted with water and applied directly to TLC plates or extracted as described for urine. Bradbury et al.⁹ used freeze-drying then extraction with MeOH before concentrating the sample using rotary evaporation. All extracts were applied to TLC plates and subjected to a variety of solvents including isopropanol, water/ammonia, butan-1-ol, chloroform, and acetic acid. These extraction and chromatographic conditions are far harsher than those used in this study, as the bile and urine samples were simply diluted with water and injected on to a reverse phase column with mobile phase systems consisting of MeOH buffered with either formic acid (0.1%, v/v) or ammonium acetate (5 mM, w/v).

Foulkes⁴ reported a reductive decarboxylation metabolite but also described photochemical degradation of fenclozic acid to the reductive decarboxylation product when extracted into dilute chloroform. As no reductive decarboxylation product was

detected in this study, it is likely that this metabolite was an analytical artifact.

Foulkes and Bradbury did not detect any GSH-related adducts in their *in vivo* studies in the rat (or in any animal species), while our *in vivo* study in the rat did confirm their presence. This would suggest that the analytical methodology applied during the development of fenclozic acid was unsuitable for the detection of GSH adducts.

It is plausible that under the harsh conditions applied in the previous analyses the GSH-related conjugates could have degraded to the oxidative dechlorination product, which was not detected in this study. Apart from the differences in sample preparation procedures, the vastly improved chromatography and sensitivity of modern Fourier transform-mass spectrometers undoubtedly aided the detection of the larger number of metabolites described here in this study. Only one *in vivo* study has been conducted on fenclozic acid in recent years¹⁰ with hepatic CYP reductase null (HRN) mice which lack functional hepatic cytochrome P450, leading to the formation of conjugated metabolites only. The team did not uncover any additional phase II/conjugated metabolites to those reported by Foulkes⁴ and Bradbury.⁹

Here, in this study, 7 additional metabolites (not including the multiple GSH-related adducts) were identified that had not been reported in any of the previous studies, which include a carnitine conjugate, additional oxidation products, and additional amino acid conjugates (see Table 1). The amino acid, taurine, and carnitine conjugates imply the formation of a coenzyme A intermediate. This potentially reactive intermediate has been associated with the toxicity of carboxylic acid-containing xenobiotics and could explain the observed toxicity of fenclozic acid in the clinic. However, as the coenzyme A thioester is not formed in rat, human, and dog microsomal incubations, it cannot be responsible for the covalent protein binding observed by Rodrigues et al.³ Likewise, the detection of an acylglucuronide metabolite, which showed evidence of acyl migration in both rat urine and bile samples, is a potential contributor to the toxicity observed in humans. The reactivity of acyl glucuronides and the associated protein binding (Hapten hypothesis) and idiosyncratic toxicity is well documented in the literature.^{11,12} However, as with the potential coenzyme A intermediate, it could not be formed in the microsomal incubations (due to a lack of active UGT) and, hence, cannot contribute to the covalent binding observed in the microsomal incubations.

In contrast, the observed bioactivation via epoxidation on the chlorobenzene ring is likely to be responsible for the NADPH dependent covalent binding in microsomes. Yet, the covalent binding studies conducted by Rodrigues et al.,³ which included GSH and cysteine microsomes trapping experiments, contradict this theory. If the epoxide reactive intermediate was the cause of covalent binding, then a GSH adduct should have been detected. However, fenclozic acid was shown to have very little metabolic turnover in the microsomal experiments as no metabolites were detected by radiochemical detection following the 2 h incubation period, supported by measurements of the intrinsic clearance of fenclozic acid in HLMs (measured $Cl_{int} < 3$ ($\mu\text{L}/\text{mL}/\text{mg}$), unpublished data). It is therefore possible that epoxide intermediate formation was low, which in combination with the formation of 4 isomers (consisting of positional and diastereoisomers) upon GSH conjugation suggests that the GSH-derived metabolites were likely not present at sufficiently high concentrations to be detected even by top-end mass spectrometers.

This is one of the problems facing current reactive metabolite screening strategies which are often focused on eliminating potential problematic compounds with medium to high *in vitro* metabolic turnover. While improvements have been made in analytical technology which enables better detection of metabolites, the current *in vitro* techniques to aid reactive metabolite detection such as GSH trapping in human liver microsomes still require refining especially for compounds with very low *in vitro* metabolic clearance.

CONCLUSION

After careful consideration of the data generated in this study, in comparison to all the data from previous literature, we propose the reactive epoxide intermediate/metabolite to be the agent responsible for the observed covalent binding in rat microsomes and likely the cause of covalent binding in human microsomes. While the intact GSH adducts were not detected previously in human or any other species *in vivo*,⁴ the identification of oxidation metabolites on the chloro-benzene ring, identified here and by Foulkes,⁴ is consistent with the formation of an epoxide intermediate. It is also important to note that the analytical approach by Foulkes was not suitable for the detection of GSH or the GSH-related adducts. This is in contrast to the recent *in vitro* microsomal GSH trapping work by Rodrigues et al.,³ where the lack of detection of the GSH adducts could be attributed to the very slow *in vitro* metabolic turnover of fenclozic acid.

The observed covalent binding in human and rat microsomes could also not be attributed to the formation of the acylglucuronide or thioester, as these metabolites are not generated in microsomes (which produce exclusively phase I metabolites). It is plausible that they contributed to or caused the observed toxicity in the clinic; however, the acylglucuronide and amino acid conjugates (indicating the formation of a coenzyme A thioester) were also detected in rat and dog where no significant toxicity was observed.

Hepatotoxicity was not prevalent in any of the preclinical species. It is therefore possible that the biotransformation to the epoxide intermediate is a minor metabolic pathway in the rat or that it is more efficiently detoxified by GSH than in humans.

Hence, we propose that the observed covalent binding in rat and human microsomes together with the GSH metabolites detected in the rat (predominantly in the bile samples) are an indicator for the cause of the observed hepatotoxicity in the clinic. Unfortunately, without dosing humans and collecting excreta for metabolite identification studies, direct comparisons cannot be made.

ASSOCIATED CONTENT

Supporting Information

Detailed table of fragment ions from all fenclozic acid metabolites, including their theoretical accurate mass, molecular formula, and proposed structure. This material is available free of charge via the Internet at <http://pubs.acs.org>.

AUTHOR INFORMATION

Corresponding Author

*Tel. +44-1625-518479. Fax: +44-1625-230614. E-mail: Scott.Martin2@astrazeneca.com.

Notes

The authors declare no competing financial interest.

REFERENCES

- (1) Chalmers, T.; Kellgren, J.; Platt, D. *Ann. Rheum. Dis.* **1969**, *28*, 595–601.
- (2) Chalmers, T. M.; Pohl, J. E.; Platt, D. S. *Ann. Rheum. Dis.* **1969**, *28*, 590–594.
- (3) Rodrigues, A. V.; Rollison, H. E.; Martin, S.; Sarda, S.; Schulz-Utermoehl, T.; Stahl, S.; Gustafsson, F.; Eakins, J.; Kenna, J. G.; Wilson, I. D. *Arch. Toxicol.* **2013**, *87*, 1569–1579.
- (4) Foulkes, D. M. *J. Pharmacol. Exp. Ther.* **1970**, *172*, 115–121.
- (5) Newbould, B. *Br. J. Pharmacol.* **1969**, *35*, 487–497.
- (6) Hart, F. D.; Bain, L. S.; Huskisson, E.; Littler, T.; Taylor, R. *Ann. Rheum. Dis.* **1970**, *29*, 684.
- (7) Alcock, S. J. *Proc. Eur. Soc. Study Drug Toxic.* **1971**, *12*, 184–190.
- (8) Thompson, R. A.; Isin, E. M.; Li, Y.; Weidolf, L.; Page, K.; Wilson, I.; Swallow, S.; Middleton, B.; Stahl, S.; Foster, A. J. *Chem. Res. Toxicol.* **2012**, *25*, 1616–1632.
- (9) Bradbury, A.; Powell, G.; Curtis, C.; Rhodes, C. *Xenobiotica* **1981**, *11*, 665–674.
- (10) Pickup, K.; Wills, J.; Rodrigues, A.; Jones, H. B.; Page, C.; Martin, S.; Sarda, S.; Wilson, I. *Xenobiotica* **2014**, *44*, 164–173.
- (11) Bailey, M. J.; Dickinson, R. G. *Chem. Biol. Interact.* **2003**, *145*, 117–137.
- (12) U.S. FDA. *Guidance for Industry: Safety Testing of Drug Metabolites*; U.S. FDA: Rockville, MD, 2008.
- (13) Skonberg, C.; Olsen, J.; Madsen, K. G.; Hansen, S. H.; Grillo, M. P. *Expert Opin. Drug Metab. Toxicol.* **2008**, *4*, 425–438.
- (14) Van Wouwe, J. P. *Int. J. Vitam. Nutr. Res.* **1995**, *65*, 211–214.
- (15) Raskind, J. Y.; El-Chaar, G. M. *Ann. Pharmacother.* **2000**, *34*, 630–638.

**4. REACTION OF HOMOPIPERAZINE WITH ENDOGENOUS
FORMALDEHYDE: A CARBON HYDROGEN ADDITION
METABOLITE/PRODUCT IDENTIFIED IN RAT URINE AND BLOOD**

Reprinted with permission of the American society for Pharmacology and Experimental therapeutics. All rights reserved.

Reaction of Homopiperazine with Endogenous Formaldehyde: A Carbon Hydrogen Addition Metabolite/Product Identified in Rat Urine and Blood

Scott Martin, Eva M. Lenz, Dave Temesi, Martin Wild, and Malcolm R. Clench

DMPK Department, Alderley Park, AstraZeneca UK Ltd., Macclesfield, Cheshire, United Kingdom (S.M., E.M.L., D.T., M.W.); and Biomedical Research Centre, Sheffield Hallam University, Sheffield, United Kingdom (M.R.C.)

Received February 3, 2012; accepted May 1, 2012

ABSTRACT:

Drug reactivity and bioactivation are of major concern to the development of potential drug candidates in the pharmaceutical industry (*Chem Res Toxicol* 17:3-16, 2004; *Chem Res Toxicol* 19:889-893, 2006). Identifying potentially problematic compounds as soon as possible in the discovery process is of great importance, so often early *in vitro* screening is used to speed up attrition. Identification of reactive moieties is relatively straightforward with appropriate *in vitro* trapping experiments; however, on occasion unexpected reactive intermediates can be found later during more detailed *in vivo* studies. Here, we present one such example involving a series of compounds from an early drug discovery cam-

paign. These compounds were found to react with endogenous formaldehyde from a rat *in vivo* study, resulting in the formation of novel +13-Da bridged homopiperazine products (equivalent to the addition of one carbon and one hydrogen atom), which were detected in urine and blood. The identification of these +13-Da products and their origin and mechanism of formation are described in detail through analyses of a representative homopiperazine compound [*N*-(3-(3-fluorophenyl)-1,2,4-thiadiazol-5-yl)-4-(4-isopropyl-1,4-diaze-pane-2-carbonyl)piperazine-1-carboxamide (AZX)] by liquid chromatography-UV-mass spectrometry, ¹H NMR, and chemical tests.

Introduction

Understanding the metabolic fate of putative drug candidates both *in vitro* and *in vivo* is a key component of drug discovery. Rapid production of early information describing the rate of clearance and site of metabolism is essential for directing iterative synthetic chemistry make-test cycles toward promising structural templates with the requisite properties for an effective drug.

Reactive drug metabolites are of great concern in the pharmaceutical industry (Evans et al., 2004; Baillie 2006, 2009). Although their identification is relatively straightforward with appropriate *in vitro* trapping experiments, sometimes additional reactive compounds are found unexpectedly. In general, early metabolism studies involve incubation in hepatocytes or microsomes to mimic the most prevalent metabolic processes occurring in the liver. Incubate samples at *t* = 0 min and at a terminal time point (usually 30-60 min) are then compared by LC-UV-MS/MS. These studies can be both challenging and time-consuming even when only a small number of metabolites are identified. Simply mining the raw data to find the metabolites in the terminal sample often requires the use of a variety of techniques, ranging from simple UV comparison to complex common fragment searching (commonly referred to as broad band or MS²) or the use of

sophisticated MS subtraction routines such as mass defect filtering. Experiments are therefore normally performed using state-of-the-art instruments offering a variety of options to aid detection and structure identification. The information is then used to direct and modify the chemistry toward compounds with favorable metabolic properties.

Improved understanding of bioactivation mechanisms, reactive intermediate formation (so-called reactive metabolites), and adverse toxicity has led to the front loading of biotransformation studies. In response, most pharmaceutical companies now employ reactive metabolite trapping screens using liver microsomes (usually human) fortified with nucleophiles such as GSH, cysteine, KCN, and methoxylamine (Prakash et al., 2008). The nucleophiles trap reactive electrophilic species at sufficient concentration to favor the formation of a stable product identified by their unique MS/MS spectral characteristics. Both early site of metabolism and reactive metabolite trapping studies rely on *in vitro* systems to generate the metabolites. However, metabolites can also be formed in complete biological systems, which could be missed if the metabolic pathways are unknown and/or the endogenous reagents are not represented in these *in vitro* systems. Hence, in our laboratories potential drug candidates undergo nonradiolabeled *in vivo* metabolite identification studies. These generally involve either a bile duct-cannulated study in rats, with collection of urine and bile over a 24-h period or collection of blood and urine from a high-dose rat pharmacokinetic study. The studies aid the identification of the excreted metabolites and ensure

Article, publication date, and citation information can be found at <http://dmd.aspetjournals.org>.
<http://dx.doi.org/10.1124/dmd.112.044917>.

ABBREVIATIONS: LC, liquid chromatography; MS/MS, tandem mass spectrometry; MS, mass spectrometry; AZX, *N*-(3-(3-fluorophenyl)-1,2,4-thiadiazol-5-yl)-4-(4-isopropyl-1,4-diaze-pane-2-carbonyl)piperazine-1-carboxamide; ACN, acetonitrile; MeOH, methanol; UPLC, ultra high-performance liquid chromatography; ESI, electrospray ionization; HCD, higher energy collisional dissociation; COSY, correlation spectroscopy; ROESY, rotating frame Overhauser effect spectroscopy; +ESI, positive ion electrospray ionization; RT, retention time.

identification of any unexpected reactive metabolites not generated or detected in the preliminary *in vitro* systems.

During recent rat *in vivo* metabolite identification studies with a series of lead compounds, cyclized GSH adducts were detected, similar to those reported by Doss et al. (2005), highlighting a potential reactive metabolite alert. This alert was not raised in the conventional GSH trapping screen, because of the type of the GSH rearrangement (data not shown). The reactophore in these lead compounds consisted of a terminal piperazine, which was responsible for this bioactivation. To preserve the potency of the compounds and remove the reactive metabolite risk, the chemistry was changed to a homopiperazine series.

Hence, several promising homopiperazine compounds from this series were dosed to rats to assess whether these GSH adducts were also formed. Instead, the analyses led to the observation of unusual, novel products with a molecular weight gain of 13 Da (while showing an apparent increase of +12 Da by mass spectrometry) as the major parent-related material in the urine and blood samples, which were not detected in the preliminary *in vitro* studies. The formation of these products, referred to as *N*-(3-(3-fluorophenyl)-1,2,4-thiadiazol-5-yl)-4-(4-isopropyl-1,4-diaza-panc-2-carbonyl)piperazine-1-carboxamide (AZX) + 13 throughout, is subject to further investigation in this article, with compound AZX (Fig. 1) as a representative structure for the "homopiperazine series."

Materials and Methods

Chemicals and Suppliers. Compound AZX was synthesized and developed at AstraZeneca UK Ltd. (Macclesfield, UK). Acetonitrile (ACN), meth-

anol (MeOH), ammonium acetate (analytical reagent grade), and formic acid were acquired from Thermo Fisher Scientific (Loughborough, UK). Potassium cyanide, formaldehyde (37% in H₂O), and the deuterated NMR solvents were sourced from Sigma-Aldrich (Poole, UK).

Standard/Stock Solutions. *AZX stock solution.* AZX was dissolved in MeOH at a concentration of 200 μ M.

AZX test solution. AZX was dissolved in MeOH/water (30:70%, v/v) to a concentration of 10 μ M. The test solution was prepared from the stock solution. (Equivalent stock and test solutions were prepared in ACN to assess whether MeOH was a contributing factor in AZX + 13 formation.)

Formaldehyde. Formaldehyde (37% in H₂O) was used undiluted in all spiking experiments.

KCN. KCN was prepared in water to a concentration of 50 mM.

Animal Dosing and Sample Collection (Urine and Blood). *Dosing solution.* AZX was prepared in a formulation of dimethylamine-water (40:60, v/v) at a concentration of 1 mg/ml.

Rats. Male Han Wistar rats ($n = 4$) were divided into two groups ($n = 2$ /group), each receiving a single dose of AZX at 2 mg/kg i.v. at a dose volume of 2 ml/kg. Urine was collected predose and at 0 to 6, 6 to 12, and 12 to 24 h from group 1, whereas group 2 provided blood via the tail vein predose and at 20 min, 1.5 h, 6 h (at a volume of 0.3 ml), and finally 24 h (at a volume of 1.3 ml). Rat urine and blood were stored frozen at -20°C until further analysis. Additional predose/control rat urine samples were provided on request, throughout the study.

Sample Preparation. *Urine.* Urine samples (0–24 h postdose) were pooled using a set volume (100- μ l aliquots) from each time point before analysis. Predose urine (190- and 90- μ l aliquots) was spiked with 10 μ l of the AZX stock solution (200 μ M) to give a final concentration of 10 and 20 μ M, respectively. Both the predose and 0 to 24 h urine samples were centrifuged at approximately 12,000g for 5 min before analysis. The supernatant was then

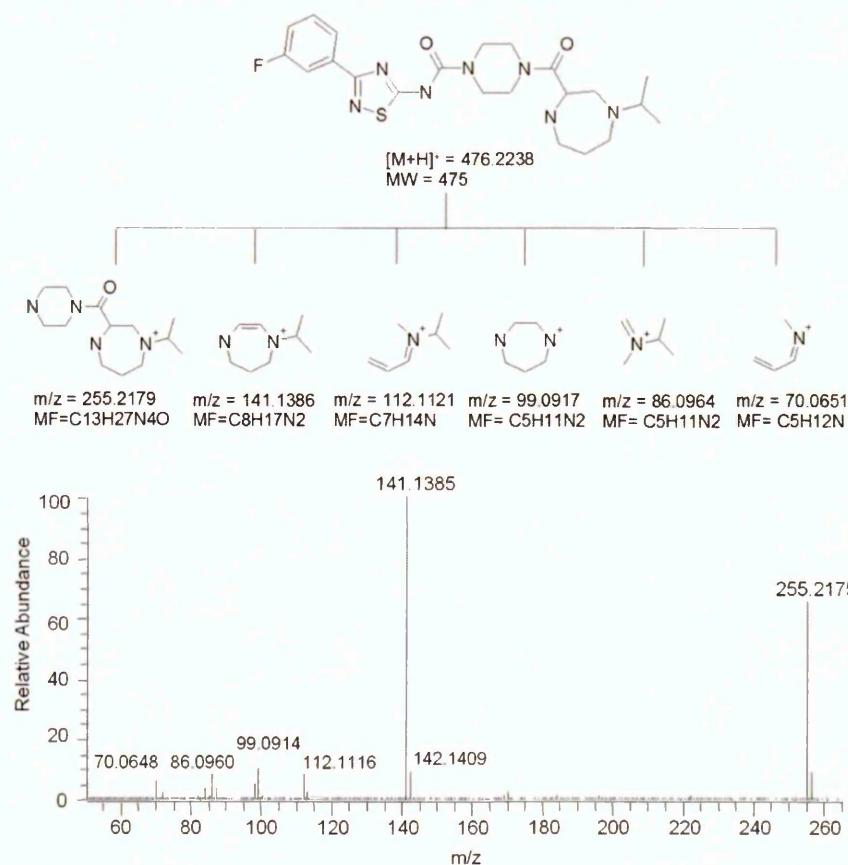


FIG. 1. Proposed LTQ Orbitrap collision cell fragmentation of compound AZX (top) with accurate mass spectrum (bottom). MW, molecular weight; MF, molecular formula.

transferred to Agilent high-performance liquid chromatography 2-ml vials with 200- μ l inserts for LC-MS analysis.

Blood. Blood samples (0–24 h postdose) were pooled using a set volume (50- μ l aliquots) from each time point. Blank/predose rat blood was spiked with 10 μ l of the AZX stock solution (200 μ M). Both the predose/blank and 0 to 24 h blood were diluted 1:1 with H₂O and quenched with chilled (4°C) ACN (1:3, v/v) followed by centrifugation at 12,000g for 5 min, and the supernatant was transferred to Agilent high-performance liquid chromatography 2-ml vials for LC-MS analysis.

Formaldehyde Addition. The formaldehyde-spiked AZX test solution was prepared by adding 10 μ l of formaldehyde (37% in water) to 500 μ l of the AZX test solution (10 μ M, MeOH/H₂O, 30:70, v/v) and analyzed by LC-MS immediately.

Potassium Trapping Experiments. Ten-microliter aliquots of the KCN solution (50 mM KCN/water) were added to a) 90 μ l of the 0 to 24 h rat urine pool, b) 90 μ l of predose rat urine, which was spiked with 10 μ l of AZX (200 μ M, i.e., the stock solution) to give a final concentration of 20 μ M, and c) 90 μ l of the formaldehyde-spiked AZX test solution (detailed above). Both the urine samples and the formaldehyde-spiked AZX test solution were left at room temperature for 24 h before injection onto the LC-MS system.

Preparation of NMR Samples. Here, a more concentrated solution of AZX was prepared, at a concentration of 1 mM in ACN. For NMR spectroscopy, three solutions were prepared: a) 2 ml of AZX/ACN (1 mM); b) solution a with 100 μ l of formaldehyde (37% in H₂O); and c) 1 ml of solution b with 100 μ l of KCN (50 mM). Each of the solutions was stored for 24 h (to allow complete formation of the products) before evaporation of the solvents. The solvents were evaporated under nitrogen; each sample was freeze-dried and reconstituted in 200 μ l of MeOH-d₄ for ¹H NMR spectroscopic analysis.

Identification and Structural Characterization of AZX + 13 by UPLC-LTQ Orbitrap. Accurate mass structural characterization was acquired on a LTQ Orbitrap XL connected to a Waters Acquity UPLC system. The Waters Acquity system consisted of a binary UPLC PUMP, a column oven, an autoinjector, and a photodiode array detector. Separations were performed out on a Kinetix C18 column (100 \times 2.0 mm, 2.6 μ m; Phenomenex, Macclesfield, UK) preceded by a guard filter in a column oven at 50°C. The mobile phase consisted of different solvent systems to assess the contribution of solvent/buffer/acidifier to the AZX + 13 formation: 1) ammonium acetate (5 mM, eluent A) and methanolic ammonium acetate (5 mM, eluent B) and 2) formic acid (0.1%, eluent A) and formic acid/ACN (0.1%, eluent B).

The AZX stock and test solution were found to be stable in both mobile phase systems. For the in vivo samples, the AZX + 13 product was detected at approximately the same concentrations in either solvent system used. Hence, solvent system 1 was subsequently used routinely.

The elution profile was linear gradient 90% A to 10% A, 0.00 to 8.00 min; isocratic hold, 10% A 8.00 to 10.00 min; and reequilibration 90% A, 10.01 to 13.00 min. The flow rate was 0.6 ml/min, and the eluent was introduced into the mass spectrometer via the LTQ divert valve at 1 min. The injection volume was 20 μ l, and UV spectra were acquired over 190 to 330 nm. The LTQ Orbitrap XL was equipped with an electrospray ionization (ESI) source (Thermo Fisher Scientific, Bremen, Germany), which was operated in positive mode. Source settings were as follows: capillary temperature, 350°C; sheath gas flow, 25; auxiliary gas flow, 17; sweep gas flow, 5; source voltage, 3.5 kV; source current, 100.0 μ A; capillary voltage, 18 V; and tube lens, 75.0 V. Full-scan MS data were obtained over the mass range of 100 to 1000 Da at a peak resolution of 7500. Targeted MS/MS experiments were acquired using higher energy collisional dissociation (HCD) fragmentation, isolation width 2 Da, normalized collision energy 45, and activation time 30 ms. HCD fragment ions were monitored by the Orbitrap using 7500 resolution. LTQ and Orbitrap mass detectors were calibrated within 1 day of commencing the work using ProteoMass LTQ/FT-Hybrid ESI positive mode calibration mix (Supelco, Bellefonte, PA).

¹H NMR Spectroscopy for Structure Verification. ¹H NMR analyses were performed to confirm and structurally characterize AZX + 13 and the AZX + 13 + CN adduct. ¹H NMR data were acquired on a Bruker AVANCE 600 MHz spectrometer, operating at 600.13 MHz ¹H resonance frequency. The NMR spectrometer was equipped with a 2.5-mm SE1 ¹H/¹⁹F probe.

One-dimensional ¹H NMR spectra of substrate and product were acquired without solvent suppression into 65K data points over a spectral width of

12,376 Hz, resulting in an acquisition time of 2.64 s. A relaxation delay of 2.4 s was used to ensure T1 relaxation between successive scans and, depending on concentration, approximately 64 to 512 scans were acquired per sample.

Two-dimensional ¹H-¹H COSY (gradient enhanced; Bruker Biospin Ltd., Coventry, UK) experiments were used on the samples to determine signal connectivities. Here, spectra were acquired into 4K data points in F2, and 128 increments in F1. The spectral width was set to 8012 Hz, resulting in an acquisition time of 0.26 s. A relaxation delay of 1.5 s was used between successive scans; 128 increments were acquired in F1, consisting of four scans each. Before Fourier transformation, the data were apodized with a sine bell window function, linearly predicted to 512 data points and zero-filled in F1 to 1024 data points. Selective excitation experiments were performed to confirm the structure of the AZX + 13 + CN adduct.

A one-dimensional selective ROESY experiment (selrogp; Bruker Biospin Ltd.) was performed. The data were collected into 65K data points, over a spectral width of 12,019 Hz, resulting in an acquisition time of 2.77 s. A relaxation delay of 2.4 s was used and a spin lock time of 100 ms.

Results

Structural Characterization of Compound AZX. Test compounds often contain structural motifs similar to those of their metabolites; it is therefore common practice to first fully characterize the structure of the test/parent compound with accurate mass MS/MS fragmentation. Characteristic fragment ions identified from the test compound MS/MS can then be used to find and elucidate metabolite structures.

Analysis of AZX by LC-UV-MS-MS/MS yielded a protonated molecular ion with an accurate mass of [M + H]⁺ 476.2243 (+0.9 ppm). The proposed fragmentation pattern and LTQ Orbitrap HCD MS/MS spectrum of compound AZX (Fig. 1) revealed two intense key fragments, *m/z* 255.2175 (corresponding to the loss of the fluorophenyl-thiadiazol group of AZX) and *m/z* 141.1385 (corresponding to the homopiperazine isopropyl moiety).

Detection of the Novel Metabolite with *m/z* 488 (AZX + 13) in the In Vivo Samples. Typically, in early in vivo metabolite identification studies, temporal blood and urine samples are typically combined to obtain a single pooled sample for each matrix. The sample is then analyzed on a LC-UV-MS/MS system in conjunction with a predose sample spiked with analyte to obtain a final concentration of 10 μ M (a concentration shown to produce a discernible UV response in the biological matrix).

Spiking of the predose serves two purposes: it helps to rule out synthetic impurities that could be misinterpreted as metabolites and to discount endogenous material visually or by automated data subtraction.

In this study, only low levels of compound AZX were detected upon analysis by UPLC-UV-MS/MS in both the 0 to 24 h rat urine-pooled sample and the AZX-spiked predose urine sample. However, an unexpected major parent-related peak was detected with a molecular ion of *m/z* 488. This observation was confirmed by respiking of parent compound into samples of fresh predose/control urine (representing final AZX concentrations of 10 and 20 μ M), which, once again, resulted in the spontaneous formation of the *m/z* 488 product as the major parent-related component, at an average ratio of approximately 95:5 (*m/z* 488: AZX parent) (data not shown).

It was initially assumed that either the wrong compound was dosed or that the parent had either degraded/formed chemical adducts, because the molecular ion, i.e., the mass addition, could not be explained. Therefore, to verify the identity and stability of the parent, the solvent standards (i.e., the 200 μ M AZX stock solution and the 10 μ M AZX test solution) and the actual dose solution (diluted to 10 μ M in 30:70, methanol/water, v/v) were analyzed in conjunction with repeat predose and 0 to 24 h rat urine samples. A comparison of the UV chromatograms (extracted at λ = 240–245 nm) for the AZX-

spiked predose urine samples (at 10 and 20 μM final concentrations) and the AZX solvent standards showed that in urine the UV peak for AZX (RT = approximately 5.32 min) was depleted, whereas the m/z 488 product (RT = approximately 4.45 min) was abundant (Fig. 2). However, the AZX solvent standards and the dose solution resulted in the observation of the correct molecular ion of $[\text{M} + \text{H}]^+$ 476, confirming that the compound had not degraded in solution over time.

Similar observations were made with the 0 to 24 h rat blood, in which the m/z 488 product was also observed, although at a reduced amount (at an approximate ratio of 40:60, m/z 488: AZX) as assessed by UV (data not shown). Furthermore, the spiking experiments with predose blood, as conducted with the urine samples, again confirmed the formation of the m/z 488 product. From these data it was surmised that AZX was reacting with a component present in the urine and blood, which is the subject of this investigation.

A thorough review of the 0 to 24 h sample data (urine and blood) confirmed that this m/z 488 metabolite/product (RT = approximately 4.45 min), represented the majority of the AZX-related material in urine as determined by UV and mass spectrometry. The mass of the m/z 488 product was equivalent to an increase of 12 Da from parent (AZX, $[\text{M} + \text{H}]^+$ 476), although it represented an actual increase of 13 Da when molecular weights were compared (as detailed in the following section).

Structural Characterization of the Novel Metabolite/Product, m/z 488 (AZX + 13) by UPLC-MS/MS. From accurate mass measurement this apparent metabolite was determined to have a mono-isotopic mass of 488.2242, almost exactly an increase of 12.0000 Da over the parent $[\text{M} + \text{H}]^+$ 476.2243, suggesting addition of one carbon atom. This was further substantiated after an elemental composition analysis in which no rational alternative molecular formula could be identified.

The proposed fragmentation pattern and LTQ Orbitrap HCD MS/MS spectrum of this metabolite/product (RT = approximately 4.45 min) (Fig. 3) contained diagnostic fragment ions m/z 267.2184 and m/z 153.1386. These ions corresponded to the addition of 12 Da to the key fragments m/z 255 and m/z 141 in the MS/MS spectrum of AZX. The observation of the fragment ions m/z 267.2184 and m/z 153.1386 with accurate mass (± 2 ppm) and elemental composition analysis appeared to confirm the addition of a single carbon atom to the homopiperazine ring. The exact position of the carbon addition could not be determined by MS; however, it was possible to postulate the structure as a bridged homopiperazine (as shown in Fig. 3).

Difference between Theoretical Molecular Weight and Measured Molecular Ion of the Proposed Bridged Homopiperazine. The proposed bridged structure equates to the addition of one carbon and one hydrogen atom, i.e., a gain of 13 Da, which is inconsistent with the 12-Da increase as determined by the mass spectrometry data. However, because the bridged product has a fixed permanent positive charge (M^+), it cannot produce a protonated molecular ion $[\text{M} + \text{H}]^+$ by positive ion electrospray (+ESI). Hence, whereas the calculated nominal mass of the parent (AZX) is 475 and the mass measured by +ESI mass spectrometry ($[\text{M} + \text{H}]^+$) is 476 (Fig. 1), the calculated nominal mass and the mass measured by +ESI MS of the bridged ion are both 488. Therefore, a comparison of the theoretical molecular weights of AZX and AZX + 13 results in a mass difference of 13 Da, compared with the 12-Da difference in the measured molecular ions by mass spectrometry. To highlight the +13 Da addition of this structurally unique product compared with the +12 carbon addition products reported in the literature (see *Discussion*), the product is referred to as AZX + 13.

KCN Addition as a Chemical Test to Confirm the Presence of a Quaternary Nitrogen. Cyanide chemically forms adducts with iminium ions and is used widely in reactive metabolism trapping

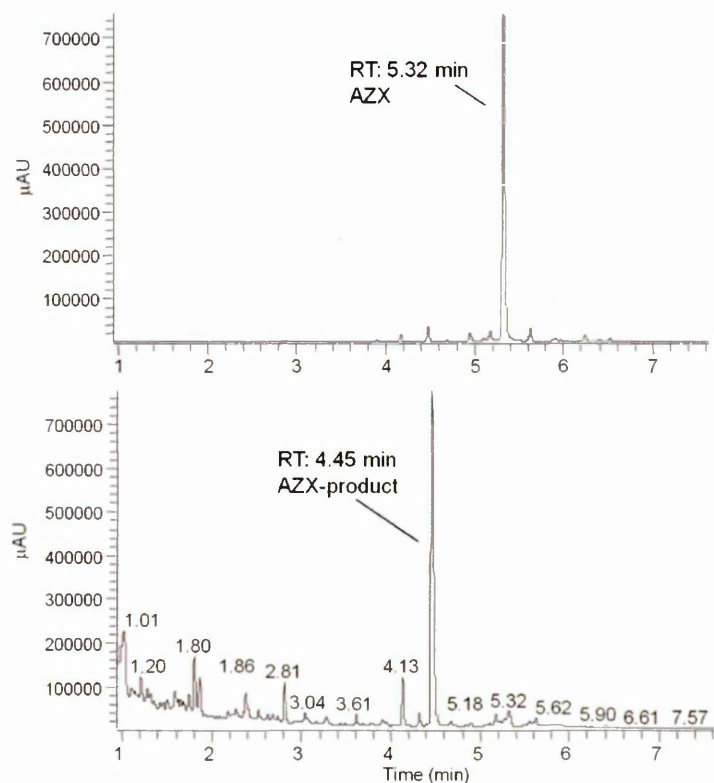


FIG. 2. UV chromatograms of the AZX test solution (10 μM) (top) compared with a predose rat urine sample after spiking with AZX (10 μM) (bottom). μAU , micro-absorption units.

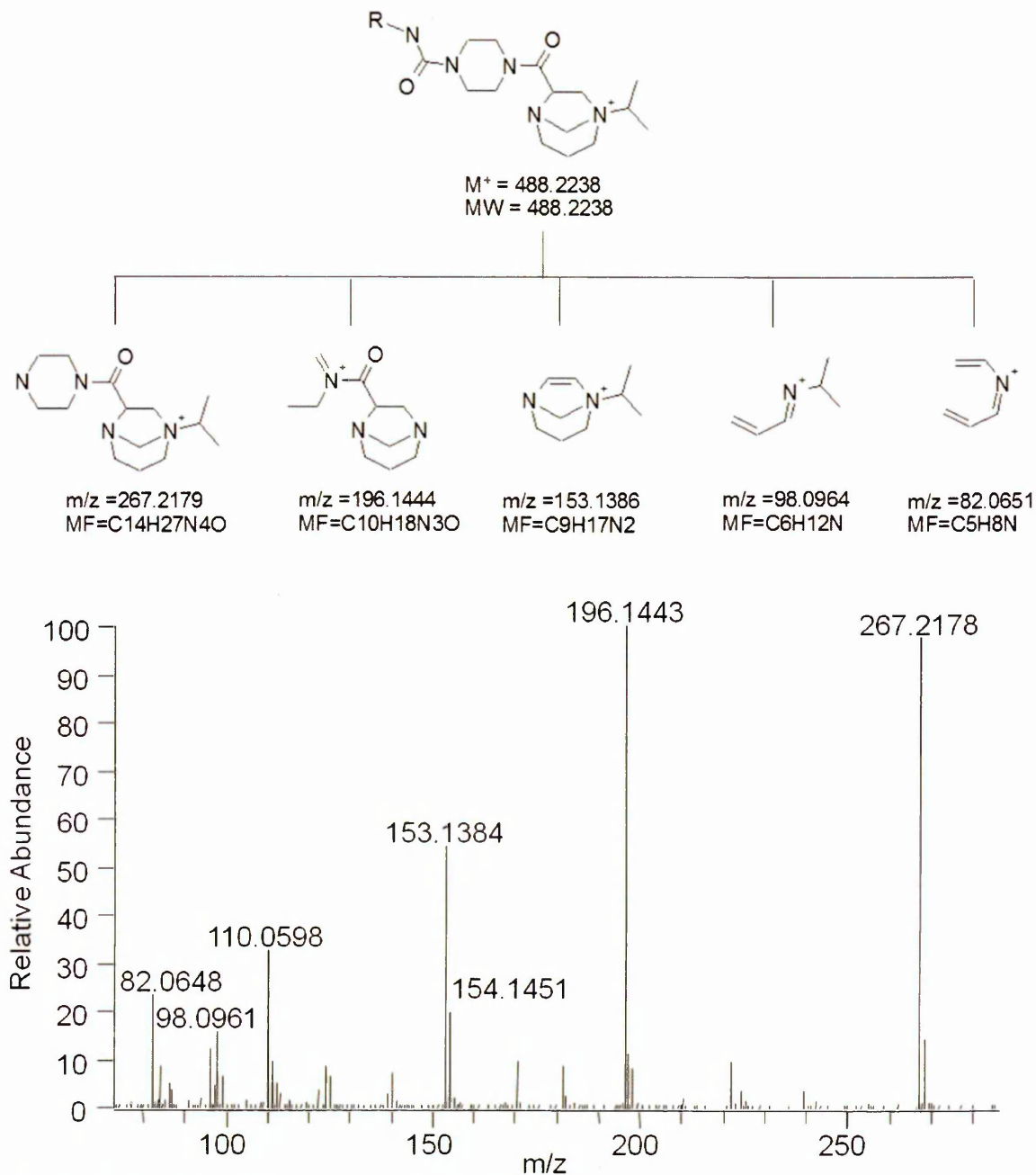


FIG. 3. Proposed LTQ Orbitrap collision cell fragmentation of the postulated bridged homopiperazine (AZX + 13) (top) with accurate spectrum (bottom). MW, molecular weight; MF, molecular formula.

studies in biological samples across the pharmaceutical industry (Argoti et al., 2005). To confirm the presence of a quaternary nitrogen (i.e., the bridged homopiperazine moiety as shown in Fig. 3), KCN was added to the AZX-spiked predose and the pooled 0 to 24 h urine sample. On addition of KCN, the AZX + 13 product peak (m/z 488, RT = approximately 4.45 min) reduced in size (based on its UV response), whereas an additional peak $[M + H]^+$ 515 (RT = approximately 5.85) was detected in each of the samples (Fig. 4). Further investigation by MS/MS fragmentation determined the addition of 27 Da (CN) on the homopiperazine ring,

by the presence of the key fragment ions m/z 294.2289 and m/z 180.1497, corresponding to +27 Da on m/z 267.2179 and m/z 153.1386, respectively. Confirmation of the presence of the quaternary nitrogen on the homopiperazine led to the investigation of the mechanism of formation of AZX + 13.

Investigation of the Formation of AZX + 13. On the basis of the MS results and the KCN trapping experiment (confirming the quaternary nitrogen), it appeared that AZX was reacting with a component in the urine to produce a one carbon and one hydrogen atom addition bridged homopiperazine.

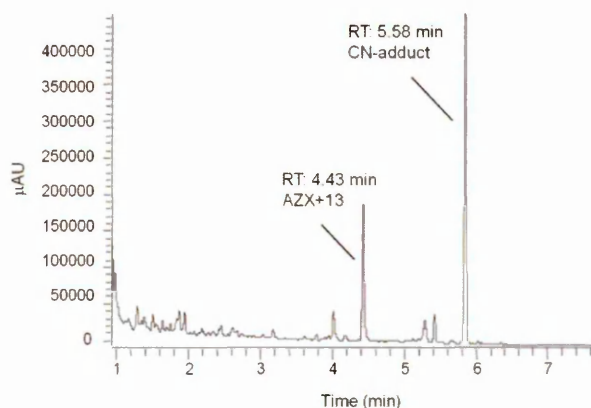


Fig. 4. The UV chromatogram of the predose urine after addition of KCN. μ AU, micro-absorption units.

The same product was observed with pooled blood, albeit to a lesser extent. Formaldehyde, reported to occur naturally in living systems (Heck and Casanova, 2004), was suggested as a likely candidate to generate AZX + 13, via a quaternary Schiff base intermediate (iminium ion), which is then intramolecularly stabilized by forming the bridged homopiperazine (as shown in Fig. 5).

To test this hypothesis, formaldehyde (10 μ l, 37% in H₂O) was spiked into the AZX test solution (10 μ M, 500 μ l), which was analyzed immediately on the UPLC-MS system. A product was formed at nearly 100% yield within the time taken to inject the sample, confirming that formaldehyde reacts rapidly with AZX at room temperature. This chemical product was verified as the AZX + 13 product, which was identical to that detected in the biological samples (urine and blood), as assessed by chromatographic retention time, UV, accurate mass, and MS/MS fragmentation. This now provided an efficient means to generate AZX + 13 at a sufficient scale for full structural confirmation by ¹H NMR spectroscopy, as detailed under *Methods and Materials*. Not only was the confirmation of the bridged homopiperazine structure of importance, but the resultant structure of the AZX + 13 CN adduct was also of interest to confirm the exact position of the CN addition, in view of several possible isomeric products.

Confirmation of AZX + 13 and the AZX + 13 + CN Adduct by ¹H NMR Spectroscopy. After identification by MS, the structures of the parent (AZX), the AZX + 13 product, and the AZX + 13 + CN adduct were verified by ¹H NMR spectroscopy (Fig. 6, A, B, and C, respectively). After the addition of formaldehyde, no changes in the spectra were observed in the aromatic regions of AZX and AZX + 13 spectra, indicating that the site of modification is remote (data not shown).

However, the aliphatic region highlighted several chemical shift changes supporting the proposed formation of the bridged homopiperazine (Fig. 6, A and B). These mainly comprised changes in the chemical shifts of the protons on the homopiperazine moiety, such as the isopropyl methyl doublets, which have shifted from 0.94 and 0.98 to 1.34 and 1.38 ppm, respectively. Likewise, all the residual

homopiperazine protons experienced a shift to higher frequency. In addition to the chemical shift changes, two doublets (labeled Ha and Hb), not initially present in the parent spectrum, were observed at 4.68 and 3.91 ppm, with a coupling constant of ³J = 9.82 Hz and an integral value of one proton per doublet, which showed a clear connectivity in the two-dimensional COSY spectrum (data not shown). The suggested structure is consistent with the proposed one carbon bridge across the homopiperazine.

Figure 6C shows the ¹H NMR spectrum of the AZX + 13 + CN adduct. The -CN addition was shown to have largely reversed the chemical shift changes induced by the addition of formaldehyde (the formation of the bridged homopiperazine), yet an additional set of doublets (an AB system, labeled Hc and Hd) was noted at 3.7 and 3.5 ppm, which showed a strong connectivity in the two-dimensional COSY spectrum (data not shown). On the basis of this evidence, two isomeric possibilities could be suggested (Fig. 7, isomers 1 and 2). Selective irradiation experiments were used to determine the correct structure of the AZX + 13 + CN adduct.

The selective ROESY experiment, irradiating the isopropyl methyl signals (labeled 8,8'), showed clear through-space interactions to the isopropyl proton (labeled 9 in the structure), as well as the homopiperazine protons 2 and 3 (Fig. 7). There was no enhancement of the bridged protons (labeled a and b), indicative of the six-membered ring (isomer 2), hence providing evidence that this was not the preferred structure. Instead, the spectral data supported the presence of the NCH₂CN side chain (isomer 1), after addition of KCN.

Discussion

This study demonstrated that compound AZX and various analogs containing a homopiperazine moiety reacted rapidly with formaldehyde in biological matrices to form a carbon and hydrogen addition bridged homopiperazine (+13-Da products). However, the origin/source of formaldehyde was still unclear, because it could have been endogenous, as reported by Heck and Casanova (2004) or, indeed, derived from the solvent system (methanol or formic acid), although it was shown to form irrespective of the mobile phase combination or spiking solvent used. A series of publications have described the formation of a +12-Da product from a reaction with formaldehyde, which was suggested to have derived from methanol, as discussed below.

It has to be pointed out that in these articles the reaction with formaldehyde resulted in +12-Da heterocyclic products (having gained one carbon atom over their respective parent compounds), whereas our example, through a different mechanism, yielded a novel bridged homopiperazine with a quaternary nitrogen (after addition of one carbon and one hydrogen). Hence, Yin et al. (2001) described the addition of +12 Da to the parent compound identified in/derived from *in vitro* experiments, in which S9 fractions/hepatic incubations were spiked with an analyte in methanol. However, it was concluded that the MeOH was first metabolized to formaldehyde (Teschke et al., 1974), which then reacted with a basic group on the incubated compound. Each of the compounds tested, containing either 1,2-amino hydroxyl or 1,2-diamino reacted with the metabolic formalde-

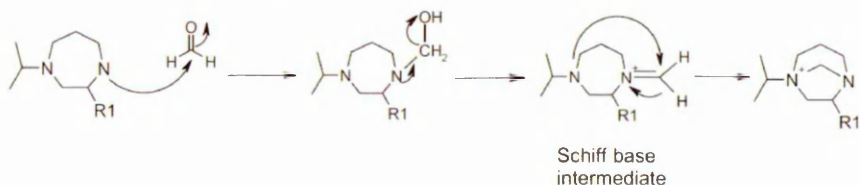


Fig. 5. The proposed structure and formation of the bridged homopiperazine (AZX + 13) through a quaternary Schiff base intermediate.

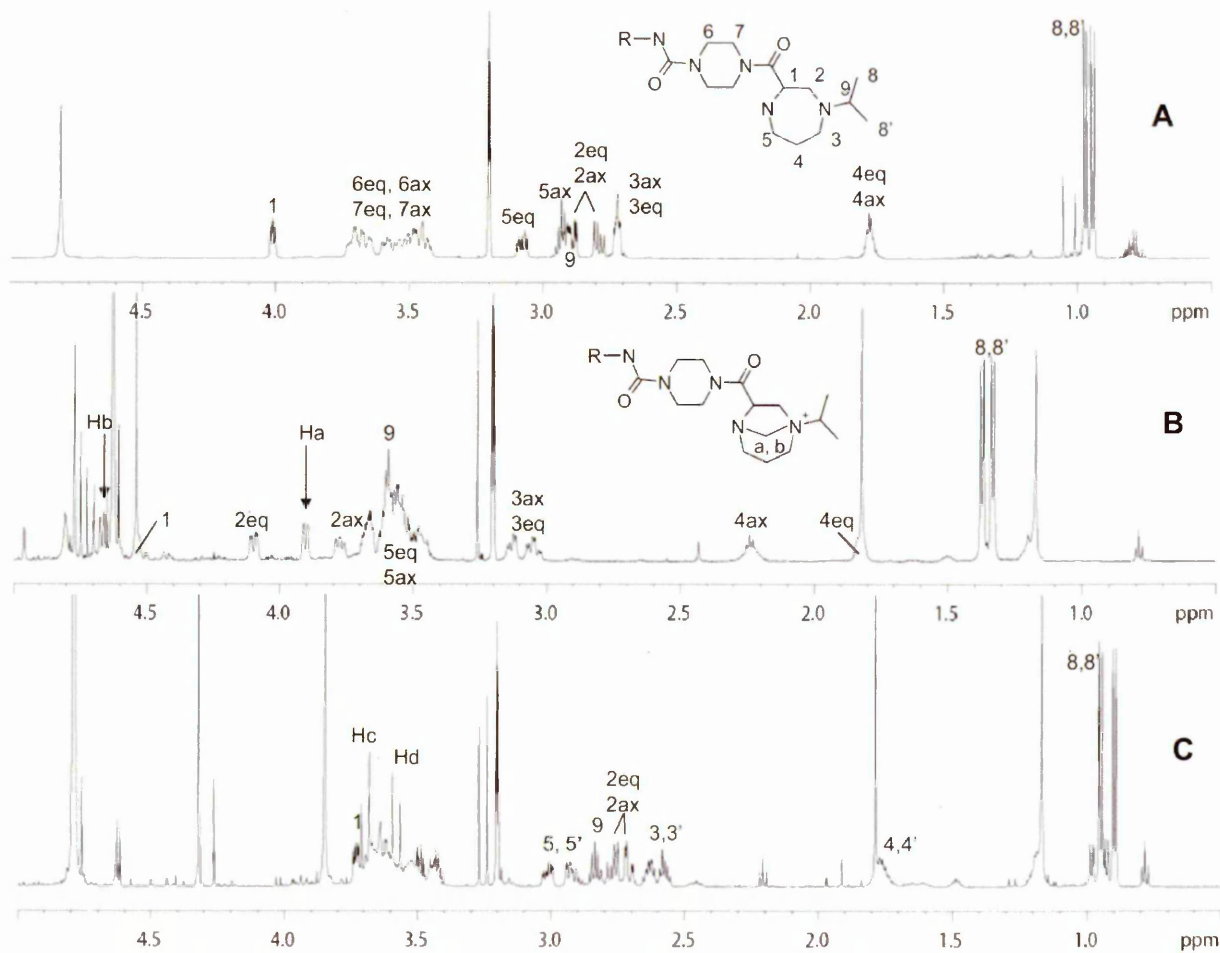


FIG. 6. ¹H NMR spectra of (A) the parent (AZX), (B) the AZX + 13 product, and (C) the CN adduct (AZX + 13 + CN).

hyde to generate ring-closed heterocyclic or +12-Da products. Cunningham et al. (1990) reported a similar problem with diaminotoluene reacting with formaldehyde generated from the use of methanol as a spiking solvent for *in vitro* incubations. The product was formed through cross-linking of two molecules of 2,4-diaminotoluene with formaldehyde to give bis(2,4-diamino-5-tolyl)methane.

Köppel et al. (1991) described the formation of +12-Da products from the gas chromatographic analyses of several drugs by addition of formaldehyde and subsequent loss of water. It was suggested that the formaldehyde was formed by thermal degradation of MeOH in the gas chromatographic source.

These reported cases describe an analytical or *in vitro* artifact from the use of MeOH as a diluent or solvent, which is then believed to be oxidized chemically or metabolically to formaldehyde. In this study AZX + 13 (the formaldehyde addition product) was derived directly from an *in vivo* investigation, suggesting a potentially different (i.e., natural) source of formaldehyde for the reaction. AZX + 13 was not detected in any preliminary *in vitro* experiments because test compounds are typically spiked into incubations using ACN and not MeOH. However, we have also demonstrated that the MeOH used as mobile phase constituent and/or indeed as the AZX diluent (used in the stock and test solutions) did not cause the formation of AZX + 13.

Further investigations were performed to rule out MeOH as the source of the formaldehyde or indeed as the reagent itself. The experiments are not described in detail here; however, a brief summary is provided.

On spiking of compound AZX/MeOH into "freshly collected" predose/control rat urine, using the MeOH/H₂O gradient, AZX + 13 was produced spontaneously with 90 to 100% yield (based on the UV response) and remained constant over 1 month (with the urine stored at 4°C). However, on spiking of AZX/MeOH into "old" predose/control rat urine, there was very little evidence of the formation of the AZX + 13 product. Here, the urine was stored cold (at 4°C) for approximately 2 months before spiking, allowing degradation/evaporation of the formaldehyde, on the basis of the half-life of formaldehyde (Organization for Economic Cooperation and Development Screening Information Data Set, Formaldehyde, 2002, <http://www.inchem.org/documents/sids/sids/FORMALDEHYDE.pdf>). After the 2-month aging period, upon spiking of AZX, only approximately 5 to 10% of the product was formed, the ratio remaining constant over a further month.

Additional evidence on the formation of the *in vivo* AZX + 13 was provided by spiking fresh rat urine samples with AZX, as conducted in the experiments detailed above, using ACN as the spiking solvent. The UPLC-UV-MS/MS analysis was also performed in the

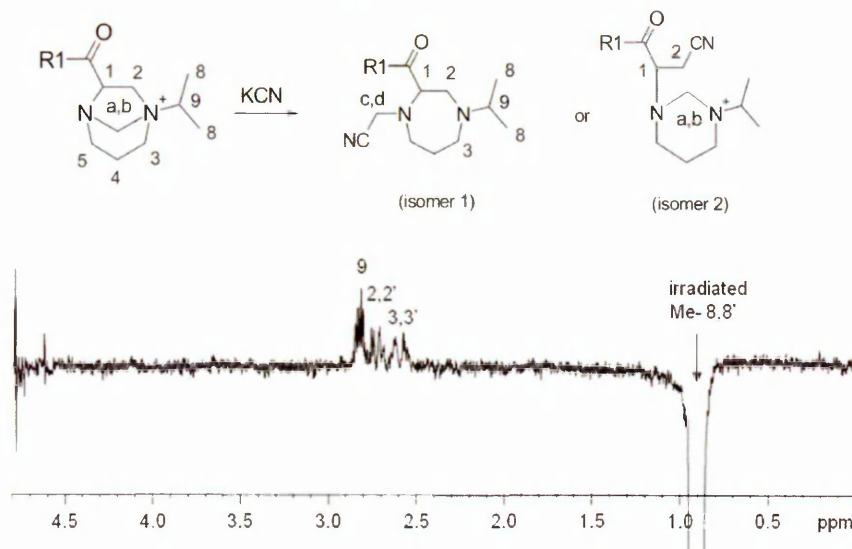


FIG. 7. ^1H NMR selective ROESY experiment (bottom) verifying the correct structure of the AZX + 13 + CN adduct as isomer 1 (top) after addition of KCN.

absence of MeOH, using ACN (containing 0.1% formic acid) as the mobile phase, revealing that AZX + 13 was still formed as the major product (between 90 and 100%), as assessed by UV quantification and MS analysis (data not shown). However, the AZX standards (the stock and test solutions, prepared in ACN) did not produce the product when subjected to UPLC-UV-MS/MS analysis, ruling out ACN and formate as possible reagents.

These simple experiments suggested not only that the formaldehyde in the urine was naturally present but also that it was depleted over time. In addition, they proved that AZX + 13 was not likely to be an analytical artifact from the MeOH, ACN, or formate used in the analyses.

The findings from our research appear to support the evidence in the literature, namely that the formaldehyde occurs naturally in all mammalian tissues, cells, and bodily fluids and that it is present in rat blood at approximately, 0.1 mM concentration (Heck and Casanova, 2004). Formaldehyde and its oxidation product formate are reported to be key intermediates in the "one-carbon pool" (Neuberger, 1981). Certain xenobiotics such as MeOH, N-, O-, or S-Me compounds, and methylene chloride apparently can also contribute to this pool. The one-carbon pool is used for the biosynthesis of purines, thymidine, and certain amino acids, which are incorporated into the DNA, RNA, and proteins during macromolecular synthesis. It is therefore suggested that compound AZX scavenges endogenous formaldehyde *in vivo*, similar to aminoguanidine, which was reported by Kazachkov et al. (2007).

Formaldehyde is known to be responsible for cross-linking proteins (e.g., Metz et al., 2004; Toews et al., 2008) and some xenobiotics (Cunningham et al., 1990) through a Schiff base intermediate. Considering that basic amine groups are ubiquitous on many xenobiotics and proteins, it is worth noting the potential for formaldehyde to cause cross-linking between xenobiotics and proteins *in vivo*. Hence, susceptibility to formaldehyde addition via a direct or metabolic route could lead to the formation of covalently bound protein adducts. However, the reaction *in vitro* relies on the presence of MeOH, e.g., used as spiking solvent, as a source of the formaldehyde [as outlined by Yin et al. (2001) and Cunningham et al. (1990)]. Therefore, the potential for some basic xenobiotics to covalently bind to protein may not be flagged by reactive metabolite screening or radiolabeled *in vitro* covalent binding studies.

Here, the Schiff base reactive intermediate, trapped because of the proximity of the two nitrogens (as in a twisted boat conformation), formed a very stable bridged homopiperazine detectable by LC-UV-MS. However, in most other basic xenobiotics the Schiff base intermediate would not be intramolecularly trapped to form a stable product detectable by subsequent analyses. Hence, there is potential for this reactive intermediate to be missed in *in vivo/in vitro* metabolite identification studies, even when formaldehyde is present.

Because the initial terminal piperazine series was found to generate electrophilic, reactive intermediates metabolically, the homopiperazine series was thought to provide a safer suitable alternative. Therefore, the formation of a bridged homopiperazine through a reactive quaternary Schiff base intermediate was an unexpected observation. The homopiperazine ring is neither planar nor symmetrical, so the conformation adopted clearly proved favorable for the formation of a one-carbon bridge.

Various other homopiperazine analogs of compound AZX have also been investigated for +13-Da product formation and as demonstrated in this study with compound AZX, these products have been formed rapidly *in vivo*, as well as being confirmed in spiking experiments with formaldehyde (data not shown). These studies have highlighted the fact that the homopiperazine moiety appears to be a highly reactive group, and the observations made in this study support the decision to change the chemistry of these compounds.

In conclusion, this study has demonstrated that compound AZX and various analogs containing the homopiperazine moiety reacted rapidly with formaldehyde present in biological fluids, as a constituent of the one-carbon pool, suggesting that it is a metabolite, as well as a chemical product. The homopiperazine moiety was initially included in the lead compounds as an inert/unreactive alternative to the terminal piperazine, which was shown to be prone to bioactivation and subsequent covalent binding with GSH. Hence, the addition of the terminal homopiperazine group was believed to retain the potency of the compounds while decreasing their reactivity. However, as we have shown in this study, this group is itself highly reactive with endogenous formaldehyde, forming bridged homopiperazines.

The findings in this article suggests that compound AZX and its homopiperazine analogs scavenge endogenous formaldehyde *in vivo* similar to aminoguanidine, which was reported by Kazachkov et al.

(2007). What appears to be a desired effect with aminoguanidine proved to be a toxicity alert with the AZX-derived compounds.

Apart from the reactivity aspect itself, quantitation of parent drug in blood and urine would be greatly compromised, creating problems for lead optimization and pharmacokinetic assessments. In addition, the formation of this adduct could artificially distort metabolite profiles in human metabolism studies, affecting (metabolites in safety testing) investigations (U.S. Food and Drug Administration guidance on Safety Testing of Drug Metabolites, 2008, <http://www.fda.gov/downloads/Drug/GuidanceComplianceRegulatoryInformation/Guidances/ucm079266.pdf>).

However, overall the study demonstrated that the bridged homopiperazine was readily formed in vivo, producing a stable product/metabolite, which did not degrade in urine for at least 1 month. This finding has provided a suitable method and an easy and highly efficient means (>95% yield) for the generation of a bridged homopiperazine synthetically by a simple reaction with formaldehyde.

Authorship Contributions

Participated in research design: Martin, Lenz, Temesi, Wild, and Clench.

Conducted experiments: Martin and Lenz.

Contributed new reagents or analytic tools: Martin and Lenz.

Performed data analysis: Martin and Lenz.

Wrote or contributed to the writing of the manuscript: Martin, Lenz, Temesi, Wild, and Clench.

References

- Argoti D, Liang L, Conteh A, Chen L, Bersbas D, Yu CP, Vouros P, and Yang F (2005) Cyanide trapping of iminium ion reactive intermediates followed by detection and structure identification using liquid chromatography-tandem mass spectrometry (LC-MS/MS). *Chem Res Toxicol* **18**:1537–1544.
- Baillie TA (2006) Future of toxicology-metabolic activation and drug design: challenges and opportunities in chemical toxicology. *Chem Res Toxicol* **19**:889–893.
- Baillie TA (2009) Approaches to the assessment of stable and chemically reactive drug metabolites in early clinical trials. *Chem Res Toxicol* **22**:263–266.
- Cunningham ML, Matthews HB, and Burka LT (1990) Activation of methanol by hepatic postmitochondrial supernatant: formation of a condensation product with 2,4-diaminotoluene. *Chem Res Toxicol* **3**:157–161.
- Doss GA, Miller RR, Zhang Z, Teffera Y, Nargund RP, Palucki B, Park MK, Tang YS, Evans DC, Baillie TA, et al. (2005) Metabolic activation of a 1,3-disubstituted piperazine derivative: evidence for a novel ring contraction to an imidazoline. *Chem Res Toxicol* **18**:271–276.
- Evans DC, Watt AP, Nicoll-Griffith DA, and Baillie TA (2004) Drug-protein adducts: an industry perspective on minimizing the potential for drug bioactivation in drug discovery and development. *Chem Res Toxicol* **17**:3–16.
- Heck H and Casanova M (2004) The implausibility of leukemia induction by formaldehyde: a critical review of the biological evidence on distant-site toxicity. *Regul Toxicol Pharmacol* **40**:92–106.
- Kazachikov M, Chen K, Babiy S, and Yu PH (2007) Evidence for in vivo scavenging by aminoguanidine of formaldehyde produced via semicarbazide-sensitive amine oxidase-mediated deamination. *J Pharmacol Exp Ther* **322**:1201–1207.
- Köppel C, Tenczer J, and Peixoto-Menezes KM (1991) Formation of formaldehyde adducts from various drugs by use of methanol in a toxicological screening procedure with gas chromatography-mass spectrometry. *J Chromatogr* **563**:73–81.
- Metz B, Kersten GF, Hoogerhout P, Brugghe HF, Timmermans HA, de Jong A, Meiring H, ten Hove J, Henmink WE, Crommelin DJ, et al. (2004) Identification of formaldehyde-induced modifications in proteins: reactions with model peptides. *J Biol Chem* **279**:6235–6243.
- Neuberger A (1981) The metabolism of glycine and serine, in *Comprehensive Biochemistry*, vol. 19A (Neuberger A and van Deenen LLM eds) pp. 257–303, Elsevier, Amsterdam.
- Prakash C, Sharma R, Gleave M, and Neiderman A (2008) In vitro screening techniques for reactive metabolites for minimizing bioactivation potential in drug discovery. *Curr Drug Metab* **9**:952–964.
- Teschke R, Hasumura Y, and Lieber CS (1974) NADPH-dependent oxidation of methanol, ethanol, propanol and butanol by hepatic microsomes. *Biochem Biophys Res Commun* **60**:851–857.
- Toews J, Rogalski JC, Clark TJ, and Kast J (2008) Mass spectrometric identification of formaldehyde-induced peptide modifications under in vivo protein cross-linking conditions. *Anal Chim Acta* **618**:168–183.
- Yin H, Tran P, Greenberg GE, and Fischer V (2001) Methanol solvent may cause increased apparent metabolic instability in in vitro assays. *Drug Metab Dispos* **29**:185–193.

Address correspondence to: Scott Martin, DMPK Department, Alderley Park, AstraZeneca UK Ltd., Macclesfield, Cheshire SK10 4TG, UK. E-mail: scott.martin2@astrazeneca.com

5. REACTIVE METABOLITE TRAPPING SCREENS AND POTENTIAL PITFALLS: BIOACTIVATION OF A HOMOMORPHOLINE AND FORMATION OF AN UNSTABLE THIAZOLIDINE ADDUCT

Reproduced with permission from Chem. Res. Toxicol. (2014) 27:968-980.

Copyright 2014 American Chemical Society.

Reactive Metabolite Trapping Screens and Potential Pitfalls: Bioactivation of a Homomorpholine and Formation of an Unstable Thiazolidine Adduct

Eva. M. Lenz,^{*,†} Scott Martin,[†] Ralf Schmidt,^{‡,§} Pierre-Emmanuel Morin,[‡] Robin Smith,[†] Daniel J. Weston,[†] and Malken Bayrakdarian^{‡,||}

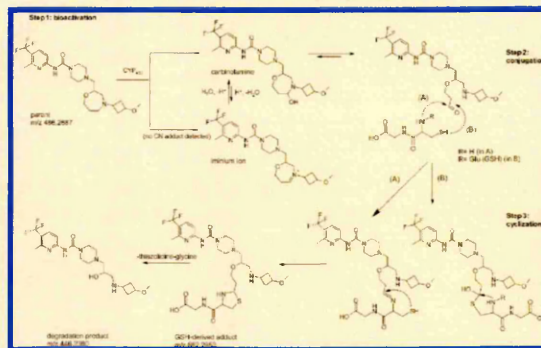
[†]DMPK Department, Alderley Park, AstraZeneca UK Ltd., Macclesfield, Cheshire SK10 4TG, United Kingdom

[‡]DMPK and Medicinal Chemistry Department, AstraZeneca R&D Montreal, St. Laurent, QC Canada H4S 1Z9

Supporting Information

ABSTRACT: Successful early attrition of potential problematic compounds is of great importance in the pharmaceutical industry. The lead compound in a recent project targeting neuropathic pain was susceptible to metabolic bioactivation, which produced reactive metabolites and showed covalent binding to protein. Therefore, as a part of the backup series for this compound several structural modifications were explored to mediate the reactive metabolite and covalent binding risk. A homomorpholine containing series of compounds was identified without compromising potency. However, when these compounds were incubated with human liver microsomes in the presence of GSH, Cys-Gly adducts were identified, instead of intact GSH conjugates. This article examines the formation of the Cys-Gly adduct with AZX ($[M+H]^+$ 486) as a representative compound for this series. The AZX-Cys-Gly-adduct ($[M+H]^+$ 662)

showed evidence of ring contraction by formation of a thiazolidine-glycine and was additionally shown to be unstable. During its isolation for structural characterization by ^1H NMR spectroscopy, it was found to have decomposed to a product with $[M+H]^+$ 446. The characterization and identification of this labile GSH-derived adduct using LC-MS/MS and ^1H NMR are described, along with observations around stability. In addition, various structurally related trapping reagents were employed in an attempt to further investigate the reaction mechanism along with a methoxylamine trapping experiment to confirm the structure of the postulated reactive intermediate.



INTRODUCTION

Reactive metabolites are of great concern in the pharmaceutical industry.^{1–3} Hence, great emphasis is placed on the early identification of potentially reactive metabolites, which has led to the front loading of biotransformation studies. Reactive metabolite trapping screens with liver microsomes (usually human) fortified with nucleophiles such as GSH, cysteine, potassium cyanide, and methoxylamine⁴ are routinely employed to trap reactive electrophilic species at sufficient concentration to form stable, recognizable products/adducts which can be identified by their expected MS changes. However, unexpected or structurally unusual products from nonstandard biotransformations such as structural rearrangements^{5–11} could escape detection during the MSMS investigations due to changes in molecular structure, molecular weight, and the lack of expected fragmentation patterns. Of particular concern are cyclized GSH adducts^{5–10} which can produce a false negative result in conventional LC-MSMS GSH trapping screens, as GSH adducts are generally identified by their expected target mass, a neutral loss of 129 Da in positive

ion mode, or/and a m/z of 273 in a precursor ion scan in negative ion mode.

A recent *in vitro* reactive metabolite investigation of a series of potential lead compounds using human liver microsomal incubations fortified with GSH revealed the formation of unexpected Cys-Gly adducts instead of intact GSH-adducts. However, only those compounds containing a homomorpholine moiety produced the Cys-Gly adduct, implying the homomorpholine was the site of bioactivation. Compound AZX (Figure 1, with $[M+H]^+$ 486), the lead compound for this series, however, was shown to produce the Cys-Gly adduct ($[M+H]^+$ 662) exclusively in human liver microsomes, indicating the potential to produce a human specific reactive metabolite. While the $[M+H]^+$ 662 adduct was clearly detected, the intact GSH adduct was not observed in the AZX-human liver microsomal incubations. From the accurate mass fragmentation pattern of the $[M+H]^+$ 662 adduct, it was possible to propose a GSH rearrangement product through the loss of the glutamate

Received: February 6, 2014

Published: May 23, 2014

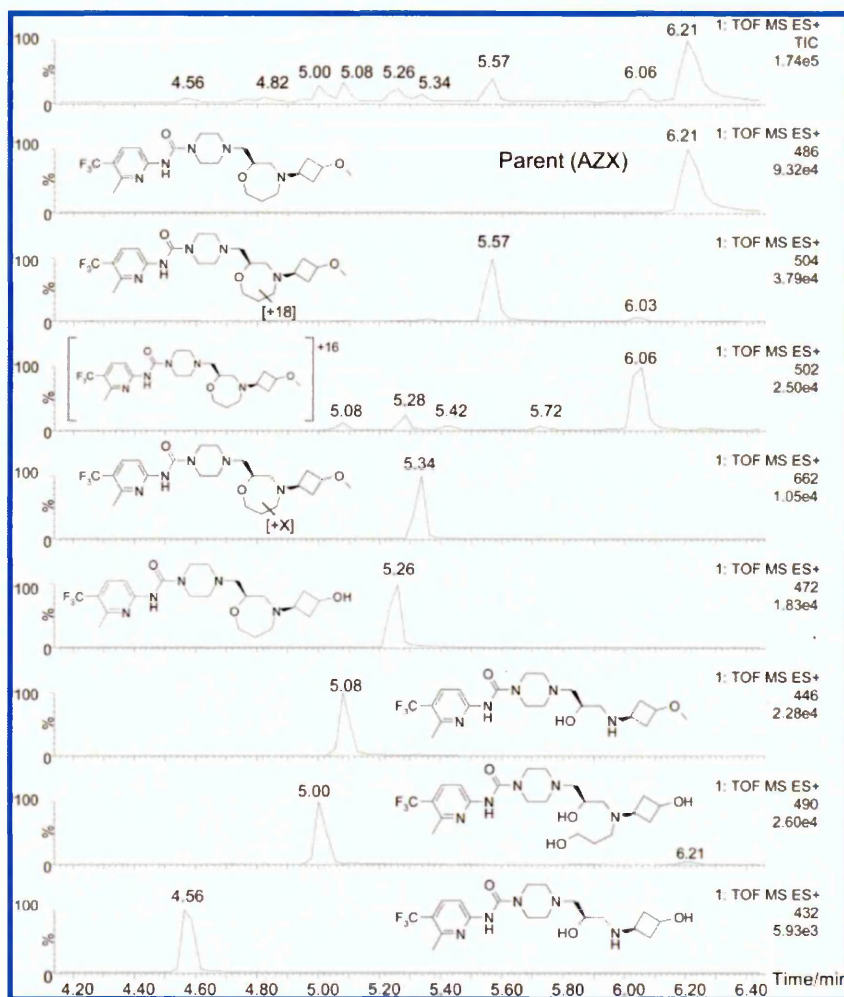


Figure 1. Total ion chromatogram (TIC) of the scaled-up bacterial cytochrome enzyme ($t = 16$ h) incubation with selected ion chromatograms of the metabolites characterized. Data generated on the UPLC-Q-TOF. Key: [+X] = GSH-derived moiety.

and intramolecular cyclization of the Cys-Gly moiety. However, the $[M+H]^+ 662$ adduct was shown to degrade to $[M+H]^+ 446$ during its isolation for subsequent structural identification by ^1H NMR spectroscopy.

The human liver microsome incubations also showed a minor signal for a compound with $[M+H]^+ 446$, suggesting it was both a metabolite and a decomposition product of $[M+H]^+ 662$. The formation of the $[M+H]^+ 662$ adduct and its stability are subject to further investigation in this article.

EXPERIMENTAL PROCEDURES

Chemicals and Reagents. Compound AZX (4-[[4-(3-methoxy-cyclobutyl)-1,4-oxazepan-2-yl]methyl]-N-[6-methyl-5-(trifluoromethyl)-2-pyridyl]piperazine-1-carboxamide) was synthesized at Astra Zeneca R&D Montreal, Canada. The structure of AZX is novel; however, its synthesis was based on the described procedure of similar analogues (AZ patent WO200606740 and, for the homomorpholine subunit, WO2006105262).

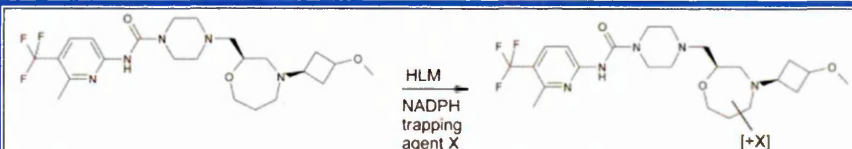
Ammonium formate, dithiothreitol (DTT), and β -nicotinamide adenine dinucleotide sulfate reduced tetrasodium salt (NADPH) were purchased from Sigma-Aldrich (Oakville, Canada) and acetonitrile (CH_3CN), methanol (MeOH), ammonium acetate, and formic acid from Fisher-Scientific (Loughborough, UK). Methoxylamine, potas-

sium cyanide (KCN), and the deuterated NMR solvents were sourced from Sigma-Aldrich (Poole, UK).

Incubation of Parent (AZX) and Trapping Conditions. AZX was incubated at a concentration of $10 \mu\text{M}$ with human and rat liver microsomes (1 mg/mL of protein, respectively) (BD-Gentest) in 0.1 M potassium phosphate buffer at pH 7.4 in the presence of 2 mM of the respective trapping reagent and 1 mM NADPH at 37°C for 30 min. After precipitation with 2 equiv (v/v) of CH_3CN and cooling for 20 min at 4°C , the samples were centrifuged at $8000g$ for 30 min. In the trapping experiment with dansyl- γ Glu-Cys-Lys (dECK), precipitation was executed with 2 volumes (v/v) of MeOH containing 5 mM DTT. The supernatant diluted with water (1:1, v/v) was analyzed by LC-MSMS. Clozapine was used in the trapping experiments (see Table 1) as the positive control.

The incubations were carried out with a range of different trapping agents that were of commercial origin (Sigma-Aldrich, Oakville, Canada), such as γ Glu-Cys-Gly (GSH), γ Glu-Cys-Gly- ^{15}N , $^{13}\text{C}_2$, N-Ac-Cys, Cys-Gly, Cys, γ Glu-Cys, and γ Glu-Cys-Gly-OEt, or synthesized in-house, such as γ Glu-Cys-Lys (ECK), dansyl-ECK (dECK), ^{18}O Glu-Cys-Gly, and β Asp-Cys-Gly, using the conditions of the standard GSH fortified trapping human liver microsomal incubation, as detailed above.

Scale-Up Incubations with Bacterial Cytochrome Enzyme Variants. A 1 mM solution of AZX in incubation buffer was prepared by the addition of MeOH not exceeding 0.2% (v/v) organic solvent in a 24-well MicroCyp plate (Codexis, Redwood City, CA, USA)

Table 1. Human Liver Microsome Incubations of AZX with Different Trapping Reagents^a


	Trapping reagent	characteristics	structure	Adduct m/z	Adduct formed
1	GSH	γ Glu-Cys-Gly		662	yes*
2	GSH (¹⁵ N, ¹³ C)	labelled Gly-[¹⁵ N, ¹³ C ₂]		665	yes
3	Glu-Cys-Gly	α Glu-Cys-Gly (no iso-peptide bond)		662	yes
4	β Asp-Cys-Gly	[β Asp]-GSH		662	yes
5	ECK	γ Glu-Cys-Lys		733	yes*
6	dECK	Dansyl- γ Glu-Cys-Lys (blocked γ Glu N-terminus)		733	no
7	N-Ac-Cys	blocked N-terminus		647	no
8	γ Glu-Cys	no Gly		605	no
9	Cys-Gly	no γ Glu		662	yes
10	Cys	no γ Glu, no Gly		605	no
11	GSH-OEt (GSEE)	γ Glu-Cys-Gly-OEt (Gly ethyl ester)		690	yes*

^aThe observation of adduct peaks was performed by LC-MS (UPLC-Q-ToF). Analyses were conducted in duplicate, with some incubations (*) repeated twice. The GSH-adduct was detected in the control incubation with clozapine (data not shown), providing evidence that intact GSH was available for reaction. However, no GSH-adducts were observed with any of the trapping agents (data not shown).

containing variants of a bacterial cytochrome enzyme. GSH was added to obtain a trapping reagent concentration of 10 mM and the incubation mixture was shaken for 16 h at 30 °C. Following precipitation with 2 equiv (v/v) of ice-cold CH₃CN, the plate was centrifuged at 8000g at 4 °C for 30 min before the supernatants were collected and analyzed by LC-MS. The content of vials with similar metabolite profile were pooled to produce 5 distinct samples, then lyophilized before shipping to the UK for further structural characterization of the [M+H]⁺ 662 adduct. At time = 0 h, CH₃CN was added to one reaction vial without GSH, thus containing

exclusively the parent compound, which served as both a control incubation and a structural control.

The Codexis MicroCyp screening plates contain engineered cytochrome P450 (CYP) variants of CYP102A1 from *Bacillus megaterium*, which do not contain γ -glutamyl transferase (GGT).

Analysis of the Human Liver Microsome and Bacterial Cytochrome Enzyme Samples by LC-MS (Ultrahigh-Performance LC (UPLC)-Q-TOF). The incubate samples were initially analyzed (at AstraZeneca R&D, Montreal) on an Acquity UPLC-Q-TOF Premier system (Waters, USA). The mobile phase consisted of aqueous 10 mM ammonium formate (w/v) containing 5% CH₃CN

(v/v, eluent A) and CH₃CN (eluent B). A linear gradient from 0% to 80% B over 7 min at 60 °C at a flow rate of 0.5 mL/min was employed and separation achieved on a HSS T3 column (1.8 μm, 2.1 × 100 mm) connected to the mass spectrometer operating in positive electrospray ionization without flow split. Data was acquired on a Q-TOF Premier in positive ion full scan mode, and fragmentation data were obtained by collision energy ramping using MS^E. MetaboLynx 4.1 (Waters, USA) was used to analyze the Q-TOF MS^E data, and the structure of trapped adducts was characterized in MSMS experiments. Total ion chromatograms were produced generating a metabolic profile for each of the bacterial cytochrome enzyme-GSH-incubate samples (data not shown).

Sample Preparation of the Bacterial Cytochrome Enzyme Samples for Structural Characterization of [M+H]⁺ 662. Upon arrival in the UK, the protein precipitated scaled-up bacterial cytochrome enzyme incubate samples were re-lyophilized, extracted into 5 mL of MeOH, and centrifuged at 8000g. The supernatant was transferred and the MeOH evaporated under a stream of nitrogen. The dried methanolic extracts were stored at 4 °C until subsequent analyses.

Each of the scaled-up bacterial cytochrome enzyme incubate samples was used for a different purpose: samples 1 and 2 were utilized for LC-MS (UPLC-DAD-LTQ-Orbitrap) method developments, sample 3 was used for the semiprep LC-separation, and sample 4 was used to assess the stability of the GSH-derived metabolite. Sample 5, when finally analyzed, was found to contain no residual [M+H]⁺ 662. For the LC-MS analyses (UPLC-DAD-MS, LTQ-Orbitrap), the bacterial cytochrome enzyme samples were reconstituted in 0.5 mL of MeOH, to which 1 mL of deionized water was added. For ¹H NMR analysis, sample 6, serving as a source of the parent compound (AZX), and the isolated fractions from sample 3, were reconstituted in 0.5 mL of MeOH-*d*₄.

Identification and Structural Characterization of [M+H]⁺ 662 by LC-MS (UPLC-DAD-LTQ-Orbitrap). Accurate mass structural characterization work was acquired (at AstraZeneca R&D, Alderley Park) on a LTQ Orbitrap XL connected to a Waters Acquity UPLC system, which consisted of a binary UPLC PUMP, column oven, autoinjector, and a photodiode array detector (DAD).

The eluent was introduced into the mass spectrometer via the LTQ divert valve at 1 min, and UV spectra were acquired over 190–330 nm. The LTQ-Orbitrap XL was equipped with an electrospray ionization (ESI) source (Thermo Fisher Scientific, Bremen, Germany), which was operated in positive mode. Source settings were as follows: capillary temperature, 350 °C; sheath gas flow, 25; auxiliary gas flow, 17; sweep gas flow, 5; source voltage, 3.5 kV; source current, 100.0 μA; capillary voltage, 18 V; and tube lens, 75.0 V. Full scan MS data were obtained over the mass range of 100 to 1000 Da at a peak resolution of 7500. Targeted MSMS experiments were acquired using higher energy collisional dissociation (HCD) fragmentation, with an isolation width of 3 Da, a normalized collision energy of 45 eV, and an activation time 30 ms. HCD and ion trap MSⁿ fragment ions were monitored by the Orbitrap using 7500 resolution. LTQ and Orbitrap mass detectors were calibrated within 1 day of commencing the work using Proteomass LTQ/FT-Hybrid ESI positive mode calibration mix (Supelco Bellefonte USA).

Method 1: Initial method development was carried out with bacterial cytochrome enzyme sample 1 on an analytical column (Acquity BEH C18, 1.7 μm, 100 × 2.1 mm, Waters, USA) at a flow rate of 0.45 mL/min, with a column temperature of 50 °C. The separation was monitored at 280 nm.

The mobile phase consisted of aqueous 5 mM ammonium acetate (w/v, eluent A) and MeOH, buffered with 5 mM ammonium acetate (w/v, eluent B). The elution profile was a linear gradient of 90% to 20% A, from 0.00 to 8.00 min; followed by a column wash of 5% A for 3 min (8.01 to 11 min) and re-equilibration with 90% A, 11.01 to 15.00 min. The maximum column loading capacity was assessed as 20 μL.

The adduct eluted at ca. *t*_R = 6.1 min and produced a molecular ion of [M+H]⁺ 662 and an in-source fragment ion of *m/z* 446.

Isolation of [M+H]⁺ 662 by Semiprep LC Linked to a HTC-Fraction Collector. Method 2: The separation method and sample loading capacity were assessed with BCE sample 2 (on the UPLC-DAD-LTQ-Orbitrap), on a semiprep AQUITY HSS T3 150 × 3 mm UPLC (Waters, USA) column. The same mobile phase eluents as those in Method 1 were used. The elution profile was modified to a sharp linear gradient of 90% to 40% A, from 0.00 to 0.1 min; held isocratically at 40% A from 0.1 to 8.00 min; followed by a linear gradient of 40% to 5% A from 8.01 to 11.00 min; and re-equilibration at 90% A, 11.01 to 19.00 min. The flow rate was 0.45 mL/min, and the sample loading was assessed as 40 μL. The UV detector was set to 280 nm. Here, the [M+H]⁺ 662 adduct eluted at ca. *t*_R = 5.1 min with a peak-width of approximately 12 s.

The isolation of [M+H]⁺ 662 was carried out with bacterial cytochrome enzyme sample 3 and captured on a HTC PAL fraction-collector/autosampler (CTC Analytics, Presearch UK) collecting at approximately 2.6 s intervals (ca. 18 μL/fraction) under full automation (using Cycle Composer (CTC Analytics, Presearch UK)) overnight (35 sequential injections representing ca. 1.4 mL of sample) into 4x 96 well plates. The well contents were evaporated to dryness and freeze-dried prior to analysis by ¹H NMR spectroscopy.

¹H NMR Spectroscopic Structure Verification. ¹H NMR structural characterization of the parent (extracted from bacterial cytochrome enzyme sample 6) and of the isolated [M+H]⁺ 662 GSH-derived adduct was performed on a Bruker AVANCE 600 MHz spectrometer (Bruker Biospin Ltd., Coventry, UK), operating at 600.13 MHz ¹H resonance frequency. The NMR spectrometer was equipped with a 5 mm SEI ¹H probe. The 1D ¹H NMR spectra of AZX and the isolated fractions were acquired without solvent suppression into 65k data points over a spectral width of 9615 Hz, resulting in an acquisition time of 3.4 s. A relaxation delay of 2.6 s was employed to ensure T1 relaxation between successive scans, and depending on concentration, approximately 64–1024 scans were acquired per sample. All spectra were referenced to MeOH-*d*₄ at δ¹H 3.32.

2D ¹H–¹H COSY (COrelation SpectroscopY, gradient enhanced) and 2D ¹H–¹H TOCSY (TOtal COrelation SpectroscopY) (Bruker Biospin Ltd., Coventry, UK) experiments were acquired into 4k data points in F2 and 256 increments in F1, consisting of 8 scans each. The spectral widths were set to 8012 Hz, resulting in an acquisition time of 0.26 s. A relaxation delay of 2 s was employed between successive scans. In the TOCSY experiment, a spin lock of 2.5 ms and a mixing time of 70 ms were used. Prior to Fourier Transformation, the data were apodized with a sine bell window function, linearly predicted to 512 data points, and zero-filled in F1 to 1024 data points.

Selective 1D TOCSY experiments (Bruker Biospin Ltd., Coventry, UK) were collected into 65k data points, over a spectral width of 8389 Hz, resulting in an acquisition time of 3.9 s. A relaxation delay of 2 s was employed with a spin lock of 2.5 ms and a mixing time of 70 ms. Selective spectra were acquired with approximately 64 scans (for the parent) and up to 2k scans (for the isolated metabolite).

Incubation of the Parent (AZX) with Potassium Cyanide (KCN) and Methoxylamine. This experiment was carried out in duplicate to confirm the presence of the iminium ion or aldehyde intermediate as postulated in the mechanism of formation of [M+H]⁺ 662. AZX was incubated at 10 μM with human liver microsomes (2 mg protein/mL, BD-Gentest 150 donor ultrapool) in 0.1 M potassium phosphate buffer at pH 7.4 in the presence of either 10 mM KCN or methoxylamine trapping reagent and 2.5 mM NADPH at 37 °C. After 60 min of incubation, an aliquot was removed and the reaction stopped by the addition of ice cold CH₃CN (1:3, v/v). An incubation containing no AZX was performed as described above with AZX added after the reaction was stopped with CH₃CN. This was used to obtain a background sample. Both samples were centrifuged at 8000g for 15 min, and the supernatants were removed and combined with water (1:1, v/v) before LC-MSMS analysis.

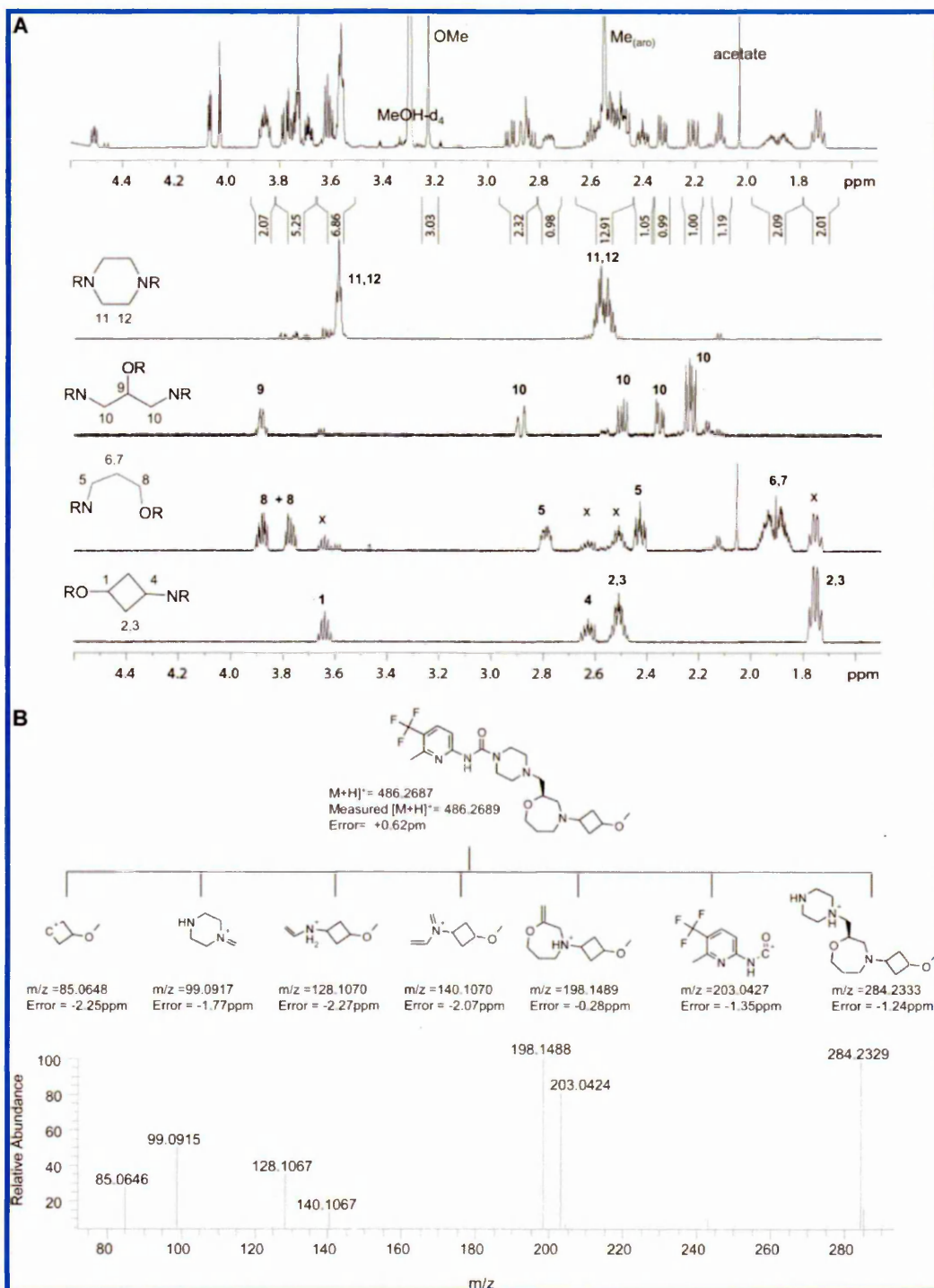


Figure 2. (A) Aliphatic regions of the ^1H NMR spectrum of the parent (AZX) (top) and of the selective 1D ^1H NMR TOCSY spectra of the individual ring moieties (below, in descending order: the piperazine ring, the individual chain-moieties of homomorpholine (i.e., the 1,3-diaminopropan-2-ol and the 3-amino-propanol), and the 3-amino-cyclobutanol moiety). Key: X indicates "coexcitation" (spectral contamination with the 3-amino-cyclobutanol) moiety. MeOH- d_4 is deuterated MeOH, the NMR solvent used. (B) Diagnostic MS-fragments (top) from the mass spectrum of the parent (AZX). Note: mass errors are within ± 3 ppm.

RESULTS

Identification of the Metabolites and Adducts of AZX in the Human Liver Micosome and Scaled-Up Bacterial

Cytochrome Enzyme Incubations with GSH. Several metabolites and adducts of AZX were detected and tentatively characterized in the incubate samples during the initial LC-MS (UPLC-Q-TOF) analyses. The main metabolites and adducts

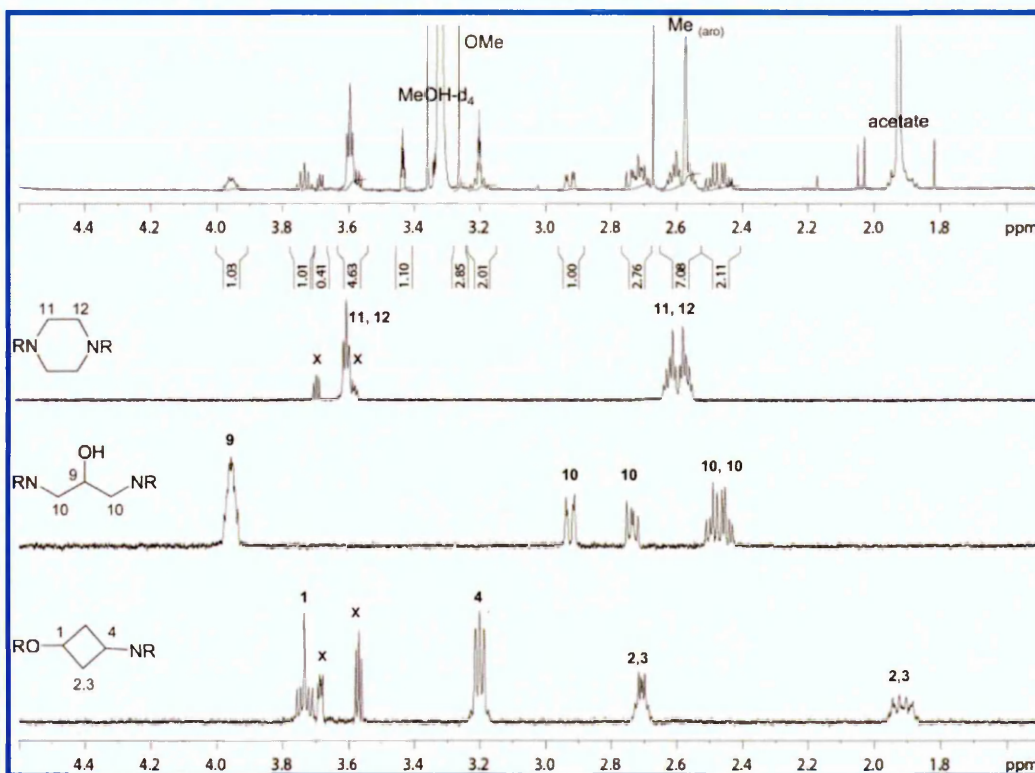


Figure 3. Aliphatic regions of the ^1H NMR spectrum of the isolated GSH-derived metabolite $[\text{M}+\text{H}]^+$ 662 (top) and of the selective 1D ^1H NMR TOCSY spectra of the individual ring moieties (below, in descending order: the piperazine ring, the 1,3-diamino-propan-2-ol of the homomorpholine, and the 3-aminocyclo-butanol). Key: X indicates “coexcitation” (spectral contamination) with an impurity. $\text{MeOH-}d_4$ = deuterated MeOH, the NMR solvent used. Note: the 3-amino-propanol moiety of the homomorpholine ring could not be detected.

in both the human liver microsome ($t = 30$ min) and the scaled-up bacterial cytochrome enzyme ($t = 16$ h) incubations were found to be identical, albeit present at different ratios (data not shown).

The total ion chromatogram of the scaled-up bacterial cytochrome enzyme-incubate (together with the selective ion chromatograms) are shown in Figure 1. The parent (AZX), eluting at 6.21 min, produced a molecular ion at $[\text{M}+\text{H}]^+$ 486. A minimum of six structurally different metabolites were identified. These included several oxidation products, such as a ring opened product (+18) with $[\text{M}+\text{H}]^+ = 504$ ($t_R = 5.57$ min), and a number of +16 oxidation products with $[\text{M}+\text{H}]^+ = 502$ ($t_R = 5.08, 5.28, 5.42, 5.72,$ and 6.06 min). Additionally, an O-demethylated metabolite was observed with $[\text{M}+\text{H}]^+ = 472$ ($t_R = 5.26$ min); an O-des-methyl homomorpholine hydrolysis product with $[\text{M}+\text{H}]^+ = 490$ ($t_R = 5.00$ min), as well as a dealkylated metabolite with $[\text{M}+\text{H}]^+ = 446$ ($t_R = 5.08$ min) together with its O-demethylated analogue with $[\text{M}+\text{H}]^+ = 432$ ($t_R = 4.56$ min) were also observed. However, the peak of interest was the GSH-derived adduct with $[\text{M}+\text{H}]^+ = 662$, eluting at $t_R = 5.34$ min.

The intact GSH-conjugate was not observed in the human liver microsome or bacterial cytochrome enzyme incubations.

Structural Characterization of the Parent (AZX) by ^1H NMR Spectroscopy and LC-MS. While the aromatic protons of the pyridine ring (2 doublets at $\delta^1\text{H}$ 7.90 and $\delta^1\text{H}$ 7.76, spectral region not shown) and both the aromatic ($\delta^1\text{H}$ 2.57) and the methoxy ($\delta^1\text{H}$ 3.27) methyls could be easily assigned, the aliphatic region of the spectrum was very complex due to

excessive signal overlap. The application of 2D NMR experiments (such as ^1H - ^1H COSY and ^1H - ^1H TOCSY) helped greatly in the assignments of the signals (data not shown), with the ^1H - ^1H COSY experiment showing 2- and 3-bond connectivities between neighboring protons, and the ^1H - ^1H TOCSY experiment creating correlations between all protons within a given spin system. In order to resolve and deconvolute the individual aliphatic ring-moieties and to preserve the signal multiplicities, 1D selective TOCSY experiments produced the most conclusive data (Figure 2A).

The aliphatic region of the spectrum was comprised of numerous multiplets from the piperazine ring protons ($\delta^1\text{H}$ 3.57 and $\delta^1\text{H}$ 2.56), from the 1,3-diamino-propan-2-ol ($\delta^1\text{H}$ 3.88, $\delta^1\text{H}$ 2.58 (an AM system) and $\delta^1\text{H}$ 2.41 (an AB system)), and the 3-amino-propanol ($\delta^1\text{H}$ 3.83 (AB), $\delta^1\text{H}$ 2.79, $\delta^1\text{H}$ 2.41, and $\delta^1\text{H}$ 1.89 (AB)) moieties of the homomorpholine ring, and from the 3-amino-cyclobutanol ($\delta^1\text{H}$ 3.64, $\delta^1\text{H}$ 2.62, $\delta^1\text{H}$ 2.51, and $\delta^1\text{H}$ 1.73).

The LC-MS data (UPLC-DAD-LTQ-Orbitrap) of AZX highlighted a molecular ion of $[\text{M}+\text{H}]^+ = 486.2689$, with fragment ions of $m/z = 203.0424$, $m/z = 284.2329$, $m/z = 128.1067$, $m/z = 198.1488$, $m/z = 140.1067$, $m/z = 85.0646$, and $m/z = 99.0915$. The mass spectrum and fragment ions (including mass errors in ppm) of AZX are shown in Figure 2B.

Isolation of the $[\text{M}+\text{H}]^+$ 662 Adduct by LC-DAD-MS Fraction Collection. The $[\text{M}+\text{H}]^+$ 662 adduct contained in the bacterial cytochrome enzyme samples (analyzed on the UPLC-DAD-LTQ-Orbitrap) showed a protonated molecular

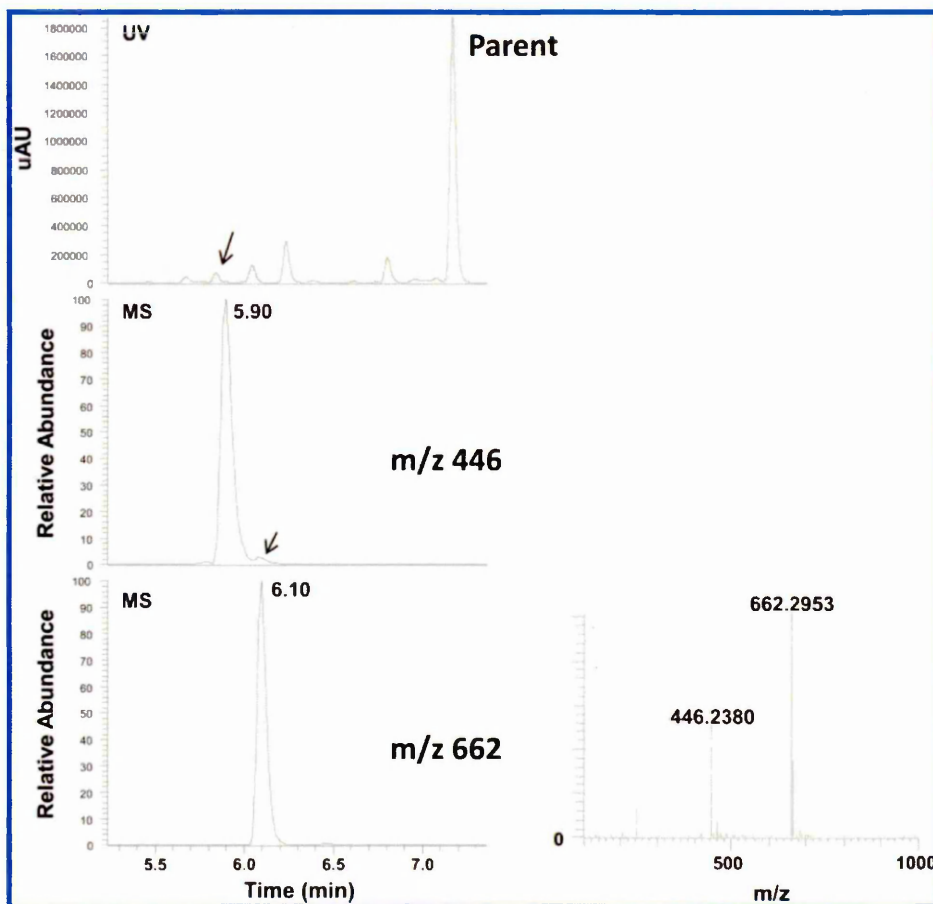


Figure 4. LC-MS data of the scaled-up bacterial cytochrome enzyme-GSH incubate sample 1 showing the UV chromatogram (at $\lambda = 280$ nm) and the selective ion chromatograms for $[M+H]^+$ 446 and $[M+H]^+$ 662. Data were generated on the UPLC-DAD-LTQ Orbitrap (Method 1). Key: The arrow indicates the small $[M+H]^+$ 446 in-source contribution from the $[M+H]^+$ 662 component ($t_R = 6.1$ min), highlighting that $[M+H]^+$ 446 is also formed in the gas-phase from $[M+H]^+$ 662. Note the small delay between the UV and MS detection.

ion with an accurate mass of $[M+H]^+$ 662.2953 and also revealed an in-source fragment at m/z 446.2380.

The isolation of $[M+H]^+$ 662 was conducted with bacterial cytochrome enzyme sample 3 (Method 2) collected into 96-well plates. On the basis of the MS-data and UV-response, the wells of interest were identified as wells 5–8 in row B, which were paired (wells B5–6 and B7–8) and subjected to ^1H NMR analysis, together with those (B9–10, B11–12, and B1–2, B3–4) representing the fronting and tailing edges of the peak, respectively.

Structural Characterization of the Isolated $[M+H]^+$ 662 Adduct by ^1H NMR Spectroscopy. The ^1H NMR spectra of the fractions confirmed that the majority of the AZX-related material was contained in fractions B5–6 and B7–8 and that these were found to be identical.

The ^1H NMR spectra showed that there were no changes in the chemical shifts of the aromatic protons (doublets at $\delta^1\text{H}$ 7.90 and $\delta^1\text{H}$ 7.76) or of the aromatic methyl signal ($\delta^1\text{H}$ 2.57); however, changes in the aliphatic region of the spectrum were evident. Selective ID TOCSY experiments (Figure 3) confirmed the presence of the piperazine ring (multiplets at $\delta^1\text{H}$ 3.58 and $\delta^1\text{H}$ 2.57) and 3-amino-cyclobutanol (multiplets at $\delta^1\text{H}$ 3.74, $\delta^1\text{H}$ 3.21, $\delta^1\text{H}$ 2.71, and $\delta^1\text{H}$ 1.92). Selective irradiation of either multiplets (at $\delta^1\text{H}$ 2.45 or $\delta^1\text{H}$ 3.94)

resolved the same signals, consistent with 1,3-diamino-propan-2-ol ($\delta^1\text{H}$ 3.94, $\delta^1\text{H}$ 2.81 (an AB system), and $\delta^1\text{H}$ 2.45 (an AB system)). However, the 3-amino-propanol moiety of the homomorpholine ring could not be detected. Signals representing the GSH-moiety were not detected either, implying that the metabolite in question was consistent with a dealkylated metabolite (with a theoretical mass of 446), as shown in Figure 3.

Structural Recharacterization of the Isolated $[M+H]^+$ 662-Adduct by LC-MS. The LC-MS (UPLC-DAD-LTQ Orbitrap) analyses of the ^1H NMR samples confirmed that the contents were consistent with $[M+H]^+$ 446. Analysis of all the wells in row B (B1–12) highlighted that $[M+H]^+$ 662 was undetectable, indicating that it had degraded to $[M+H]^+$ 446 during fraction collection. Although baseline separation between the two UV-peaks was not fully achieved in the semiprep separation ($t_R = 5.00$ min for $[M+H]^+$ 446 and 5.09 min for $[M+H]^+$ 662, i.e., approximately 5.4 s between peaks, with a peak width of 12 s), the high speed HTC collection was considered adequate for their initial separation. However, the LC-DAD data showed that soon after the initial injections the peaks started to merge, mirroring the conversion of $[M+H]^+$ 662 to $[M+H]^+$ 446. The observation of m/z 446 as an in-

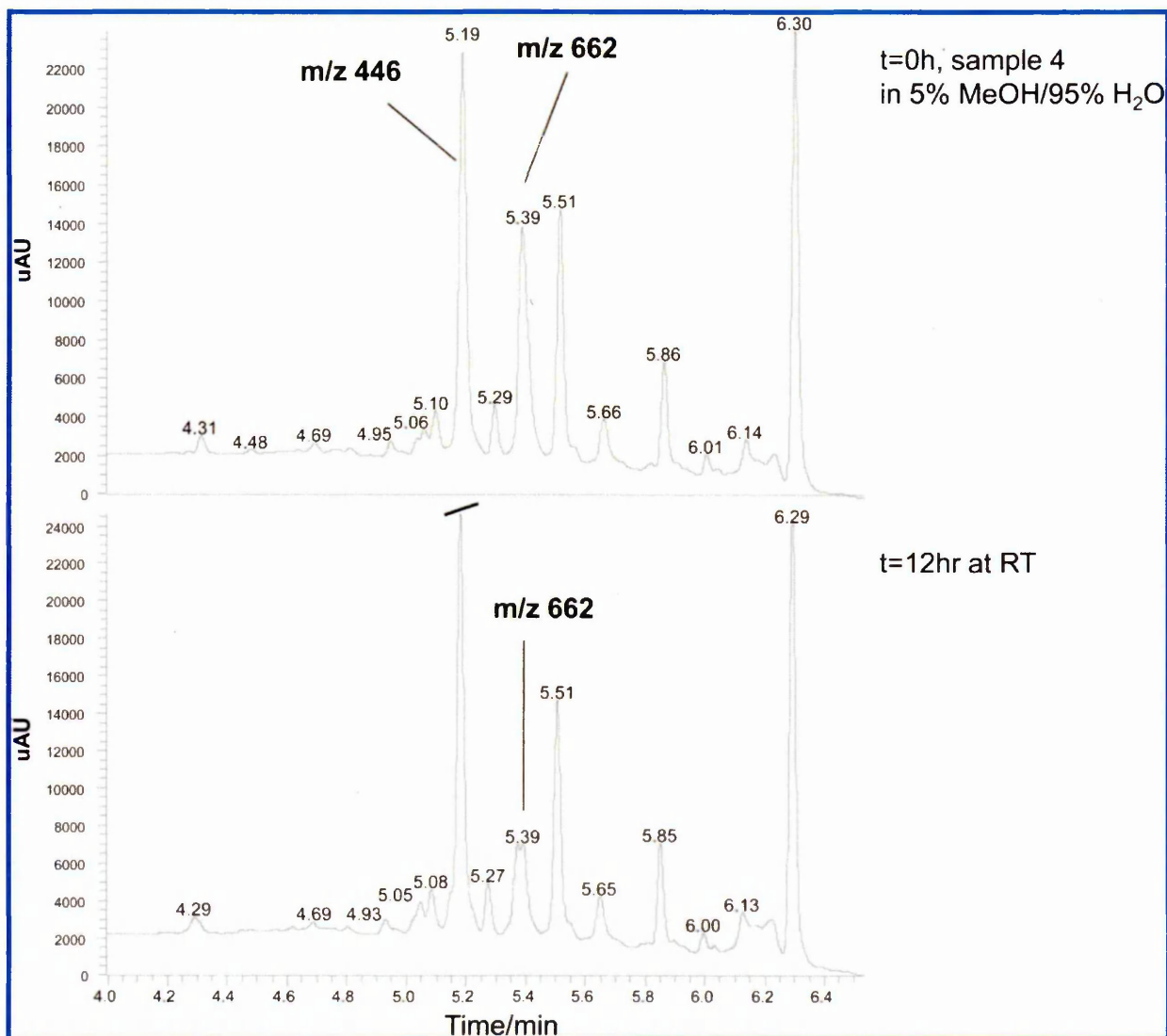


Figure 5. UV chromatogram ($\lambda = 280$ nm) assessing the stability of the GSH-derived metabolite $[M+H]^+$ 662 of a bacterial cytochrome enzyme extract (sample 4) comparing $t = 0$ h with $t = 12$ h. The peak identity was derived from the MS data. Key: RT = room temperature.

source fragment (as shown in Figure 4) additionally masked the degradation process.

Stability of $[M+H]^+$ 662 Investigated by LC-MS. The bacterial cytochrome enzyme sample 4 was analyzed immediately after reconstitution on the UPLC-DAD-LTQ Orbitrap with analytical LC Method 1 to ensure separation of the two components. Comparison of the UV-peak intensities at $t = 0$ and 12 h showed that the $[M+H]^+$ 662 peak decreased, while $[M+H]^+$ 446 increased (Figure 5). The stability of the $[M+H]^+$ 662 metabolite was also examined in acidic and basic conditions, which confirmed that under non-neutral conditions the degradation was accelerated (acid > base > neutral) (data not shown).

The $[M+H]^+$ 662 adduct was also shown to degrade upon storage. Reanalysis of the residual bacterial cytochrome enzyme-incubate samples (samples 1 and 2, used for method development, and sample 5, stored at 4 °C until the end of the investigations) showed that $[M+H]^+$ 662 was depleted while $[M+H]^+$ 446 was abundant. Reanalysis of residual aliquots

(stored at 4 °C for approximately 1 month) of the original incubate samples also confirmed that $[M+H]^+$ 662 had degraded (data not shown). This finding helped to address the question whether $[M+H]^+$ 446 was a metabolite or degradation product. The LC-MS data collected (on the UPLC-Q-ToF) during the original incubations showed $[M+H]^+$ 662 in vast excess in the human liver microsome-(30 min)-incubations compared to the scale-up bacterial cytochrome enzyme-(16 h)-incubations where $[M+H]^+$ 446 was abundant (data not shown), suggesting that $[M+H]^+$ 662 was converted to $[M+H]^+$ 446 either metabolically during the extended incubation time or, more likely, chemically.

Structural Characterization of the $[M+H]^+$ 662-Adduct by LC-MS/MS. The MS/MS fragmentation data (generated on the UPLC-DAD-LTQ-Orbitrap) of the $[M+H]^+$ 662.2953 adduct (Figure 6) provided evidence of Cys-Gly cyclization and formation of a thiazolidine moiety. The mass spectrum showed the in-source fragment of $[M+H]^+$ 446.2380 (with a mass error of +1.45 ppm), as well as 2 further diagnostic fragments at m/z

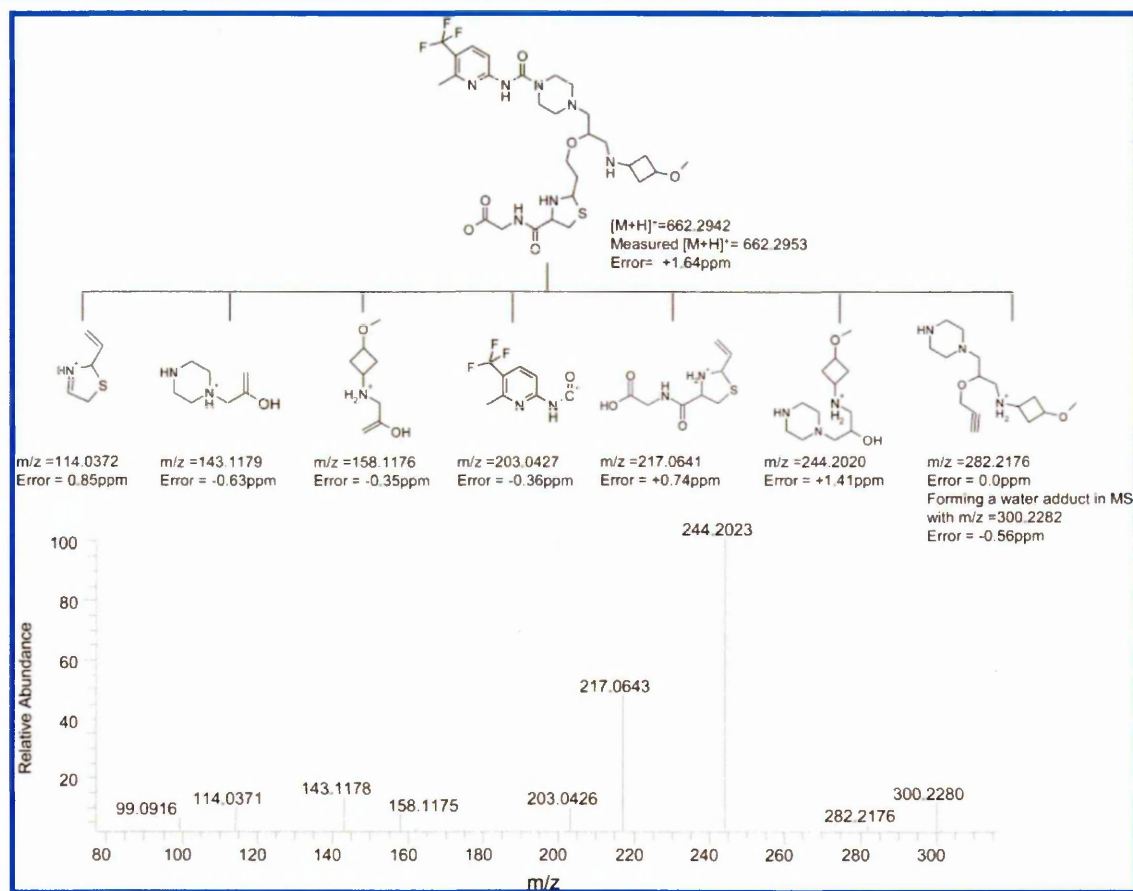


Figure 6. Diagnostic MS-fragments (top) from the mass spectrum (bottom) of the GSH-derived metabolite $[M+H]^+$ 662. Note: the mass errors are within ± 3 ppm.

217.0643 and m/z 114.0371, representing the thiazolidine–glycine moieties. A clear change in the homomorpholine ring fragmentation from the parent (AZX) was also observed (lacking fragments at m/z 198.1488 and m/z 140.1067), while the presence of the m/z 158.1175 and m/z 143.1178 fragments were indicative of major structural differences in the homomorpholine region of the molecule. The m/z 203.0427 fragment indicated that the aromatic region of the molecule was unchanged.

Incubation of AZX with KCN and Methoxylamine. The incubation of AZX with methoxylamine produced an adduct with $[M+H]^+$ 531.2886 with a characteristic fragment of m/z 329.2544 (Figure 7), producing (MS³) fragments at m/z 282.2175 and m/z 244.2019, indicative of the bioactivation to an carbinolamine, ring-opening of the homomorpholine, and the formation of the aldehyde functional group. However, incubating AZX in human liver microsomes in the presence of KCN did not produce a detectable quantity of the expected CN adduct for an iminium ion intermediate (mass ion $[M+H]^+$ 511), suggesting the equilibrium favored the carbinolamine/aldehyde.^{12–14}

Proposed Mechanism of Formation of $[M+H]^+$ 662. The proposed mechanism of formation of $[M+H]^+$ 662 involves initial oxidation of the homomorpholine moiety via cytochrome P450-mediated bioactivation to a carbinolamine intermediate, followed by ring-opening to a reactive aldehyde intermediate^{12,13} (Figure 8, Step 1) and conjugation with either

the amino^{15–17} or thiol⁵ group of the cysteine moiety (Figure 8, Step 2, A and B, respectively). The resulting Schiff base^{15–17} (A) or substituted mercaptomethanol⁵/carbosulfonium (B) intermediates then ring-contrast to a thiazolidine (Figure 8, Step 3) with cleavage of the iso-peptide bond (liberating the glutamic acid) prior to (A) or after the intermolecular conjugation (B).

The failure to detect the intact GSH-conjugate in the human liver microsomes or bacterial cytochrome enzyme incubations suggests either facile hydrolysis of the glutamate or a preference of route A. The subsequent loss of the thiazolidine–glycine moiety then results in the observed formation of the $[M+H]^+$ 446 degradation product.

Incubation of AZX in Human Liver Microsomes with Different Trapping Agents. Further experiments were conducted with structurally modified trapping reagents (Table 1) using clozapine as the positive control (individual data not shown) to further investigate the mechanism. Incubations of AZX with agents 3 and 4, characterized by variations in the peptide bonds and modifications in the N-terminus, produced adducts with the same molecular weight, retention time, and fragment ions (data not shown) as the GSH-derived adduct 1, indicating the loss of the Glu (γ or α) or β -Asp residue. Reagent 5 (C-terminal substitution of Gly with Lys) produced an adduct (with $[M+H]^+$ 733) also characterized by the expulsion of Glu. No adduct was observed with 6 (dansylation of γ Glu¹⁸) suggesting either the necessity of a free N-terminal amino

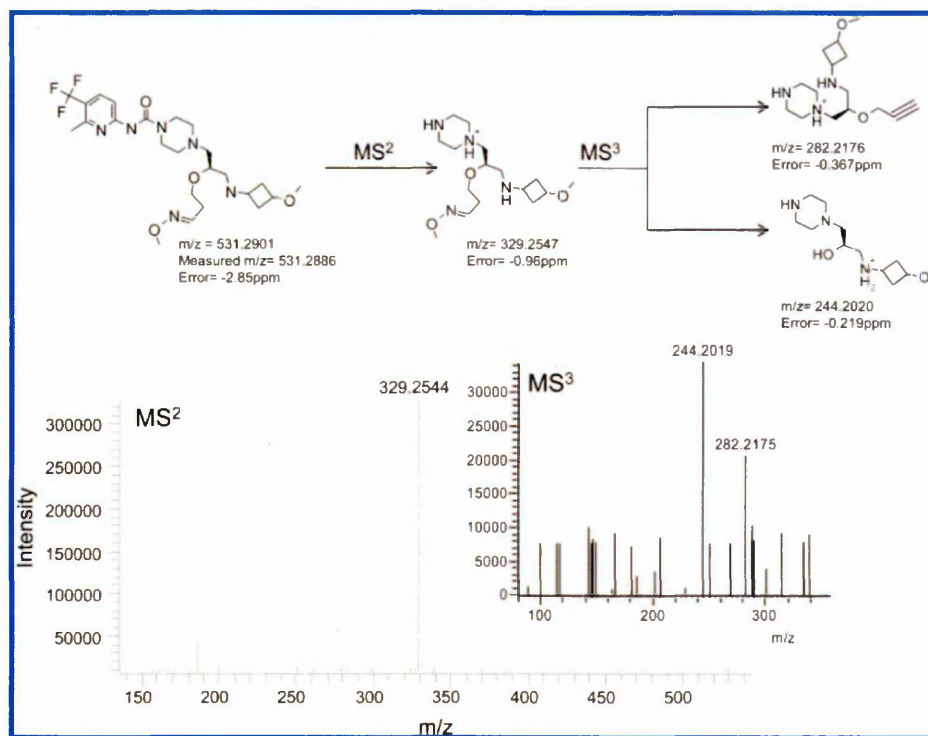


Figure 7. Diagnostic MS-fragments (MS^2 and MS^3 , top) derived from the fragmentation of the AZX-methoxylamine adduct (m/z 531.2886). The MS^2 spectrum of m/z 531 and the MS^3 mass spectrum of m/z 531 to 329 are shown below. Note: the mass errors are within ± 3 ppm.

group on Glu or prevention of cleavage of the Glu-Cys bond, or simply steric hindrance. The GSH-derivative **8** (containing the γ Glu but lacking the C-terminal Gly) did not produce any trapped adduct, whereas **9** (retaining the Gly but lacking the N-terminal γ Glu) produced the $[M+H]^+$ 662 adduct with the same structural properties as those in **1**. Contrary to the piperazines forming adducts with Cys (**10**) or N-Ac-Cys (**7**),¹⁰ no adduct was observed with AZX with either of these agents. The $[M+H]^+$ 662 adduct was also observed with GSEE (**11**, ethyl-esterification of Gly). The MS-data (i.e., relative quantification by MS, Q-ToF) showed a $[M+H]^+$ 690/662 ratio of 1:5 (data not shown). The assumption that commercial GSEE had partially hydrolyzed to GSH (either metabolically or chemically) was disproved by incubation with clozapine, as the corresponding hydrolysis product for the clozapine GSEE adduct (with an expected $[M+H]^+$ 632) was not detected under the same conditions (data not shown). Similarly, the presence of clozapine-GSH adducts in the control incubations proved that intact GSH was available for reaction.

DISCUSSION

This study demonstrated that the bioactivated homomorpholine moiety of compound AZX reacted rapidly with GSH and various other trapping agents, of which most of them contained the Cys-Gly-moiety (as shown in Table 1).

Unexpectedly, the Cys-Gly adduct $[M+H]^+$ 662 of AZX proved to be unstable, degrading readily during its isolation to the desalkyl product with $[M+H]^+$ 446, which was observed as an in-source fragment in the LC-MS analyses but also as a metabolite in the human liver microsome and bacterial cytochrome enzyme incubations. The presence of m/z 446 as in-source fragment, however, initially obscured the detection of

the $[M+H]^+$ 662 decomposition process. The very failure in successfully characterizing the isolated $[M+H]^+$ 662 adduct by 1H NMR spectroscopy prompted the reinterrogation of the LC-MS data, as the 1H NMR spectrum showed the structure to be exclusively consistent with the dealkylated metabolite $[M+H]^+$ 446, lacking the 3-aminopropanol moiety of the homomorpholine ring. The LC-DAD-MS data, acquired on the LTQ-Orbitrap after the isolation, confirmed the degradation of $[M+H]^+$ 662 to $[M+H]^+$ 446. In addition, the LC-MS data (generated on the Q-ToF) of the original human liver microsome (30 min) and scaled-up bacterial cytochrome enzyme (16 h) incubations highlighted that the $[M+H]^+$ 446 metabolite featured more prominently in the bacterial cytochrome enzyme incubates, due to enzymatic transformation during the extended incubation time or chemical degradation, or a mix of both. Reanalysis of the stored samples, however, supported the facile chemical degradation of $[M+H]^+$ 662.

Although the proposed Cys-Gly-thiazolidine adduct could not be structurally verified by 1H NMR spectroscopy, the successful structural characterization of $[M+H]^+$ 662 (by LC-MS/MS) and its $[M+H]^+$ 446 degradation product (by LC-MS and 1H NMR spectroscopy), as well as the MS^n fragmentation data of the methoxylamine adduct allowed us to propose the mechanism of its formation. This involved initial enzymatic oxidation of AZX to a carbinolamine and the formation of the aldehyde^{12,13} followed by adduct formation with Cys-Gly or GSH (via route A or B) and rearrangement to the thiazolidine. The proposal of both routes derived from the data in Table 1, as the free thiol group, present in every trapping agent, did not ensure adduct formation. Likewise, the presence of the glutamate (α - or γ -) or aspartate moieties provided no

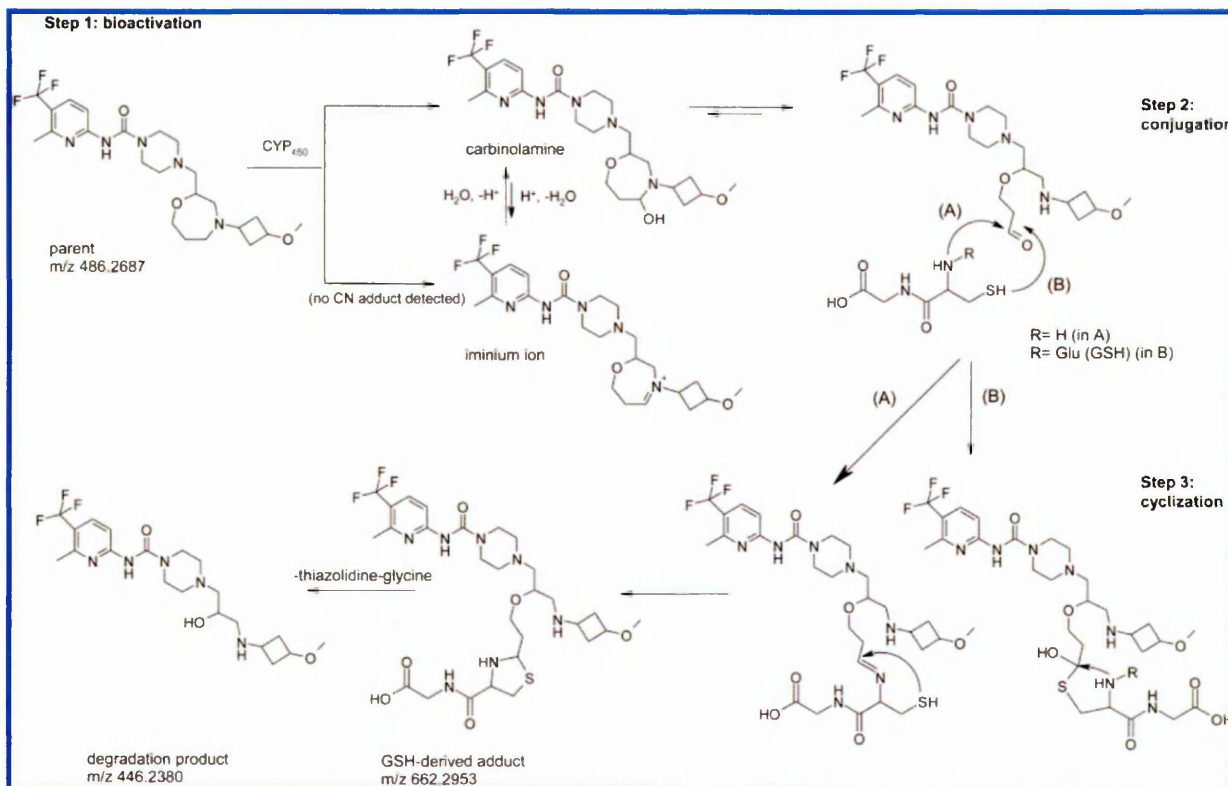


Figure 8. Proposed mechanism of formation of $[M+H]^+ 662$ and its subsequent decomposition to $[M+H]^+ 446$. Step 1: bioactivation to the aldehyde. Step 2: (A) nucleophilic addition of the free Cys-Gly amine group or (B) nucleophilic addition of GSH via the thiol group followed by loss of the glutamate moiety. Step 3: cyclization to form the thiazolidine, followed by the elimination of the ethylene-thiazolidine-glycine moiety.

indication of preference, as these moieties were expelled in either route producing the $[M+H]^+ 662$ adduct.

Both routes have literature precedents, with route A^{15–17} describing nucleophilic addition of the primary amino group of Cys (forming a carbinolamine), followed by elimination of water forming an imine (a reactive Schiff base) intermediate. Nucleophilic attack of the Cys-thiol function on the imine carbon produces thiazolidine-glycine. The mechanism has been previously detailed for the detoxification of the ethanol metabolite acetaldehyde.¹⁶

Route B⁵ describes the nucleophilic addition of the Cys-thiol group to the aldehydic carbon generating the substituted mercaptomethanol intermediate and subsequently, following elimination of water, a carbosulfonium intermediate.⁵ Here, ring contraction occurs via nucleophilic attack of the Cys-amino group on the carbosulfonium intermediate to form the thiazolidine-glycine-adduct.^{5,15–17}

While recent literature data highlighted examples of desired reversible binding, such as saxagliptin (Onglyza) where prolonged binding via the cyanide functional group¹⁹ to the target peptidase inhibitor balanced maximizing pharmacodynamic effects with minimizing drug levels,^{20,21} the formation of the reactive aldehyde intermediate as described in this article was an entirely unexpected and undesired effect.

The mechanism of the chemical degradation of the $[M+H]^+ 662$ adduct to the observed $[M+H]^+ 446$ product was initially unclear with two possible routes to the final alcohol, hydrolysis, or elimination. However, an experiment with water, labeled with oxygen-18, showed no oxygen-18 incorporation, thereby

disproving the hydrolysis route (experimental details and results are in the Supporting Information). Hence, elimination assisted by either an intramolecular hydrogen bond between one of the amines on the core of the molecule and the ether oxygen or by protonation of the oxygen by acid present in the solution could weaken the oxygen-carbon bond. A base either from the molecule or from solution could then deprotonate the 2-position of the ethyl chain thereby leading to elimination of the alkene to afford the alcohol.

The observations made in the human liver microsome incubation experiments (Table 1) allowed us to come to the following conclusions. First, the data suggest that the hydrolysis of the GSH γ -glutamyl-cysteine isopeptide bond is not reliant on the presence of GGT,⁹ based on the observation that modifications of the X-Cys peptide bond, represented by α Glu and β Asp, did not have any negative impact on $[M+H]^+ 662$ formation (Table 1). In fact, as the $[M+H]^+ 662$ adduct was formed with GSH, α GSH, and β Asp-Cys-Gly, as well as Cys-Gly alone, the release of any residue blocking the cysteine amino group appeared to be a requirement for successful adduct formation. Although a GSH-adduct was produced in the control incubations with clozapine (data not shown), no intact GSH adducts were detected for any of the trapping agents with AZX (data not shown). This suggested that hydrolysis of the glutamate (or β Asp) moiety must have occurred readily^{22,23} or that the aldehyde intermediate of AZX had a preference for the amino-group of hydrolyzed GSH (and its derivatives) (route A). This observation is mirrored in the literature. A study on acetaldehyde¹⁷ showed that there was only limited adduct

formation with intact GSH (nucleophilic attack of the thiol), while rapid equimolar adduct formation was reported with Cys-Gly, following the addition of γ GTP.

Second, adduct formation not only requires either the unsubstituted/free amino group (A) or the thiol function of cysteine (B) but also a C-terminal amino acid, as neither Cys or γ Glu-Cys produced an adduct with AZX. Successful adduct formation appeared to rely on the presence of a terminal glycine or lysine group. However, the importance of these groups in either the intramolecular rearrangement or the initial addition of Cys-Gly to the aldehydic carbon would require further investigation.

In summary, we were able to determine the structure of the Cys-Gly adduct and confirm the presence of the aldehyde intermediate responsible for its formation. However, as the Cys-Gly $[M+H]^+$ 662 adduct was observed with GSH as well as with several other trapping agents (as outlined in Table 1), the possibility of additional alternative mechanisms of formations cannot be ruled out.

■ ASSOCIATED CONTENT

■ Supporting Information

Synthesis of dECK, incubation of the enantiomer of AZX with GSH, and an investigation of the degradation of $[M+H]^+$ 662 in the presence of $H_2^{18}O$. This material is available free of charge via the Internet at <http://pubs.acs.org>.

■ AUTHOR INFORMATION

Corresponding Author

*Tel: +44-1625-518479. Fax: +44-1625-230614. E-mail: Eva.Lenz@astrazeneca.com.

Present Addresses

§(R.S.) EMD Serono Research and Development Institute, 45A Middlesex Turnpike, Billerica, MA 01821.

|| (M.B.) IntelliSyn R&D, Department of Medicinal Chemistry, 7171 Frederick-Banting, Montreal, QC, Canada H4S 1Z9.

Funding

This study was fully financed by AstraZeneca Ltd.

Notes

The authors declare no competing financial interest.

■ ACKNOWLEDGMENTS

We thank Dr. Chad Elmore (AstraZeneca R&D, Moelndal, Sweden) for his helpful advice regarding the mechanism of formation and decomposition of the reactive metabolite.

■ ABBREVIATIONS

AZX, 4-[[4-(3-methoxycyclobutyl)-1,4-oxazepan-2-yl]methyl]-N-[6-methyl-5-(trifluoromethyl)-2-pyridyl]piperazine-1-carboxamide; UPLC, ultrahigh-performance liquid chromatography; DAD, diode array detector; MSMS, tandem mass spectrometry; MSⁿ, multistage tandem mass spectrometry; HCD, higher energy collisional dissociation; ESI, electrospray ionization; +ESI, positive ion electrospray ionization; CH₃CN, acetonitrile; MeOH, methanol; COSY, correlation spectroscopy; TOCSY, total correlation spectroscopy; ROESY, rotating frame Overhauser effect spectroscopy; t_R , retention time; dECK, dansyl- γ Glu-Cys-Lys

■ REFERENCES

(1) Evans, D. C., Watt, A. P., Nicoll-Griffith, D. A., and Baillie, T. A. (2004) Drug-protein adducts: an industry perspective on minimizing

the potential for drug bioactivation in drug discovery and development. *Chem. Res. Toxicol.* 17, 3–16.

(2) Baillie, T. A. (2006) Future of toxicology: metabolic activation and drug design: Challenges and opportunities in chemical toxicology. *Chem. Res. Toxicol.* 19, 889–893.

(3) Baillie, T. A. (2009) Approaches to the assessment of stable and chemically reactive drug metabolites in early clinical trials. *Chem. Res. Toxicol.* 22, 263–266.

(4) Prakash, C., Sharma, R., Gleave, M., and Nedderman, A. (2008) *In vitro* screening techniques for reactive metabolites for minimizing bioactivation potential in drug discovery. *Curr. Drug Metab.* 9, 952–964.

(5) Singh, S., and Dryhurst, G. (1992) Metabolism of 5-hydroxytryptamine by brain synaptosomes and microsomes in the presence of cysteine and glutathione. *J. Med. Chem.* 35, 2667–2672.

(6) Ludwig, E., and Eyer, P. (1995) Reactivity of glutathione adducts of 4-(dimethylamino) phenol. Formation of a highly reactive cyclization product. *Chem. Res. Toxicol.* 8, 310–315.

(7) Monks, T. J., and Lau, S. S. (1997) Biological reactivity of polyphenolic-glutathione conjugates. *Chem. Res. Toxicol.* 10, 1296–1313.

(8) Mutlib, A., Chen, H., Shockcor, J., Espina, R., Chen, S., Cao, K., Du, A., Nemeth, G., Prakash, S., and Gan, L. S. (2000) Characterization of novel glutathione adducts of a non nucleoside reverse transcriptase inhibitor, (S)-6-chloro-4-(cyclopropylethynyl)-4-(tri-fluoromethyl)-3,4-dihydro-2(1H)-quinazolinone (DPC 961), in rats. Possible formation of an oxirene metabolic intermediate from a disubstituted alkyne. *Chem. Res. Toxicol.* 13, 775–784.

(9) Fliege, R., and Metzler, M. (2000) Electrophilic properties of Patulin. N-Acetylcysteine and glutathione adducts. *Chem. Res. Toxicol.* 13, 373–381.

(10) Doss, G. A., Miller, R. R., Zhang, Z., Teffera, Y., Nargund, R. P., Palucki, B., Park, M. K., Tang, Y. S., Evans, D. C., and Baillie, T. A. (2005) Metabolic activation of a 1, 3-disubstituted piperazine derivative: evidence for a novel ring contraction to an imidazoline. *Chem. Res. Toxicol.* 18, 271–276.

(11) Yu, J., Mathisen, D. E., Burdette, D., Brown, D. G., Becker, C., and Aharony, D. (2010) Identification of multiple glutathione conjugates of 8-amino-2-methyl-4-phenyl-1,2,3,4-tetrahydroisoquinoline maleate (Nomifensine) in liver microsomes and hepatocyte preparations: evidence of the bioactivation of Nomifensine. *Drug Metab. Dispos.* 38, 46–60.

(12) Kalgutkar, A. S., Dalvie, D. K., Aubrecht, J., Smith, E. B., Coffing, S. L., Cheung, J. R., Vage, C., Lame, M. E., Chiang, P., McClure, K. F., Maurer, T. S., Coelho, R. V., Jr., Soliman, V. F., and Schildknecht, K. (2007) Genotoxicity of 2-(3-chlorobenzoyloxy)-6-(piperazinyl) pyrazine, a novel 5-hydroxytryptamine 2c receptor agonist for the treatment of obesity: role of metabolic activation. *Drug Metab. Dispos.* 35, 848–858.

(13) Mašič, L. P. (2011) Role of cyclic tertiary amine bioactivation to reactive iminium species: Structure toxicity relationship. *Curr. Drug Metab.* 12, 35–50.

(14) Huang, T.-C., Huang, L.-Z., and Ho, C.-T. (1998) Mechanistic studies on thiazolidine formation in aldehyde/cysteamine model systems. *J. Agric. Food Chem.* 46, 224–227.

(15) Kallen, R. G. (1971) The mechanism of reactions involving Schiff base intermediates, thiazolidine formation from L-cysteine and formaldehyde. *J. Am. Chem. Soc.* 93, 6236–6248.

(16) Anni, H., Pristatsky, P., and Israel, Y. (2003) Binding of acetaldehyde to a glutathione metabolite: mass spectrometric characterization of an acetaldehyde-cysteinylglycine conjugate. *Alcohol: Clin. Exp. Res.* 10, 1613–1621.

(17) Kera, Y., Kiriya, T., and Komura, S. (1985) Conjugation of acetaldehyde with cysteinylglycine, the first metabolite in glutathione breakdown by gamma-glutamyltranspeptidase. *Agents Actions* 17, 48–52.

(18) Schmidt, R., Walles, M., and Panetta, R. (2008) *Comparison of New Peptide Based Reagents to Conventional Glutathione and Methoxyl Amine for the Trapping of Reactive Metabolites*, 15th North America

Regional ISSX Meeting, Oct 12–16, 2008, San Diego, CA. *Drug Metab. Rev.* 40 (s3), 221.

(19) Kurti, L., and Czako, B. (2005) Pinner Reaction, in *Strategic Applications of Named Reactions in Organic Synthesis* (Hayhurst, J., Ed.) pp 352–353, Elsevier Academic Press, London.

(20) Wang, A., Dorso, C., Kopcho, L., Locke, G., Langish, R., Harstad, E., Shipkova, P., Marcinkeviciene, J., Hamann, L., and Kirby, M. S. (2012) Potency, selectivity and prolonged binding of saxagliptin to DPP4: maintenance of DPP4 inhibition by saxagliptin in vitro and ex vivo when compared to a rapidly-dissociating DPP4 inhibitor. *BMC Pharmacol.* 12, 1–11.

(21) Fura, A., Khanna, A., Vyas, V., Koplowitz, B., Chang, S.-Y., Caporuscio, C., Boulton, D. W., Christopher, L. J., Kristina, D., Chadwick, K. D., Hamann, L. G., Humphreys, W. G., and Kirby, M. (2009) Pharmacokinetics of the dipeptidyl peptidase 4 inhibitor Saxagliptin in rats, dogs, and monkeys and clinical projections. *Drug Metab. Dispos.* 37, 1164–1171.

(22) Kohjin Co., Ltd. (2008) Revised GRAS Notice for L-Glutathione for Use as a Food Ingredient. Submitted to Center for Food Safety and Applied Nutrition, FDA. http://www.accessdata.fda.gov/scripts/cfn/gras_notices/804895A.PDF.

(23) Deshmukh, M., Kutscher, H., Stein, S., and Sinko, P. (2009) Nonenzymatic, self-elimination degradation mechanism of glutathione. *Chem. Biodiversity* 6, 527–539.

6. METHANOL ADDUCTS LEADING TO THE IDENTIFICATION OF A REACTIVE ALDEHYDE METABOLITE OF CPAQOP IN HUMAN LIVER MICROSOMES BY ULTRA-HIGH PERFORMANCE LIQUID CHROMATOGRAPHY/MASS SPECTROMETRY

Reproduced with permission from John Wiley and Sons. All rights reserved.

Rapid Commun. Mass Spectrom. 2017, 31, 145–151
(wileyonlinelibrary.com) DOI: 10.1002/rcm.7772

Methanol adducts leading to the identification of a reactive aldehyde metabolite of CPAQOP in human liver microsomes by ultra-high-performance liquid chromatography/mass spectrometry

Scott Martin^{1*}, Eva M. Lenz¹, Robin Smith², David G. Temesi^{2,†}, Alexandra L. Orton¹ and Malcolm R. Clench³

¹Oncology iMED, Hodgkin Building, Chesterford Science Park, AstraZeneca UK Ltd., Saffron Walden, Essex CB10 1XL, UK

²Oncology iMED, Alderley Park, AstraZeneca UK Ltd., Macclesfield, Cheshire SK10 4TG, UK

³Biomedical Research Centre, Sheffield Hallam University, Howard Street, Sheffield S1 1WB, UK

RATIONALE: The incubation of CPAQOP (1-[(2R)-2-[[4-[3-chloro-4-(2-pyridyloxy)anilino]quinazolin-5-yl]oxymethyl]-1-piperidyl]-2-hydroxy) with human liver microsomes generated several metabolites that highlighted the hydroxyacetamide side chain as a major site of metabolism for the molecule. The metabolites were derived predominantly from oxidative biotransformations; however, two unexpected products were detected by liquid chromatography/ultraviolet/mass spectrometry (LC/UV/MS) and identified as methanol adducts. This observation prompted further LC/MS investigations into their formation.

METHODS: Three separate incubations of CPAQOP were conducted in human liver microsomes; Naïve, fortified with methoxyamine and fortified with glutathione. Separation was achieved *via* ultra-high-performance liquid chromatography with either methanol or acetonitrile gradients containing formic acid. MS analysis was conducted by electrospray ionisation LTQ Orbitrap mass spectrometry acquiring accurate mass full scan, data-dependent MS² and all ion fragmentation.

RESULTS: No methanol adducts were detected by MS when acetonitrile was used in the mobile phase instead of methanol, verifying that a metabolite was reacting with methanol on column. Although this reactive metabolite could not be isolated or structurally characterised by LC/MS directly, product ion spectra of the methanol adducts confirmed addition of methanol on the hydroxyacetamide side chain. Additional experiments using methoxyamine showed the disappearance of the two methanol adducts and appearance of a methoxyamine adduct, confirming the presence of an aldehyde. Product ion spectra of the methoxyamine adduct confirmed addition of methoxyamine to the hydroxyacetamide side chain.

CONCLUSIONS: The proposed bioactivation of CPAQOP occurred *via* the reactive aldehyde intermediate, which readily reacted with methanol in the mobile phase to form a pair of isomeric hemiacetal methanol adducts. In acidified methanol the equilibrium favoured the methanol adduct and in acidified acetonitrile it favoured the hydrate; therefore, the reactive aldehyde metabolite was not detected and could not be structurally characterised directly. Copyright © 2016 John Wiley & Sons, Ltd.

Metabolite identification studies within drug discovery are generally used to identify; metabolically labile sites on chemical structures, human metabolites which may not be represented in the toxicological species, active metabolites or potential reactive/toxic metabolites, which are of concern for the pharmaceutical industry.^[1–3] These discovery studies are conducted *in vitro* and generally involve incubation of a test compound in hepatocytes or microsomes, which mimic the most prevalent metabolic processes occurring in the liver. Typically, samples are taken from the test compound incubates, then added to acetonitrile to quench the reaction at $t = 0$ min

(control) and at a terminal time point (usually 30–60 min). Subsequently, samples are analysed on high-resolution accurate mass ultra-high-performance liquid chromatography/tandem mass spectrometry (UHPLC/MS/MS) systems and comparison of the $t = 0$ min vs the $t = 60$ min samples enables easier identification of metabolites from endogenous components. The analyses can be both challenging and time consuming even when identifying only a small number of metabolites. Often the data has to be generated and reported quickly to impact the chemistry design and unusual unexpected metabolites/products are not fully investigated due to time constraints. Such products can occasionally be formed through reactive or toxic metabolites.

Here we present an unusual finding from an *in vitro* metabolite identification study of CPAQOP (1-[(2R)-2-[[4-[3-chloro-4-(2-pyridyloxy)anilino]quinazolin-5-yl]oxymethyl]-1-piperidyl]-2-hydroxy), a representative compound from a structurally related chemical series, in human liver microsomes (HLM). CPAQOP (Fig. 1) generated several

* Correspondence to: S. Martin, Oncology iMED, AstraZeneca UK Ltd., Hodgkin Building, Chesterford Science Park, Saffron Walden, Essex CB10 1XL, UK.
E-mail: scott.martin2@astrazeneca.com

Present address: (DGT) Recipharm, Vale of Bardsley, Ashton-under-Lyne, Lancashire OL7 9RR, UK

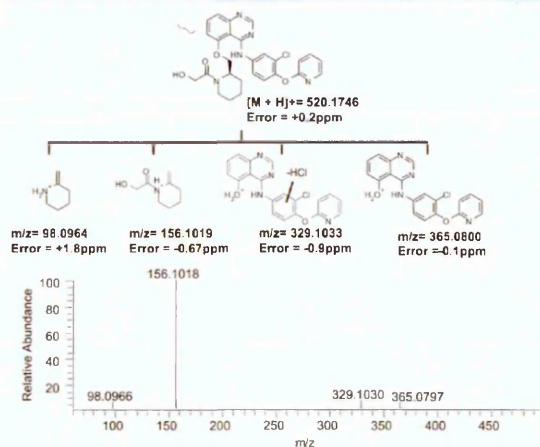


Figure 1. Accurate mass HCD-MS positive product ion mass spectrum of CPAQOP (bottom) and proposed product ions with theoretical exact mass and mass error in ppm (top).

metabolites in HLM that were predominantly oxidative biotransformation products, which highlighted the hydroxyacetamide side chain as a major site of metabolism for the molecule. However, two unexpected methanol adduct products were also detected with different retention times yet identical mass. Methanol adducts are fairly common in mass spectrometry and are normally identified as analytical artefacts of the parent drug, generated during the positive ion electrospray ionisation process. Pozo *et al.*^[4] reported the analysis of steroids using electrospray-generated adducts such as $[M + \text{methanol}]$ or $[M + \text{Na} + \text{methanol}]$. In this case, CPAQOP reacted with methanol in the mobile phase prior to the MS ionisation process. The methanol adducts not only eluted at a different retention time to the parent drug, but two chromatographically separate methanol adduct peaks were observed, indicating the presence of isomers. These adducts were not detected in the control sample or in the analysis where acetonitrile replaced methanol as the mobile phase. This inferred a metabolic transformation to a reactive metabolite formed in the $t = 60$ sample, which subsequently generated the methanol adducts on injection onto the UHPLC column. The formation of these methanol adducts is subject to further investigation in this paper.

EXPERIMENTAL

Chemicals

CPAQOP was synthesised at AstraZeneca R&D (Alderley Park, Macclesfield, UK).

Methanol, acetonitrile and formic acid were all of analytical grade and supplied by Fisher Scientific (Loughborough, UK). Methoxyamine hydrochloride was sourced from Sigma-Aldrich (Poole, UK). All other chemicals or solvents were purchased from commercial suppliers and were of analytical grade. No specific safety considerations apply to any of these agents, although the agents should be handled with care in a fume hood to avoid inhalation or ingestion.

CPAQOP stock solution

Solid CPAQOP was dissolved in dimethyl sulfoxide (DMSO) to a concentration of 10 mM. The purity of CPAQOP was determined to be $>98\%$ by LC/MS and LC/UV.

In vitro incubation spiking solution

CPAQOP DMSO stock was diluted with 0.1 M potassium phosphate buffer (pH 7.4) to a concentration of 2 mM. This solution was then spiked into the *in vitro* incubation at 1:100 (v/v) to give a final concentration in the incubation of 20 μM .

In vitro incubation experimental methods

Three separate incubations were performed with the parent compound (CPAQOP): (A) CPAQOP was incubated at 20 μM with HLM (2 mg protein/mL, Corning 150 donor ultrapool) in 0.1 M potassium phosphate buffer at pH 7.4 and 2.5 mM nicotinamide adenine dinucleotide phosphate (NADPH) at 37°C. An aliquot was removed after 0 min (control) and 60 min and the reaction stopped by the addition of ice cold acetonitrile (1:1, v/v). (B) CPAQOP was incubated as described in (A), but with 10 mM methoxyamine trapping agent added. An aliquot was removed after 60 min and the reaction stopped by the addition of ice-cold acetonitrile (1:1, v/v). (C) CPAQOP was incubated as described in (A). An aliquot was removed after 60 min and the reaction stopped by the addition of ice-cold acetonitrile (1:1, v/v) containing 10 mM methoxyamine. The extract was then incubated for a further 10 min at 37°C. (D) CPAQOP was incubated as described in (A), but with 10 mM glutathione (GSH) trapping agent added. An aliquot was removed after 60 min and the reaction stopped by the addition of ice-cold acetonitrile (1:1, v/v).

Sample preparation

Quenched incubates were centrifuged at ca. 3000 g for 15 min, and the supernatant retained. An aliquot of the supernatant was transferred to a 2 mL HPLC vial (Waters, Milford, MA, USA) and diluted 1:3 (v/v) with ultra-purified distilled water prior to the LC/MS analyses.

Profiling and structural characterisation of metabolites by UPLC/LTQ-Orbitrap mass spectrometry

Accurate mass structural characterisation work was performed on a LTQ-Orbitrap XL instrument (Thermo Fisher Scientific, Bremen, Germany) connected to an Acquity UPLC™ system (Waters). The Acquity system consisted of a binary UPLC pump, column oven, a sample manager and a photodiode array detector. Separation was carried out on a BEH C18 column (100 \times 2.1 mm, 1.7 μM ; Waters) preceded by a guard filter in a column oven at 50°C.

Two chromatographic methods were used. Method 1: The mobile phase consisted of formic acid (0.1% in water, eluent A) and methanolic formic acid (0.1%, eluent B). Method 2: The mobile phase consisted of formic acid (0.1% in water, eluent A) and acetonitrile containing formic acid (0.1%, eluent B). The elution profile for both methods was: Initial conditions 95% A, then a linear gradient to 20% A from 1.01 to 9.00 min, isocratic hold at 2% A from 9.01 to 11.00 min and re-equilibration 95% A from 11.00 to 14.00 min. The flow

rate was 0.45 mL/min and the eluent was introduced into the mass spectrometer *via* the LTQ divert valve at 1 min. The injection volume was 20 μ L and UV spectra were acquired over 200–350 nm. The LTQ-Orbitrap XL was equipped with an electrospray ionisation (ESI) source which was operated in positive ion mode. Positive ion source settings were: capillary temperature 300°C, sheath gas flow 25, auxiliary gas flow 17, sweep gas flow 5, source voltage 3.5 kV, source current 100.0 μ A, capillary voltage 18 V, and tube lens 75.0 V. Full scan MS data were obtained over the mass range 100–1200 Da. Targeted MS/MS experiments were acquired in the Orbitrap using Higher Energy Collisional Dissociation (HCD) fragmentation, isolation width 3 Da, normalised collision energy 60 eV, and activation time 30 ms. All ions acquired in the Orbitrap were monitored at 7500 resolution full width at half maximum. LTQ and Orbitrap mass detectors were calibrated within one day of commencing the work using Proteomass LTQ/FT-Hybrid electrospray positive mode calibration mix (Supelco, Bellefonte, USA).

Data analysis

Mass spectrometric data were collected using Xcalibur version 2.1 (Thermo Fisher Scientific, Bremen, Germany). Components were identified as being derived from CPAQOP by common fragments, isotopic pattern (Chlorine), UV absorbance and accurate mass. Comparisons with $t = 0$ incubations were conducted to minimise the potential for false positives from system impurities and endogenous components.

RESULTS

The initial full characterisation of a test compound with accurate mass MS/MS data often allows structural motifs and characteristic product ions to be identified, which assist the elucidation of the metabolite structures. MS/MS product ion experiments were undertaken in positive ion mode for the structural characterisation of metabolites or chemical addition products. All accurate mass measurements including the MS/MS product ions were within ± 3 ppm of the theoretical exact mass.

Structural characterisation of CPAQOP by LC/MS/MS

In positive ion mode CPAQOP yielded a protonated molecule $[M + H]^+ = 520.1749$ Da (+0.56 ppm mass error) and showed a characteristic chlorine pattern. The proposed dissociation pattern and LTQ Orbitrap HCD-MS product ion spectrum (Fig. 1) revealed three key product ions at m/z 365.0797 (corresponding to loss of the methylpiperidylethanone), 156.1018 (methylpiperidylethanone) and 98.0964 (methylpiperazine).

Structural characterisation of the acid metabolite (+O –H2) by LC/MS/MS

In positive ion mode the acid metabolite yielded a protonated molecule displaying the characteristic chlorine pattern with a measured accurate mass of $[M + H]^+ = 534.1539$ Da (0.0 ppm mass error), which is consistent with addition of one oxygen and loss of two hydrogen atoms. The proposed fragmentation

pattern and LTQ Orbitrap HCD-MS product ion spectrum (Fig. 2) revealed diagnostic product ions; m/z 365.0789, 170.0808, 126.0911 and 98.0963. The product ion at m/z 170.0808 corresponded to the addition of 14 Da (+O, –H₂) to m/z 156.1018 observed in CPAQOP. Detection of the methylpiperazine product ion (m/z 98.0963, also observed in CPAQOP) confirmed the piperazine ring was unchanged and the biotransformation had occurred on the hydroxyacetamide side chain. The product ion m/z 126.0911 represents loss of CO₂ from the hydroxyacetyl side chain, which is consistent with an acid on the terminal side chain carbon.

Structural characterisation of the hydrate product (+O) by LC/MS/MS

The hydrate metabolite was only detected at trace levels when methanol was used in the mobile phase, but it was the predominant species when methanol was substituted by acetonitrile. Therefore, the MS/MS spectra (shown in Fig. 3) for the hydrate have been taken from the LC/MS analysis where acetonitrile mobile phase eluent was employed. In positive ion mode the hydrate product yielded a protonated molecule displaying a characteristic chlorine pattern with a measured accurate mass of $[M + H]^+ = 536.1691$ Da (–0.04 ppm mass error), which is consistent with addition of one oxygen atom. The proposed dissociation pattern and LTQ Orbitrap HCD-MS product ion spectrum (Fig. 3) revealed diagnostic product ions; m/z 172.0964, 126.0911 and 98.0963. The m/z 172.0964 product ion corresponded to the addition of 16 Da to the m/z 156.1018 product ion observed in CPAQOP and the accurate mass confirmed addition of one oxygen atom to the methylpiperidylethanone group. Detection of the methylpiperazine product ion (m/z 98.0963, also observed in CPAQOP) confirmed the piperazine ring was unchanged

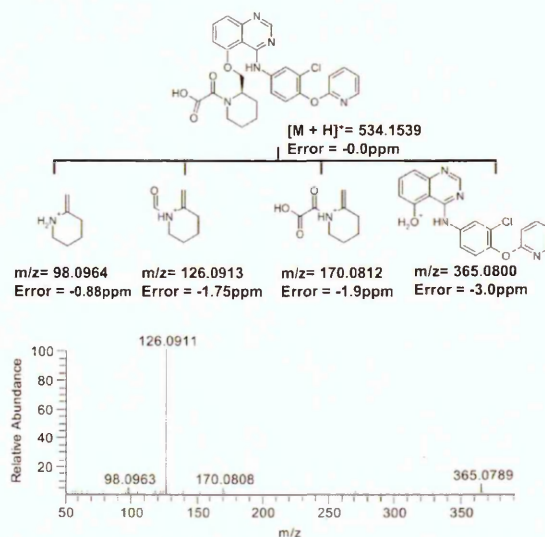


Figure 2. Accurate mass HCD-MS positive product ion mass spectrum of the acid metabolite (bottom) and proposed product ions with theoretical exact mass and mass error in ppm (top).

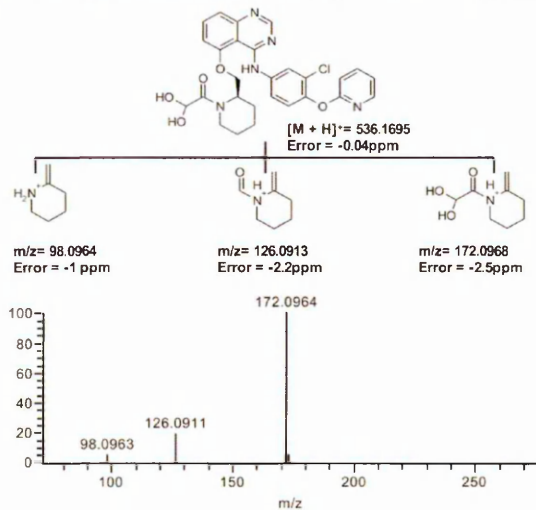


Figure 3. Accurate mass HCD-MS positive product ion mass spectrum of the hydrate (bottom) and proposed product ions with theoretical exact mass and mass error in ppm (top).

and the oxygen atom addition had occurred on the hydroxyacetamide side chain. The m/z 126.0911 product ion represents loss of CH_2O_2 from this side chain, which is consistent for a hydrate on the terminal carbon.

Structural characterisation of the methanol addition product (a hemiacetal) by LC/MS/MS

Two distinct LC/UV/MS peaks were detected in the chromatogram for this product. In positive ion mode the methanol addition products yielded protonated molecules displaying characteristic chlorine patterns with measured accurate masses of $[\text{M} + \text{H}]^+ = 550.1854$ Da (+0.41 ppm mass error) and $[\text{M} + \text{H}]^+ = 550.1852$ Da (+0.12 ppm), which is consistent with addition of one carbon, two hydrogens and an oxygen atom. The proposed dissociation pattern and LTQ Orbitrap HCD-MS product ion spectrum for both adducts (Fig. 4) revealed diagnostic product ions m/z 186.1121, 126.0911 and 98.0963. The product ion m/z 186.1121 corresponded to the addition of 30 Da to m/z 156.1018 observed in the MS/MS spectrum of CPAQOP, and accurate mass confirmed addition of one carbon, two hydrogens and an oxygen to the methylpiperidylethanone group. Detection of the methylpiperazine product ion (m/z 98.0963, also observed in CPAQOP) confirmed the piperazine ring was unchanged and addition of CH_2O occurred on the hydroxyacetamide side chain. The m/z 126.0911 product ion represents loss of $\text{C}_2\text{H}_4\text{O}_2$ from this side chain, confirming it as the site of methanol addition.

The observation of two distinct LC/UV/MS peaks both with measured accurate masses within 2 ppm of the theoretical exact mass of CPAQOP + CH_2O ($[\text{M} + \text{H}]^+ = 550.1854$ Da) and identical MS/MS fragmentation (Fig. 4) suggested formation of isomers. The addition of methanol to the terminal carbon on the hydroxyacetamide side chain creates a second chiral centre and therefore diastereoisomers, which could be separated chromatographically (Fig. 5(a)).

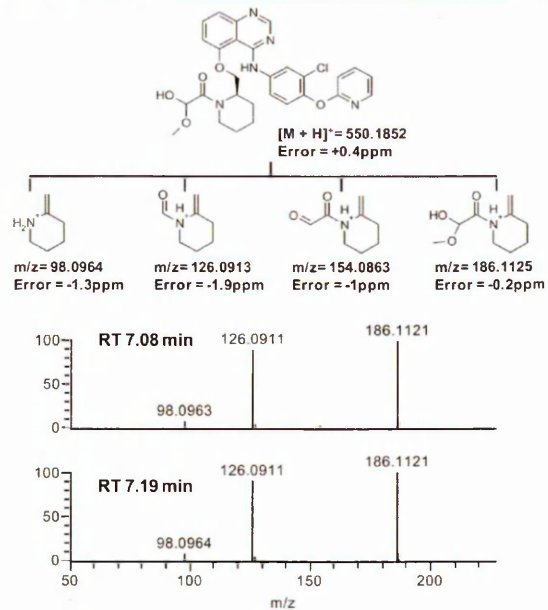


Figure 4. Accurate mass HCD-MS positive product ion mass spectra of the hemiacetal methanol adducts (bottom) and proposed product ions with theoretical exact mass and mass error in ppm (top).

The data (the observation of the hydrate and the hemiacetal) suggested that the potential reactive intermediate had undergone structural changes on the hydroxyacetyl side chain, producing a reactive aldehyde, whilst the formation of the acid indicated further oxidation of this functional group.

Glutathione (GSH) and methoxyamine trapping experiments

To confirm the reactive intermediate, the proposed reactive aldehyde, two trapping experiments in HILM were undertaken. The first involved GSH, the routine industry standard for trapping soft electrophilic reactive metabolites. GSH does not routinely adduct with aldehydes, though some literature data suggests this can occur.^[5] Saturated aldehydes generally require a nitrogen-based trapping agent, such as methoxyamine, which forms a stable Schiff base adduct.^[6–8] The incubation of CPAQOP with GSH did not produce an adduct (data not shown); instead, only the methanol adducts were detected, confirming that the reactive intermediate was not a soft electrophilic species. In contrast, the second involved incubation of CPAQOP with methoxyamine and generated the corresponding methoxyamine adduct, whilst the methanol adducts were not detected. Incubation of CPAQOP in HILM showed almost complete turnover of the CPAQOP at $t = 60$ min (Fig. 5(a)); however, when co-incubating with methoxyamine, the overall metabolic turnover was reduced, resulting in a significant amount of CPAQOP remaining unmetabolised (Fig. 5(b)). Additionally, hydroxyl metabolites of the methoxyamine adduct were detected at significantly greater concentration than the methoxyamine adduct itself (Fig. 5(b)). It was therefore decided to repeat the methoxyamine trapping experiment, this time spiking the

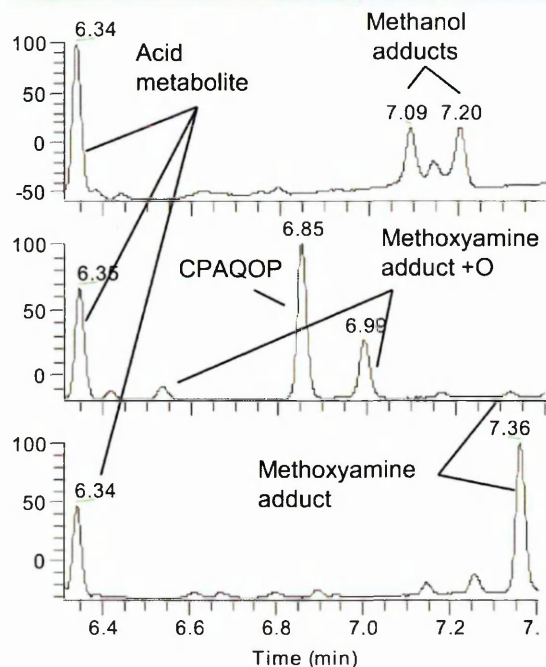


Figure 5. Extracted UV absorbance chromatograms (330 nm) of CPAQOP incubated in (a) HLM, (b) HLM + methoxyamine, and (c) HLM with addition of methoxyamine post-quake.

methoxyamine post-incubation into the HLM immediately after quenching (at $t = 60$ min). This resulted in increased metabolic turnover of CPAQOP and the formation of only one methoxyamine adduct with significantly increased yield, simplifying the data interpretation (Fig. 5(c)).

Structural characterisation of the methoxyamine adduct by LC/MS/MS

In positive ion mode the methoxyamine adduct yielded a protonated molecule displaying a characteristic chlorine pattern with a measured accurate mass of $[M + H]^+ = 547.1855$ Da (+0.35 ppm mass error), which is consistent with addition of one carbon, one hydrogen and one nitrogen (CHN). The addition of CHN was an expected modification upon reaction of an aldehyde with methoxyamine. The proposed dissociation pattern and the LTQ Orbitrap HCD-MS spectrum (Fig. 6) revealed diagnostic product ions m/z 183.1124, 152.0942, 123.0552 and 96.0808. The product ion m/z 186.1121 corresponded to the addition of 27 Da to m/z 156.1018 observed in the MS/MS spectrum of CPAQOP and accurate mass measurement confirmed addition of CHN to the methylpiperidylethanone group. The m/z 152.0942 ion corresponded to the loss of a methanol radical from the m/z 183.1124 ion.

The adduct formation with methoxyamine provided evidence of the presence of an aldehydic functional group, and therefore confirmed the formation of a reactive aldehyde intermediate following oxidation of the terminal hydroxyl group.

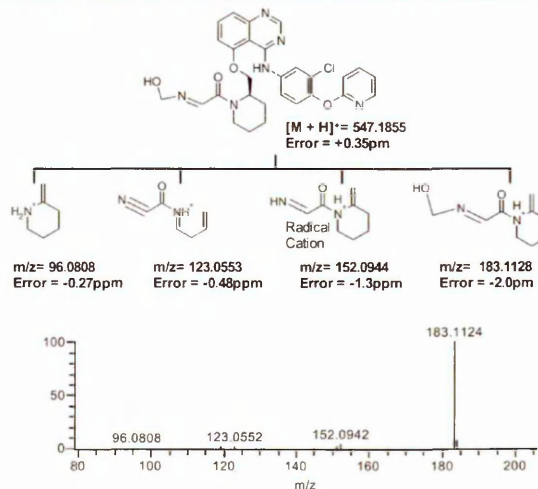


Figure 6. Accurate mass HCD-MS positive product ion mass spectrum of the methoxyamine adduct (bottom) and proposed product ions with theoretical exact mass and mass error in ppm (top).

The metabolic fate of CPAQOP, the formation of the methanol adduct and the methoxyamine adduct are summarised in Fig. 7.

DISCUSSION

This study demonstrated that the compound CPAQOP on incubation with HLM generated a reactive aldehyde metabolite that subsequently formed two methanol adduct isomers (Fig. 7). Whilst the reactive aldehyde metabolite was not directly detected and therefore could not be structurally characterised by UHPLC/MS, the methoxyamine trapping experiment verified the presence of an aldehyde. MS/MS experiments carried out on the methoxyamine adduct confirmed that addition occurred on the hydroxyacetamide side chain. Detection of the hydrate product gave further support for metabolism of the hydroxyacetamide side chain to the corresponding oxoacetamide (reactive aldehyde). The identification of two chromatographically distinct methanol adduct peaks with identical accurate masses (within ± 1 ppm) and dissociation patterns was indicative of the formation of diastereoisomers. Chemical addition of methanol to the reactive aldehyde metabolite created an additional chiral centre and resulted in the formation of diastereoisomers, which were easily separated by UHPLC (Fig. 5(a)). Overall, the metabolic profile of CPAQOP incubated in HLM showed that CPAQOP was readily metabolised, with little evidence of the parent CPAQOP in the LC/UV chromatograms (Fig. 5). The aldehyde, hydrate and methanol adducts were likely to be in equilibrium. In acidified methanol/water mobile phase the methanol adducts appeared to be the predominant products, with the hydrate detected only at trace levels and the reactive aldehyde not detected. However, in acidified acetonitrile/water mobile phase, only a single hydrate product was detected. Chemical reactions of methanol with aldehydes forming hemiacetals have been reported previously

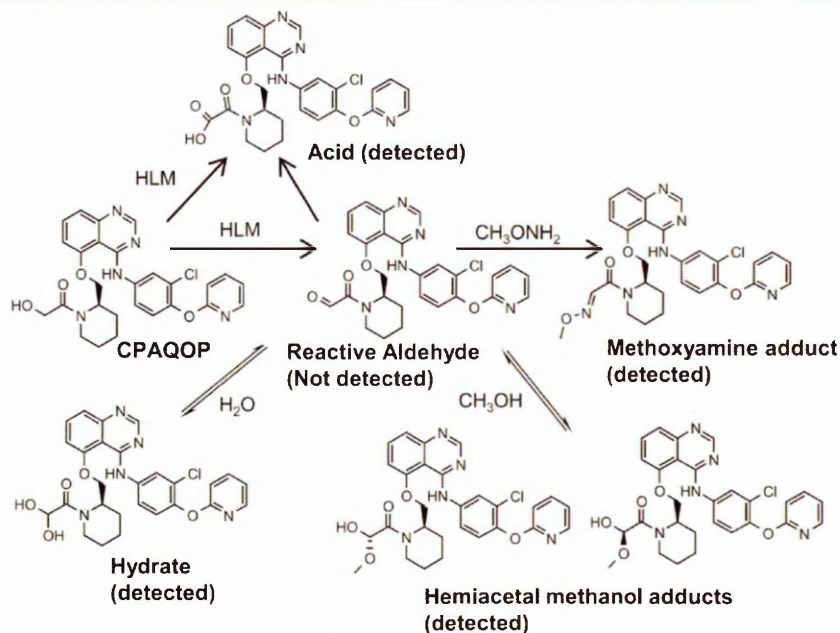


Figure 7. The proposed metabolic profile of CPAQOP generated in HLM, together with the analytical artifact, the methanol adduct, as well as the methoxyamine incubation product. The proposed reactive aldehyde intermediate is shown in the centre.

by Bateman *et al.*,^[9] who observed methanol addition to numerous components of secondary organic aerosol (a mixture of polyfunctional compounds containing alcohol, carbonyl, nitro and other functionalities) when methanol was used for extraction and/or storage. They also observed an increased rate of methanol adduct formation in acidified solutions. A series of publications have reported the formation of artefacts when methanol was used as a diluent to spike test compounds into microsomal incubations. Yin *et al.*^[10] and Li *et al.*^[11] described the formation of +12 Da artefacts (having gained one carbon atom over the incubated parent compound) from microsomal incubations, where methanol was present in the spiking diluent at 1% (*v/v*). Similarly, Cunningham *et al.*^[12] reported the formation of an unusual -CH₂ bridged dimer of 2,4-diaminotoluene again through the presence of methanol in the diluent. In these examples, methanol in the microsomal incubation was metabolised to formaldehyde, which subsequently reacted with the test compounds containing 1,2-diamino-, 1,2-aminohydroxyl- or 2,4-diaminotoluene. This is in contrast to this study, where methanol had not been added to the incubation or the sample extract prior to injection onto the LC/UV/MS system, confirming the addition occurred post-injection on the LC column, with the mobile phase the source of the methanol.

The initial methoxyamine-HLM incubation with CPAQOP resulted in a significant reduction in metabolic turnover of parent compared to the control (incubation without methoxyamine, as shown in Fig. 5(a)) and the generation of additional products due to further metabolism of the methoxyamine adduct. The reduction in metabolic turnover

was almost certainly due to enzyme inhibition by addition of methoxyamine to the incubation. Zhang *et al.*^[13] reported on the inhibitor properties of methoxyamine against P450 enzymes CYP1A2, CYP2C9, CYP2C19, CYP2D6 and CYP3A4/5 at concentrations up to 10 mM. To improve data quality and yield of the methoxyamine adduct the experiment was repeated, adding methoxyamine 'post-quake' then incubating for a further 10 min at 37°C. The result was a much cleaner metabolic profile, with no reduction in metabolic turnover and a significant increase in yield of the methoxyamine adduct (shown in Fig. 5). Although the aldehyde metabolite is reactive, it was present at a high enough concentration immediately post-incubation to produce the methoxyamine adduct. This is in agreement with the facile reaction of the reactive aldehyde and methanolic mobile phase on column forming the isomeric methanol adducts. Aldehyde metabolites are capable of reacting with macromolecules such as proteins, forming covalent adducts potentially triggering direct cell toxicity or an immune response and have been implicated in adverse drug reactions observed in the clinic. Several drugs are suspected of generating reactive aldehyde metabolites implicated in adverse drug reactions, which include acyclovir nephrotoxicity,^[14] abacavir idiosyncratic hypersensitivity with increased risk of cardiac dysfunction,^[15] and felbamate aplastic anaemia and hepatotoxicity.^[16] It is therefore prudent to identify compounds or structural moieties that form reactive aldehyde metabolites early in drug discovery to modify or change the chemistry and remove the liability. It is also important to note that CPAQOP did not form an adduct in the HLM GSH trapping experiment, thus escaping detection

from the early routine in-house reactive metabolite screen. Without the formation of the methanol adducts, the aldehyde may not have been identified until much later in drug discovery.

In conclusion, analytical artefacts (such as methanol adducts) are not desired and can complicate the analysis or lead to misinterpretation. However, here we presented an example where the methanol adducts were diagnostic and pivotal in identifying a reactive aldehyde metabolite, thus highlighting the importance of fully investigating any unusual adducts observed in metabolite identification studies.

Whilst the reactive aldehyde metabolite could be proposed from the detection of methanol adducts, the hydrate metabolite was simply addition of oxygen (+16 Da) to the parent compound, which is a very common biotransformation reaction. If the initial analysis had been undertaken in acetonitrile it is likely that the hydrate would have been reported as a hydroxylated metabolite and the reactive aldehyde liability for the chemical series missed.

CONCLUSIONS

The proposed bioactivation of CPAQOP occurred *via* the reactive aldehyde intermediate, which readily reacted with methanol in the mobile phase to form a pair of isomeric hemiacetal methanol adducts. In acidified methanol the equilibrium favoured the methanol adduct and in acidified acetonitrile it favoured the hydrate; therefore, the reactive aldehyde metabolite was not detected and could not be structurally characterised directly.

The aldehyde did not form an adduct with GSH, escaping detection in our conventional *in vitro* trapping screen; however, it was trapped with methoxyamine. A significant gain in efficiency (>20-fold increase in yield of adduct) was observed when methoxyamine was added immediately post-incubation over the traditional method, where methoxyamine is added pre-incubation.

Acknowledgement

This study was fully financed by AstraZeneca Ltd.

REFERENCES

- [1] D. C. Evans, A. P. Watt, D. A. Nicoll-Griffith, T. A. Baillie. Drug-protein adducts: an industry perspective on minimizing the potential for drug bioactivation in drug discovery and development. *Chem. Res. Toxicol.* **2004**, *17*, 3.
- [2] T. A. Baillie. Approaches to the assessment of stable and chemically reactive drug metabolites in early clinical trials. *Chem. Res. Toxicol.* **2009**, *22*, 263.
- [3] B. K. Park, A. Boobis, S. Clarke, C. E. Goldring, D. Jones, J. G. Kenna, C. Lambert, H. G. Laverty, D. J. Naisbitt, S. Nelson. Managing the challenge of chemically reactive metabolites in drug development. *Nat. Rev. Drug Discov.* **2011**, *10*, 292.
- [4] O. J. Pozo, P. Van Eenoo, K. Deventer, F. T. Delbeke. Ionization of anabolic steroids by adduct formation in liquid chromatography electrospray mass spectrometry. *J. Mass Spectrom.* **2007**, *42*, 497.
- [5] E. M. Lenz, S. Martin, R. Schmidt, P. E. Morin, R. Smith, D. J. Weston, M. Bayraktarian. Reactive metabolite trapping screens and potential pitfalls: bioactivation of a homomorpholine and formation of an unstable thiazolidine-adduct. *Chem. Res. Toxicol.* **2014**, *27*, 968.
- [6] C. Prakash, R. Sharma, M. Gleave, A. Nedderman. In vitro screening techniques for reactive metabolites for minimizing bioactivation potential in drug discovery. *Curr. Drug Metab.* **2008**, *9*, 952.
- [7] M. Colzani, G. Aldini, M. Carini. Mass spectrometric approaches for the identification and quantification of reactive carbonyl species protein adducts. *J. Proteomics* **2013**, *92*, 28.
- [8] X. Yang, W. Chen. In vitro microsomal metabolic studies on a selective mGluR5 antagonist MTEP: characterization of in vitro metabolites and identification of a novel thiazole ring opening aldehyde metabolite. *Xenobiotica* **2005**, *35*, 797.
- [9] A. P. Bateman, M. L. Walser, Y. Desyaterik, J. Laskin, A. Laskin, S. A. Nizkorodov. The effect of solvent on the analysis of secondary organic aerosol using electrospray ionization mass spectrometry. *Environ. Sci. Technol.* **2008**, *42*, 7341.
- [10] H. Yin, P. Tran, G. E. Greenberg, V. Fischer. Methanol solvent may cause increased apparent metabolic instability in in vitro assays. *Drug Metab. Dispos.* **2001**, *29*, 185.
- [11] C. Li, S. Surapaneni, Q. Zeng, B. Marquez, D. Chow, G. Kumar. Identification of a novel in vitro metabolite from liver microsomal incubations. *Drug Metab. Dispos.* **2006**, *34*, 901.
- [12] M. L. Cunningham, H. Matthews, L. T. Burka. Activation of methanol by hepatic postmitochondrial supernatant: formation of a condensation product with 2,4-diaminotoluene. *Chem. Res. Toxicol.* **1990**, *3*, 157.
- [13] C. Zhang, S. Wong, E. M. Delarosa, J. R. Kenny, J. S. Halladay, C. E. Hop, S. C. Khojasteh-Bakht. Inhibitory properties of trapping agents: glutathione, potassium cyanide, and methoxyamine, against major human cytochrome p450 isoforms. *Drug Metab. Lett.* **2009**, *3*, 125.
- [14] P. Gunness, K. Aleksa, J. Bend, G. Koren. Acyclovir-induced nephrotoxicity: the role of the acyclovir aldehyde metabolite. *Transl. Res.* **2011**, *158*, 290.
- [15] N. M. Grilo, C. Charneira, S. A. Pereira, E. C. Monteiro, M. M. Marques, A. M. Antunes. Bioactivation to an aldehyde metabolite – Possible role in the onset of toxicity induced by the anti-HIV drug abacavir. *Toxicol. Lett.* **2014**, *224*, 416.
- [16] C. D. Thompson, M. T. Kinter, T. L. Macdonald. Synthesis and in vitro reactivity of 3-carbamoyl-2-phenylpropion-aldehyde and 2-phenylpropenal: putative reactive metabolites of felbamate. *Chem. Res. Toxicol.* **1996**, *9*, 1225.

7. SUMMARY AND CONCLUSIONS

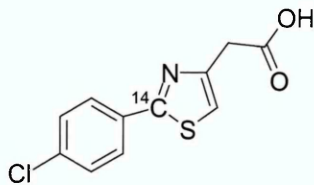
7.1 Fenclozic acid

Fenclozic acid (Myalex™) was developed by ICI pharmaceuticals in the 1960s for the treatment of rheumatoid arthritis, it was a promising compound with good pre-clinical safety profile and efficacy. Whilst it did not show adverse hepatic effects in pre-clinical animal tests or initial studies in man^{134,135} it was later withdrawn from clinical development due to hepatotoxicity in humans at daily doses of 400 mg. One of the more recent theories for the cause of the observed hepatotoxicity in the clinic is the formation of RMs. The original metabolite identification work by Foulkes^{136,133} and by Bradbury¹³⁷ showed fairly extensive metabolism, but did not detect any potential RMs other than an acyl-glucuronide.

7.1.1 In vitro studies

More recently AstraZeneca investigated this hepatotoxicity using a variety of modern *in vitro* approaches, which have been used to explore potential underlying mechanisms¹³⁸. ¹⁴C radiolabelled Fenclozic acid (Figure 31) *in vitro* CVB experiments were undertaken to determine the potential for Fenclozic acid to be bioactivated in rat, dog and human liver microsomes and hepatocytes.

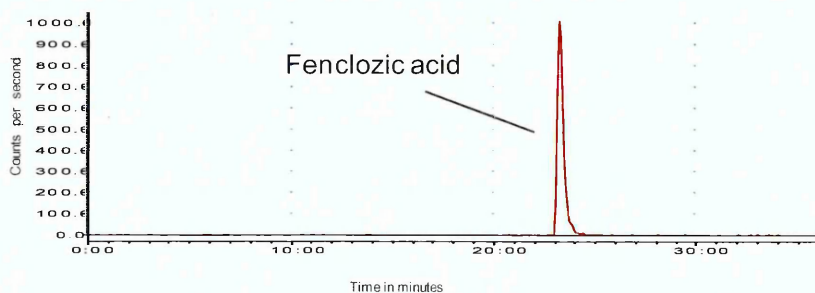
Figure 31 ¹⁴C Radiolabelled Fenclozic acid



CVB was observed for Fenclozic acid in both the hepatocytes and microsomes incubations indicating the formation of a RM. The CVB in microsomes and reduced CVB in hepatocytes in the presence of a P450 inhibitor, strongly suggested phase I metabolism was responsible for the CVB and not the previously identified acyl-glucuronide. To investigate the potential RM, several HLM trapping experiments were undertaken with ¹⁴C Fenclozic acid using a

variety of nucleophilic trapping agents for CVB and metabolite identification. The most significant drop in CVB was observed for the Cys and GSH trapping experiments, suggesting GSH/Cys were conjugating with an electrophilic RM in preference to it covalently binding to protein. The metabolite identification work was undertaken as a part of this thesis and formed the initial metabolism investigation into Fenclozic acid prior to the *in vivo* studies (Chapter 2 & 3). Analysis of each of the trapping agents by flow radio chemical detection did not show the presence of any metabolites and the only radio peak observed in each trapping experiment was Fenclozic acid (Figure 32).

Figure 32 Radio chromatogram from a Fenclozic acid GSH trapping experiment.



This was unusual considering the position of the ^{14}C in Fenclozic acid (Figure 31), as it is highly unlikely that the label was lost through metabolism. However, the samples were also analysed extensively by LC-UV-MS using a number of the MS scan/MS data stripping techniques (Section 1.3.2) and no metabolites or parent related products could be identified. Whilst there were no metabolites detected, the measured CVB in HLM and the reduction in CVB in the presence of GSH or Cys strongly suggests the presence of an electrophilic RM. The *in vitro* metabolic turnover in HLM was low with a measured $\text{Cl}_{\text{int}} < 3 \mu\text{L}/\text{mL}/\text{mg}$ (unpublished AstraZeneca data) which may help to explain the lack of metabolites. It is therefore possible that low levels of RM were formed, but were below the detection limits of the analytical instruments. In summary, all of the *in vitro* data pointed towards CYP bioactivation to a RM, however no RMs were detected. Whilst extensive analytical work was undertaken to identify metabolites from the microsomal *in vitro* trapping experiments there was only minimal contribution to the overall Fenclozic acid *in vitro* investigation paper¹³⁸,

therefore it was decided not include it in this thesis, even though this work formed the basis for the subsequent *in vivo* investigations.

7.1.2 Fenclozic acid metabolism study in HRN mice (Chapter 2)

The *in vitro* CVB observed was shown to be phase I mediated, but CVB of a drug or its metabolites does not necessarily lead to *in vivo* toxicity. To investigate the contribution of phase II metabolism to Fenclozic acid toxicity, an *in vivo* study in hepatic reductase null mice (HRN) was conducted to examine the disposition, metabolism and *in vivo* CVB of ¹⁴C Fenclozic acid. The metabolite identification work for this paper (Chapter 2) was undertaken as a part of this thesis. HRN mice have no functional hepatic CYP enzymes¹³⁹ and have been shown to produce only phase II conjugation metabolites for diclofenac¹⁴⁰.

The histopathological examination did not reveal any evidence of adverse hepatic effects for Fenclozic acid in HRN mice after a single dose of 10 mg/kg. *In vivo* CVB measured in plasma and the tissues examined was much less than 50 pmol per mg of protein, with the highest binding observed in the kidney (twice what was observed in the liver). This suggested that phase II conjugation biotransformations of Fenclozic acid in the liver did not produce a large extent of CVB. The two major metabolites detected in faeces and urine were taurine and glycine amino acid conjugates, whilst the acyl glucuronide was only detected as a minor metabolite. The taurine, glycine and acyl-glucuronide imply the formation of a coenzyme A intermediate. Coenzyme A intermediates have been associated with the toxicity of carboxylic acid containing xenobiotics¹⁴¹, however no evidence of toxicity was observed in the HRN mice in this study. Both the *in vitro* and HRN *in vivo* experiments suggested the CVB and toxicity were not due to phase II metabolism; however due to the use of HRN mice it was not possible to identify any phase I metabolites from these studies.

7.1.3 Fenclozic acid metabolism study in bile duct cannulated rats (Chapter 3)

To better characterise the metabolism of Fenclozic acid it was decided to conduct a bile duct cannulated metabolite identification study using Han Wistar

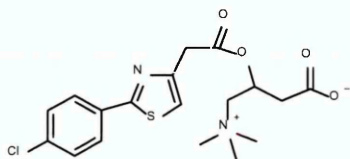
rats. Unfortunately due to the amount of radioactive material remaining it was not possible to dose rats with ^{14}C labelled Fenclozic acid, so only cold material was dosed. Using bile duct cannulated animals it is possible to collect excretory metabolites in bile and urine rather than faeces and urine. Faeces is a difficult matrix to analyse and will generally require extraction of the metabolites prior to analysis, whereas bile can be injected on to LC-MS without any need for extraction, reducing the potential loss or degradation of metabolites. Rat was chosen as it produces more sample than mouse and is a direct comparison to the original work by Foulkes and Bradbury^{136,137} who had previously profiled the metabolites in rat.

The product ions of Fenclozic acid and its metabolites identified in the rat bile duct cannulated study can be found in Appendix B.

Fenclozic acid was extensively metabolised *in vivo* in the rat with a total of 18 metabolites detected including several previously unreported metabolites. Earlier studies by Foulkes and Bradbury^{136,137} in the rat showed fairly extensive metabolism, however there was a significant difference in the type and number of metabolite identified compared to this study. A likely explanation for these differences was the extraction and chromatographic conditions employed by Foulkes and Bradbury. It is possible that a number of metabolites degraded under their extraction and chromatographic conditions, which were far harsher than the ones used in this study. For example Foulkes reported a reductive decarboxylation metabolite, but also described degradation of Fenclozic acid to this metabolite when extracted in chloroform. The reductive decarboxylation product was not detected in this study, so it is likely an analytical artefact from the extraction procedure. Foulkes and Bradbury did not detect any GSH-related conjugates, while several GSH related conjugates were detected in this study. This would suggest that the analytical methodology applied during the development of Fenclozic acid was unsuitable for the detection of GSH adducts. Apart from the differences in sample preparation, the vastly improved chromatography and sensitivity of modern high resolution MS instruments undoubtedly aided the detection of a larger number of metabolites. Unlike the HRN mouse study seven new metabolites were identified (not including the multiple GSH related product) including an unusual carnitine conjugate and

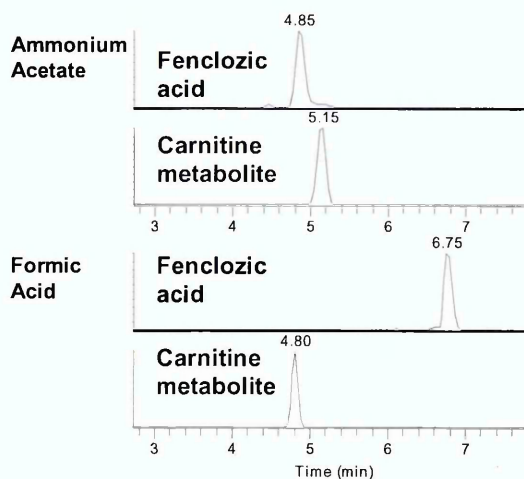
additional amino acid conjugates. The carnitine conjugate is not a common biotransformation for xenobiotics, but it has been reported as a metabolite for valproic acid¹⁴². The carnitine conjugate in Figure 33 is zwitterionic and is likely to have a low pK_a (<3) compared to Fenclozic acid and was demonstrated by changing the mobile phase from pH 6.5 to pH 4.0.

Figure 33 Fenclozic acid carnitine conjugate



At pH 4.0 Fenclozic acid would likely start to become unionised and less polar, so retain longer on a reverse phase column, whereas the carnitine conjugate will not change ionisation state or retention characteristics (Figure 34).

Figure 34 Selected ion mass chromatograms for Fenclozic acid and the carnitine metabolite at pH 6.5 (ammonium acetate) (top) and pH 4.0 (formic acid) (bottom).

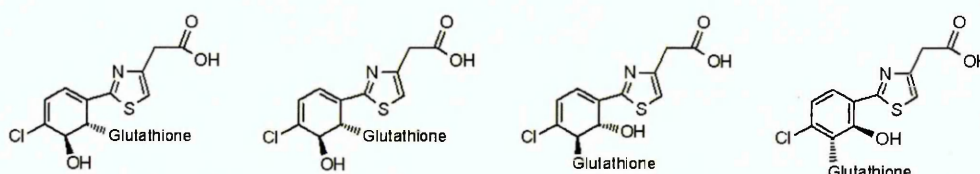


This test could be used in future to confirm the presence of a carnitine conjugate, if MS spectra are unrevealing.

The GSH related conjugates detected pointed towards a single phase I epoxide metabolite on the chlorobenzene ring, which is likely responsible for the CVB observed in rat microsomes. Whilst the CVB results indicated that a GSH conjugate was likely, the *in vitro* GSH trapping experiments contradicted this

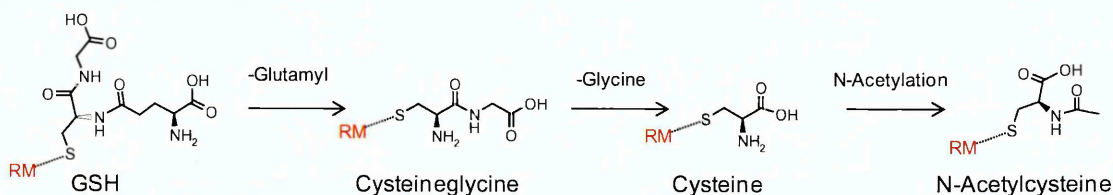
theory. If an epoxide metabolite was the cause of the CVB, then a conjugate should have been detected in either the Cys or GSH trapping experiments, which both had almost identical analytical conditions and LC-MS instrumentation to the rat bile duct cannulated study. The low metabolic turnover of Fenclozic acid in HLM ($Cl_{int} < 3 \text{ uL/mL/mg}$) would be consistent with the formation of low levels of the epoxide RM and the subsequent GSH adducts. The formation of four isomeric GSH conjugates (Figure 35) (positional and diastereoisomers) would further reduce LC-MS sensitivity, indicating that these GSH-conjugates were not present at sufficiently high concentrations to be detected.

Figure 35 Fenclozic acid Glutathione conjugate isomers



GSH conjugates can be further metabolised through enzymatic degradation of the GSH (Figure 36), often leading to multiple GSH related adducts from one RM. Many of these GSH degradation products were identified for Fenclozic and there were up to four isomers for each GSH product, so in total there were up to 16 GSH related conjugates generated from a single epoxide RM.

Figure 36 In vivo enzymatic degradation of GSH conjugates



Based on all of the data it is proposed that the reactive epoxide intermediate/metabolite is the agent responsible for the observed CVB in rat microsome and that it is likely to be the cause of CVB in human microsomes. While the intact GSH adducts were not detected in previous studies the identification of oxidation metabolites on the chloro-benzene ring by Foulkes¹³⁶, is consistent with the formation of an epoxide intermediate.

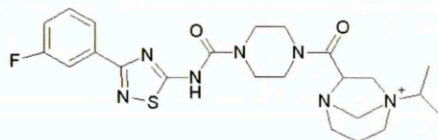
In conclusion, the reactive epoxide metabolite identified here is likely formed in humans and therefore could have contributed to the Fenclozic acid hepatotoxicity observed in the clinic.

7.2 Reaction of Homopiperazine with endogenous formaldehyde (Chapter 4)

A new series of homopiperazine compounds were introduced into a discovery project to replace a piperazine series that had a RM liability, similar to that reported by Doss *et al.*¹⁴³. No RMs were detected *in vitro* and the series of compounds had low to moderate metabolic turnover *in vitro*. However, when compounds were dosed to rats the *in vivo* CL was higher than expected from the IVIVE, suggesting there might be additional metabolic routes *in vivo*. Rat urine and plasma were collected from an AZX *i.v.* dosed rat, to identify additional *in vivo* routes specifically looking for RMs that may not be formed *in vitro*. Subsequent metabolite identification uncovered an unexpected major parent related peak with a ion arising from a molecular species at m/z 488 (not observed *in vitro*) in the 0-24 hour pooled urine sample, whilst only low levels of AZX were detected by UPLC-UV-MS. Surprisingly the AZX spiked pre-dose control urine also produced this m/z 488 product and only a minor LC-UV peak for AZX was observed. It was initially assumed that either the wrong compound was dosed or that the parent had either degraded/formed chemical adducts, as the $[M+H]^+$, i.e. the mass addition, could not be explained. Analysis of the dose solution and solvent stocks confirmed AZX ($[M+H]^+$ 476) was >95% pure and no m/z 488 was observed so this was ruled out.

Product ion spectra of m/z 488 confirmed the transformation had occurred on the homopiperazine ring and elemental composition analysis confirmed the molecular formula to be AZX +carbon. It was not possible to identify the exact position of the carbon addition however, due to the limited possibilities on the homopiperazine ring a carbon bridged structure was proposed (Figure 37). The presence of quaternary nitrogen was confirmed by reaction with cyanide.

Figure 37 AZX homopiperazine -CH₂ bridged structure



The proposed bridged structure equated to the addition of one carbon and one hydrogen atom, i.e. a gain of 13 Da which is not consistent with apparent +12 Da product observed by MS. However, the bridged structure has a fixed permanent positive charge (M^+) (Figure 37) and cannot produce a protonated molecule ($[M+H]^+$ ion) by positive ion electrospray (+ESI). Whilst the calculated MW of AZX is 475 Da and the observed $[M+H]^+$ was m/z 476, the calculated mass of the bridged homopiperazine and M^+ ion are 488 Da and m/z 488 respectively. Therefore the MW difference between AZX and the bridged homopiperazine is 13 Da (+1xC and +1xH), while the measured m/z difference is 12 Da (1xC).

Formaldehyde was identified as a potential candidate to react with AZX and form the proposed bridged homopiperazine *via* the Mannich reaction through a reactive schiff base intermediate, which is intramolecularly stabilised by forming the bridged homopiperazine. To test this hypothesis formaldehyde was spiked into a test solution of AZX and the +13 Da product was formed immediately at nearly 100%. This provided an easy method to scale up for NMR analysis, which subsequently confirmed the product was in fact the carbon bridged homopiperazine. Several experiments ruled out methanol or other analytical solvents as the source of the formaldehyde, so the question remained whether this could occur *in vivo*. The +13 Da product was also detected in rat plasma, which is highly unlikely to come into contact with formaldehyde prior to analysis. Formaldehyde occurs naturally in the body and it is present in rat blood at approximately 0.1mM¹⁴⁴. It is therefore proposed that AZX scavenges endogenous formaldehyde *in vivo*, similar to aminoguanidine which was reported by Kazachkov *et al.*¹⁴⁵.

Formaldehyde is known to be responsible for cross linking proteins^{146,147} and some xenobiotics¹⁴⁸ *via* the Mannich reaction through a Schiff base intermediate. Considering that basic amine groups are ubiquitous on many

xenobiotics and proteins, it is worth noting the potential for formaldehyde to cause cross linking between xenobiotics and proteins *in vivo*. Hence, susceptibility to formaldehyde addition *via* a direct or metabolic route could lead to the formation of covalently bound protein adducts.

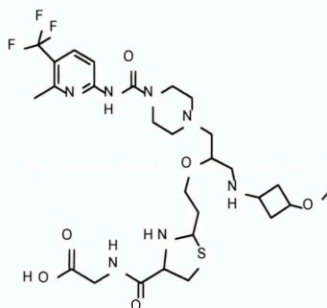
Additionally compounds with this susceptibility are likely to generate poor IVIVE, as the formaldehyde reaction products are not formed when incubated in hepatocytes or microsomes under AstraZeneca's standard incubation conditions. For these reasons compounds/chemical series with this liability should be avoided and structures containing homopiperazine rings should be tested for formaldehyde reactivity prior to any *in vivo* studies.

7.3 Bioactivation of a homomorpholine (Chapter 5)

The lead compound for drug research programme carried out within Astrazeneca had a RM liability and was shown to generate significant CVB *in vitro*. A homomorpholine backup series was investigated to mediate this RM risk, initial GSH HLM trapping results were negative in the Astrazeneca GSH screening assay. However, initial *in vitro* metabolite identification studies uncovered an unexpected cysteineglycine adduct. A representative compound was selected for a detailed investigation, AZX, which will be referred to as AZXa to avoid confusion with the compounds discussed in Chapter 4 and 6. To generate enough of the cysteineglycine adduct for NMR analysis, incubations of AZXa were scaled up using cytochrome P450 (CYP) variants of CYP102A1 from *Bacillus megaterium* (BM3) with GSH. The metabolite was isolated by fraction collection and initial LC-MS analysis confirmed the cysteineglycine product (m/z 662) had been isolated, however subsequent analysis by NMR showed the metabolite degraded during isolation. Therefore isolation of the metabolite was not possible, so more detailed MS product ion work on an LTQ-Orbitrap was undertaken on a fresh sample of AZXa to gain more structural information. It was possible to identify the molecular formula for each fragment ion using elemental composition software. Restricting the molecular formula parameters to the number and type of elements possible from the theoretical exact mass $[M+H]^+$ ion of the cysteineglycine conjugate, ensured only the correct molecular formulae were reported for each product ion.

From the product ion data it was possible to postulate a structure for the cysteineglycine adduct (Figure 38), and from this structure propose a mechanism of formation via a reactive aldehyde metabolite.

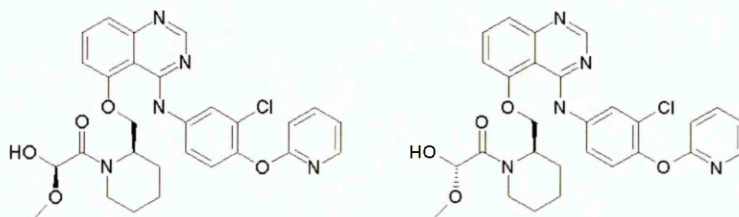
Figure 38 Proposed structure for the AZXa cysteineglycine adduct



A methoxyamine HLM trapping experiment confirmed the presence of an aldehyde metabolite, however MS³ product ion spectra were required to confirm the methoxyamine addition to the homopiperazine ring. There were two possible mechanisms of formation, the first involving the reaction of the aldehyde with the amine on the Cys moiety of GSH, forming an imine intermediate (similar to the mechanism discussed in Chapter 2), which reacts with the thiol to form the thiazolidine-glycine proposed structure. The second mechanism is via reaction of the thiol in GSH with the aldehyde, the resulting mercaptomethanol undergoes an intermolecular reaction eliminating water and forming the proposed thiazolidine-glycine product. Both mechanisms involved the loss of the glutamyl from GSH prior or in the process of reacting with the aldehyde metabolite. The loss of the glutamyl made this GSH related adduct invisible to the LC-MS GSH -129 NL & *m/z* 272 PIS screening method (Section 1.5.1.1) employed at the time of this work, thus highlighting the importance of early metabolite identification studies for the identification of RMs, rather than relying on automated LC-MS screening methods. It is recommended that homomorpholine rings are avoided in drug design if possible; if not that they are fully investigated for the formation of reactive aldehyde metabolites.

Through routine metabolite identification in HLM, two unexpected methanol adduct products were detected by LC-UV-MS for a chemical series in a drug discovery programme. Methanol adducts are common in mass spectrometry and are normally identified as analytical artefacts of the parent drug, generated during the positive ion ESI process and are therefore often ignored. In this example both methanol adducts were chromatographically separated from each other and the parent compound, so must have been generated prior to introduction into the MS ESI source. The T=0 control sample did not contain these adducts, so they were likely formed through a metabolic process, however addition of CH₃O metabolically is very unusual. The methanol adducts disappeared on re-analysis when acetonitrile replaced methanol as eluent B, which inferred a metabolite was reacting with methanol on column. A representative compound was selected for a detailed investigation, AZX, which will be referred to as AZXb to avoid confusion with the compounds discussed in Chapter 4 & 5. AZXb generated several metabolites in HLM including the two methanol adducts, which were major products. Interpretation of the methanol adduct from AZXb product ion spectra confirmed the addition of methanol to the hydroxyacetamide side chain and that both methanol adducts generated identical product ion spectra. Therefore the likely site of methanol addition was the terminal hydroxy methyl, which created a pair of diastereoisomers (Figure 39).

Figure 39 AZXb methanol adduct diastereoisomers



A plausible explanation for the chemical addition of methanol to the terminal hydroxy methyl would be metabolic oxidation of the terminal hydroxy to a reactive aldehyde that forms a hemiacetal with methanol. A methoxyamine

trapping experiment confirmed the presence of an aldehyde metabolite, so bioactivation of AZXb had occurred *via* a reactive aldehyde intermediate, which subsequently reacted with methanol to form a pair of isomeric hemiacetal methanol adducts. The reactive aldehyde metabolite was not detected and could not be structurally characterized directly, as the equilibrium favoured the methanol adduct in acidified methanol and the hydrate in acidified acetonitrile.

The initial methoxyamine trapping experiment with AZXb in HLM reduced the metabolic turnover of AZXb and produced hydroxylated metabolites of the methoxyamine adduct. This was likely caused by the P450 inhibitory properties of methoxyamine¹²¹. Repeating the methoxyamine experiment, this time adding the methoxyamine post incubation, resulted in a much cleaner metabolic profile; with no reduction in metabolic turnover and a significant increase in yield of the methoxyamine adduct. The increase in yield of the methoxyamine adduct inferred there was a significant concentration of the aldehyde post incubation, this is in agreement that the aldehyde reacted with the methanol mobile phase on column forming the isomeric methanol adducts.

Whilst the reactive aldehyde metabolite could be proposed from the detection of methanol adducts, the hydrate metabolite is simply addition of Oxygen (+16 amu) to parent compound, which is a very common biotransformation reaction. If the initial analysis had been undertaken in acetonitrile, it is likely that the hydrate would have been reported as a simple hydroxylated metabolite and the reactive aldehyde liability for the chemical series missed. This is especially true for AZXb, which when incubated in HLM fortified with GSH did not yield any GSH related conjugates. This is in contrast to the AZXb aldehyde metabolite discussed in Chapter 6 that formed a rearranged GSH adduct, but did not appear to react with the methanol mobile phase. The absence of methanol adducts for AZXa is likely due to the aldehyde forming an adduct with GSH, considering the excess GSH present, it is unlikely any aldehyde would be present at the time of the LC-MS analysis. Both AZXa and AZXb generated reactive aldehyde metabolites in HLM, which would not have been detected through the standard AZ RM trapping screens (GSH & KCN). Methoxyamine was successfully employed to trap both AZXa and AZXb reactive aldehyde metabolites. For these reasons compounds/chemical series with this liability

should be avoided and structures containing a side chain with a terminal hydroxy should be tested for aldehyde formation with methoxyamine or semicarbazide.

7.5 Limitations of GSH LC-MS trapping screening assay

There are a number of trapping experiments available to capture and detect RMs (Section 1.5.1), however the most common within drug research are HLM incubations fortified with GSH for soft electrophiles and cyanide for hard electrophiles. They are often employed in early drug discovery in LC-MS RM trapping screening assays that utilise PIS, NLS or/and automated data processing to generate a quick yes/no answer (Section 1.5.1.1). The advantage of these early RM trapping screens is their ability to process relatively large numbers of compounds quickly and inexpensively, feeding back data within design make test cycles. Adducts are generally detected based on expected precursor ions, product ions or neutral losses from the GSH or cyanide adduct. However, none of the RM examples described in this thesis were detected by the current AZ GSH or cyanide RM LC-MS screening assays. From these studies there were 4 limitations highlighted;

7.5.1 Detectability of RMs from compounds with little or no *in vitro* metabolic turnover

When a compound or chemical series have little or no *in vitro* metabolic turnover (Low Cl_{int}) in HLM, they are not likely to generate enough RM to be trapped and detected by LC-MS, even if bioactivation was a major metabolic route *in vivo* (e.g. Fenclozic acid). Prior to submission for RM trapping experiments the HLM Cl_{int} should have been determined for the test compound or chemical series, if the Cl_{int} is low then alternative studies to assess potential bioactivation should be considered. Cultured cells such as the H μ REL system¹⁴⁹ remain viable for much longer than human hepatocytes or HLM during incubations with test compounds. Thus compounds with low *in vitro* metabolic turnover can be incubated for days rather than hours, generating a more accurate Cl_{int} and significantly higher concentrations of metabolites.

An *in vitro* radiolabelled CVB experiment is likely to be more sensitive and would indicate the presence of a RM (Fenclozic acid), however these studies require a radiolabelled analogue of the test compound. For that reason they are often only conducted when a compound has been selected for progression into development. For an earlier investigation *in vivo* metabolite identification may provide further information, however the animal species used for the *in vivo* metabolite identification may generate a completely different metabolic profile to humans.

7.5.2 Bioactivation to a RM *in vivo* is not represented *in vitro*

When a compound generates a RM *in vivo*, but the RM is not generated *in vitro*, RM trapping assays will generate a false negative. This is difficult to address as the RM may only be detected from detailed *in vivo* metabolite identification studies and it is not possible to predict what will occur *in vivo* in humans until later in the drugs development after considerable investment. However, it was possible to detect a potential human RM of AZX (Chapter 4) through *in vivo* metabolite identification studies in preclinical species. It is therefore recommended that an *in vivo* metabolite identification is conducted alongside an *in vitro* incubation to determine if there is an *in vitro/in vivo* RM disconnect prior to candidate selection for progression in to development. This is not a perfect solution as the animal species used for the *in vivo* metabolite identification may generate a different metabolic profile to humans, but it could be valuable to identify potential bioactivation reactions not represented *in vitro*.

7.5.3 GSH or cyanide trapping agents are unsuitable for the RM

Whilst GSH successfully trapped the AZXa reactive aldehyde metabolite (Chapter 4), it did form an adduct with the AZXb reactive aldehyde that was formed in significant quantities in HLM and subsequently reacted with methanol (Chapter 6). There are alternative nucleophilic trapping agents available to trap aldehyde metabolites such as methoxyamine or semicarbazide.

Methoxyamine successfully trapped both the AZXa and AZXb reactive aldehyde metabolites, however, methoxyamine's inhibitory properties against P450 enzymes¹²¹ significantly reduced the metabolic turnover for AZXb in HLM

(Chapter 6). Spiking methoxyamine post incubation in HLM would prevent any inhibition from the trapping agent or further metabolism of the trapped adduct. Whilst this experiment successfully trapped the AZXb reactive aldehyde, the aldehyde was expected to be present post incubation at a significant concentration, due to its subsequent reaction with methanol from the LC-MS analysis. Therefore this may not work for all reactive aldehyde metabolites which could bind to microsomal protein during the incubation, resulting in little or no aldehyde metabolite remaining to adduct with the trapping agent post incubation. Semicarbazide adducts do not produce consistent straightforward product ions or neutral losses, so it is not possible to use automated LC-MS screening scan functions such as PIS/NLS or data processing to detect and find them.

Therefore it is unlikely that methoxyamine or semicarbazide would become part of the routine trapping screening assays employed, however they are useful for specific experiments to investigate a mechanism of bioactivation. Detailed metabolite identification experiments *in vitro* and *in vivo* are the most likely studies to identify RMs not trapped by cyanide or GSH, prior to *in vitro* radiolabelled CVB experiments conducted in late drug design. Trapping assays are useful tools for an early RM flag, but it is suggested that these do not replace more detailed metabolite identification studies for the investigation of RM liability.

7.5.4 Unexpected or unusual GSH rearrangement products not detectable by current LC-MS GSH trapping screening assays.

RMs can form rearrangement products with GSH¹⁴³ (Chapter 5) that do not generate expected $[M+H]^+$ or $[M-H]^-$ ions, product ions or neutral loss by LC-MS and thus not detected by LC-MS GSH screening assays utilising -129 NLS/*m/z* 272 PIS or predicted $[M+H]^+/[M-H]^-$ ions (Section 1.5.1.1). It is very difficult to screen for these types of RMs by LC-MS detection, and an expert metabolite identification scientist utilising high resolution accurate mass instrumentation would often be required to identify these unusual GSH rearrangements. These studies are low throughput and time consuming, so it would be impossible to do

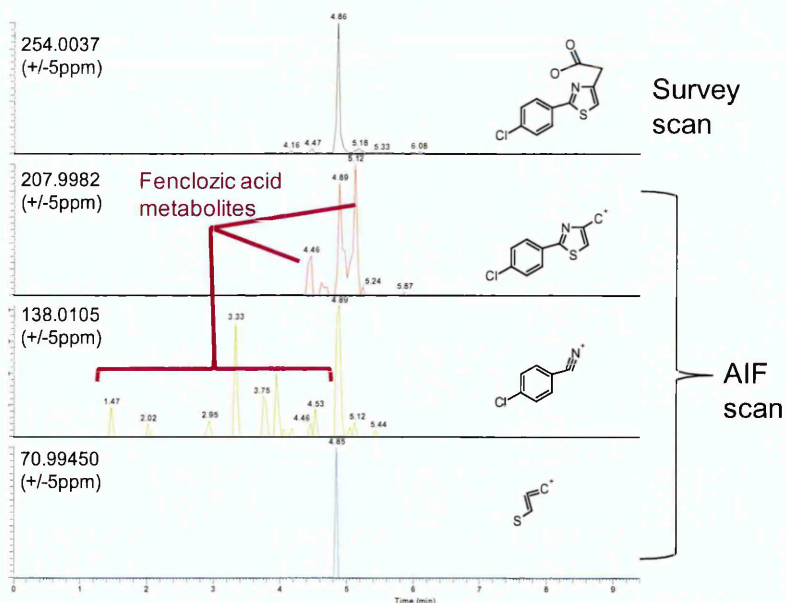
this in replacement of routine RM trapping. However checking a representative compound from a chemical series in conjunction with RM trapping is feasible.

7.6 LC-UV-MS methodology

The application of UHPLC, UV and high resolution accurate mass data was critical for the identification, separation, isolation and structural elucidation of all metabolites and products. All of the compounds studied in this thesis contained reasonable chromophores, so absorbed UV at higher more selective wavelengths. Therefore it was easy to generate relatively clean UV chromatograms at selected wavelength ranges, that were extremely useful to help find and semi-quantify metabolites.

All MS data were acquired on either a Q-ToF operated in MS^E mode or an LTQ-Orbitrap. Whilst the Q-ToF methodology was useful, accurate mass data acquired on the LTQ-Orbitrap was far superior, so superseded all Q-ToF data. The initial LTQ-Orbitrap MS analysis for all studies consisted of positive ion DDA with full scan and AIF in the orbitrap (accurate mass). Due to the scan time and LC peak widths it was not possible to acquire DDA orbitrap scans, so they were acquired in parallel in the ion trap with nominal mass. This method was successful and several metabolites were detected by post acquisition processing such as accurate mass common fragment searching using a narrow mass window (Figure 40), MDF and precursor/neutral loss searching of the DDA MS² acquisitions.

Figure 40 Selected ion mass chromatograms (+/-5 ppm narrow mass window) of Fenclozic acid (survey scan) and Fenclozic acid product ions (AIF) in rat urine.



It was also possible to gain a reasonable amount of spectral information on the metabolites using accurate mass AIF and nominal mass DDA product ion scans in combination. Once all the positive ion metabolites were identified, additional runs were required to generate discrete accurate mass MS² data that were acquired using DDA with a targeted *m/z* list. Due to the complexity of the bile and urine matrix analysed for Fenclozic acid, multiple runs were required to generate product ion spectra for all metabolites. It is not possible to acquire positive/negative switching data on a LTQ-Orbitrap or Q-ToF MS, so all negative ion data had to be acquired in separate runs. Acquiring both IT and collision cell based dissociation product ion spectra for every discrete MS² generated more product ions than each technique on its own and reduced the need for additional MSⁿ experiments. However, it was still necessary to generate IT MS³ data to confirm the site of methoxyamine addition on the AZXa reactive aldehyde.

Whilst the LC-MS methodology was successfully employed for the detection and structural elucidation of all metabolites, several repeat LC-MS analyses were required to generate sufficient data for metabolite assignment. This is a significant limitation of the LC-MS methodology especially for early discovery

work where results are time critical and small sample volumes are the norm. An optimal method would ideally, acquire negative and positive ion, AIF, DDA with CID and HCD MS² accurate mass data in a single analysis and multiple scan cycles of these across the within the width of a UHPLC peak (~ 3 seconds wide). This would significantly reduce repeat analysis, sample usage, instrument time and the number of data files simplifying interpretation. This method is beyond the capability of most LC-MS systems including; Q-ToF, LTQ-Orbitrap and Q-Exactive mass spectrometers, in fact the Fusion MS is the only instrument with this capability.

7.7 Overall conclusion

The LC-MS methodology and bespoke trapping experiments were successfully employed to determine the structure and propose a mechanism of formation for all the RMs reported in this thesis. The limitations of conventional GSH trapping assays were identified for these RM examples and potential improvements to the LC-MS methodology for metabolite identification studies were highlighted.

REFERENCES

- 1 I. Kola and J. Landis, *Nat. Rev. Drug Discovery*, 2004, **3**, 711-716.
- 2 J. A. Hasler, R. Estabrook, M. Murray, I. Pikuleva, M. Waterman, J. Capdevila, V. Holla, C. Helvig, J. R. Falck and G. Farrell, *Mol. Aspects Med.*, 1999, **20**, 1-137.
- 3 P. Anzenbacher and E. Anzenbacherova, *Cell. Mol. Life Sci.*, 2001, **58**, 737-747.
- 4 M. Ingelman-Sundberg, *Naunyn Schmiedebergs Arch. Pharmacol.*, 2004, **369**, 89-104.
- 5 D. W. Nebert and D. W. Russell, *J. Lancet*, 2002, **360**, 1155-1162.
- 6 P. Baranczewski, A. Stanczak, K. Sundberg, R. Svensson, A. Wallin, J. Jansson, P. Garberg and H. Postlind, *Pharmacol. Rep.*, 2006, **58**, 453-472.
- 7 G. K. Dresser, J. D. Spence and D. G. Bailey, *Clin. Pharmacokinet.*, 2000, **38**, 41-57.
- 8 B. Coles, B. Ketterer and J. A. Hinson, *Crit. Rev. Biochem. Mol. Biol.*, 1990, **25**, 47-70.
- 9 J. R. Mitchell, S. S. Thorgeirsson, W. Z. Potter, D. J. Jollow and H. Keiser, *Clin. Pharmacol. Ther.*, 1974, **16**, 676-684 (DOI:0009-9236(74)90055-1 [pii]).
- 10 J. P. Uetrecht, *Chem. Res. Toxicol.*, 1999, **12**, 387-395.
- 11 B. K. Park, M. Pirmohamed and N. R. Kitteringham, *Chem. Res. Toxicol.*, 1998, **11**, 969-988.
- 12 World Health Organization, *International drug monitoring: the role of national centres, report of a WHO meeting [held in Geneva from 20 to 25 September 1971]*, Geneva: World Health Organization, 1972.
- 13 K. M. Giacomini, R. M. Krauss, D. M. Roden, M. Eichelbaum, M. R. Hayden and Y. Nakamura, *Nature*, 2007, **446**, 975-977.
- 14 T. Y. Wu, M. H. Jen, A. Bottle, M. Molokhia, P. Aylin, D. Bell and A. Majeed, *J. R. Soc. Med.*, 2010, **103**, 239-250 (DOI:10.1258/jrsm.2010.100113 [doi]).
- 15 https://www.gov.uk/government/uploads/system/uploads/attachment_data/file/403098/Guidance_on_adverse_drug_reactions.pdf, (accessed 07/10).
- 16 M. Pirmohamed, A. M. Breckenridge, N. R. Kitteringham and B. K. Park, *Br. Med. J.*, 1998, **316**, 1295.

- 17 J. Uetrecht and D. J. Naisbitt, *Pharmacol. Rev.*, 2013, **65**, 779-808 (DOI:10.1124/pr.113.007450 [doi]).
- 18 A. K. Daly, *Genome Med.*, 2013, **5**, 5.
- 19 P. B. Watkins, *Toxicol. Pathol.*, 2005, **33**, 1-5 (DOI:QHH2FB19LCU9NNMX [pii]).
- 20 B. Gunawan and N. Kaplowitz, *Drug Metab. Rev.*, 2004, **36**, 301-312.
- 21 N. Kaplowitz, *Clin. Infect. Dis.*, 2004, **38 Suppl 2**, S44-8 (DOI:10.1086/381446 [doi]).
- 22 M. P. Holt and C. Ju, *AAPS J.*, 2006, **8**, E48-E54.
- 23 A. Fura, Y. Shu, M. Zhu, R. L. Hanson, V. Roongta and W. G. Humphreys, *J. Med. Chem.*, 2004, **47**, 4339-4351.
- 24 B. Testa, *Biochem. Pharmacol.*, 2004, **68**, 2097-2106.
- 25 US Food and Drug Administration, *Guidance for Industry Safety Testing of Drug Metabolites*, 2008, .
- 26 I. H. T. Guideline, *Guidance on nonclinical safety studies for the conduct of human clinical trials and marketing authorization for pharmaceuticals M3 (R2)*, 2009.
- 27 US Food and Drug Administration, *Guidance for industry. M3 (R2) nonclinical safety studies for the conduct of human clinical trials and marketing authorization for pharmaceuticals*, 2013.
- 28 E. M. Isin, C. S. Elmore, G. N. Nilsson, R. A. Thompson and L. Weidolf, *Chem. Res. Toxicol.*, 2012, **25**, 532-542.
- 29 R. A. Hamilton, W. R. Garnett and B. J. Kline, *Clin. Pharmacol. Ther.*, 1981, **29**, 408-413.
- 30 K. Vishwanathan, K. Babalola, J. Wang, R. Espina, L. Yu, A. Adedoyin, R. Talaat, A. Mutlib and J. Scatina, *Chem. Res. Toxicol.*, 2008, **22**, 311-322.
- 31 C. Yu, C. L. Chen, F. L. Gorycki and T. G. Neiss, *Rapid Commun. Mass Spectrom.*, 2007, **21**, 497-502.
- 32 S. Ma, S. K Chowdhury and K. B Alton, *Curr. Drug Metab.*, 2006, **7**, 503-523.
- 33 B. Prasad, A. Garg, H. Takwani and S. Singh, *TrAC, Trends Anal. Chem.*, 2011, **30**, 360-387.
- 34 S. M. Chesnut and J. J. Salisbury, *J. Sep. Sci.*, 2007, **30**, 30.

- 35 S. A. Wren and P. Tchelitcheff, *J. Chromatogr. A*, 2006, **1119**, 140-146.
- 36 L. Nováková, D. Solichová and P. Solich, *J. Sep. Sci*, 2006, **29**, 2433-2443.
- 37 J. Castro-Perez, R. Plumb, J. H. Granger, I. Beattie, K. Joncour and A. Wright, *Rapid Commun. Mass Spectrom.*, 2005, **19**, 843-848.
- 38 T. M. Annesley, *Clin. Chem.*, 2003, **49**, 1041-1044.
- 39 D. L. Buhrman, P. I. Price and P. J. Rudewicz, *J. Am. Soc. Mass Spectrom.*, 1996, **7**, 1099-1105.
- 40 R. King, R. Bonfiglio, C. Fernandez-Metzler, C. Miller-Stein and T. Olah, *J. Am. Soc. Mass Spectrom.*, 2000, **11**, 942-950.
- 41 P. J. Taylor, *Clin. Biochem.*, 2005, **38**, 328-334.
- 42 P. Wright, Z. Miao and B. Shilliday, *Bioanalysis*, 2009, **1**, 831-845.
- 43 D. Q. Liu, Y. Xia and R. Bakhtiar, *Rapid Commun. Mass Spectrom.*, 2002, **16**, 1330-1336.
- 44 P. de Bruijn, S. Sleijfer, M. Lam, R. H. Mathijssen, E. A. Wiemer and W. J. Loos, *J. Pharm. Biomed. Anal.*, 2010, **51**, 934-941.
- 45 R. Dong, Z. Fang, H. Gao, G. Hao, G. Liu, T. Shan and Z. Liu, *Chromatographia*, 2011, **73**, 75-81.
- 46 A. S. Babu, *J. Anal. Bioanal. Tech.*, 2011, **2**, 118.
- 47 J. Wittig, M. Herderich, E. U. Graefe and M. Veit, *Journal of Chromatography B: Biomedical Sciences and Applications*, 2001, **753**, 237-243.
- 48 K. Straub, P. Rudewicz and C. Garvie, *Xenobiotica*, 1987, **17**, 413-422.
- 49 N. J. Clarke, D. Rindgen, W. A. Korfmacher and K. A. Cox, *Anal. Chem.*, 2001, **73**, 430 A-439 A.
- 50 J. Qu, Y. Wang, G. Luo and Z. Wu, *J. Chromatogr. A*, 2001, **928**, 155-162.
- 51 M. R. Davis, K. Kassahun, C. M. Jochheim, K. M. Brandt and T. A. Baillie, *Chem. Res. Toxicol.*, 1993, **6**, 376-383.
- 52 W. G. Chen, C. Zhang, M. J. Avery and H. G. Fouda, in *Biological Reactive Intermediates VI*, ed. nononymous, Springer, 2001, p. 521-524.
- 53 K. Kassahun, M. Davis, P. Hu, B. Martin and T. Baillie, *Chem. Res. Toxicol.*, 1997, **10**, 1228-1233.
- 54 S. Kölliker, M. Oehme and C. Dye, *Anal. Chem.*, 1998, **70**, 1979-1985.

- 55 G. Hopfgartner, C. Husser and M. Zell, *J. Mass Spectrom.*, 2003, **38**, 138-150.
- 56 Y. Xia, J. D. Miller, R. Bakhtiar, R. B. Franklin and D. Q. Liu, *Rapid Commun. Mass Spectrom.*, 2003, **17**, 1137-1145.
- 57 E. von Roepenack-Lahaye, T. Degenkolb, M. Zerjeski, M. Franz, U. Roth, L. Wessjohann, J. Schmidt, D. Scheel and S. Clemens, *Plant Physiol.*, 2004, **134**, 548-559 (DOI:10.1104/pp.103.032714 [doi]).
- 58 M. Ibáñez, J. V. Sancho, Ó. J. Pozo, W. Niessen and F. Hernández, *Rapid Commun. Mass Spectrom.*, 2005, **19**, 169-178.
- 59 H. Zhang, D. Zhang and K. Ray, *J. Mass Spectrom.*, 2003, **38**, 1110-1112.
- 60 M. Zhu, L. Ma, D. Zhang, K. Ray, W. Zhao, W. G. Humphreys, G. Skiles, M. Sanders and H. Zhang, *Drug Metab. Dispos.*, 2006, **34**, 1722-1733 (DOI:dmd.106.009241 [pii]).
- 61 F. Cuyckens, R. Hurkmans, J. M. Castro-Perez, L. Leclercq and R. J. Mortishire-Smith, *Rapid Commun. Mass Spectrom.*, 2009, **23**, 327-332.
- 62 L. Sleno, *J. Mass Spectrom.*, 2012, **47**, 226-236.
- 63 P. R. Tiller, S. Yu, K. P. Bateman, J. Castro-Perez, I. S. McIntosh, Y. Kuo and T. A. Baillie, *Rapid Commun. Mass Spectrom.*, 2008, **22**, 3510-3516.
- 64 D. Zhang, P. T. Cheng and H. Zhang, *Drug Metab. Lett.*, 2007, **1**, 287-292.
- 65 H. Zhang, M. Zhu, K. L. Ray, L. Ma and D. Zhang, *Rapid Commun. Mass Spectrom.*, 2008, **22**, 2082-2088.
- 66 K. P. Bateman, J. Castro-Perez, M. Wrona, J. P. Shockcor, K. Yu, R. Oballa and D. A. Nicoll-Griffith, *Rapid Commun. Mass Spectrom.*, 2007, **21**, 1485-1496.
- 67 L. Xiu-Qin, J. Chao, S. Yan-Yan, Y. Min-Li and C. Xiao-Gang, *Food Chem.*, 2009, **113**, 692-700.
- 68 E. Liu, L. Qi, Y. Peng, X. Cheng, Q. Wu, P. Li and C. Li, *Biomed. Chromatogr.*, 2009, **23**, 828-842.
- 69 D. G. Temesi, S. Martin, R. Smith, C. Jones and B. Middleton, *Rapid Communications in Mass Spectrometry*, 2010, **24**, 1730-1736.
- 70 D. O'Connor, R. Mortishire-Smith, D. Morrison, A. Davies and M. Dominguez, *Rapid Commun. Mass Spectrom.*, 2006, **20**, 851-857.
- 71 X. Zhu, Y. Chen and R. Subramanian, *Anal. Chem.*, 2014, **86**, 1202-1209.

- 72 R. Bateman, R. Carruthers, J. Hoyes, C. Jones, J. Langridge, A. Millar and J. Vissers, *J. Am. Soc. Mass Spectrom.*, 2002, **13**, 792-803.
- 73 G. Hopfgartner, D. Tonoli and E. Varesio, *Anal. Bioanal. Chem.*, 2012, **402**, 2587-2596.
- 74 J. L. Bushee and U. A. Argikar, *Rapid Commun. Mass Spectrom.*, 2011, **25**, 1356-1362.
- 75 Q. Ruan, S. Peterman, M. A. Szewc, L. Ma, D. Cui, W. G. Humphreys and M. Zhu, *J. Mass Spectrom.*, 2008, **43**, 251-261.
- 76 R. Cho, Y. Huang, J. C. Schwartz, Y. Chen, T. J. Carlson and J. Ma, *J. Am. Soc. Mass Spectrom.*, 2012, **23**, 880-888.
- 77 R. F. Mayol, C. A. Cole, G. M. Luke, K. L. Colson and E. H. Kerns, *Drug Metab. Dispos.*, 1994, **22**, 304-311.
- 78 A. E. Mutlib, H. Chen, G. A. Nemeth, J. A. Markwalder, S. P. Seitz, L. S. Gan and D. D. Christ, *Drug Metab. Dispos.*, 1999, **27**, 1319-1333.
- 79 A. Ritieni, V. Fogliano, G. Randazzo, A. Scarallo, A. Logrieco, A. Moretti, L. Manndina and A. Bottalico, *Nat. Toxins*, 1995, **3**, 17-20.
- 80 S. K. Bharti and R. Roy, *TrAC, Trends Anal. Chem.*, 2012, **35**, 5-26.
- 81 S. W. Provencher, *Magn. Reson. Med.*, 1993, **30**, 672-679.
- 82 B. Atcheson, P. J. Taylor, D. W. Mudge, D. W. Johnson, P. I. Pillans and S. E. Tett, *J. Chromatogr. B*, 2004, **799**, 157-163.
- 83 M. Delamoye, C. Duverneuil, F. Paraire, P. de Mazancourt and J. Alvarez, *Forensic Sci. Int.*, 2004, **141**, 23-31.
- 84 A. Fortuna, J. Sousa, G. Alves, A. Falcão and P. Soares-da-Silva, *Anal. Bioanal. Chem.*, 2010, **397**, 1605-1615.
- 85 P. Marathe, W. Shyu and W. Humphreys, *Curr. Pharm. Des.*, 2004, **10**, 2991-3008.
- 86 N. Penner, L. J. Klunk and C. Prakash, *Biopharm. Drug Dispos.*, 2009, **30**, 185-203.
- 87 C. L. Shaffer, M. Gunduz, B. A. Thornburgh and G. D. Fate, *Drug Metab. Dispos.*, 2006, **34**, 1615-1623 (DOI:dmd.106.010934 [pii]).
- 88 T. A. Baillie and A. W. Rettenmeier, *J. Clin. Pharmacol.*, 1986, **26**, 481-484.
- 89 D. R. Knapp, T. E. Gaffney, R. E. McMahon and G. Kiplinger, *J. Pharmacol. Exp. Ther.*, 1972, **180**, 784-790.

- 90 N. Haskins, *Biol. Mass Spectrom.*, 1982, **9**, 269-277.
- 91 A. E. Mutlib, *Chem. Res. Toxicol.*, 2008, **21**, 1672-1689.
- 92 A. Mutlib, H. Chen, J. Shockcor, R. Espina, S. Chen, K. Cao, A. Du, G. Nemeth, S. Prakash and L. Gan, *Chem. Res. Toxicol.*, 2000, **13**, 775-784.
- 93 Z. Yan and G. W. Caldwell, *Anal. Chem.*, 2004, **76**, 6835-6847.
- 94 C. Prakash, R. Sharma, M. Gleave and A. Nedderman, *Curr. Drug Metab.*, 2008, **9**, 952-964.
- 95 S. Ma and R. Subramanian, *J. Mass Spectrom.*, 2006, **41**, 1121-1139.
- 96 J. Castro-Perez, R. Plumb, L. Liang and E. Yang, *Rapid Commun. Mass Spectrom.*, 2005, **19**, 798-804.
- 97 B. Wen, L. Ma, S. D. Nelson and M. Zhu, *Anal. Chem.*, 2008, **80**, 1788-1799.
- 98 X. Zhu, N. Kalyanaraman and R. Subramanian, *Anal. Chem.*, 2011, **83**, 9516-9523.
- 99 C. Xie, D. Zhong and X. Chen, *Anal. Chim. Acta*, 2013, **788**, 89-98.
- 100 S. Liao, N. P. Ewing, B. Boucher, O. Materne and C. L. Brummel, *Rapid Commun. Mass Spectrom.*, 2012, **26**, 659-669.
- 101 C. M. Dieckhaus, C. L. Fernández-Metzler, R. King, P. H. Krolikowski and T. A. Baillie, *Chem. Res. Toxicol.*, 2005, **18**, 630-638.
- 102 S. Nakayama, H. Takakusa, A. Watanabe, Y. Miyaji, W. Suzuki, D. Sugiyama, K. Shiosakai, K. Honda, N. Okudaira, T. Izumi and O. Okazaki, *Drug Metab. Dispos.*, 2011, **39**, 1247-1254 (DOI:10.1124/dmd.111.039180 [doi]).
- 103 W. Jian, H. Liu, W. Zhao, E. Jones and M. Zhu, *J. Am. Soc. Mass Spectrom.*, 2012, **23**, 964-976.
- 104 S. Kitada, M. Leone, S. Sareth, D. Zhai, J. C. Reed and M. Pellecchia, *J. Med. Chem.*, 2003, **46**, 4259-4264.
- 105 J. Gan, T. W. Harper, M. Hsueh, Q. Qu and W. G. Humphreys, *Chem. Res. Toxicol.*, 2005, **18**, 896-903.
- 106 M. Zhu, L. Ma, H. Zhang and W. G. Humphreys, *Anal. Chem.*, 2007, **79**, 8333-8341.
- 107 J. Gan, T. W. Harper, M. Hsueh, Q. Qu and W. G. Humphreys, *Chem. Res. Toxicol.*, 2005, **18**, 896-903.

- 108 J. R. Soglia, S. P. Harriman, S. Zhao, J. Barberia, M. J. Cole, J. G. Boyd and L. G. Contillo, *J. Pharm. Biomed. Anal.*, 2004, **36**, 105-116.
- 109 J. R. Soglia, L. G. Contillo, A. S. Kalgutkar, S. Zhao, C. E. Hop, J. G. Boyd and M. J. Cole, *Chem. Res. Toxicol.*, 2006, **19**, 480-490.
- 110 Z. Yan, N. Maher, R. Torres, G. W. Caldwell and N. Huebert, *Rapid Commun. Mass Spectrom.*, 2005, **19**, 3322-3330.
- 111 N. R. Hartman, R. L. Cysyk, C. Bruneau-Wack, J. Thénot, R. J. Parker and J. M. Strong, *Chem. Biol. Interact.*, 2002, **142**, 43-55.
- 112 D. Argoti, L. Liang, A. Conteh, L. Chen, D. Bershas, C. P. Yu, P. Vouros and E. Yang, *Chem. Res. Toxicol.*, 2005, **18**, 1537-1544.
- 113 J. W. Gorrod, C. M. Whittlesea and S. P. Lam, in *Biological Reactive Intermediates IV*, ed. nonymous, Springer, 1991, p. 657-664.
- 114 M. Zhang, C. M. Resuello, J. Guo, M. E. Powell, C. S. Elmore, J. Hu and K. Vishwanathan, *Drug Metab. Dispos.*, 2013, **41**, 1023-1034 (DOI:10.1124/dmd.112.050450 [doi]).
- 115 M. D. Mitchell, M. M. Elrick, J. L. Walgren, R. A. Mueller, D. L. Morris and D. C. Thompson, *Chem. Res. Toxicol.*, 2008, **21**, 859-868.
- 116 J. E. Laine, S. Auriola, M. Pasanen and R. O. Juvonen, *Toxicol. In Vitro*, 2011, **25**, 411-425.
- 117 F. Goldszer, G. L. Tindell, U. K. Walle and T. Walle, *Res. Commun. Chem. Pathol. Pharmacol.*, 1981, **34**, 193-205.
- 118 X. Yang and W. Chen, *Xenobiotica*, 2005, **35**, 797-809.
- 119 T. Rousu, O. Pelkonen and A. Tolonen, *Rapid Commun. Mass Spectrom.*, 2009, **23**, 843-855.
- 120 J. P. O'Donnell, D. K. Dalvie, A. S. Kalgutkar and R. S. Obach, *Drug Metab. Dispos.*, 2003, **31**, 1369-1377 (DOI:10.1124/dmd.31.11.1369 [doi]).
- 121 C. Zhang, S. Wong, E. M. Delarosa, J. R. Kenny, J. S. Halladay, C. E. Hop and S. C. Khojasteh-Bakht, *Drug Metab. Lett.*, 2009, **3**, 125-129.
- 122 V. Ravindranath and M. R. Boyd, *Toxicol. Appl. Pharmacol.*, 1985, **78**, 370-376.
- 123 W. Jian, M. Yao, D. Zhang and M. Zhu, *Chem. Res. Toxicol.*, 2009, **22**, 1246-1255.
- 124 M. J. Bailey and R. G. Dickinson, *Chem. Biol. Interact.*, 2003, **145**, 117-137.

- 125 S. Bolze, O. Lacombe, T. Hulot, G. Durand, P. Chaimbault, N. Bromet, F. Massiere and C. Gay-Feutry, *Curr. Sep.*, 2002, **20**, 55-60.
- 126 Z. Chen, T. G. Holt, J. V. Pivnichny and K. Leung, *J. Pharmacol. Toxicol. Methods*, 2007, **55**, 91-95.
- 127 N. Jinno, S. Ohashi, M. Tagashira, T. Kohira and S. Yamada, *Biol. Pharm. Bull.*, 2013, **36**, 1509-1513.
- 128 S. Zhong, R. Jones, W. Lu, S. Schadt and G. Ottaviani, *Drug Metab. Dispos.*, 2015, **43**, 1711-1717 (DOI:10.1124/dmd.115.066159 [doi]).
- 129 J. R. Gillette, *Biochem. Pharmacol.*, 1974, **23**, 2785-2794.
- 130 D. C. Evans, A. P. Watt, D. A. Nicoll-Griffith and T. A. Baillie, *Chem. Res. Toxicol.*, 2004, **17**, 3-16.
- 131 S. Nakayama, R. Atsumi, H. Takakusa, Y. Kobayashi, A. Kurihara, Y. Nagai, D. Nakai and O. Okazaki, *Drug. Metab. Dispos.*, 2009, **37**, 1970-1977 (DOI:10.1124/dmd.109.027797 [doi]).
- 132 R. A. Thompson, E. M. Isin, Y. Li, L. Weidolf, K. Page, I. Wilson, S. Swallow, B. Middleton, S. Stahl and A. J. Foster, *Chem. Res. Toxicol.*, 2012, **25**, 1616-1632.
- 133 J. N. Bauman, J. M. Kelly, S. Tripathy, S. X. Zhao, W. W. Lam, A. S. Kalgutkar and R. S. Obach, *Chem. Res. Toxicol.*, 2009, **22**, 332-340.
- 134 T. Chalmers, J. Kellgren and D. Platt, *Ann. Rheum. Dis.*, 1969, **28**, 595-601.
- 135 T. M. Chalmers, J. E. Pohl and D. S. Platt, *Ann. Rheum. Dis.*, 1969, **28**, 590-594.
- 136 D. M. Foulkes, *J. Pharmacol. Exp. Ther.*, 1970, **172**, 115-121.
- 137 A. Bradbury, G. Powell, C. Curtis and C. Rhodes, *Xenobiotica*, 1981, **11**, 665-674.
- 138 A. V. Rodrigues, H. E. Rollison, S. Martin, S. Sarda, T. Schulz-Utermoehl, S. Stahl, F. Gustafsson, J. Eakins, J. G. Kenna and I. D. Wilson, *Arch. Toxicol.*, 2013, , 1-11.
- 139 Y. Le and B. Sauer, *Mol. Biotechnol.*, 2001, **17**, 269-275.
- 140 K. Pickup, A. Gavin, H. B. Jones, E. Karlsson, C. Page, K. Ratcliffe, S. Sarda, T. Schulz-Utermoehl and I. Wilson, *Xenobiotica*, 2012, **42**, 195-205.
- 141 T. Lassila, J. Hokkanen, S. Aatsinki, S. Mattila, M. Turpeinen and A. Tolonen, *Chem. Res. Toxicol.*, 2015, **28**, 2292-2303.

- 142 J. Y. Raskind and G. M. El-Chaar, *Ann. Pharmacother.*, 2000, **34**, 630-638.
- 143 G. A. Doss, R. R. Miller, Z. Zhang, Y. Teffera, R. P. Nargund, B. Palucki, M. K. Park, Y. S. Tang, D. C. Evans and T. A. Baillie, *Chem. Res. Toxicol.*, 2005, **18**, 271-276.
- 144 H. A. Heck and M. Casanova, *Regul. Toxicol. Pharmacol.*, 2004, **40**, 92-106.
- 145 M. Kazachkov, K. Chen, S. Babiy and P. H. Yu, *J. Pharmacol. Exp. Ther.*, 2007, **322**, 1201.
- 146 B. Metz, G. F. A. Kersten, P. Hoogerhout, H. F. Brugghe, H. A. M. Timmermans, A. de Jong, H. Meiring, J. Hove, W. E. Hennink and D. J. A. Crommelin, *J. Biol. Chem.*, 2004, **279**, 6235.
- 147 J. Toews, J. C. Rogalski, T. J. Clark and J. Kast, *Anal. Chim. Acta*, 2008, **618**, 168-183.
- 148 M. L. Cunningham, H. B. Matthews and L. T. Burka, *Chem. Res. Toxicol.*, 1990, **3**, 157-161.
- 149 E. Novik, T. J. Maguire, P. Chao, K. Cheng and M. L. Yarmush, *Biochem. Pharmacol.*, 2010, **79**, 1036-1044.

WORD COUNT

Chapter 1 (Introduction): 16995

Chapter 2: 4700

Chapter 3: 3900

Chapter 4: 5000

Chapter 5: 4300

Chapter 6: 3400

Chapter 7 (summary) 5306

Total word count: 43601

The metabolic fate of [¹⁴C]-Fenclozic acid in the hepatic reductase null (HRN) mouse:

Contributed to the writing of the introduction, methods, results and conclusion.

Conducted all of the LC-MS analysis and interpretation.

Identification of the Reactive Metabolites of Fenclozic Acid in Bile Duct Cannulated Rats:

First Author and corresponding author.

Designed the study, planned, prepared, and wrote the majority of the manuscript (>95%). Conducted all sample preparation, LC-MS analysis and interpretation.

Reaction of Homopiperazine with Endogenous Formaldehyde: A Carbon Hydrogen Addition Metabolite/Product Identified in Rat Urine and Blood:

First Author and corresponding author.

Designed the study, planned, prepared, and wrote the majority of the manuscript (>75%). Conducted all sample preparation, LC-MS analysis and interpretation.

Reactive Metabolite Trapping Screens and Potential Pitfalls: Bioactivation of a Homomorpholine and Formation of an Unstable Thiazolidine Adduct:

Contributed to the writing of the introduction, methods, results and conclusion.

Conducted the metabolite isolation, detailed LC-MS analysis and interpretation to identify the thiazolidine adduct (including methoxyamine trap) and contributed to the interpretation of the multi-trapping agent experiments.

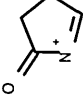
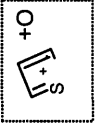
Methanol adducts leading to the identification of a reactive aldehyde metabolite of AZX in human liver microsomes

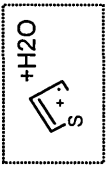
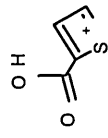
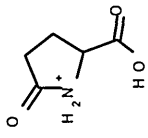
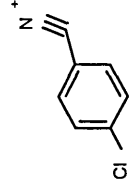
First Author and corresponding author.

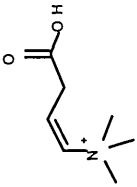
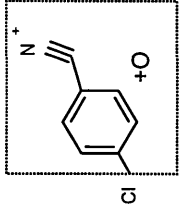
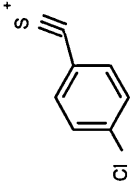
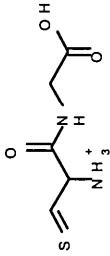
Designed the study, planned, prepared, and wrote the majority of the manuscript (>90%). Conducted all the LC-MS analysis and interpretation.

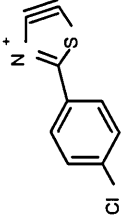
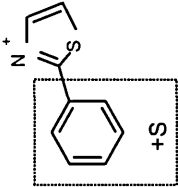
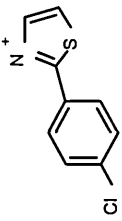
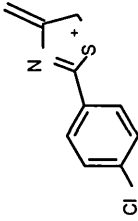
APPENDIX B: PROPOSED STRUCTURES FOR PRODUCT IONS IDENTIFIED FROM FENCLOZIC ACID AND IT'S METABOLITES

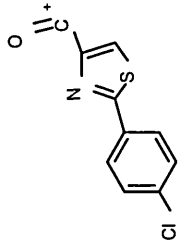
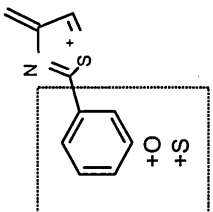
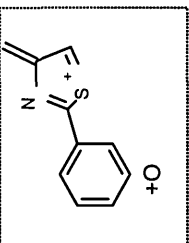
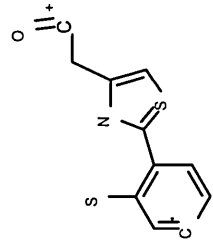
Table C1

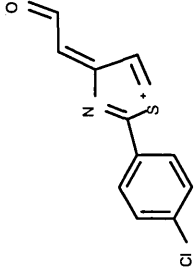
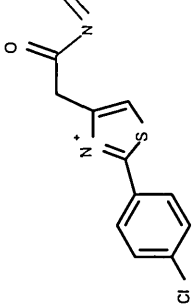
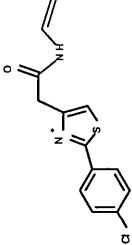
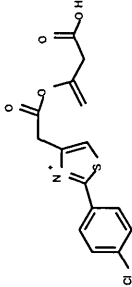
Fragment	Metabolite	Fragment <i>m/z</i>	Elemental composition	Proposed structure	Comment
1	Fenclozic acid M1, M2, M3, M4, M5, M10, M12, M15 M16 and M17	70.9950	C ₃ H ₃ S		
2	M12	84.0444	C ₄ H ₆ NO		Fragment from Glutaryl
3	M1	86.9899	C ₃ H ₃ OS		

4	M6 and M7	89.0056	C_3H_5OS		
5	M1	114.9848	$C_4H_3O_2S$		
6	M13	126.0219	$C_2H_8O_3NS$		Fragment from Taurine
7	M12 and M18	130.0499	$C_5H_8NO_3$		Fragment from Glutaryl
8	Fenclozic acid, M6 and M7	138.0105	C_7H_5ClN		

9	M11	144.1019	$C_7H_{14}NO_2$		Fragment from Carnitine
10	M8 and M9	150.0105	C_8H_5ClN		
11	M2, M3, M4, M5, M15, M16, M17 and M18	154.0054	C_7H_5ClNO		
12	M1 M6 and M7	154.9717	C_7H_4ClS		
13	M18	177.0328	$C_5H_9N_2O_3S$		Fragment from Glutathione

14	M8 and M9	193.9826	C ₉ H ₅ CINS		
15	M15 and M16	194.0093	C ₉ H ₈ NS ₂		
16	M1, M6 and M7	195.9982	C ₉ H ₇ CINS		
17	Fenclozic acid, M10, M11 M12 and M14, M15 and M16	207.9982	C ₁₀ H ₇ CINS		

18	M8 and M9	221.9775	C ₁₀ H ₅ CINOS		
19	M15	222.0042	C ₁₀ H ₈ NOS ₂		
20	M1, M2, M3, M4, M5, M15, M16 and M17	223.9931	C ₁₀ H ₇ CINOS		
21	M15	235.0120	C ₁₁ H ₉ NOS ₂		<p>Odd electron ion. Cl Radical loss (Not shown in figure 4)</p>

22	M12, M13 and M14	235.9931	$C_{11}H_7ClNOS$		
23	M14	265.0197	$C_{12}H_{10}ClN_2OS$		
24	M13	279.0353	$C_{13}H_{12}ClN_2OS$		
25	M11	338.0248	$C_{14}H_{13}ClNO_4S$		

Note- The exact Product ion structures are proposed for illustrative purposes.

APPENDIX C: COPYRIGHT PERMISSION

I declare that the copyright has been granted for all publications included in this thesis.

Signed *S. Mart*



informa
healthcare

Title: The metabolic fate of [14C]-fenclozic acid in the hepatic reductase null (HRN) mouse
Author: Kathryn Pickup, Jonathan Wills, Alison Rodrigues, et al
Publication: Xenobiotica
Publisher: Taylor & Francis
Date: Feb 1, 2014
Copyright © 2014 Taylor & Francis

LOGIN
If you're a copyright.com user, you can login to RightsLink using your copyright.com credentials. Already a RightsLink user or want to learn more?

Thesis/Dissertation Reuse Request

Taylor & Francis is pleased to offer reuses of its content for a thesis or dissertation free of charge contingent on resubmission of permission request if work is published.



ACS Publications
Most Trusted. Most Cited. Most Read.

Title: Identification of the Reactive Metabolites of Fenclozic Acid in Bile Duct Cannulated Rats
Author: Scott Martin, Eva M. Lenz, Warren Keene, et al
Publication: Analytical Chemistry
Publisher: American Chemical Society
Date: Nov 1, 2014
Copyright © 2014, American Chemical Society

LOGIN
If you're a copyright.com user, you can login to RightsLink using your copyright.com credentials. Already a RightsLink user or want to learn more?

PERMISSION/LICENSE IS GRANTED FOR YOUR ORDER AT NO CHARGE

This type of permission/license, instead of the standard Terms & Conditions, is sent to you because no fee is being charged for your order. Please note the following:

- Permission is granted for your request in both print and electronic formats, and translations.
- If figures and/or tables were requested, they may be adapted or used in part.
- Please print this page for your records and send a copy of it to your publisher graduate school.
- Appropriate credit for the requested material should be given as follows: "Reprinted (adapted) with permission from (COMPLETE REFERENCE CITATION). Copyright (YEAR) American Chemical Society." Insert appropriate information in place of the capitalized words.
- One-time permission is granted only for the use specified in your request. No additional uses are granted (such as derivative works or other editions). For any other uses, please submit a new request.

Council

David R. Sibley
President
Bethesda, Maryland

John D. Schuetz
President-Elect
St. Jude Children's Research Hospital

Kenneth E. Thummel
Past President
University of Washington

Charles P. France
Secretary/Treasurer
The University of Texas Health
Science Center at San Antonio

John J. Tesmer
Secretary/Treasurer-Elect
University of Michigan

Dennis C. Marshall
Past Secretary/Treasurer
Ferring Pharmaceuticals, Inc.

Margaret E. Gnegy
Councilor
University of Michigan Medical School

Wayne L. Backes
Councilor
Louisiana State University Health
Sciences Center

Carol L. Beck
Councilor
Thomas Jefferson University

Mary E. Vore
Chair, Board of Publications Trustees
University of Kentucky

Brian M. Cox
FASEB Board Representative
Uniformed Services University
of the Health Sciences

Scott A. Waldman
Chair, Program Committee
Thomas Jefferson University

Judith A. Siuciak
Executive Officer

August 19, 2016

Scott Martin
Oncology DMPK
AstraZeneca
Hodgkin Bldg Chesterford Research Park
Saffron Walden
Essex CB10 1XL
UK

Email: scott.martin2@astrazeneca.com

Dear Scott Martin:

This is to grant you permission to include the following article in your thesis entitled "Identification and mechanistic study of novel drug metabolites by LC-MS" for Sheffield Hallam University:

Scott Martin, Eva M. Lenz, Dave Temesi, Martin Wild, and Malcolm R. Clench, Reaction of Homopiperazine with Endogenous Formaldehyde: A Carbon Hydrogen Addition Metabolite/Product Identified in Rat Urine and Blood, *Drug Metab Dispos* August 2012 40:1478-1486; doi:10.1124/dmd.112.044917

On the first page of each copy of this article, please add the following:

Reprinted with permission of the American Society for Pharmacology and Experimental Therapeutics. All rights reserved.

In addition, the original copyright line published with the paper must be shown on the copies included with your thesis.

Sincerely yours,



Richard Dodenhoff
Journals Director

Title: Reactive Metabolite Trapping Screens and Potential Pitfalls: Bioactivation of a Homomorpholine and Formation of an Unstable Thiazolidine Adduct

Author: Eva. M. Lenz, Scott Martin, Ralf Schmidt, et al

Publication: Chemical Research in Toxicology

Publisher: American Chemical Society

Date: Jun 1, 2014

Copyright © 2014, American Chemical Society

LOGIN

If you're a **copyright.com user**, you can login to RightsLink using your **copyright.com** credentials. Already a **RightsLink user** or want to [learn more?](#)

PERMISSION/LICENSE IS GRANTED FOR YOUR ORDER AT NO CHARGE

This type of permission/license, instead of the standard Terms & Conditions, is sent to you because no fee is being charged for your order. Please note the following:

- Permission is granted for your request in both print and electronic formats, and translations.
- If figures and/or tables were requested, they may be adapted or used in part.
- Please print this page for your records and send a copy of it to your publisher/graduate school.
- Appropriate credit for the requested material should be given as follows: "Reprinted (adapted) with permission from (COMPLETE REFERENCE CITATION). Copyright (YEAR) American Chemical Society." Insert appropriate information in place of the capitalized words.
- One-time permission is granted only for the use specified in your request. No additional uses are granted (such as derivative works or other editions). For any other uses, please submit a new request.

JOHN WILEY AND SONS LICENSE

TERMS AND CONDITIONS

Dec 19, 2016

This Agreement between Scott Martin ("You") and John Wiley and Sons ("John Wiley and Sons") consists of your license details and the terms and conditions provided by John Wiley and Sons and Copyright Clearance Center.

License Number	4012450309927
License date	Dec 19, 2016
Licensed Content Publisher	John Wiley and Sons
Licensed Content Publication	Rapid Communications in Mass Spectrometry
Licensed Content Title	Methanol adducts leading to the identification of a reactive aldehyde metabolite of CPAQOP in human liver microsomes by ultra-high-performance liquid chromatography/mass spectrometry
Licensed Content Author	Scott Martin,Eva M. Lenz,Robin Smith,David G. Temesi,Alexandra L. Orton,Malcolm R. Clench
Licensed Content Date	Nov 28, 2016
Licensed Content Pages	7
Type of use	Dissertation/Thesis
Requestor type	Author of this Wiley article
Format	Print and electronic
Portion	Full article
Will you be translating?	No
Title of your thesis / dissertation	IDENTIFICATION AND MECHANISTIC STUDY OF NOVEL DRUG METABOLITES BY LC-MS
Expected completion date	Feb 2017
Expected size (number of pages)	180
Requestor Location	Scott Martin Astrazeneca Hodgkin building c/o Darwin building 310 Cambridge Science park Milton road Cambridge, CB4 0WG United Kingdom Attn: Scott Martin
Publisher Tax ID	EU826007151
Billing Type	Invoice
Billing Address	Scott Martin Astrazeneca Hodgkin building c/o Darwin building 310 Cambridge Science park Milton road Cambridge, United Kingdom CB4 0WG Attn: Scott Martin